STRATEGIES FOR ENHANCING THE FIRE RESISTANCE OF STEEL FRAMED STRUCTURES THROUGH COMPOSITE CONSTRUCTION

By

Rustin Fike

A DISSERTATION

Submitted to
Michigan State University
in partial fulfillment of the requirements
for the degree of

DOCTOR OF PHILOSOPHY

Civil Engineering

2010

ABSTRACT

STRATEGIES FOR ENHANCING THE FIRE RESISTANCE OF STEEL FRAMED STRUCTURES THROUGH COMPOSITE CONSTRUCTION

BY

Rustin Fike

Steel framed structures often utilize concrete due to several advantages composite construction offers over other types of construction. The composite action that develops between steel and concrete significantly enhances structural performance under ambient and fire conditions. However, the beneficial effects of composite action are not often taken into consideration in evaluating the fire response of structures due to poor understanding on the behavior of composite structural systems, and lack of design methodologies for evaluating fire resistance. With the aim of developing an understanding on the behavior of composite structural systems under fire exposure, both experimental and numerical studies were carried out as part of this study.

The experimental studies consisted of analyzing the response of four composite beam slab assemblies under fire exposure. The assemblies consisted of a network of five steel beams, atop which was cast various types of concrete slabs. The assemblies were tested under design fire exposure and realistic load levels. In the fire tests, special attention was given to monitor the development of composite action and tensile membrane behavior under realistic loading and fire conditions.

Data from the fire resistance tests and the literature were utilized to validate the response of composite column, beam slab assembly, and full-scale steel framed structural models created in SAFIR finite element based computer program. The validity of the program is established by comparing measured temperatures, deflections, and failure modes observed in testing with those

predicted by SAFIR. These validated models were then applied to study the influence that critical factors have on the fire response of composite structural systems at the element, assembly, and system levels. In total, more than 2000 numerical simulations were conducted to quantify the effect of critical parameters on the fire response of steel framed structures. In each of the simulations, the failure times were evaluated based on strength limit states.

Data generated from the parametric studies was applied to develop design methodologies for evaluating the fire resistance of concrete filled HSS columns, and composite beam slab assemblies. The design methodology for concrete filled HSS columns is based on equivalent fire severity principals, and utilizes the equal area concept to establish equivalency between severity of a design fire, and that of ASTM E-119 fire exposure for predicting failure of concrete filled HSS columns under design fire exposure. For beam-slab assemblies, a relationship between maximum design fire temperature and fire response is utilized to establish a correlation between fire resistance under standard ASTM E-119 fire exposure and under design fire exposure. The validity of the proposed methods is established by comparing the predictions from these methods with results from SAFIR analysis.

To further demonstrate the validity of the proposed methodologies, fire resistance calculations have been carried out for a typical eight story steel framed office building, and compared with SAFIR predictions. The building was analyzed under various fire scenarios and structural configurations to illustrate the improvements in fire resistance achieved through composite construction. Initially, with unprotected steel members, failure occurred in less than 20 minutes in the structure, after incorporating concrete filled HSS columns and SFRC beam-slab assemblies, fire resistance was enhanced to such an extent that fire protection can be eliminated from columns and secondary beams while still providing the required level of fire resistance.

ACKNOWLEDGMENT

I would like to express my gratitude to my advisor, Prof. Venkatesh Kodur for his continued support and guidance during the course of my studies. I would also like to thank Prof. Ronald Harichandran, Prof. Rigoberto Burgueño, and Prof. Indrek Wichman for joining my Ph.D. committee, and for their valuable advice throughout my education at MSU.

For his support, not just in graduate school, but in my life as well, I am thankful to my father Dr. Randall Fike. I am also thankful for the friends who have accompanied me on this journey, especially: Dr. Alicia Findora, Dr. Gilbert Baladi, Nick Brake, and Tyler Dawson.

For her continued support, love, and encouragement, I am thankful to my fiancée Ashleigh Brewer.

I would like to thank the lab manager, Mr. Siavosh Ravanbakhsh for his support and help during the experimental program in this research.

Obviously, I would like to extend my thanks to Laura Taylor, Mary Mroz, and Margaret Conner for all the help they provided.

I would like to thank Aqeel Ahmad, Megan Vivian, Nickolas Hatinger, Nikhil Raut, Purushutham Pakala, Wasim Khaliq, Mahmud Dwaikat, Monther Dwaikat, Jim Stein, and Emily Wellman for their support, particularly in the experimental part of this study.

Additionally, I would like to thank all the faculty members and students at the Civil and Environmental Engineering department at Michigan State University for their help and support during my Ph.D. study.

Finally, I would like to thank my Lord for the abilities, opportunities, and people he has given me to accomplish all that I have in life, and for life itself.

TABLE OF CONTENTS

LIST OF TABLES

LIST OF FIGURES

CHAPTER 1

1 INTRODUCTION

1.1 General

Fire represents one of the most severe environmental conditions to which structures may be subjected, and hence, the provision of appropriate fire safety measures for structural members is an important aspect in the design of high-rise buildings. Steel is often used as the primary structural material in high-rise buildings, and these steel structural members have to satisfy appropriate fire resistance requirements prescribed in building codes. Unprotected steel members exhibit a fire resistance of about 20-25 minutes, and hence, have to be provided with some level of fire protection to enhance their fire resistance level to 1 to 4 hours as stipulated in building codes. This is generally achieved by providing external fire insulation to steel members. Such fire proofing measures, which are based on prescriptive provisions, add to the cost of construction and do not permit the feasibility of having exposed steel in buildings. Also, durability (adhesion and cohesion) of fire insulation is often an unreliable issue, and hence requires periodic inspection and regular maintenance. This, in turn, incurs additional cost during the lifetime of the structure (FEMA 2002, NIST 2004).

The amount of fire proofing (insulation) to structural members is usually determined by testing single structural elements such as beams, columns, etc., under standard fire conditions. This traditional approach of evaluating fire resistance based on element level tests is overly conservative and may not be realistic, since a number of factors such as composite action, moment redistribution, member interactions, restraint conditions, and load intensity cannot be accounted for in single element behavior. Further, compartment characteristics and location, as well as realistic fire scenarios, which influence the behavior and eventual failure of a structure, are not taken into consideration.

In recent years, there is a growing recognition that structural performance under fire conditions should be based on realistic fire, restraint, and loading conditions. It is widely believed that a structural system performs better under actual design (realistic) scenarios, and this might lead to reduced (or eliminated) fire protection requirements. In fact, there is significant evidence that shows steel framed structures in high-rise office buildings have historically survived major fires extremely well, for example, the First Interstate Bank Building Fire in Los Angeles in 1988 (FEMA 1990), and the One Meridian Plaza fire in Philadelphia in 1991 (FEMA 1994). The large scale fire tests carried out on a steel framed building (British Steel 1998) further confirm the fact that the fire performance of a whole structure, under design fire scenarios, is much better than that of individual members under standard fire scenarios.

In addition, fire statistics have shown that the risk to life in office buildings is very low and rarely do fires develop into the post flashover stage where the stability of the building is threatened. Further, in the event of fire, fire safety measures such as fire detection, fire suppression, smoke management, occupant evacuation, and brigade fire fighting provide many levels of defense. However, in the current practice of evaluating fire resistance, based on standard fire tests, none of the above factors are fully taken into consideration. Thus, the current prescriptive approaches have not only major drawbacks, but also do not permit an engineering approach to evaluate realistic fire safety in steel structures. The development of engineering approaches is critical for undertaking rational fire design in a performance-based environment.

1.2 Behavior of Steel Structures Under Fire Conditions

Steel, similar to other building materials, loses its strength and stiffness with an increase in temperature. The rate of loss of strength is faster in steel as compared to concrete. Further, the high thermal conductivity of steel results in faster heat transmission through the member cross-section. To overcome this, steel has traditionally been provided with external fire insulation to limit the temperature rise in the steel section. Fig. 1.1 illustrates the variation of normalized (with respect to ambient temperature properties) strength and elastic modulus of steel as a function of temperature (SFPE 2005). Of particular significance in Fig. 1.1, is the observation that the normalized yield strength and elastic modulus drop to about 50% at 550 °C, this has a considerable impact on the fire resistance of steel structures.

Under fire conditions, the loading on a structure does not significantly change, but, the capacity (strength) of the member decreases with time of fire exposure due to increasing temperatures in steel. This decrease in strength continues until the time at which the capacity of the member is below the applied load, at which point the member fails. This type of response is contrary to what happens under other conventional loading conditions wherein failure is due to progressive increase in loading.

Fig. 1.2 illustrates the development of failure in a simply supported steel beam (protected with fire insulation) exposed to loading under conventional loading conditions, and under fire exposure conditions. In the conventional loading case, the simply supported beam is subjected to increasing load levels as encountered in earthquake or wind loads, while in the second case the beam is exposed to fire and the load level remains constant. In both cases, the beam initially has an ultimate moment capacity of 400 kip-ft. Under service loads, the applied moment on the beam is only 200 kip-ft, which is well below the ultimate moment capacity (400 kip-ft.).

However, as the applied load increases, the moment demand on the beam increases until failure occurs.

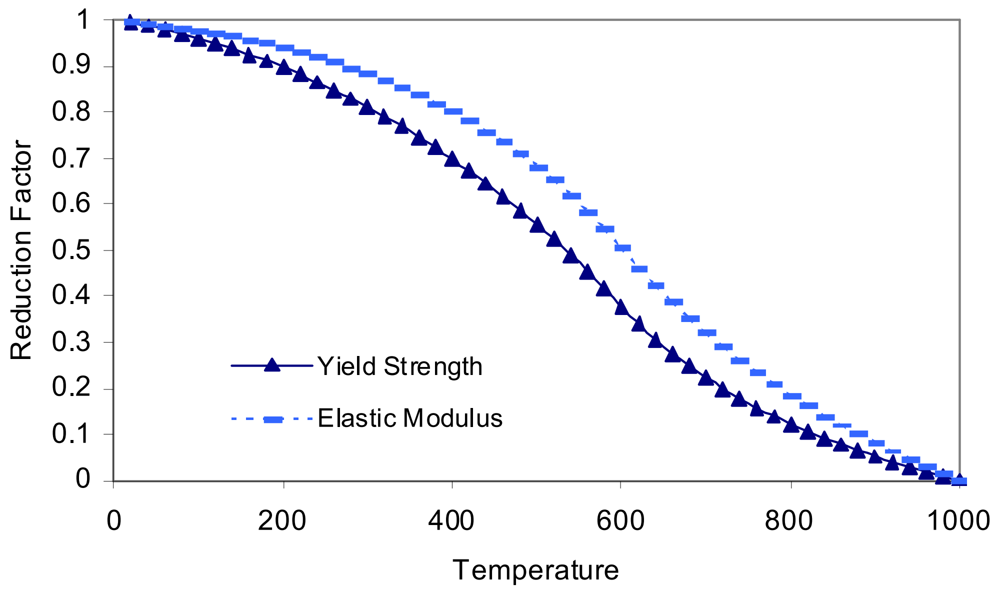

Fig. 1.1: Variation of strength and elastic modulus of steel with temperature

For interpretation of the references to color in this and all other figures, the reader is referred to the electronic version of this dissertation

Likewise, in the case of fire exposure, the load under service conditions, just prior to fire exposure produces a moment of 200 kip-ft. However, as the time of fire exposure increases, the load level remains the same (200 kip-ft), but the moment capacity decreases due to softening of steel with an increase in temperatures (Fig. 1.1). As an illustration, in about 20 minutes the moment capacity decreases to about 350 kip-ft., while at 40 minutes it goes down to about 300 kip-ft. Finally, at 60 minutes, the capacity reaches 200 kip-ft. and failure occurs in the beam.

In both cases, the deflection increases either with increasing load or under fire exposure until failure of the beam. In the case of increasing load, failure occurs when the applied load exceeds the capacity of the beam, however, in the case of fire, failure occurs when the capacity of the beam (at the critical section) drops below the applied load (moment). The duration of time from the initiation of fire exposure until the capacity of the section drops below the applied load (moment) is termed as the fire resistance of the member. The decrease in moment capacity and increase in deflection of a structural member under fire conditions are primarily dependent on the temperature rise in steel. By limiting the fire induced temperature rise in steel, it is possible to delay the failure of a structural member.

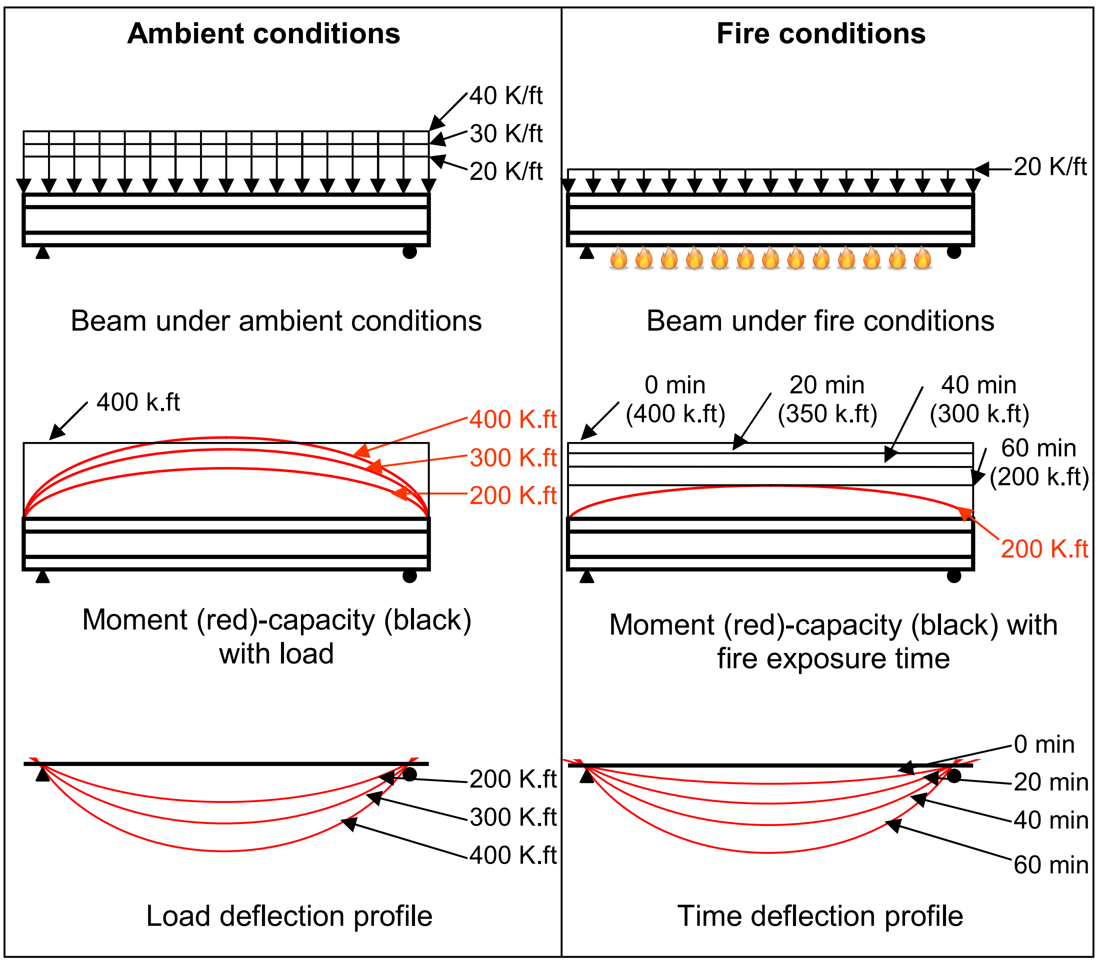

Fig. 1.2: Progression of failure in a steel beam under conventional and fire loading scenarios

This case of a simply supported beam illustrated the propagation of failure for a very simplistic case. In actual buildings, the performance of a structural member is quite complex and is dependent on a number of factors such as type of fire exposure, continuity, restraint, composite action, and system characteristics.

1.3 Methods of Achieving Fire Resistance

Unprotected steel structural members when exposed to fire exhibit a fire resistance on the order of 20-25 minutes. However, in medium to high-rise office buildings, structural members are required to have fire resistance on the order of 1-3 hours. Thus, steel structural members are typically provided with some form of fire protection to achieve the required fire resistance. There are three methods through which fire resistance requirements can be achieved, namely; applying external protection, providing capacitive protection, or composite construction.

The principle behind external fire protection is to limit heat transmission from fire to the steel section. This is accomplished through the application of layers of insulation between steel and probable fire exposure zones. This is often achieved through spray applied fire protection or intumescent paints. Spray applied fire protection consists primarily of vermiculite and cementations materials. Layers of insulation on the order of 0.5-2 inches thickness are required to achieve a fire resistance of 1-3 hours for most structural members. The low thermal conductivity of these insulating materials limits the temperature rise in steel for the required length of time.

Intumescent paints can also be applied in much thinner layers, and have the appearance of paint at ambient temperatures. When exposed to elevated temperatures, intumescent paint undergoes an endothermic carbonation reaction that results in the production of an inert gas (often CO_2) that does not burn, but is retained in the paint layer causing it to "foam" to a much thicker layer (FEMA 2003). This expanded foam layer has a low thermal conductivity that serves to insulate the structural member after the endothermic reaction has ended, thus limiting the temperature rise in the steel.

Both of these methods of protecting the steel sections with external insulation have severe limitations. They add to construction costs and time, reduce usable space, require inspection (adding additional operation cost), and have problems with adhesion and cohesion characteristics. Adhesion of these materials was found to be poor during fire tests, and some specimens delaminated while they were being placed in the testing frame (Sorathia et al. 2003, FEMA 2002).

As an alternative to external protection, capacitive protection can be used to enhance the fire resistance of steel structural members. Capacitive methods that have been employed include filling hollow structural section (HSS) columns with concrete or water. Capacitive protection limits the temperature rise in steel by absorbing heat from the steel. Since heat is constantly transferred from the steel to the capacitive material, the temperature in the steel remains low for a considerable length of time. Though water has been employed in a few cases, due to the inherent problems of using liquid to increase heat capacity, concrete is preferred in most situations. The main advantage of concrete is that it can be utilized to carry a portion of the load at ambient conditions (as composite construction) thus economizing the design (Kodur and Fike 2009a,b).

In lieu of external insulation or capacitive protection, the inherent fire resistance present in steel structural systems can effectively be utilized to satisfy the required fire resistance ratings. Such inherent fire resistance exists in all structures, and can be significant in the case of composite steel-concrete structural systems. In these systems, inherent fire resistance is facilitated by structural interactions between various connected structural members, composite action, tensile membrane action, and redistribution of forces from fire weakened members to other cooler parts of the structure. Composite construction is generally accounted for in the ambient temperature strength design of the members, but is often neglected in evaluating fire response. When composite action between steel and concrete is accounted for with realistic fire exposures (with a decay phase to limit the temperature rise in structural members), application of realistic failure limit states, and load level, it may be possible to achieve the required fire resistance in some situations without the need for additional fire protection measures (Kodur and Fike 2008, Ponto 2006, Lamont and Lane 2006).

Elimination of external fire protection measures decreases construction time, reduces construction cost, increases usable space, and provides a more reliable fire resistance mechanism. While detailed fire resistance analysis may be required to demonstrate inherent fire resistance, the benefits on the construction side more than offset the additional design effort.

1.4 Fire Resistance Evaluation

The fire resistance of structural members is currently evaluated through standard fire resistance tests. In these tests, a structural member is exposed to a standard fire in a specially built fire furnace for a specified fire duration. The fire conditions and procedures used in the fire test are governed by specifications in applicable standards such as ASTM E-119 (ASTM 2007), and internationally ISO 834 (ISO 1975). There are a number of limitations that result from these standard fire tests. The most restrictive limitations are:

- The use of a one-size fits all prescriptive standard fire exposure that is often more severe than commonly experienced by structural members in buildings. In the standard fire exposure, the fire temperature increases throughout the duration of the fire exposure and there is no decay phase, despite the fact that most building fires die down after a certain length of time due to a lack of either fuel or air.

- Structural elements are tested as individual components (columns or beams) and the beneficial effects such as redistribution of moments, and composite action, which occur through interconnected structural members are neglected.
- Failure is often defined by a limiting critical temperature in steel, and thus does not capture the actual failure under strength or deflection limit states.

Hindered by these limitations, the current practice of evaluating fire resistance through prescriptive based approaches does not lead to rational assessment of structural performance under realistic fire, loading, and restraint conditions. To overcome these limitations, it is necessary to implement a performance-based methodology for evaluating fire resistance.

Performance-based fire resistance evaluation takes into account realistic (probable) fire scenario, loading, restraint, and boundary conditions of the structural system. Determination of realistic fire exposure is accomplished by taking into account the compartment fuel load and ventilation characteristics, as well as other details, such as the presence of sprinklers, on the fire growth and development. Several methods can be employed to determine the probabilistic (design) fire exposure. Eurocode and SFPE provide simplified approaches for determining the time temperature relationship under design fire exposure (Eurocode 2005a, SFPE 2005). Fig. 1.3 shows time-temperature plots for a mild and severe design fire determined according to SFPE, and the current ASTM E-119 standard fire. The temperatures in the standard fire exposure increase throughout the fire duration as seen in Fig. 1.3. Both of the design fires however have temperatures that initially increase, which subsequently start to decay. This is because initially the fire is fueled by the contents of the compartment, and is supported by the ventilation (air) present in the compartment. As fire progresses, either the contents of the compartment are fully consumed, or the ventilation is insufficient to support combustion, and the fire dies down (often referred to as burnout). As such, while the temperatures in the initial part of a design fire may be more severe than the standard fire (as seen in Fig. 1.3), the decay phase of fire allows the structural elements to cool down and enhance the fire resistance. Under design fires, it is possible for structural elements to survive complete compartment burnout.

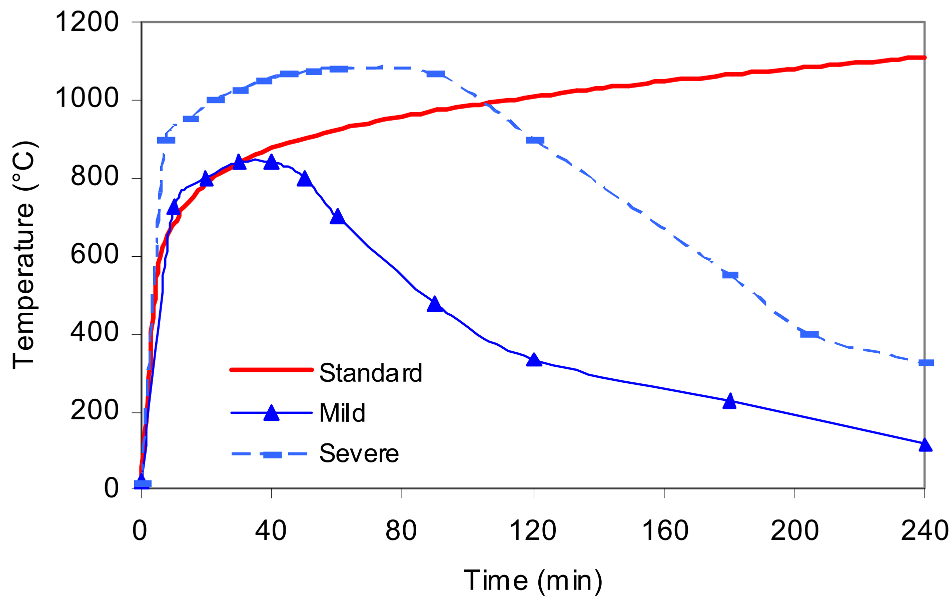

Fig. 1.3: Time-temperature relationships for different fire scenarios

In recent years, most high-rise buildings have been equipped with automatic fire suppression systems (sprinklers). The current method of assessing fire resistance through standard fire exposures makes no provision for the contribution of these suppression systems. The effect of sprinklers can be accounted for through modified time-temperature relationships. Given the ability of design fires to account for automatic suppression systems, and the actual characteristics of the compartment in which the structural member is located, it is necessary to consider design fires for realistic assessment of fire resistance.

In addition to fire exposure, a number of other factors also influence the fire performance of structural systems. These include restraint effects, redistribution of forces, member interactions, and steel-concrete composite action. Many of these effects can be accounted for in the fire resistance analysis by applying a system-level approach (rather than an element-level approach). Fig. 1.4 illustrates the conventional method of assessing fire resistance based on the response of single elements. Note that no consideration is given to the effect of the members surrounding the fire exposed element or the presence of composite construction. Also shown in Fig. 1.4 is the system-level approach wherein the effect of connectivity between members, composite action, realistic loads, realistic fires, and realistic failure criterion can be taken into consideration.

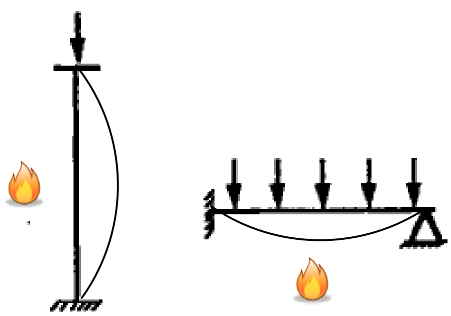

Conventional element approach

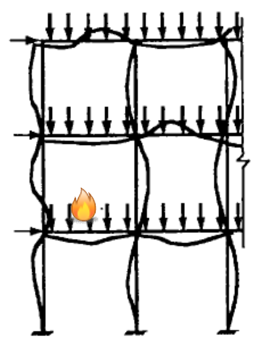

Improved system-level approach

Fig. 1.4: Conventional and improved structural configuration for evaluating fire resistance

By applying a system based approach, composite construction and member interactions in the structural system can be utilized, and in some cases, it may be possible to achieve the required fire resistance without the need for additional external fire insulation.

1.5 Research Objectives

Recently there is a growing recognition that fire resistance assessment should be based on overall structural behavior under realistic fire and loading scenarios. A number of studies have been undertaken in this direction. There is, however, no framework for fully utilizing the inherent fire resistance exhibited by steel structural systems. Specifically, the beneficial effects of composite action in beam-slab assemblies and in columns are overlooked. This research is aimed at developing a better understanding of the inherent fire resistance present in steel framed structures. The main objective is to develop methodologies for utilizing inherent fire resistance in steel structural systems. To accomplish this, the following specific research objectives were developed.

- Conduct a detailed state-of-the-art review on the fire response of steel and composite structures. This review will cover experimental and numerical work that has been done, high temperature material properties, and code provisions pertaining to the fire response of steel and composite structures.
- Conduct an experimental investigation to assess the beneficial effects of composite action in steel beam-concrete slab assemblies. For this, four test assemblies will be constructed, three with traditional lightweight concrete and one with SFRC concrete. The objective is to assess the relative response of the assemblies under fire exposure and to maximize the effect of tensile membrane action.
- Develop numerical models and conduct parametric studies to investigate the effect a variety of parameters have on the fire resistance of steel framed structures.
- Develop simplified design methodologies for evaluating the fire response of concrete-filled HSS columns and composite floor assemblies.

- Conduct a series of case studies to verify the feasibility of unprotected steel in framed buildings under realistic fire, restraint, composite action, and failure criterion.

1.6 Scope

This dissertation is organized into 8 chapters as follows:

- Chapter 1: Provides an introduction to fire resistance, fire performance, and fire design as it applies to steel and composite structures.
- Chapter 2: Reviews the state-of-the-art on the fire response of steel and composite structures at the element, assembly, and system level. Additionally, high temperature material properties and fire provisions in current codes and standards are also reviewed.
- Chapter 3: Presents the fire resistance experiment on four beam slab assemblies and the previous work on concrete filled HSS columns.
- Chapter 4: Addresses the need for a comprehensive computational program for parametric studies, and provides an overview of the computational program SAFIR. Following the overview of SAFIR, element, assembly, and system level models are validated against test data.
- Chapter 5: Presents the results (factors affecting fire resistance) from a series of parametric studies at the element, assembly, and system levels.
- Chapter 6: Overviews the development of simplified design methodologies based on the factors influencing fire resistance, and shows the methodologies to be effective through a series of numerical examples.
- Chapter 7: Presents an overview of performance-based design followed by a system-level case study to illustrate the use of the developed methodologies.
- Chapter 8: Summarizes conclusions and recommendations for future work.

CHAPTER 2

2 STATE-OF-THE-ART REVIEW

2.1 General

Since the 1990's there has been a growing recognition that the current approach of evaluating fire resistance based on standard fire tests has a number of drawbacks. Further, observations from a number of accidental fires pointed to the fact that steel structural systems possess higher inherent fire resistance under realistic fire, loading, and restraint scenarios. A number of experimental and numerical studies have been undertaken to demonstrate the inherent fire resistance present in steel structural systems. Many of these studies focused on illustrating enhanced fire resistance through system-level analysis of steel framed structural systems. A critical review of these studies is presented in this section. Based on the review, the knowledge gaps in the area relating to fire performance of composite steel framed structures are identified.

2.2 Fire Incidents

A review of accidental fire incidents in Europe, Australia, and North America, clearly indicate that steel framed structures exhibit higher fire resistance than typically observed in standard fire tests on singe structural elements. This section presents a summary of the most notable fire incidents. A comprehensive review of these fires is presented elsewhere (Wang and Kodur 2000, Nwosu and Kodur 1999)

- A fire broke out on the 12th story of the First Interstate Bank building in Los Angeles, California, late in the evening on May 4th 1988 and burned for over three hours. By the time it was extinguished, the fire had burned out almost five stories of the building. Over half a million gallons of water were used to extinguish the blaze (FEMA 1990). However, the building withstood complete compartment burnout of almost five stories without structural collapse, thus indicating that buildings in actual (real) fire incidents exhibit higher fire resistance than that based on standard fire tests on single elements. It should be noted that the structural elements in the building were designed to have a fire resistance between 1 and 3 hours.

- On the evening of June 3rd 1990, a major fire broke out in a construction contractors hut located on the first floor of the partly completed 14-story Broadgate building in London, UK. The building was equipped with sprinklers, but since the building was still under construction, the sprinklers were not operational after workers left for the day. Additionally, much of the structural fire protection was not yet applied to the building, thus, the unprotected steel framing was directly exposed to fire. The fire burned for a total of 4.5 hours with temperatures estimated to be in excess of 1000 °C for two of those hours. There was some contraction in columns and large deflections were observed in the beams, however, the structure did not collapse, thus reinforcing the hypothesis that steel framed structural systems possess higher fire resistance than individual elements tested in a furnace. The total damage to the building was £25 million, that associated with the repairs to the structural frame were approximately £2 million, and repairs took only 30 days to complete (Newman et al. 2006).
- In another incident, a major accidental fire started on the 22nd floor of the 38 story steel framed One Meridian Plaza building (Philadelphia, Pa) on the evening of Feb. 23rd, 1991. The structural elements were designed to have fire resistance ratings on the order

of 1-3 hours depending on the element. When fire fighters arrived, the fire was completely developed on the 22nd floor and was spreading to the 21st floor. Due to early loss of electrical power and failure of emergency generators, fire fighting efforts were seriously hindered. By the end, the fire had burned for 19 hours consuming 8 stories of the building. Again, despite the severity and duration of the fire, no structural collapse was observed, reinforcing that steel framed buildings possess higher fire resistance under realistic conditions (loading, fire, and restraint) than that exhibited by a single element tested in a standard test furnace. The total direct cost of fire was $100 million, litigation related to the reusability of the structure continued for years and cost more than the damage to the actual building (FEMA 1994).

The above real fire incidents clearly demonstrate that steel framed structural systems exhibit higher inherent fire resistance than that observed in standard fire resistance tests. The fire resistance of the overall structural frame can be much greater that that of individual structural members and depends on a number of parameters. Characteristics inherent to the structure such as composite construction and member interactions appreciably enhance fire resistance when considered under realistic fire exposure, loading and failure criterion. However, these beneficial effects are seldom considered in current design approaches due to the complexity of the analyses, and the lack of a well defined framework for fire resistance assessment.

In order to define this framework for fire resistance assessment, the following section presents the previous experimental and numerical studies on the response of steel composite structures under fire exposure. Subsequent sections present realistic factors to be considered in fire resistance assessment, fire correlation methodologies, and material properties for steel, concrete, and insulation respectively.

2.3 Previous Experimental and Numerical Studies

The above real fire incidents have stimulated researchers to develop an understanding of the overall response of steel framed structures exposed to fire. The objective of most of the studies was to illustrate the enhanced fire resistance achieved through two categories, namely, steel-concrete composite action and system-level structural response. A review of the research studies on composite construction (namely CFHSS columns and beam slab assemblies) under fire exposure is presented first, followed by the state-of-the-art with respect to system-level structural response of composite steel frames under fire exposure.

2.3.1 Composite Construction

As illustrated in Chapter 1, composite construction consisting of steel and concrete can significantly enhance the fire resistance of structural systems. This higher fire resistance is mainly derived from the good fire resistance properties of concrete as well as the high mass of concrete. The beneficial concrete properties include lower thermal conductivity, higher heat capacity, and slower degradation of strength and stiffness with temperature. Generally, the composite construction in steel framed buildings is in the form of composite columns or steel beam-concrete slab assemblies. Of these, concrete filled HSS columns offer numerous benefits (construction speed and economy) over other forms of composite columns and thus are widely used in low-rise buildings. Steel beam-concrete slab assemblies are commonly used due their efficiency as floor systems in steel framed buildings. These floor systems also have the added benefit of significantly enhancing fire resistance. A review of previous studies on the fire performance of composite construction (CFHSS columns and composite beam assemblies) is presented in the following sections.

CFHSS Columns

Alternate approaches for achieving fire resistance in columns have been studied for the last three decades. Methods such as filling HSS columns with water and concrete are among the most popular approaches studied by researchers (Kodur and Lie, 1995a, Bond, 1975, Klingsch and Wittnecker, 1988). However, the use of concrete-filling is the most attractive and feasible proposition developed thus far.

Fire resistance tests on CFHSS columns were predominantly carried out at the National Research Council of Canada (NRCC), a few organizations in Europe, and more recently in China. The experimental program at NRCC consisted of fire tests on about 80 full-scale CFHSS columns (Kodur and Lie, 1995a,b, Lie and Chabot 1992, Lie and Caron, 1988, Lie and Irwin, 1991). Both square and circular HSS columns were tested with three types of concrete filling, namely, plain (PC), bar reinforced (RC), and steel fiber reinforced (FC). The influence of various factors including type of concrete filling, concrete strength, type and intensity of loading, and column size were investigated under the ASTM E-119 (2007) standard fire exposure. The tests reported by European and Chinese studies (Klingsch and Wittbecker 1988, and Grandjean et al., 1981) are similar to NRCC tests, but the fire exposure was that of the ISO 834 (1975) standard fire; which has a time-temperature curve similar to that of ASTM E-119 (2007).

Data reported from NRCC tests and numerical studies can be used to illustrate the typical behavior, as well as beneficial effects, of concrete-filled HSS columns under standard fire conditions. Fig. 2.1a shows a schematic of a typical CFHSS columns, while Fig. 2.1b shows the axial deformation as a function of fire exposure time for three typical HSS columns filled with plain concrete (PC), steel fiber reinforced concrete (FC) and bar reinforced concrete (RC) respectively (Kodur and Lie, 1995b). The three columns were of similar size and were subjected to similar load levels, hence, the results presented in Fig. 2.1b can be used to illustrate the comparative behavior of the three types of concrete filling.

At ambient conditions, the applied load on a composite (CFHSS) column is carried by both the concrete and the steel. When the CFHSS column is exposed to fire, steel carries most of the load during the early stages of fire since the steel section expands more rapidly than the concrete core. As time progresses and temperatures increase, the steel section gradually yields due to loss of strength at elevated temperatures, and the expansion phase gives way to a contraction phase in about 20 minutes into fire exposure. At this stage, concrete starts to carry an increased portion of the load. As fire progresses, the strength of concrete also deteriorates to a level where the column strength is less than the applied load, and at this point failure of the column occurs. The elapsed time from ignition to failure is termed the fire resistance of the column.

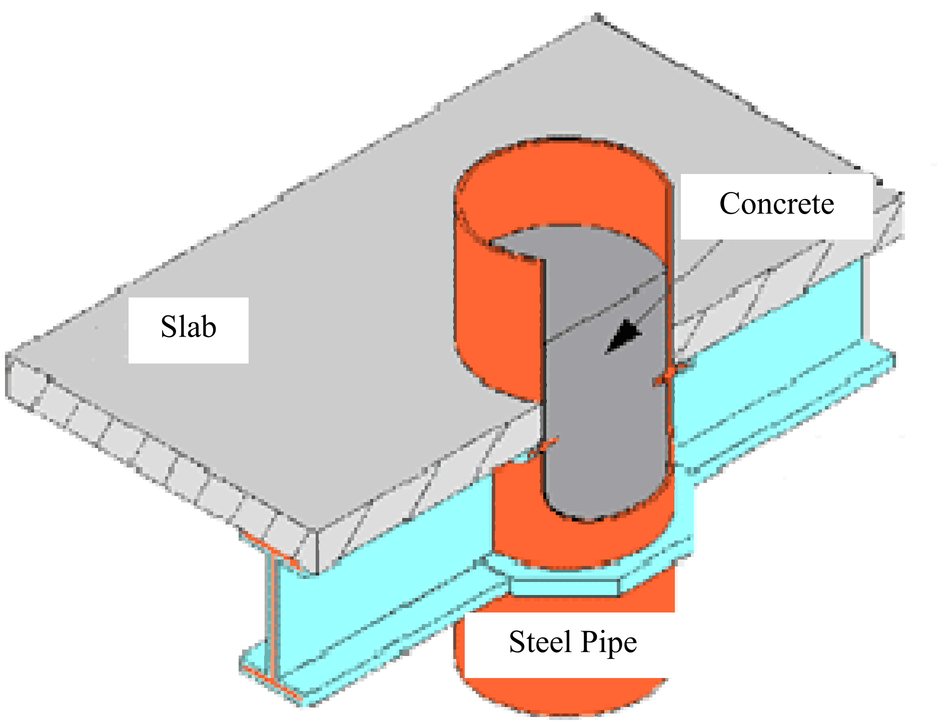

(a): Schematic of a typical CFHSS column

Fig. 2.1: Illustration of construction and fire behaviour of CFHSS columns under standard fire exposure

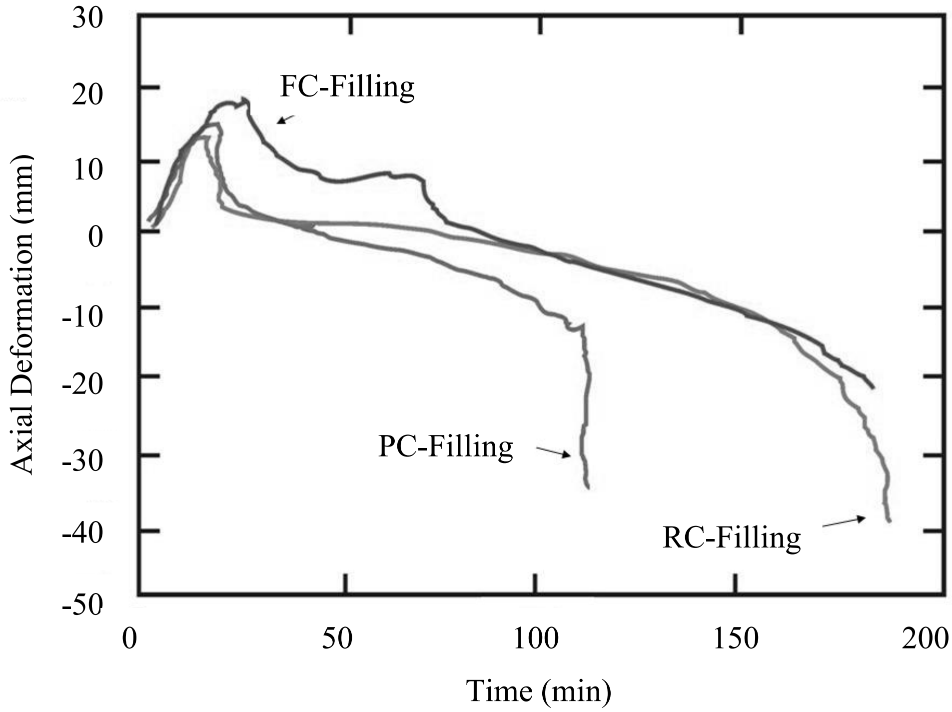

(b): Behaviour of a typical HSS column with different types of concrete filling

Fig. 2.1 (Continued): Illustration of construction and fire behaviour of CFHSS columns under standard fire exposure

Based on the experimental and numerical studies reported in literature (Kodur and Lie 1996, Kodur and Lie 1997, Lie and Stringer 1994), it was found that the parameters with the most influence on fire resistance of CFHSS columns are: type of concrete filling (plain, bar-reinforced, and fiber-reinforced), outside diameter or width of the column, applied load, effective length of the column, concrete strength, and type of aggregate. Using these influencing factors as the basis, the following unified design equation was developed to calculate the fire resistance of circular and square HSS columns filled with any of the three types of concrete (Lie and Stringer 1994, Kodur 1999, Kodur and MacKinnon 2000).

$$R = f\frac{(f_C^{'} + 20)}{(KL - 1000)} D^2 \sqrt{\frac{D}{C}} \qquad [2.1]$$

where: R = fire resistance in minutes, f'_c= specified 28-day concrete strength in MPa, D = outside diameter or width of the column in mm, C = applied load in kN, K = effective length factor, L = unsupported length of the column in mm, f = a parameter to account for the type of concrete filling (PC, RC, and FC), the type of aggregate used (carbonate or siliceous) in concrete, the percentage of reinforcement, the thickness of concrete cover, and the cross-sectional shape of the HSS column (circular or square), values of which can be found in reference (Kodur and Lie 1996).

The design equation and research presented above, though representing a significant advancement in the understanding of CFHSS columns exposed to fire, have a number of limitations. The most restrictive of these limitations are:

- No consideration was given to design (realistic) fire exposure
- Full range of length and cross sections, as encountered in real applications, were not investigated due to limitations in furnace dimensions
- System-level response of structural systems including 2^{nd} order effects was not considered due to complexities in the analysis

These limitations do not facilitate the use of CFHSS columns in applications such as airports, schools, atriums, and hotels, where exposed steel is highly desired. Thus, in order to utilize inherent fire resistance of steel framed structures (and realize unprotected steel), it is necessary to study the response of full-scale CFHSS columns exposed to realistic design scenarios in a system-level environment.

The fire test data, numerical models, and resulting design equation available in literature represent a considerable contribution to the understanding of the performance of CFHSS columns under fire exposure. While forming a good basis for comparison of column fire resistance, the exclusive use of standard fire exposure in the fire resistance assessment precludes determination of the actual failure time of a CFHSS column exposed to real fires. Standard fire exposure does not take into account the compartment characteristics such as ventilation or fuel supply, and thus presents a monotonically increasing time temperature relationship without a decay phase, thus representing an unrealistic and overly conservative fire condition. It is therefore necessary to develop an understanding on the response of CFHSS columns to design fire exposure, and to develop a simplified fire resistance design methodology for CFHSS columns.

Composite Beam-Slab Assemblies

Composite construction in the form of CFHSS columns has been shown to clearly enhance fire resistance over that of unprotected steel columns. In a similar fashion, composite floor systems have been shown to have a higher fire resistance than steel beams considered individually. The beneficial effect of composite floor systems was clearly seen in the Cardington tests (as discussed in the next section), as well as in the performance of various buildings under fire accidents. Following the Cardington tests, a number of researches have attempted to develop models to account for composite action in steel framed structures. Finite element packages that have been employed include ABAQUS (Gillie, et al. 2001a,b Gillie et al. 2002), VULCAN (Huang et al. 2000, Huang et al. 2001, Huang et al. 2003a,b), SAFIR (Moss and Clifton 2004) and ADAPTIC (Elghazouli and Izzuddin 2000, Elghazouli and Izzuddin 2001). In an effort to focus on the beneficial effects of composite floors, researchers have also conducted small-scale tests to simulate the behavior of concrete slabs under fire (Lim et al. 2004, Bailey et al. 2000).

Data from the reported tests can be used to illustrate the behavior of beam-slab assemblies exposed to fire (Kodur and Fike 2009). A typical detail of a composite steel beam-concrete slab assembly is show in Fig. 2.2a. The tensile membrane action observed in such an assembly under fire conditions is illustrated in Fig. 2.2b, where the response of the assembly is pictorially shown at various fire exposure times. Prior to fire exposure, the beam slab assembly resists bending wherein the steel beam takes predominantly tensile forces and the concrete takes compressive forces, (see the case of "T = 1" in Fig. 2.2b). Under fire exposure, the temperature of the steel beam gradually increases leading to loss of strength and stiffness. As the steel gets progressively weaker, the composite assembly begins to undergo large deflections (case of "T = 30" in Fig. 2.2b). This deterioration of strength/stiffness properties of steel and concrete continues with time and at about 64 minutes the slab has undergone large deflections and the steel beam is providing very little strength to the composite assembly. Due to the large deflections at this stage, the reinforcement within the concrete (shrinkage steel) if properly anchored, acts as a cable and transfers load through a mechanism called tensile membrane action (TMA). This serves to transfer the load from the fire weakened portion of a structure to the cooler surrounding parts as illustrated in Fig. 2.2b in the "T=64" row. The perimeter of the slab is in compression while tensile forces develop in the central heated region as illustrated in Fig. 2.2c. This load transfer mechanism delays the failure of the assembly and thus enhances the fire resistance of a composite beam slab assembly. Under design (realistic) fire conditions TMA can be quite beneficial, and might lead to the beam slab assembly surviving burnout conditions.

Following the Cardington test program, many researchers explored developing a full understanding of TMA under fire conditions. Bailey (Bailey et al. 2000) postulated that under fire exposure, the ribbed steel deck on the bottom of a concrete slab offered no structural contribution. This postulate was based on the observation that the ribbed steel deck rapidly achieved temperatures exceeding 900 °C in fire, thus causing the ribbed steel deck to have

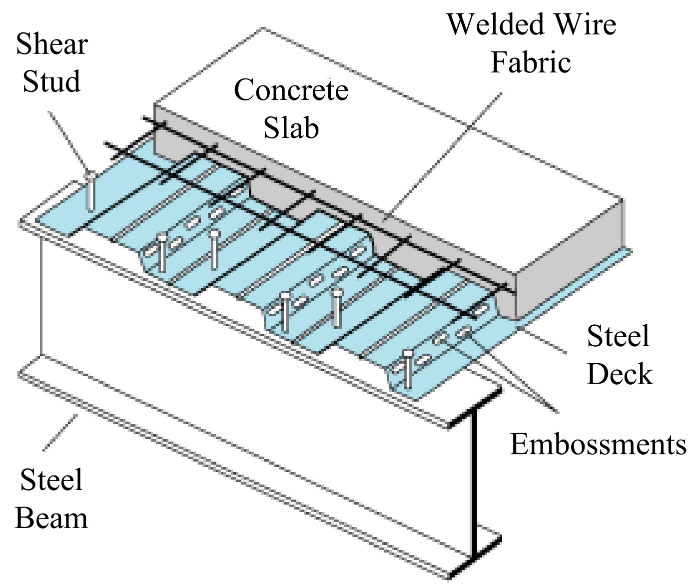

(a): Schematic of composite steel beam-concrete slab assembly

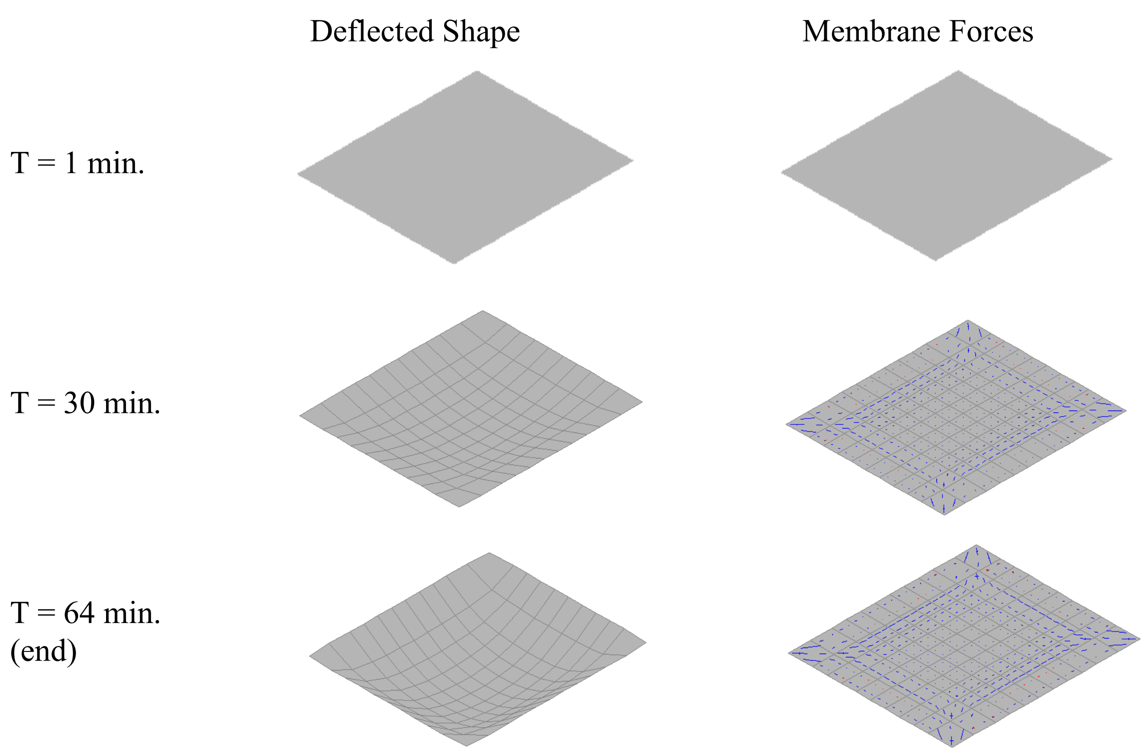

(b): Deflected shape and force distribution in the slab resulting from TMA

Fig. 2.2: Illustration of construction and tensile membrane action in a composite beam slab assembly

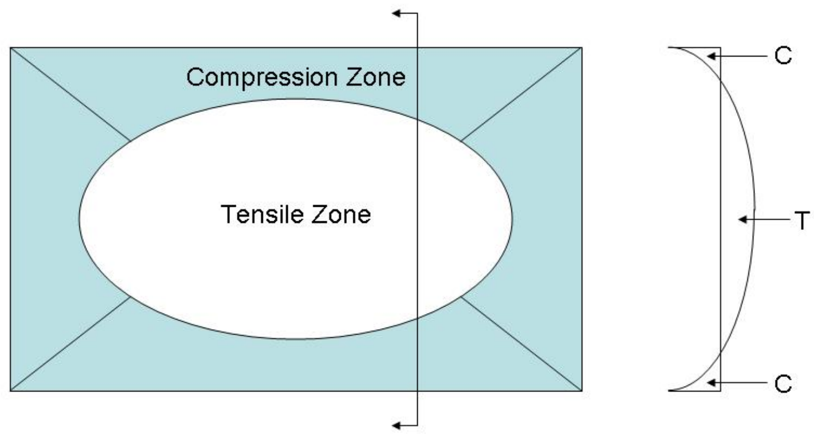

(c): Compressive and tensile zones in TMA

Fig. 2.2 (Continued): Illustration of construction and tensile membrane action in a composite beam slab assembly

minimal strength (Bailey et al. 2000). To further investigate the failure mechanism of the slab without the ribbed steel deck, Bailey et al. (2000) cast a concrete slab on a ribbed steel deck, then removed the deck from the bottom of the slab. This slab was then loaded to failure at ambient temperature to determine the probable failure patterns that might result under fire conditions. Based on these experimental studies, Bailey extended the work of Hayes (1968) and developed a simplified numerical approach to determine the load (moment) capacity of the slab under fire loading. Utilizing the results from Bailey's studies, the Building Research Establishment (BRE) in U.K. has developed guidelines and a simple calculation method to determine the load carrying capacity of slabs experiencing TMA during fire exposure. Implicit assumptions to the method developed by BRE are that the reinforcing mesh in the concrete floor slab is fractured over protected steel members, and that membrane action is based on a lower bound yield line pattern. Specifics of the methodology are given in references (Bailey and Moore 2000a,b).

Recently Zhang and Li (2008) proposed a calculation method based on first principles for estimating the load carrying capacity of slabs under fire conditions. In this approach, the slab was considered to consist of 5 zones: an elliptical center, and four rigid parts around the edge.

Through the use of moment equilibrium, a series of equations were developed to determine the ultimate load carrying capacity of the slab exposed to fire. The explicit assumptions in the method are that the slab is rectangular with an aspect ratio less than 2, the supporting beams below the slab are protected with insulation and are strong enough to support the load from the slab under fire conditions, the slab is vertically restrained around the perimeter with no horizontal restraint, and that the reinforcement in the slab is continuous and arranged in two orthogonal directions. Validation of this numerical method showed that there was good agreement between the predictions from this method and test data. (Zhang and Li 2008)

An experimental study on the ultimate failure of reinforced concrete slabs in fire was conducted by Cashell et al. (2008). In this study, the failure of a slab via rupture of the reinforcement was investigated. The tests were based on the assumption that the concrete floor slab behaves as a lightly reinforced beam under fire conditions. This is mainly due to the high temperatures attained in the ribbed metal deck under fire exposure. The quick rise in temperature is believed to eliminate the structural contribution of the ribbed metal deck, thus the concrete floor slab is postulated to act as a lightly reinforced concrete beam supported by the reinforcing steel in the slab. Preliminary analysis and modeling of the tested slabs has been used to show the correlation between specific parameters used in modeling and the ultimate deflection of the slab at failure. Based on these studies, and subsequent numerical simulations, the authors concluded that the stress-strain curves of steel, and bond slip characteristics between steel and concrete assumed in modeling, have a significant influence on fire resistance of concrete slabs as determined by computational models.

Lim et al. (2004) studied the response of slabs to fire through experimental and numerical studies. The fire experiments consisted of three reinforced concrete slabs of 3.3 by 4.3 meters and 90, 100, and 130 mm in thickness respectively. Data from these tests was then utilized to validate the shell element subroutine recently introduced in SAFIR (Talamona 2005). The validation process indicated that SAFIR is able to track the deflections and predict the locations of the tensile and compressive zones in the slab with good accuracy. The results from fire tests and the SAFIR analysis showed that the simply supported concrete slab contributes to the overall fire resistance of steel structures.

While the above studies offer considerable insight into the behavior and response of steel framed structures under fire exposure, there are still a considerable number of limitations to the state of the art. In Bailey's studies, the assumed ultimate defections (at failure) in this method are notably less than those observed in the Cardington tests, and do not take into account the beneficial beam-slab interactions. The method developed by Zhang and Li (2008) assumed that the perimeter beams were sufficiently large to support the increased loads from the deflecting slab, but additionally assumed that the slab had no horizontal restraint. This is unlikely to occur in reality that a beam will have high vertical restraint with little lateral restraint. In addition, this study only considered the standard fire exposure and omitted the effects of the beam-slab interactions. Tests conducted by Cashell et al. (2008) have two primary limitations, the assumption that two-way bending in a slab can be characterized as two orthogonal strips with a shared deflection point in the middle, and the fire exposure used in the fire test and numerical studies was the standard fire exposure.

The tests conducted by Wellman et al. (2010) offer considerable insight into the response of composite construction made with lightweight concrete under fire exposure. From these tests, it is observed that there is a benefit to composite construction, though lightweight concrete with shrinkage reinforcing does not provide sufficient strength to enhance the fire resistance of the assembly to the levels required in codes and standards. As such, from these tests it can be concluded that there is a clear need for the development of material systems that can enhance fire resistance though composite construction.

Additional information on the response of composite construction to fire exposure can be gained from the experimental and numerical studies which have been carried out on composite steel structures at the system level. A review of this work is presented in the following section.

2.3.2 System-Level Structural Response

Numerous fire resistance tests on isolated members or small assemblies have been conducted in the past 30 to 40 years, however, there have been only few tests on full-scale steel structures. There have been a total of eight significant experimental studies on full-scale structures exposed to fire since 1976 (Wald et. al), of these, three of them were conducted to assess non-structural aspects, (Pettersson 1976, Latham et al. 1987, and Thomas et al. 1992) while the remaining five were conducted to assess the structural response of the frame during fire exposure (Witteveen et al. 1977, Rubert and Schaumann 1986, Cooke and Latham 1987, Genes 1982, and British Steel 1998). Due to the current research interest in specifically the structural response under fire exposure, no information on the non-structural tests will be presented here, for those details the interested reader is directed to the literature (Pettersson 1976, Latham et al. 1987, and Thomas et al. 1992).

The first tests to consider the structural response of structures under fire exposure were conducted by Witteveen et al. (1977). In these testes, the stability of both braced and un-braced frames were assessed under fire exposure. It was found that the temperature distribution achieved in columns in standard fire tests as stipulated in ASTM E-119 are not realistic. In these tests, columns are place in a furnace where the ends are not exposed to fire, and hence, experience much cooler temperatures. This adds stability to the column and causes much higher failure temperatures to be observed than would be if the entire column were exposed to fire. It was determined that failure temperatures could be over predicted by as much as 100 °C in the standard fire resistance test.

To assess the failure temperature of steel frames, Rubert and Schaumann (1986) constructed a series of three quarter scale steel frames, loaded them, and exposed them to elevated temperatures using electric heaters. One of the primary observations from these tests is that due to the heating of only the steel frame, it was necessary to provide considerable restraint against torsional failure. The only appreciable data reported from these test was the failure temperatures, no information was provided on either strains or displacements. These testes serve as the benchmark used to check many finite element models.

Cooke and Latham (1987) tested a steel frame consisting of two columns and a steel beam under fire exposure. The connections between the steel beam and the column were made with shear tab connections. Atop the steel beam, a concrete slab was cast on a composite steel deck. To avoid any contribution from composite action, a ceramic blanket was placed between the beam and the slab to isolate the behavior of the beam. The fire exposure was provided by the combustion of wood cribs beneath the assembly. Despite the provision of shear connections, significant hogging moments developed in the beam due to the fire exposure. It was however observed that the unprotected steel beam withstood the effect of fire for an ASTM E-119 equivalency of 32 minutes, significantly more than observed in single element tests.

To assess the ability of lightly protected steel beams to resist fire exposure without a loss of stability, Genes (1982) tested two stories of a larger 28 story building under fire exposure. It was observed that indeed the lightly protected members can provide some level of fire resistance without loss of structural stability though little additional information is available regarding the tests.

The most notable experimental studies on the fire response of full-scale steel framed buildings were conducted by the Building Research Establishment in the U.K. in collaboration with British Steel (British Steel 1998). For these studies, an eight story steel frame building was constructed within an aircraft hanger located in Cardington, U.K. This building was designed in accordance with BS 5950 (British Steel 1998) and represented a typical office building as constructed in London. Eight fire tests were conducted in the building and a detailed description of each of these tests is provided in the testing report published by British Steel (1998). A brief summary of the most relevant tests to the current research is presented below.

Four of these fire tests have direct implications to the research here presented, namely the "restrained beam" test, "plane frame" test, "corner" test, and "demonstration" test. The first two tests focused on a specific feature of the structure, (a restrained beam and plane frame respectively) and the behavior of that member when exposed to standard fire as provided by a furnace. The latter two fire tests simulated realistic fire exposure in a compartment of a steel famed building fueled by the combustion of compartment contents.

Since the objective of these fire tests was to exploit the inherent fire resistance of a steel framed building, all of the structural members, with the exception of columns, were left unprotected. In the plane frame test, the columns were only insulated up to about 300 mm below the connection. This un-insulated portion of the column became too hot during the fire test and underwent local failure (buckling with significant deformation), though no global failure occurred as can be seen in Fig. 2.3a. From this observation, it was concluded that in the rest of the tests, the columns were to be protected over their entire length.

The duration of the fire exposures simulated in the fire tests was dependent on the fuel source. Fires lasting 2.5 to 3 hours were simulated when furnaces were used. When combustion of compartment contents fueled the fires, they were allowed to reach burnout conditions in the fire compartment. In all of the tests, significant deflections in the beams were observed. Despite the large deflections that occurred in all of the fires, no global failure (full collapse) occurred (British Steel 1998) as seen in Fig. 2.3, all figures from Cardington tests are reprinted with permission as indicated in Appendix A.

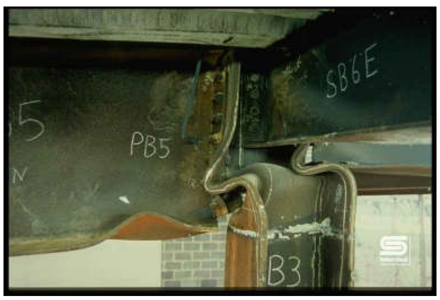

a) Column contraction in plane frame test

b) End buckling of beam in corner test

c) Large beam deflection observed during demonstration test

d) Connection deformation resulting from restrained beam test

Fig. 2.3: Post fire pictures from the Cardington tests

The primary observation from these tests was that the composite steel beam concrete slab assemblies demonstrated considerable fire resistance though none of the beams were protected. It was postulated that this was in large part due to the contribution of the steel beam-concrete slab interactions and the development of tensile membrane action (TMA) (Bailey and Moore 2000a,b). Also, due to the local failure observed in unprotected columns in the plane frame test, the importance of protecting columns for overall structural stability during fire exposure was highlighted.

Following the experiments conducted at Cardington, several researchers focused their attention on system-level response of steel structural systems through numerical simulations. Initially, this research was primarily conducted in Europe, and focused on the response of steel framed structures representing typical European construction practices (Gillie et al. 2001a,b, Lamont and Lane 2006, Cameron 2003). While this work has aided in understanding the failure mechanisms of steel framed buildings exposed to fire, the use of primarily European construction practices necessitates similar, independent, investigations utilizing North American construction practices.

Following the collapse of the World Trade Center buildings, researches have accelerated efforts to develop an understanding on the fire resistance of steel framed structures. Several research programs have been undertaken to better understand the response of steel framed structures exposed to fire (Lew et al. 2005, Usmani 2005, Usmani et al. 2003, Flint et al. 2006, Duthinh 2004, and Flint et al 2007). Though providing considerable insight to the behavior of steel framed buildings exposed to fire, these studies do not fully account for all of the factors that contribute to inherent fire resistance making it necessary to conduct additional studies. The significant findings from these research programs are highlighted below:

- Full-scale structures demonstrate higher fire resistance than indicated in standard (element-level) fire tests
- Structural systems perform better under real fires than standard fires, and survive burnout conditions under most design (real) fires situations

- Composite construction, specifically steel beam-concrete slab assemblies, significantly enhances the fire resistance of the entire assembly
- Steel columns are critical to structural stability of the building and must be provided with fire protection to maintain structural integrity during fire exposure.

In addition to the explicit findings from the experiential studies presented in this and the previous section, these studies can be used to identify the realistic factors that need to be taken into consideration for a holistic fire resistance assessment. These factors are discussed in the following section.

2.4 Realistic Design Parameters

In addition to composite action, a few other factors influence the fire resistance of steel framed structural systems. The prominent factors include fire scenario, load level, and the limit state used to evaluate failure. These parameters, as elaborated upon below, are to be properly accounted for when evaluating the inherent fire resistance in steel framed structures.

- The current practice of evaluating fire resistance of structural members is based mainly on standard fire tests or empirical calculation methods, in which the member is exposed to a standard fire as specified in standards such as ASTM E-119 (ASTM 2007) or ISO 834 (ISO 1975). In the standard fire exposure, the fire size is the same (irrespective of compartment characteristics), and fire temperatures increases with time throughout the fire duration with no decay phase. However, in realistic fire exposure, the resulting fire size is a function of compartment characteristics, such as ventilation, fuel load, compartment size, and lining materials, and there is always a decay phase following the initial growth phase. As the temperatures in the structural member decrease in the decay phase of the fire, the materials recover part of their strength and stiffness. This recovery of material strength and stiffness helps to withstand the applied loads on the member and might be sufficient to overcome the destructive effect of fire.

- Load level has a significant influence on the fire resistance of structures. The lower the load, higher is the fire resistance of a structural member. In prescriptive based methodologies, fire resistance is often evaluated based on the maximum design load on a structural member. In recent years there is a growing recognition that the level of loading in a building under fire conditions is less than the full service loads. A load level of 1.2DL + 0.5LL is the recommendation of ASCE 7 (ASCE 2005) while Eurocode recommends using 1.2DL + 0.4LL (Eurocode 2002). Adoption of realistic load levels will enable realization of inherent fire resistance in structural members.
- In fire resistance evaluation, the limit state applied to determine failure has a significant influence on the resulting fire resistance of the structural member. The different criterion that can be applied to define failure include thermal (barrier), strength (stability), and integrity limit states. In the current prescriptive based approaches, fire resistance is often evaluated based on critical temperature attained in the steel. Failure is said to occur when the critical temperature reaches 538 °C in columns and 593 °C in beams. The rational for this criterion is that steel looses 50% of its room temperature strength at about 550 °C, thus, the structural member has 50% of its load capacity remaining. Since service load levels under fire conditions correspond to about 50% of the ultimate load, failure is assumed to occur when the steel member reaches 538 °C in columns and 593 °C in beams (ASTM 2007). While this definition of failure based on critical temperature is simple and convenient in application since only temperature measurements (predictions) are required in tests (or analysis), it does not represent

realistic failure of a structural member which is a function of load level, restraint, and other factors. While this aspect has been partially recognized in Eurocode (Eurocode 2005b), fire resistance in North American standards continue to be based on critical temperature in the steel. For realistic assessment of failure, actual strength and deflection limit states are to be used. This aspect is especially critical in the case of composite construction (beam-slab assemblies and composite columns) where the concrete can continue to carry the load well after the steel reaches a predefined critical temperature. Thus, realistic failure limit states such as strength or deflection criterion should be applied to realize the inherent fire resistance of a structural member.

- Other factors that have a minor to moderate effect on the fire resistance of composite structural systems include concrete strength, aggregate type in concrete, concrete cover thickness (to reinforcement), restraint etc. Giving due consideration to these factors will enable realization of inherent fire resistance in composite structural systems.

2.5 Fire Resistance Evaluation Methods

Fire exposure has been clearly shown to have an influence on the fire resistance of a structure, there are however an infinite number of fire exposures possible in a given compartment. To avoid conducting fire resistance experiments under a wide range of fire exposures, several simplified approaches for establishing equivalent fire resistance based on the ASTM E-119 fire exposure have been developed. A review of these methods and their applicability to composite construction is presented in the following sections.

2.5.1 Equal Area Concept

The equal area concept, as the name implies, establishes fire resistance equivalency using the principle of equivalent fire exposure wherein the area under the standard (ASTM E-119 or ISO

834) time temperature curve is compared to the area under the design fire time temperature curve. In this method, the area under the design fire time temperature curve at the time the structural member fails is determined (area A1 in Fig. 2.4) (Buchanan 2005). Then, the area under the standard fire curve is estimated at different time steps. The time at which the area under the standard fire curve is equal to that under the design fire curve (at the time of structural member failure) is the equivalent fire resistance of the member under standard fire exposure (area A2 in Fig. 2.4). This approach has been validated for steel structural members and reasonable agreement between predicted and measured values has been observed (Buchanan 2005). However, the main limitation of the method is that it is not applicable for design fires that are either very hot and short, or cold and long as compared to the standard fire (Buchanan 2005). Thus, the method does not accurately correlate the fire resistance time due to the reliance on the area under the time-temperature curve. Additionally, the equal area concept has not been validated for use on composite structural members.

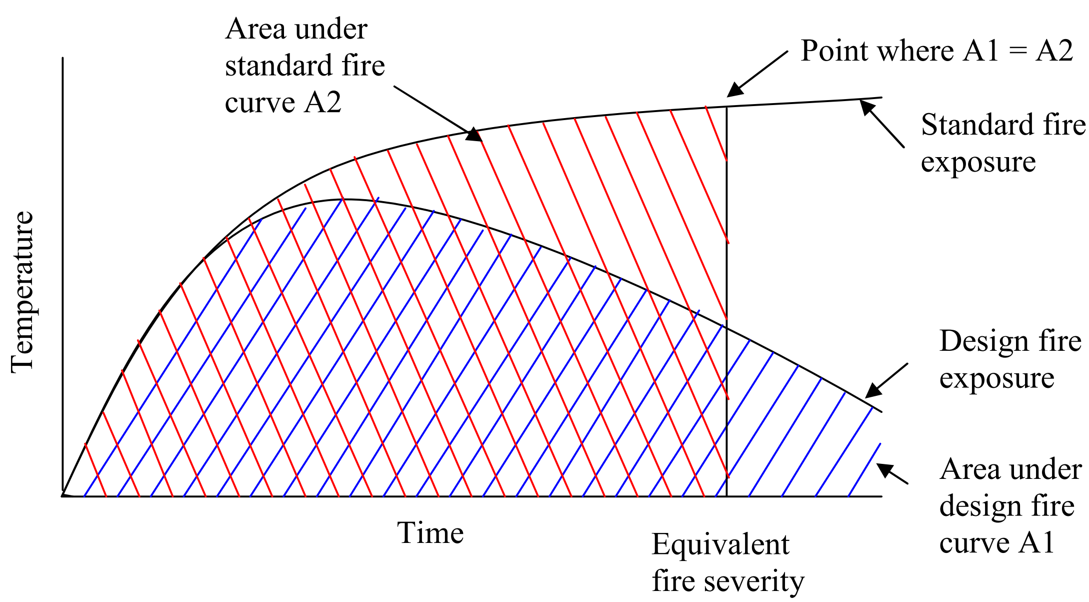

Fig. 2.4: Illustration of equal area concept for equivalent fire severity

2.5.2 Maximum Temperature Concept

This method was developed based on the assumption that steel structural members fail when steel reaches a critical temperature. For steel members the critical temperature is often taken as 550 °C. To use this method, the maximum steel temperature achieved under a given design fire is determined as shown in Fig. 2.5. The time it takes under standard fire exposure to reach the maximum temperature observed under the design fire is the equivalent ASTM E-119 fire severity as illustrated in Fig. 2.5. The limitation to this method is that when the temperatures reached in the design fire are well above or below those that would cause failure in the section, the method is not as accurate. Also, this method cannot be directly applied to composite members, since a limiting temperature in steel does not necessarily indicate failure of the member due to the composite action between the steel and the concrete.

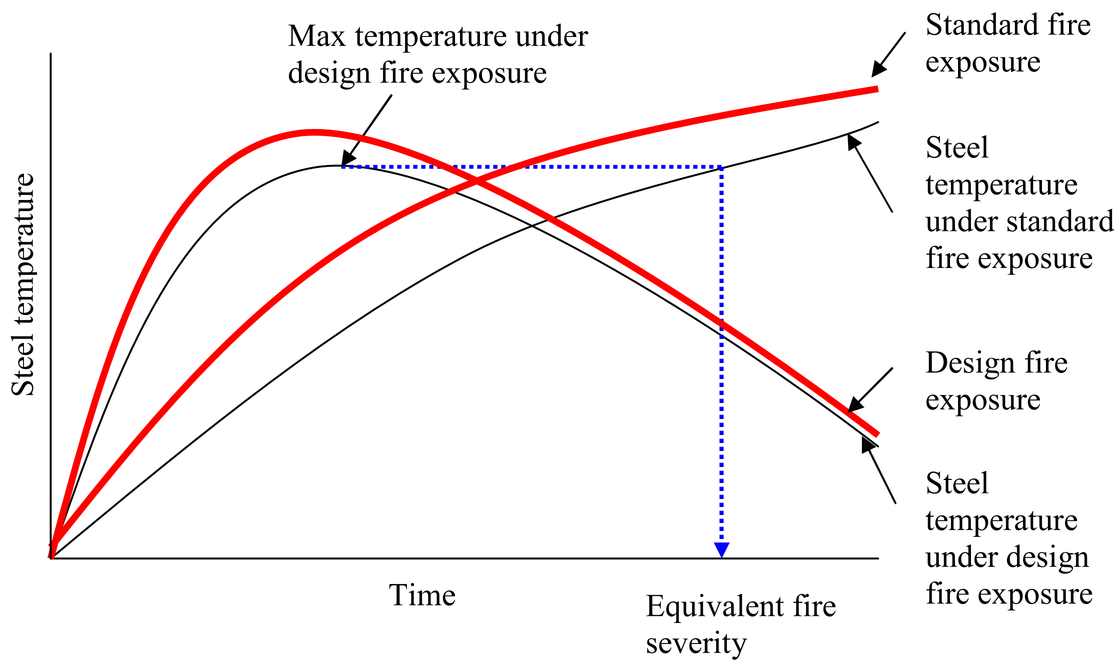

Fig. 2.5: Illustration of maximum temperature concept for equivalent fire severity

2.5.3 Minimum Load Capacity Concept

This approach utilizes a strength failure limit state to establish equivalency between a standard and a design fire exposure. Similar to the maximum temperature concept, the minimum load capacity concept compares the time that it takes to reach a certain load capacity of the section under the two fires. The minimum load capacity of the section under the design fire is determined as shown in Fig. 2.6. The load capacity under the standard fire exposure is then determined as shown in Fig. 2.6. The point where the load capacity of the member under the standard fire is the same as that under design fire exposure is the equivalent fire severity as illustrated in Fig. 2.6. The limitation to this method is the assumption that load level is about 50% of the room temperature capacity of the member, and it does not take into account the actual load level on the structural member. Further, the method cannot fully account for the effect of composite action.

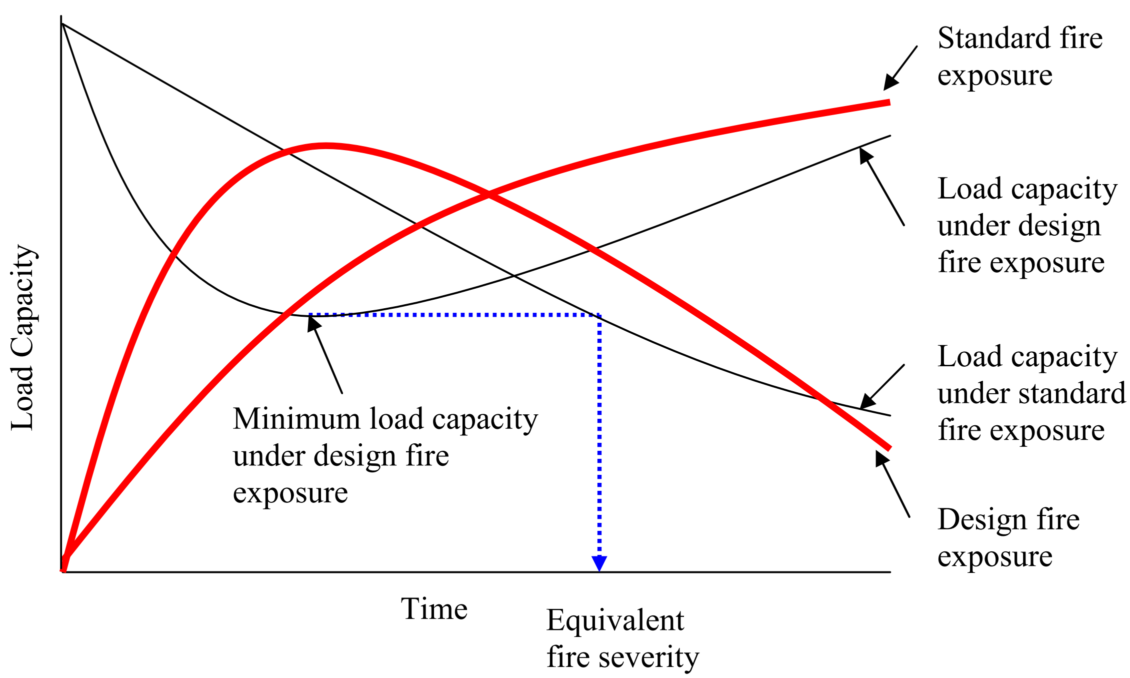

Fig. 2.6: Illustration of minimum load capacity concept for equivalent fire severity

2.5.4 Time-Equivalent Formula

In addition to the above approaches, several empirical relationships such as the CIB and Law formulae have been proposed to establish equivalency between standard and design fire exposures (Buchanan 2005). Globally, these methods were developed for protected steel sections. As such, these empirical formulae available in literature are incapable of capturing the effect of composite construction.

2.5.5 Summary

Due to the need to assess fire resistance under a wide range of fire exposures, several methods to do so based on standard fire resistance have been developed as presented in the previous sections. These methods were developed based on single element tests and do not take into consideration the effect of composite construction. The insulating functionality, capacitive protection, and load carry capacity of the concrete in composite construction are not taken into consideration in these approaches. As such, these methods are not suitable for use with composite construction, thus, there is a considerable need for development of methods that can be used to assess the fire resistance of composite members under realistic fire conditions.

2.6 High-Temperature Material Properties

The response of steel and composite structures is highly dependent on the material models used for the constituent materials. There are three basic categories of high temperature material properties that contribute to the response of composite structures, they are: (a) thermal (b) mechanical and (c) deformation properties. Thermal properties determine the temperature profile in the steel and concrete sections resulting from fire exposure, while the mechanical properties govern the loss of strength and stiffness as a function of temperature. Deformation properties determine the extent of deformations of the structural member under fire conditions.

For evaluating realistic fire performance of steel or composite structures, due consideration should be given to thermal, mechanical, and deformation properties. These properties vary with temperature and are influenced by the phase changes that occur in steel or concrete at elevated temperatures. A review of the available constitutive models for high temperature properties of steel and concrete are presented in the following sections, and the equations presented in both Eurocode (2004, 2005a) and ASCE (1992) provided in Appendix B.

2.6.1 Thermal Properties – Steel

The main thermal properties that influence the temperature rise in steel are thermal conductivity and specific heat (often expressed in terms of heat capacity). There is limited test data on the specific heat and thermal conductivity of steel. Figs. 2.7 and 2.8 show plots of the available data on thermal conductivity and specific heat of steel as a function of temperature respectively. Relationships from codes and standards (Eurocode (EC3) 2005a, ASCE 1992), as well as published test data, were used to compile Figs. 2.7 and 2.8 (Rempe and Knudson 2008, Dale et. al 2007, Touloukian 1972, Powel and Tye 1960, and Yawata 1969).

It can be seen from Fig. 2.7 that thermal conductivity decrease with temperature in an almost linear fashion, and there is little variation between the models presented in ASCE manual and Eurocode. On the contrary, published specific heat models vary considerably above 700 °C, as is seen in Fig. 2.8. In general, the specific heat of steel increases with an increase in temperature with a large spike occurring around 750 °C. The increase in specific heat with temperature is due to individual atoms in steel moving farther apart, thus achieving a higher energy state. The spike in the specific heat at around 750 °C is due to the phase change that occurs in steel in which the

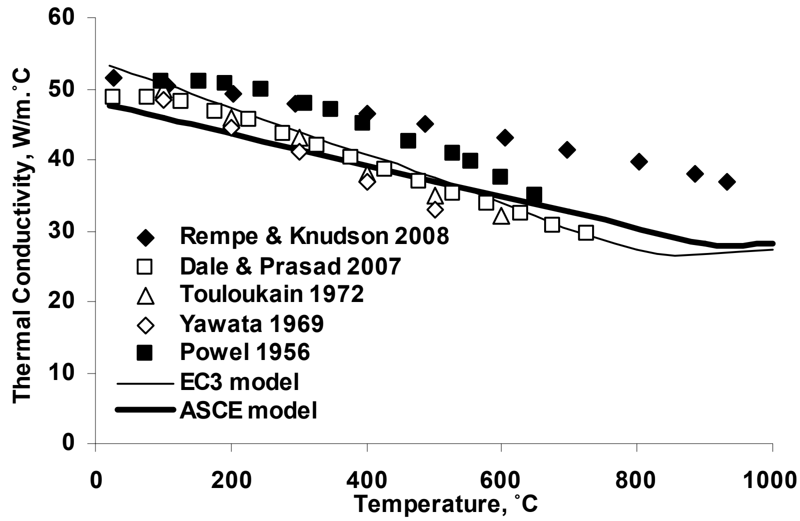

Fig. 2.7: Thermal conductivity of steel as predicted by different models and as measured in different test programs

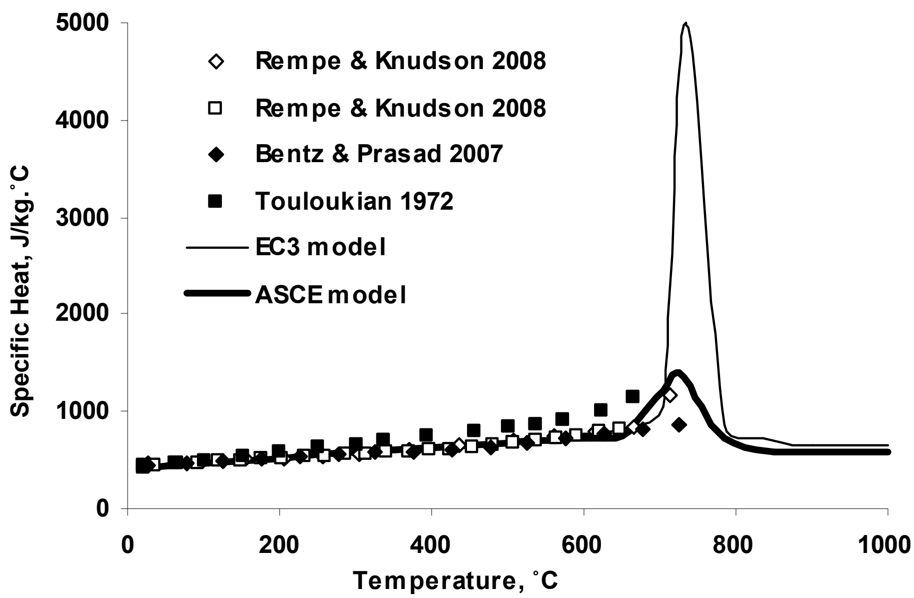

Fig. 2.8: Specific heat of steel as predicted by different models and as measured in different tests

atoms transition from a face centered cubic “FCC” to a body centered cubic “BCC” structure. This process absorbs considerable energy (heat), thus accounting for the spike around 750 °C seen in Fig. 2.8. The variation between the test data and the models shown in Fig. 2.8 is partly due to the fact that the majority of the existing data on specific heat originates from studies carried out on iron and non-structural steel alloys. Additionally, the maximum temperature reached in these studies of iron and non-structural steel was below 750 °C, thus not capturing the full range of temperatures observed in fire conditions.

2.6.2 Thermal Properties – Concrete

As is the case with steel, the thermal properties that have a significant effect on the response of concrete to fire exposure are thermal conductivity and specific heat. Thermal conductivity of concrete as a function of temperature is shown in Fig. 2.9 below. Due to the natural variability of concrete resulting from the use of unprocessed naturally occurring materials, the thermal conductivity of concrete is given as a range rather than a specific value. This range is applicable to both siliceous and carbonate based concrete. From Fig. 2.9, it can be seen that the thermal conductivity of concrete is between 1.4 and 2 W/mK at 20 °C and decreases to 0.75 W/mK at 800 °C.

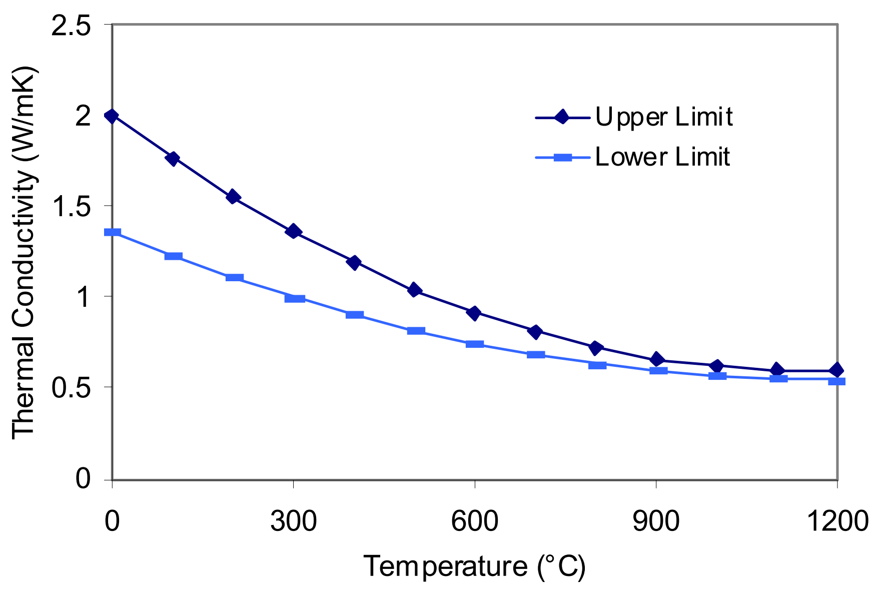

Fig. 2.9: Thermal conductivity of concrete as a function of temperature

Specific heat of concrete as a function of temperature is plotted in Fig. 2.10 according to both ASCE (1992) and Eurocode (2004) procedures. Of note is the large spike in specific heat for carbonate aggregate concrete as specified in ASCE (1992). This is attributed to the endothermic dissociation of dolomite within the carbonate aggregate, not present for siliceous aggregate. This spike is however neglected in the Eurocode (2004) (Fig. 2.10) and the same specific heat model employed for both siliceous and carbonate aggregate concrete.

2.6.3 Mechanical Properties – Steel

A review of the literature indicates that there have been more studies on the high-temperature mechanical properties of steel than on thermal properties. Tests on the high temperatures strength properties are conducted in two main ways: transient- and steady-state tests. In transient-state tests, the test specimen is subjected to a constant load and then exposed to uniformly increasing temperature. Temperature and strain are recorded continuously under constant stress. Thermal strain (evaluated from a separate test) is subtracted from the total measured strain (Outinen 2007). In the transient-state tests, the heating rate has a great influence on the strain rate, and thus different heating rates produce different strain rates. Heating rate of steel under fire conditions depends on the nature of the fire as well as on insulation and steel section properties. Generally, for a typical beam with 2 hour fire rated protection, the heating rate of steel can vary between 3-7 °C/min. However, for unprotected steel sections, the heating rate can vary between 25-40 °C/min. In the literature, (Outinen 2007) the reported transient mechanical property tests were conducted at heating rates ranging between 10 to 50 °C/min. This heating rate can be suitable for unprotected steel members, but not for protected members with slow heating rates.

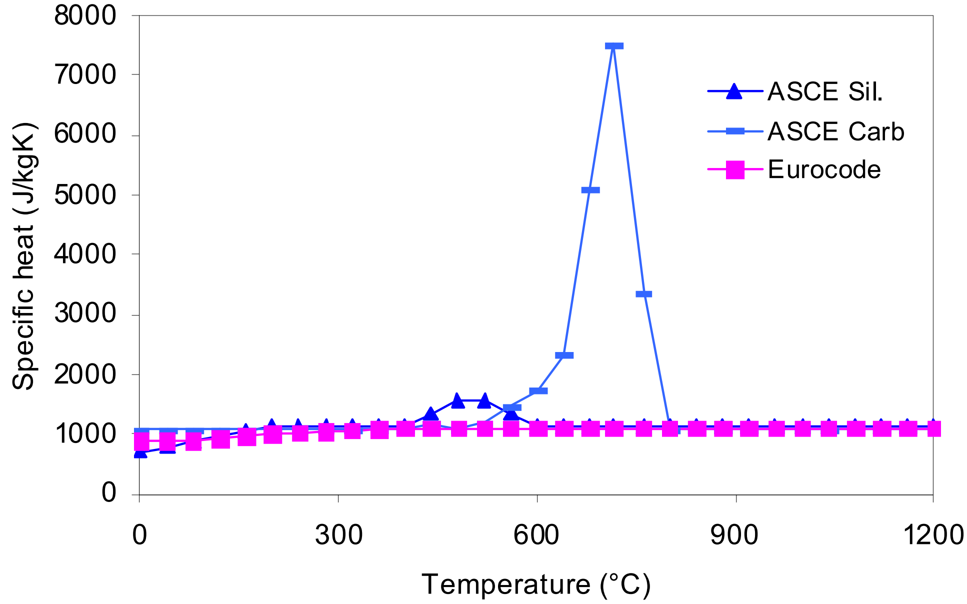

Fig. 2.10: Specific heat of concrete as a function of temperature

On the other hand, the steady-state tests are generally faster and easier to conduct than the transient-state tests. In the steady-state tests, the test specimen is heated to a specific temperature and after that a tensile test is carried out. Stress and strain values are recorded continuously under constant temperature. The test can be either load-controlled (loading rate is constant) or strain-controlled (strain rate is constant) (Outinen 2007, Anderberg 1988). Despite the fact that strain rate has a significant effect on the test results, a large amount of test data on conventional steel is published without the information on strain rates. Therefore, test standards are still concerned with defining limits for strain rates in tests (Outinen 2007, Anderberg 1988, and Cooke 1988).

These variations in test methods resulted in variations in the reported mechanical properties, which in turn resulted in variations in the constitutive models specified in codes and standards. The following sections present comparative study of these variations.

As mentioned earlier, different test regimes were used to obtain yield strength and elastic modulus of steel at elevated temperatures. The variations in test parameters resulted in different test measurements, thereby leading to differences in constitutive relationships presented in different codes and standards. Generally, tensile strength tests are conducted to obtain elastic modulus and yield strength of steel. There is lack of experiments on the modulus of steel under compression. This is because in tensile strength tests, complications that may arise due to geometric instabilities and confinement of specimen are eliminated. However, it is generally assumed that the modulus of elasticity for steel, derived based on tensile strength tests, is the same for compression state.

Figs. 2.11 and 2.12 show the yield strength and modulus of elasticity of steel as a function of temperature respectively. The test data plotted in the figures are compiled from various high temperature property tests as shown on the figures. Both the yield strength and elastic modulus decrease as temperature increases. This decrease can be attributed to the nucleus of the iron atoms in steel moving farther apart due to rising temperature in steel, leading to decreased bond strength, which in turn reduces the yield strength and elastic modulus.

It can be seen in the figures that there is significant variation in test data on yield strength and modulus of elasticity at temperatures above 300˚C. This variation can be attributed to many factors, primarily variable heating and strain/load rates during the test. For example, when the heating rate of the stressed specimen is small, the specimen will be subjected to stress at elevated temperatures for longer time duration, therefore, other factors, such as high-temperature creep (time-dependent plastic strain under constant stress and temperature), can influence the resulting temperature-stress-strain curves of the tested specimen. The yield strength and elastic modulus constitutive relationships from ASCE manual, Eurocode, and those proposed by Poh (2001) are also shown in Figs. 2.11 and 2.12 respectively.

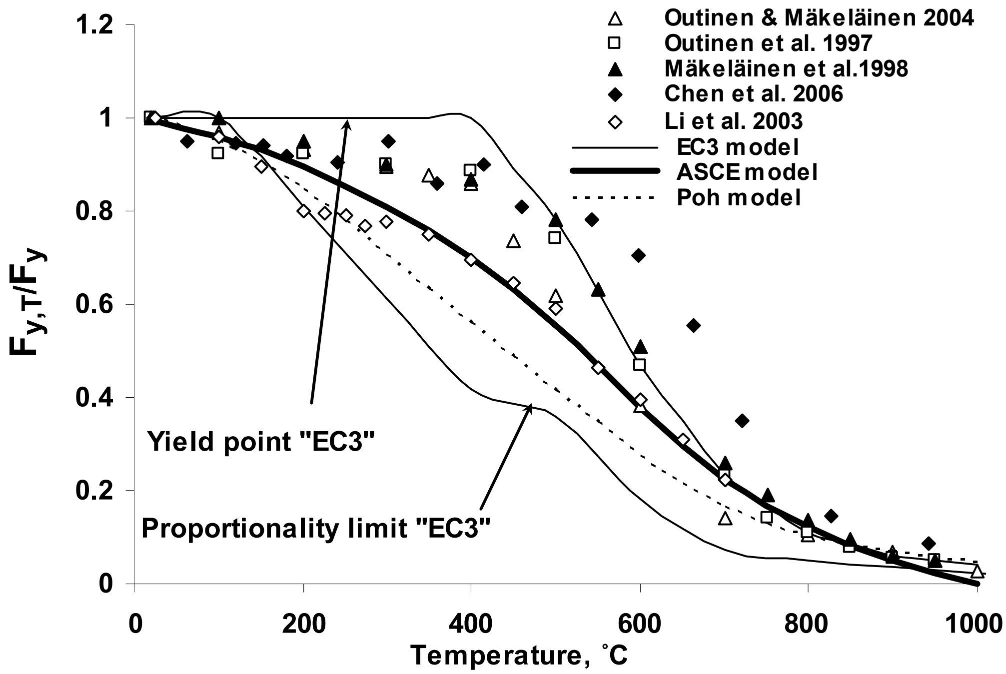

Fig. 2.11: Yield strength of steel as predicted by different models and as measured in different tests

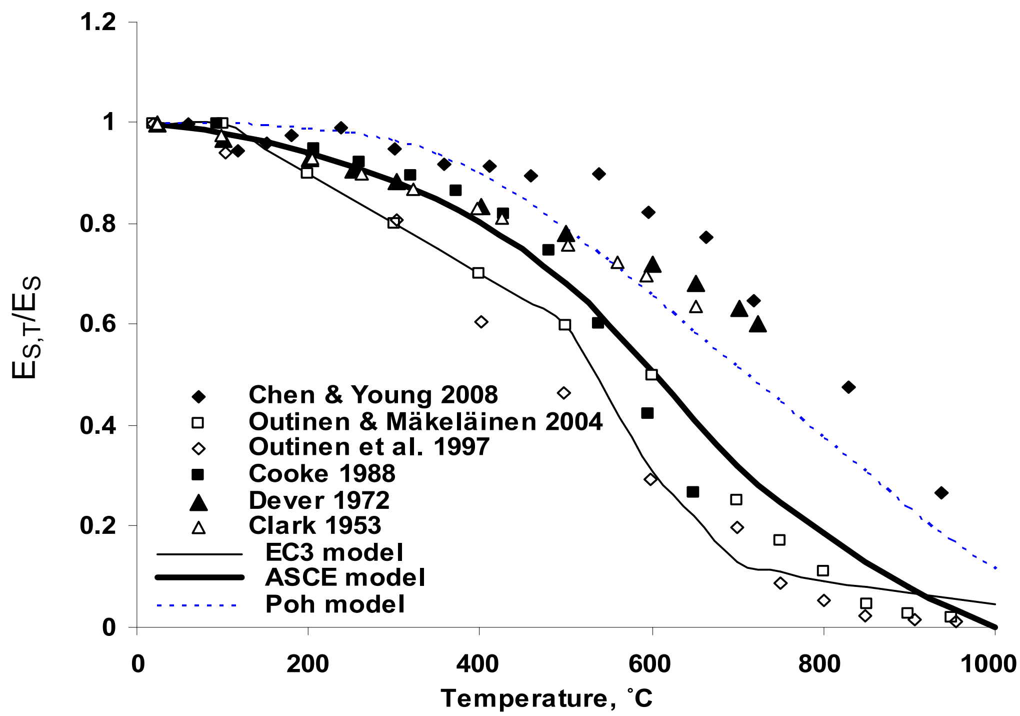

Fig. 2.12: Elastic modulus of steel as predicted by different models and as measured in different tests

As is the case with test data, there is also a considerable variation in the constitutive models for yield strength and modulus of elasticity. These variations in constitutive models are due to the large variation in the test data used to compile the respective constitutive models. A review of the models shows that the Eurocode model predicts less reduction in yield strength of steel with temperature as compared to the ASCE or Poh models (Kodur et al. 2010). However, the Eurocode model provides a higher reduction in elastic modulus of steel with temperature as compared to the ASCE and Poh models as shown in Fig. 2.12. Also, the Eurocode model assumes no reduction in steel yield strength up to 400˚C, while ASCE and Poh models assume a loss of 30% and 40%, respectively, at 400˚C, as shown in Fig. 2.11.

Fig. 2.11 also shows that the Eurocode distinguishes between two limits: the proportionality limit, and the yield limit. The proportionality limit in the Eurocode is the end of the linear portion of the stress-strain curve, after which point the stress-strain relation remains elastic but becomes nonlinear. The yield limit in Eurocode is the point after which the stress-strain becomes both nonlinear and inelastic. This feature of the stress-strain does not exist in either ASCE or Poh models which both assume a sharp point as a limit between linear-elastic and inelastic material response. The theory behind introducing proportionality limit in the Eurocode stress-strain curves (at high temperatures) is to capture visco-elastic behavior that is partly due to creep effect. The nonlinearity after the proportionality limit indicates that stress causes further strain after this point than in the linear elastic range. This simplification enables the stress-strain curves of the Eurocode to partly account for high temperature creep strain at elevated temperature.

Figs. 2.13a and 2.13b show the temperature-stress-strain curves from Eurocode 3, ASCE manual, and as proposed by Poh (2001) at room temperature and at 600˚C, respectively. The y-axis represents normalized stress and the x-axis represents normalized strain.

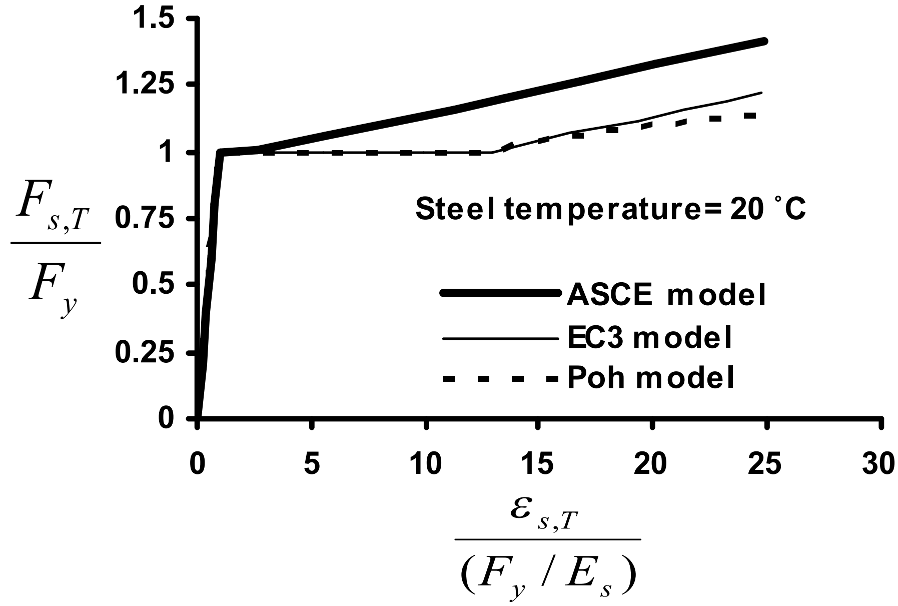

a) 20°C stress-strain relationship

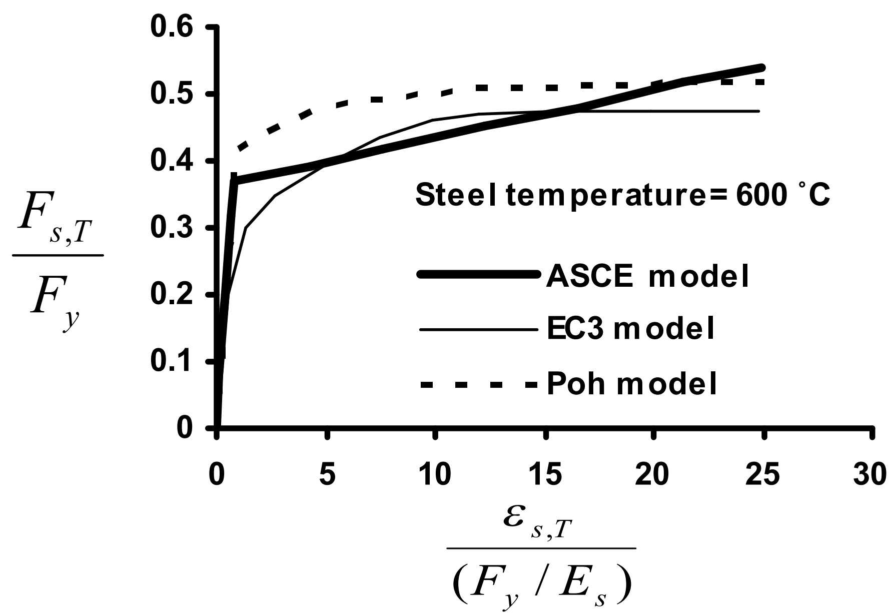

b) 600°C stress-strain relationship

Figs. 2.13a and 2.13b: Temperature-stress-strain relationships for structural steel as per ASCE, Eurocode and Poh models

Originally, the Eurocode temperature-stress-strain curves were derived based on transient-tests under slow heating rates (Twilt 1991 and Anderberg 1988). Therefore, when used in the fire resistance analysis, the Eurocode constitutive relationships generally produce slightly more flexible responses as compared to ASCE or Poh constitutive models. This is attributed to the fact that in the transient-state tests, adopted by the Eurocode, part of high temperature creep is included in the resulting temperature-stress-strain curves (Buchanan 2005). However, less information is known about the test data that were used to derive ASCE temperature-stress-strain curves of steel. On the other hand, Poh (2001) developed generalized temperature-stress-strain relations for structural steel based on a large set of experimental data. These relations account for specific features, such as the yield plateau and the effect of strain hardening. These temperature-stress-strain relations have been validated against the specified relationships in codes and standards, and they have been shown to give more realistic predictions of fire resistance when used in conjunction with high temperature creep model.

Another difference between the three constitutive models is the assumed limits for the elastic phase. ASCE manual and Poh models consider a sharp yield point as an end of the linear-elastic phase, while Eurocode considers another point, called the “proportionality limit” as an end of the linear phase, as shown in Fig. 2.14. However, the end of elasticity in the Eurocode is the yield point, and is defined as the offset stress (also known as proof stress) corresponding to 0.2% strain, as shown in Fig. 2.14.

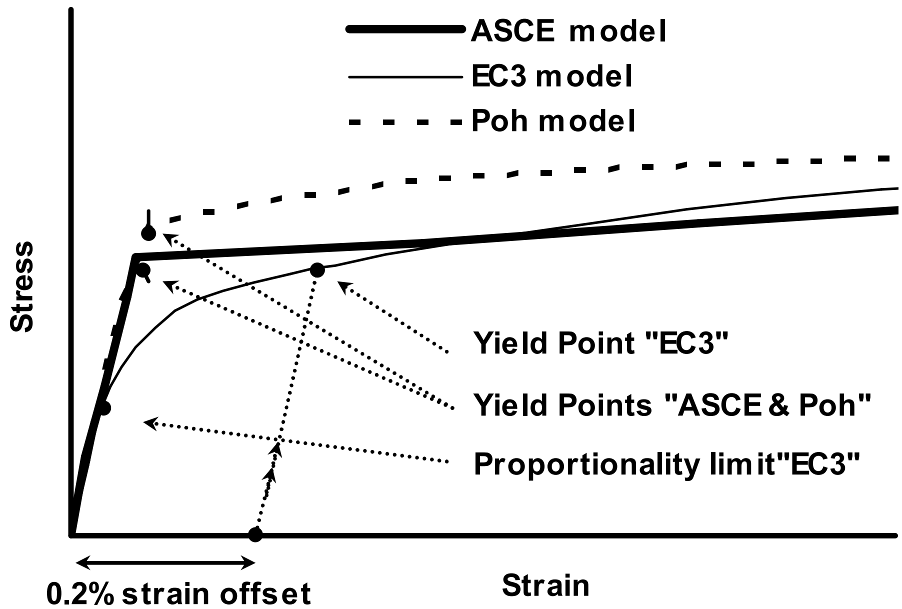

Fig. 2.14: Definition of yield point and proportionality limit in ASCE, EC3, and Poh 2001

2.6.4 Mechanical Properties – Concrete

The mechanical properties that influence the response of concrete to fire exposure differ slightly from those for steel. Of particular interest in concrete are the compressive strength, and the stress strain relationships.

Fig. 2.15 presents the compressive strength reduction factor of concrete as a function of temperature for the full range of temperatures practically achieved under fire exposure. From Fig. 2.15 it can be seen that the compressive strength reduction factor for carbonate and siliceous aggregate based concrete are significantly similar over the entire temperature range plotted in Fig. 2.15. In both instances, the reduction factor decreases monotonically with increasing temperatures.

At every temperature above 100 °C concrete has a unique stress strain relationship, for ease of presentation, the stress strain curves for only five temperatures are shown in Fig. 2.16. From Fig. 2.16 it can be seen that both the strain at peak stress and the ultimate strain increases for concrete as a function of temperature. This has a considerable effect on the response of a structure under fire exposure, as the temperatures increase, the deflections in the member will increase. In the case of floor systems, these increasing deflections allow the concrete to transfer a portion of the load via tensile membrane action, and hence, enhance the fire resistance of the structure.

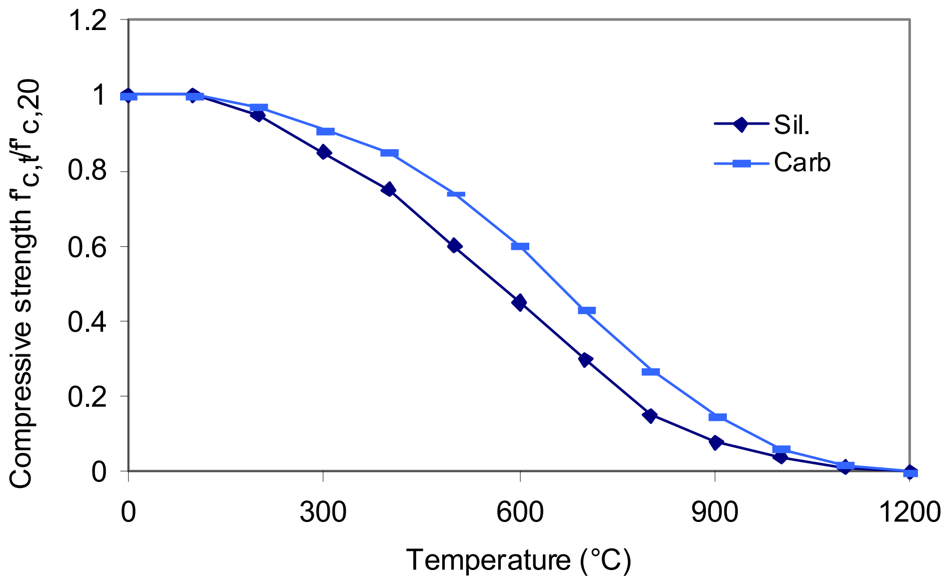

Fig. 2.15 Compressive strength of concrete as a function of temperature

Finally, with reference to the mechanical properties of concrete at elevated temperature, the Eurocode presents a series of equations to define the stress strain relationships as shown in Appendix B. These equations, as was the case for steel at elevated temperatures, encompass an infinite number of data points, as such, no graphical representation is presented here, rather, the interested user is directed to the Eurocode or Appendix B.

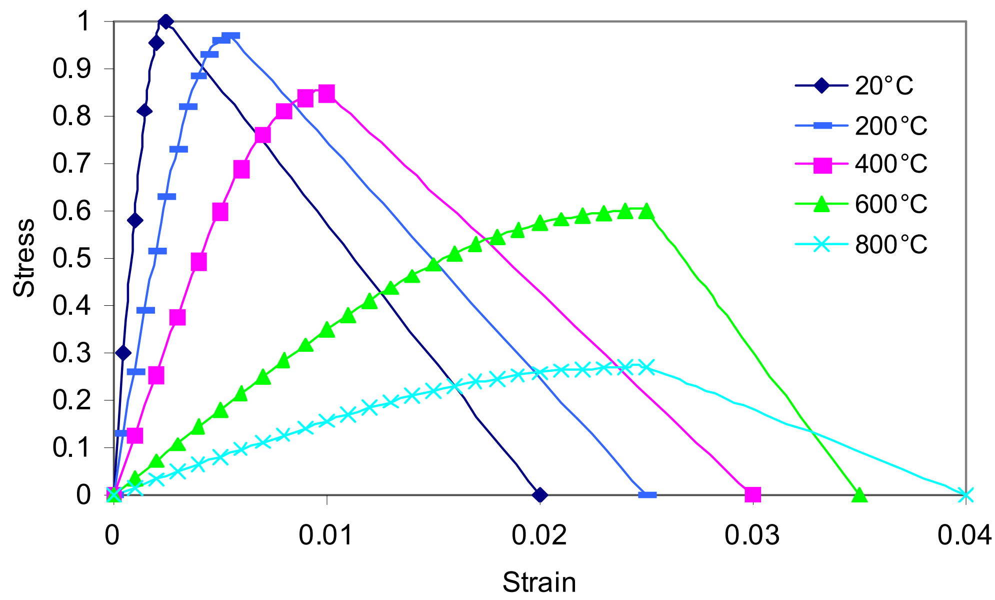

Fig. 2.16: Strain at peak stress reduction factor as a function of temperature for concrete

2.6.5 Deformation Properties – Steel

The deformation properties that influence the fire response of steel structures are thermal strain and high-temperature creep. The following sections discuss the variations in deformation properties of steel at elevated temperatures.

There have been many tests to characterize thermal strain of steel at elevated temperatures, results from some of which are compiled in Fig. 2.17 (Outinen 2004, Cooke 1988, Anderberg 1988, and Stirland 1980,). As seen in Fig. 2.17, thermal strain of steel increases with temperature up to nearly 750˚C, at which point a phase change takes place (as discussed previously) and the thermal strain becomes nearly constant up to 800 °C, after which point thermal strain starts to increase again.

Variation of thermal strain models as specified in ASCE and EC3 are also plotted in Fig. 2.17. Minimal differences exist between the Eurocode and ASCE models for thermal strain of steel up to 700 °C. However, in the temperature range of 700-850 °C the ASCE model assumes a continuously increasing thermal strain while the Eurocode model accounts for the phase change that occurs in steel in this temperature range by assuming a constant thermal strain from 750 °C to 850 °C, followed by an increasing thermal strain up to 1000 °C (See Fig. 2.8).

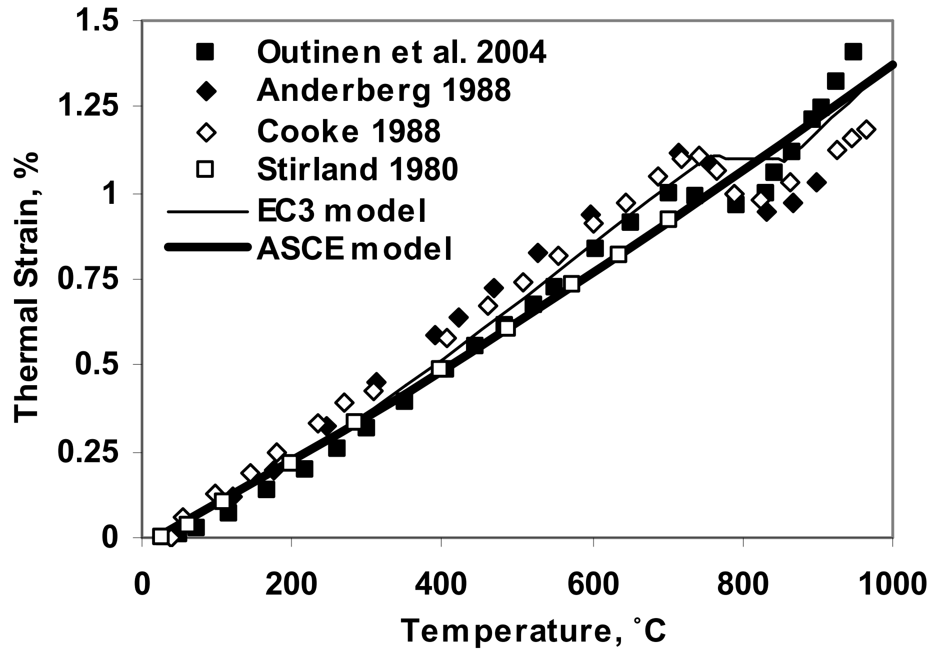

Fig. 2.17: Thermal strain of steel as predicted by different models and as measured in different tests

2.6.6 Deformation Properties – Concrete

As was the case with steel, the deformation property of concrete that has the largest influence on the fire resistance of composite steel-concrete construction is thermal expansion. Fig. 2.18 presents a plot of the thermal expansion of concrete as a function of temperature for both siliceous and carbonate aggregate based concrete. It is observed from Fig. 2.18 that the coefficient of thermal expansion for carbonate aggregate is lower than that of siliceous aggregate concrete at all temperatures practically achieved under fire exposure. While for both concrete types, the coefficient of thermal expansion is nearly zero at ambient temperatures, it increases to

0.014 by 700 °C for siliceous aggregate concrete, and 0.012 by 805 °C for carbonate aggregate concrete.

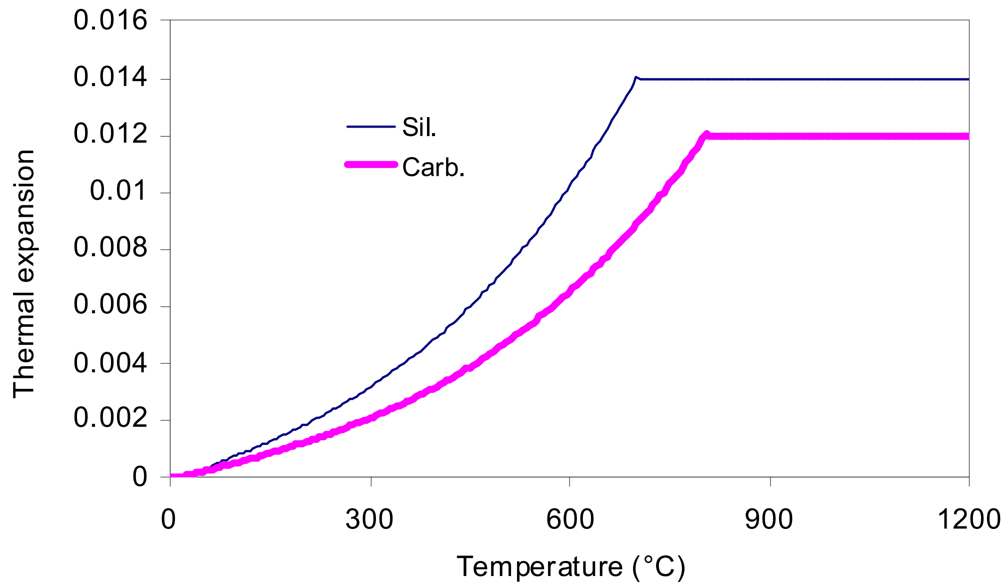

Fig. 2.18: Coefficient of thermal expansion for concrete as a function of temperature

2.6.7 High Temperature Properties of Insulation

Steel and concrete have as their primary function in any structure to resist the applied loads on the structure. Insulation on the other hand has as its primary objective to prevent heat transfer, specifically, it is to offer no structural contribution. As such, the properties of insulation materials that are of interest to the current research are all thermal in nature. These properties include thermal conductivity, specific heat, density, and moisture content (SFPE 2005). Given the wide range of insulations available in the market, and the proprietary nature of many of them, only the desirable thermal properties of insulation will be discusses. It is desired that insulation have a low thermal conductivity, high specific heat, low density, and high moisture content to optimize the protection offered to a structural member. It is base on these criterion, and supporting fire resistance experiments, that insulation is selected for use in a specific application.

2.7 Knowledge Gaps

The current state-of-the-art presents a large amount of information on the behavior and mechanics of composite steel structures under fire exposure. The previous research presented in this chapter focuses on the experimental and numerical studies conducted on the fire resistance of CFHSS columns and composite floor systems.

Studies on the fire resistance of CFHSS columns have clearly shown that composite construction in the form of CFHSS columns is capable of providing fire protection to meet the levels required in codes and standards in most practical applications. While a major contribution to structural fire engineering, the previous work on CFHSS columns does not provide a rational approach for fire resistance design. There is a critical need for a simplified design methodology to assess the fire resistance of CFHSS columns under design fire exposure. The methodology should take into consideration realistic load levels, failure criterion, and expand the range of columns considered by increasing the cross-sectional and length limitations associated with the use of Eq. 2.1.

Composite beam slab assemblies have been shown in previous experimental and numerical investigations to enhance the fire resistance of steel framed structures. Much of this enhancement is due to the development of tensile membrane action as the slab deflects due to the heat from fire reducing the mechanical properties of the constituent material. The benefit that is achieved through composite construction is however still insufficient to meet the levels required in codes and standards. To provide an improved fire resistance from composite beam-slab assemblies, it is necessary in investigate the use of alternate materials in the concrete slab to enhance the tensile strength of the concrete. Enhancing tensile strength of the concrete will allow additional load to be transferred through tensile membrane action, and thus, higher fire resistance to be achieved. In addition, after development of the material system, a simplified approach for fire resistance design using the novel material system needs to be developed. The simplified approach should permit the use of composite floor slabs for achieving fire resistance in any fire exposure, under realistic loading and failure criterion, and over a wide range of sizes.

Lastly, the previous work as presented in this chapter highlights the need for fire resistance evaluation to be considered on the system level, rather than just the element or assembly levels. This need is based on the observation that the presence of multiple connected members and composite construction at the system level enhance the fire resistance of composite structural systems. As such, to provide a holistic approach to fire resistance evaluation, any methodologies or material systems developed for CFHSS columns or composite beam slab assemblies should be modeled at the syste--m level for verification of the develop innovations.

The current research as presented in the following chapters is aimed at overcoming these knowledge gaps. The first step in accomplishing this is to conduct an experimental investigation on the response of a composite beam slab assembly incorporating steel fiber reinforced concrete to fire exposure. Details on the experimental program are presented in the following chapter.

CHAPTER 3

3 EXPERIMENTAL STUDIES

3.1 General

To develop a methodology for exploiting the beneficial effects of composite construction on the fire resistance of steel framed structures, it is necessary to undertake detailed analysis at the element, assembly and system levels. The numerical models to be used for conducting this detailed analysis require validation at the element, assembly, and system levels. It is therefore necessary to have experimental data at the element, assembly, and system levels for CFHSS columns, composite floor assemblies, and a full-scale building respectively. As seen in Chapter 2, comprehensive fire resistance experiments have been conducted on concrete-filled HSS columns, and on the steel framed structure at Cardington. However, only limited studies have been conducted on steel beam-concrete slab assemblies, and these do not fully take into consideration composite action, and specifically, the contribution of tensile membrane action to fire resistance. To overcome this limitation, four novel fire resistance experiments were carried out on steel beam-concrete slab assemblies. In this chapter, the details of these novel fire tests are presented, and the available fire test data at the element and system level reviewed.

3.2 Element Level – CFHSS Columns

A review of the literature, as presented in Chapter 2, indicates that there have been a number of studies on the fire resistance of CFHSS columns exposed to fire conditions. The most comprehensive of the research programs for which test data is available, is that conducted at the National Research Council of Canada (NRCC). In this research program, fire resistance experiments on 85 CFHSS columns were conducted (Kodur and Lie, 1996, Lie and Kodur, 1996, Lie and Chabot, 1992, Lie and Irwin, 1995, Chabot and Lie, 1992). The columns tested at NRCC were both round and square HSS columns with three different types of concrete filling, bar reinforced (RC), steel fiber reinforced (FC) and plain concrete (PC). A figure illustrating the three different types of fillings and the two different HSS cross sections is presented as Fig. 3.1. The rebar used in RC filled HSS columns was standard deformed rebar ranging in size depending on the size of the columns. Steel fibers were 50 mm long crimped fibers with yield strength of 620 MPa as commonly used in construction. Specific details and response parameters needed for validation of the SAFIR computer model are summarized below.

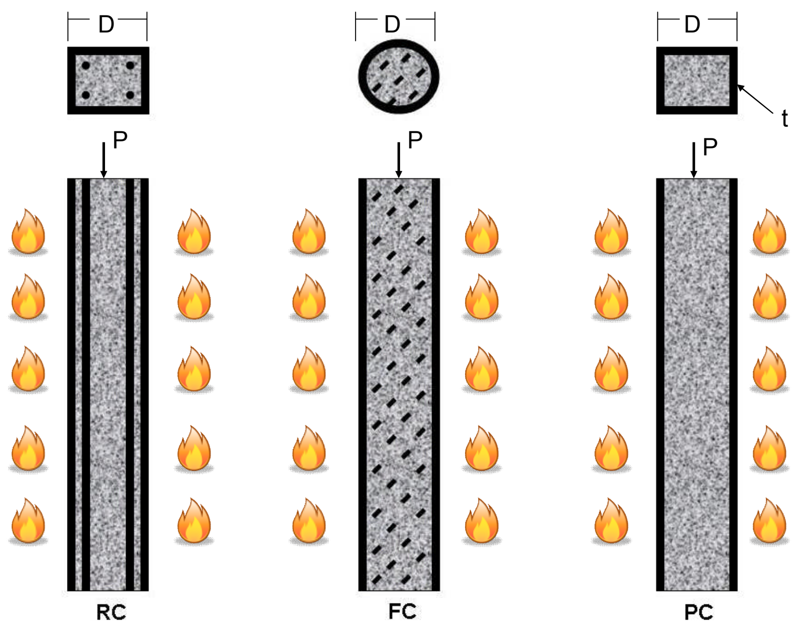

Fig. 3.1: Illustration of RC, FC, and PC square and round column cross-sections tested at NRCC

3.2.1 Dimensions

All of the tested columns were 3810 mm long from one end plate to the other. Both circular and square cross-sections were considered in the research program. The circular cross-sections had wall thicknesses ranging from 1.78 to 12.70 mm, and outside diameters ranging from 141.3 to

406.4 mm. The square cross-sections ranged from 152.4 to 304.8 mm in outside width, with a wall thickness of 6.35 mm.

3.2.2 Materials

Steel strength was not taken as a primary variable in this research program, the steel was specified as either 300 or 350 MPa in accordance with CSA standard G40.21-M (Kodur and Lie, 1996, Lie and Kodur, 1996, Lie and Chabot, 1992, Lie and Irwin, 1995, Chabot and Lie, 1992). The concrete used as infill was normal weight aggregate concrete with a 28-day compressive strength of concrete ranging from 23 to 85 MPa for the different CFHSS columns. Two primary types of concrete were considered, that made with carbonate aggregate, and that made with siliceous aggregate. In the majority of cases, the cement used was typical (No. 10) cement, however, some minor consideration was given to the use of high early strength cement. For all of the pours done in the research program, the full mix design is provided in the respective internal test reports (Kodur and Lie, 1996, Lie and Kodur, 1996, Lie and Chabot, 1992, Lie and Irwin, 1995, Chabot and Lie, 1992). Typical mix proportions for selected concrete mixes (Lie and Chabot 1992) are reproduced in Table 3.1 to illustrate the detailed information available in the test reports.

Table 3.1: Sample mix proportions for concrete used in CFHSS columns (Lie and Chabot 1992, Lie and Kodur 1994)

	PC	FC	RC
Cement (Kg/cu.m)	355	439	439
Course Agg. (Kg/cu.m)			
19 mm	-	788	788
9.5 mm	1014	340	340
Total	1014	1128	1128
Fine agg.	855	621	621

Table 3.1 (Continued): Sample mix proportions for concrete used in CFHSS columns (Lie and Chabot 1992, Lie and Kodur 1994)

	PC	FC	RC
Steel fibers (Kg/cu.m)	-	42	-
Rebar (mm)	-	-	Various
Water (Kg/cu.m)	173	161	161
Water/cement Ratio	0.49	0.37	0.37
Superplasticizer	-	Mighty 150	-
Retarding admixture	Master Builders 100XR	Master Builders 100XR	-
28 day comp. str. (MPa)	33.0	43.2	41.3

3.2.3 Fabrication

In order to attach the columns to the loading apparatus, and to provide the desired type of end restraint, all of the columns had a steel end plate welded to the top and bottom. To allow for the pouring of concrete into the column, the plate on the top was provided with a hole just smaller than the inside dimension of the column. In addition to the hole in the top plate on the column, a total of four 13 mm holes were drilled in the columns to act as steam vent holes, two 457 mm from the top of the column, and two 457 mm from the bottom of the column. Additionally, a 25 mm hole was placed at the top of the column to allow for entry of the thermocouple wires to the inside of the column.

For concrete filling, the columns were placed in the upright position and concrete was poured from a mixing truck. After being filled, the columns were allowed to remain in the upright position for 28 days, after which point they were placed in the horizontal position until testing.

3.2.4 Instrumentation

Instrumentation in the columns consisted of thermocouples and axial displacement transducers. Thermocouples inside the column were attached to a thermocouple tree in all of the columns and to rebar in the RC columns. The thermocouple tree consisted of a steel rod running down the length of the column with additional small pieces of rod attached to it allowing temperatures to be measured at several points across the cross section as seen in Fig. 3.2. Type K chromel-allumel thermocouples with a thickness of 0.91 mm were used.

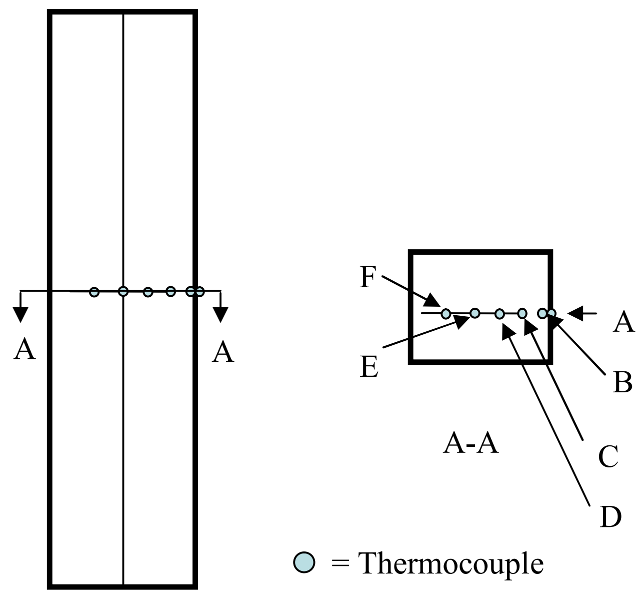

Fig. 3.2: Schematic of thermocouple tree used in testing at NRCC

Displacement of the columns was monitored by a displacement transducer which measured the motion of the loading jack on the top of the column. The transducer used in testing had a tolerance of 0.002 mm.

3.2.5 Test Conditions

The columns were tested at NRCC's fire test furnace by exposing them to fire and loading. Loading to the columns was provided via a single hydraulic jack with a capacity of 9778 kN which was located at the top of the column. With one exception, loading on the columns was applied concentrically. Loading ranged from 9-47% of the total composite column strength or from 46-165% of the concrete core strength.

Most of the columns were tested in the simulated fixed-fixed end condition. To achieve this condition, eight 19 mm bolts were passed through the plates on the ends of the columns and attached to the loading frame of the furnace.

Fire exposure was simulated as specified in ASTM E-119 standard fire exposure. Heat to the furnace was provided via 32 propane gas burners evenly spatially distributed in the furnace. Temperatures within the furnace chamber were also measured with Type K chromel-alumel thermocouples. A total of eight of them were inserted into the combustion chamber. The average of all eight of these thermocouples was used to monitor the temperatures inside the furnace.

3.2.6 Measured Data

Data from fire tests was recorded at one minute intervals depending on the stage of the test. This data has been made available in the raw form through internal reports and several journal publications. Test data provided in these reports consists of temperatures at various cross section locations, furnace temperature, and axial deformation. Sample plots of the temperature at various locations and axial deformations are presented for column RP-168 (Table 3.2) as Figs. 3.3 and 3.4 below respectively, see Fig. 3.2 for key to labeling used in Fig. 3.3.

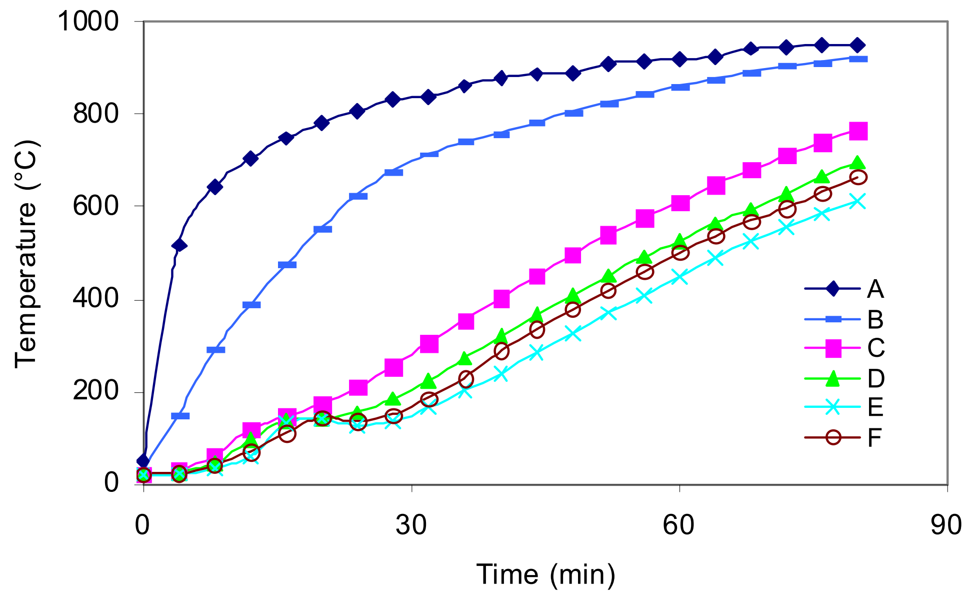

Fig. 3.3: Thermal response recorded during fire test at NRCC for CFHSS column RP-168

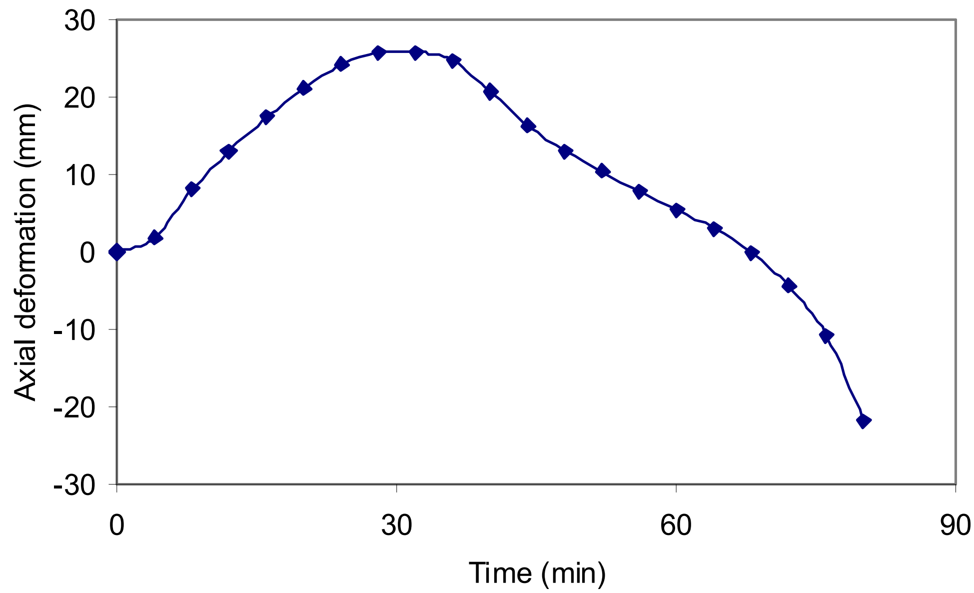

Fig. 3.4: Axial deformation recorded during fire test at NRCC for CFHSS column RP-168

3.2.7 Data for Model Calibration

Detailed data on test parameters and column response is available for all of the 85 columns tested at NRCC. Given that this information is readily available, it is not prudent, considering the high cost of testing, to duplicate these tests for the purpose of this research. Rather, the data from NRCC will be used to validate numerical models constructed in SAFIR, such that parametric studies can be carried out numerically. For this purpose, 14 CFHSS columns were selected as a representative sample from the 85 tested at NRCC. Pertinent information from these columns is presented in Table 3.2. In the designation of columns (ex: RP-355), the first letter (R) represents section shape (round or square), the second letter (P,F,B) denotes filling type (plain, steel fiber and bar-reinforced concrete), and the number (355) denotes the diameter (for circular) or width (for square) of the HSS column section in mm.

Table 3.2: Summary of test parameters and fire resistance values for selected CFHSS columns tested at NRCC

Column Designation	Dia. or Width mm (in.)	AISC Factored Load kN (kip)	Load Ratio	Fire Resistance (min)	Concrete Filling	Aggregate Type
RP-168	168.3 (6.63)	1197 (269)	0.13	81	Plain	Sil.
RP-273	273.1 (10.75)	3508 (788)	0.15	143	Plain	Sil.
RP-355	355.6 (14.0)	5120 (1151)	0.18	170	Plain	Sil.
SP-152	152.4 (6.0)	1409 (317)	0.20	86	Plain	Carb.
SP-178	177.8 (7.0)	1976 (444)	0.28	80	Plain	Sil.
RF-324	323.9 (12.75)	4573 (1028)	0.35	199	Fiber	Carb.
RF-356	355.6 (14.0)	6616 (1487)	0.23	227	Fiber	Carb.
SF-203	203.2 (8.0)	3506 (788)	0.26	128	Fiber	Carb.
SF-219	219.1 (8.63)	3793 (852)	0.16	174	Fiber	Carb.
RB-273a	273.1 (10.75)	3323 (747)	0.32	188	Bar	Carb.
RB-273b	273.1 (10.75)	3333 (749)	0.57	96	Bar	Carb.
SB-203	203.2 (8.0)	2345 (527)	0.21	150	Bar	Carb.
SB-254a	254 (10.0)	3405 (765)	0.42	113	Bar	Carb.
SB-254b	254 (10.0)	3405 (765)	0.65	70	Bar	Carb.

3.3 Assembly Level – Composite Floor System

In the previous chapter, it was observed that composite floor systems demonstrate higher fire resistance than observed for steel beams in single element tests. This was attributed to the development of tensile membrane action in the concrete slab supporting a portion of the applied load. To study this, tests were carried out on four composite beam slab assemblies under various configurations and loadings. Initially, three plain concrete floor slabs were constructed and tested under fire exposure, based on the results from these tests, it was decided to test an additional, similar assembly made with SFRC.

3.3.1 Test Specimens

The test specimens were specifically designed such that the response of the central beam under fire exposure could be evaluated. The three plain lightweight concrete assemblies are referred to as PC-1, PC-2, and PC-3, while the SFRC assembly is referred to as SFRC, the different construction parameters for each assembly are shown in Table 3.3. The assemblies comprised of a network of five steel beams and a concrete deck cast on the top. The beam networks consisted of three W10X15 beams connected to a pair of W12X16 girders (Fig. 3.5) via the connections denoted in Table 3.3. The W12X16 beams were 3.96 m long while the W10X15 beams were 2.13 m in length. The spacing of the connections on the W12X16 beam was 1.98 m, leaving 152.4 mm of the W12X16 beam extending past the connection of the end W10X15 beam. The detailing of all steel work was done according to AISC (2005) specifications. The steel used in the beams was A992 with a specified yield strength of 344 MPa, while the steel used in the connections was of Grade A36 with a specified yield strength of 248 MPa. Bolts used in the assembly of the specimen were 19 mm Grade A325 with a shear strength of 68.8 kN.

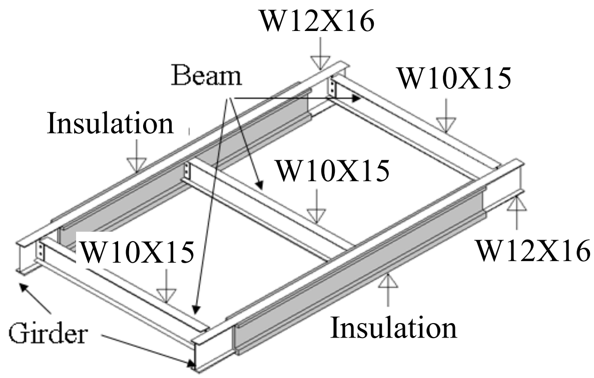

Fig. 3.5: Configuration of beams in the tested assembly

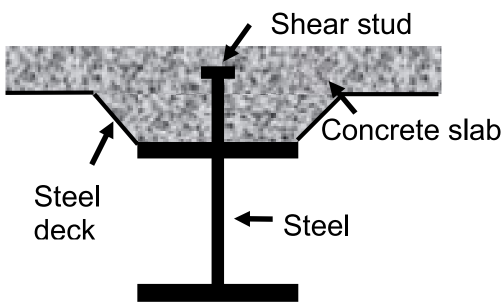

(a) Cross-section of beam slab assembly

(b) Deck assembly with shear studs

Fig. 3.6: Details of deck and shear studs in beam-slab assembly

Table 3.3: Details of tested beam slab assemblies

	PC-1	PC-2	PC-3	SFRC
Concrete type	Lightweight	Lightweight	Lightweight	Normal weight SFRC
Slab thickness (mm)	101.6	101.6	101.6	127
Concrete strength (MPa)	45.3	44.8	43.8	46.6
Connection type	Fin plate	Fin plate	Double angle	Fin plate
Girder protection	1 hour (14.3 mm)	1 hour (14.3 mm)	1 hour (14.3 mm)	2 hour (22 mm)
Beam protection	1 hour (14.3 mm)	None	None	None

Atop the network of steel beams was attached a ribbed 20 gauge 38 mm galvanized deck. Through the galvanized deck, shear studs were welded to the top flange of both the W12X16 and the W10X15 beams. The shear studs used had a shank diameter of 16 mm and a length of 76 mm for slabs PC-1 to PC-3, and a diameter of 19 mm with a length of 101.6 mm for the SFRC slab. Shear studs were affixed to the W12X16 section every 178 mm and attached to the W10X15 section in the valley of every rib, giving them a center to center spacing of 154 mm. A schematic of the shear stud placing is presented as Fig. 3.6a, and a picture of the as constructed specimen is shown in Fig. 3.6b.

Following completion of the beam network and attachment of the shear studs to the beams, the two W12X16 girders and W10X15 beams were provided with fire protection sufficient to achieve the fire resistance ratings shown in Table 3.3. Carboline Type 5GP fire protection was applied to the beams and was measured at several points to ensure that the thickness was uniform over the entire surface. Fire protection was terminated approximately 300 mm from the end of the W12X16 beams (all of which is outside the fire exposed region) to allow the steel beams to rest directly on the supports during testing. Fig. 3.7 shows the insulation on the W12X16 beams shortly after application of the fire protection. The properties of the insulation are tabulated in Table 3.4.

Fig. 3.7: Fire protection on the girder just after application

Table 3.4: Properties of fire insulation

Density (wet):	832kg/m^3
Density (dry):	240kg/m^3
Adhesion:	>4255kPa
Comp strength:	112kPa

After application of fire protection, the remaining galvanize deck was placed, formwork installed around the perimeter of the assembly, and the concrete poured. The deck was 4.57 m by 3.96 m, with a maximum thickness of 101.6 mm for slabs PC-1 through PC-3, and 127 mm for the SFRC slab. The specified compressive strength was 28 MPa with the strengths shown in Table 3.3 corresponding to the strength measured on the day of testing for the respective slabs. The course aggregate was either lightweight or carbonate (limestone) based depending on the concrete type shown in Table 3.3. Once the normal weight concrete for use in SFRC was placed in the truck, steel fibers with a length of 63.5 mm (aspect ratio = 67) were added to the concrete, the mix proportions are shown in Table 3.5.

Table 3.5: Mix proportions used in the tested composite beam-slab assembly

	SFRC	Lightweight
Type 1 cement	338 kg/m^3	332 kg/m^3
Course agg. (19 mm)	1023 kg/m^3	89 kg/m^3
Lightweight agg. (19 mm)	-	495 kg/m^3
Boarl material	-	60 kg/m^3
Fine agg.	965 kg/m^3	753 kg/m^3
Water	160 kg/m^3	161 kg/m^3
Steel fibers	42 kg/m^3	-
Air	4.28%	5.74%
W/C	0.47	0.48
Unit weight	2459 kg/m^3	1762 kg/m^3
Slump*	90 mm	163 mm

*Slump is not required for SFRC, this value was however obtained for comparison purposes.

After the slabs were cast, they were covered with a vapor barrier and allowed to cure for a minimum of 90 days at ambient temperature to achieve a relative humidity level below 75% prior to testing.

3.3.2 Instrumentation

The test specimens were instrumented with thermocouples, strain gauges, and displacement transducers to monitor thermal and mechanical response of the specimen during fire testing. Temperatures were measured with 0.91 mm thick type K chromel-alumel thermocouples, which were placed on the upper and lower flanges, and on the web of the steel beam at the nine cross sections indicated in Fig. 3.8a.

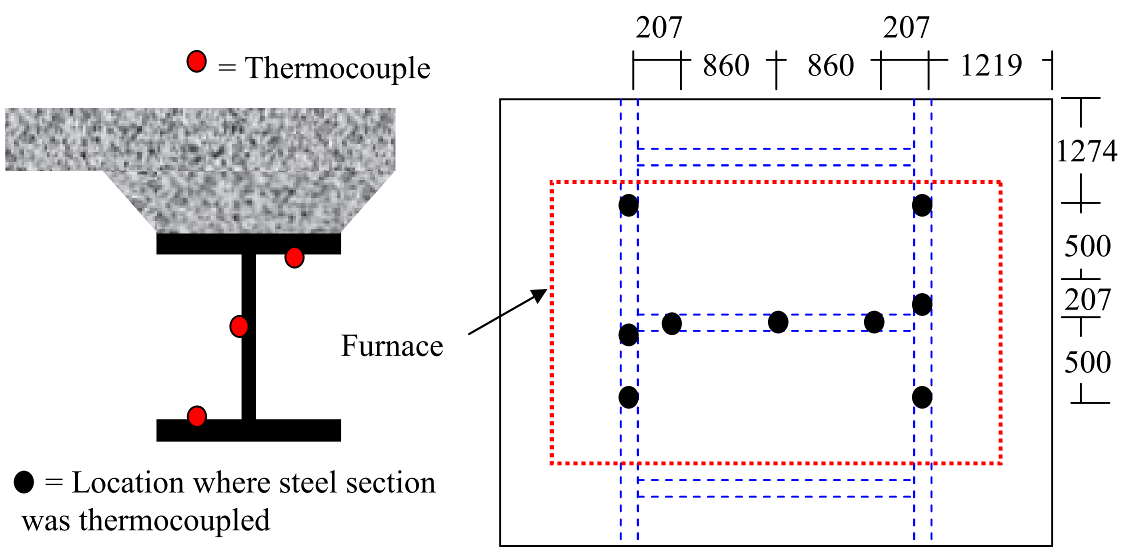

(a): Thermocouple layout on beam cross section

Fig. 3.8: Instrumentation scheme used in testing of the beam-slab assembly (mm)

In addition, the temperatures were also monitored at two points in the depth of the concrete at four cross-sections, and on the exposed surface of the assembly at seven locations as shown in Figs. 3.8b and c respectively. Since high temperatures are quickly generated in the furnace, strains and displacements were measured only on the unexposed surface of the slab. Strains were measured using 60 mm long 120 Ω strain gauges located at the 10 locations shown in Fig. 3.8d. Vertical displacements were measured at 9 locations as shown in Fig. 3.8e using linear varying displacement transducers (LVDT's) connected to the top surface of the slab.

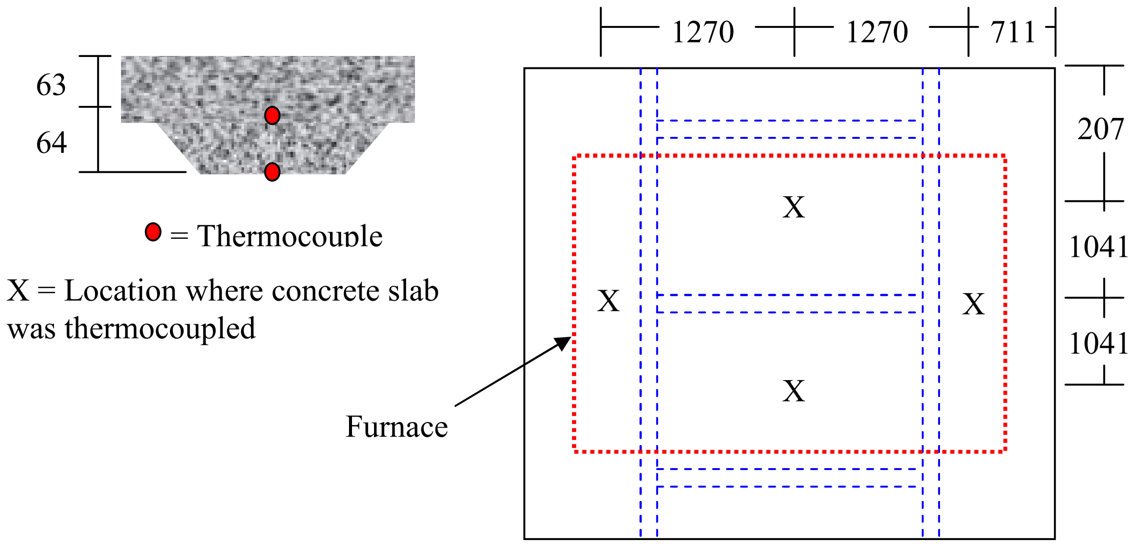

(b): Thermocouple layout on slab cross section

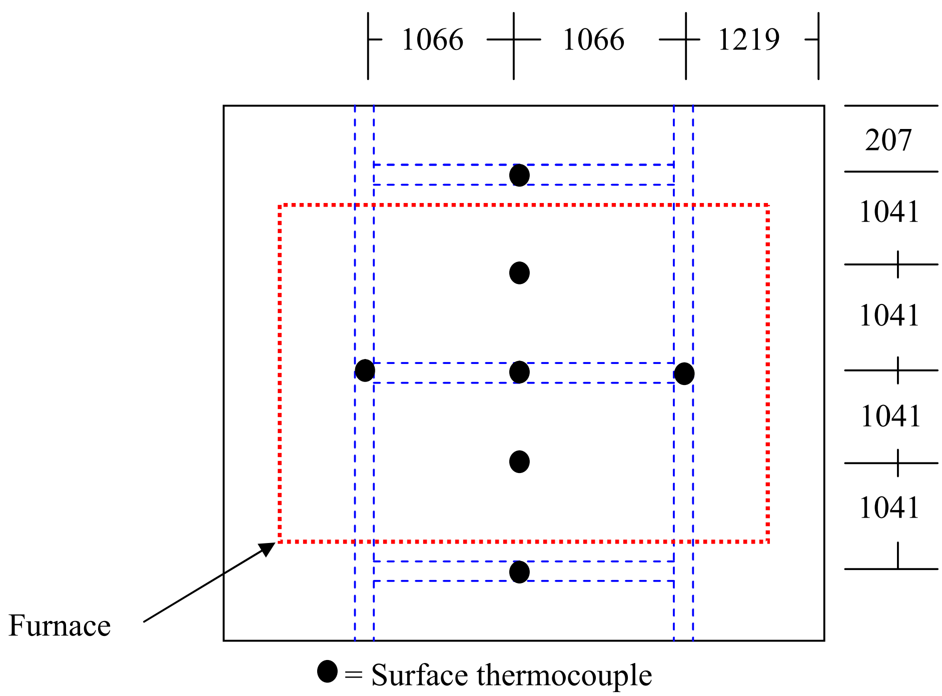

(c): Thermocouple layout on unexposed side of slab

Fig. 3.8 (Continued): Instrumentation scheme used in testing of the beam-slab assembly (mm)

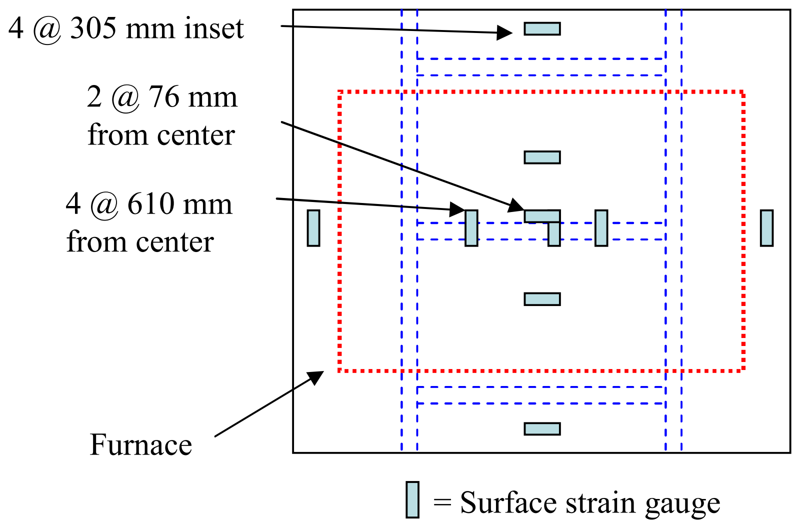

(d): Strain gauge layout on unexposed side of slab

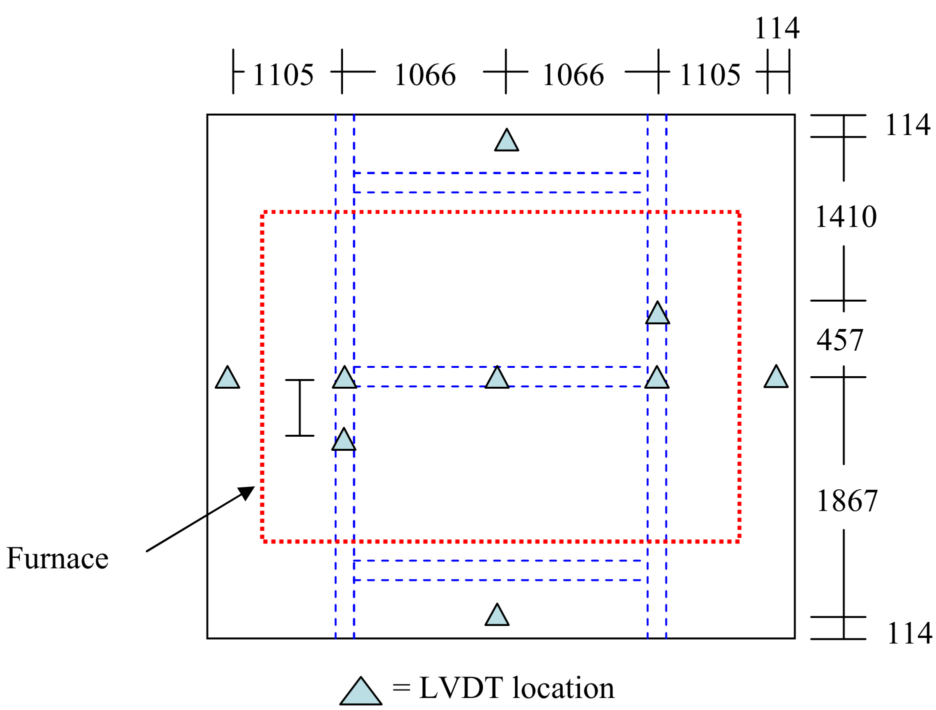

(e): LVDT Layout

Fig. 3.8 (Continued): Instrumentation scheme used in testing of the beam-slab assembly (mm)

3.3.3 Test Equipment

The fire resistance tests were conducted at Michigan State University's Structural Fire Testing Furnace shown in Fig. 3.9. The test furnace is design to simulate as closely as possible the thermal and structural loading to which a structure would be exposed in a building fire. Heat is provided to the furnace by six independent natural gas burners. The gas is fed into the furnace at approximately 0.02 MPa and is regulated to assure this pressure is maintained. A main control valve which trips at sensing any irregularities in pressure (such as a rapid shutdown) is incorporated to assure that in the case of an emergency, the fuel supply is shut off almost instantly. In addition to this, if left unused for more than 2 minutes, the valve will again shut itself off requiring a purge cycle before operation can be resumed. The maximum total gas consumption of the furnace is approximately 230 m^3/ hr with a consumption of 100 m^3/hr while in the maintenance stage of the ASTM E119 time-temperature relationship. Each of the burners is capable of producing 406 kW. The six burners are located on the furnace as indicated in Fig. 3.10. Each of the burners is located 1.2 m from the top of the furnace, and can be independently turned off during the course of the test. Using the integrated UV detectors, the burners automatically adjust the fuel to air ratio to achieve a clean burn and minimize pollutants.

As seen in Fig. 3.10, there are two observation ports which allow test specimens to be viewed. These ports are equipped with high temperature resistant glass, and are large enough to accommodate a video camera or other similar device.

A constant load was applied to the specimen for the entire duration of testing using hydraulic actuators. The loading frame used in testing the floor assemblies has the configuration shown in Fig. 3.11. Two independent load zones exist allowing for several configurations to be used depending on test requirements. The central hydraulic pump can reach a maximum pressure of

20.7 MPa and a minimum pressure of 3.44 MPa. The large actuators have a maximum extension of 152.4 mm while that of the smaller actuators is 305 mm.

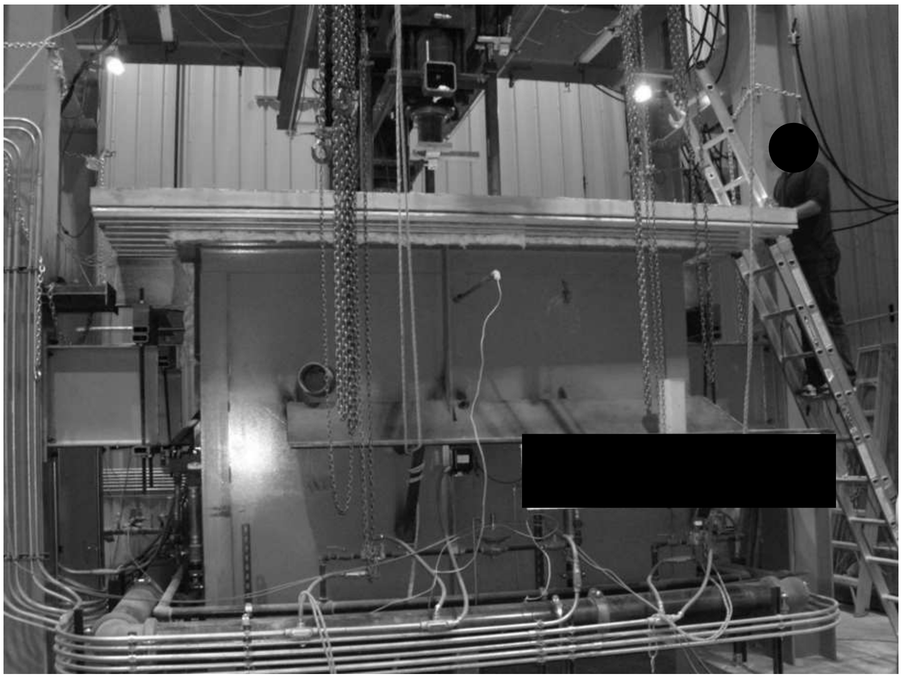

Fig. 3.9: View of MSU structural fire testing facility

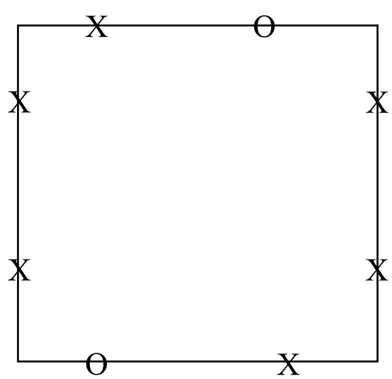

X – Burner
O – Observation port

Fig. 3.10: Layout of burners and observation ports in fire test furnace

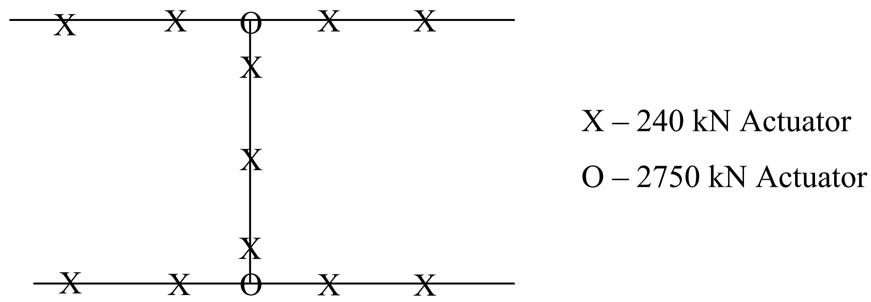

Fig. 3.11: Actuator locations in the furnace

There are separate fans for combustion air and exhaust. Exhaust flow is controlled manually and can be adjusted such that either positive or negative pressure is present in the furnace at any given time. Input air however, as indicated above, is governed by the UV detectors to optimize combustion at each burner. Exhaust air is taken from the top of the furnace to reduce the combustion products in the furnace at any given time.

The temperature within the combustion chamber is manually controlled allowing for any time temperature profile to be simulated. The furnace has been calibrated for ASTM E-119 (ASTM 2007) and E-1529 (ASTM 2001) hydrocarbon fires. The manual control facilitates simulating a design fire scenario with ease. The sensitivity of the controls allows good control to achieve less than 1% error while following the ASTM E-119 time-temperature relationship.

There are a total of 90 inputs for the data acquisition system. 10 of these positions were used for strain gages, 10 are for LVDT's, while the remaining 70 were used for thermocouples. Data was collected from all of the channels in five second intervals and recorded in Excel (*.CSV) format for later analysis.

3.3.4 *Test Specimen Installation*

After curing of the concrete, the test specimens were placed into the testing furnace and all of the instrumentation attached. For lifting purposes, four of the shear studs were replaced with threaded rod of equivalent shear strength, and the rods were long enough for them to pass through the slab and leave approximately 75 mm of threaded rod exposed past the top surface of the slab. On this protruding threaded rod, a hook eye was attached for use in lifting the specimen as shown in Fig. 3.12a.

As seen in Fig. 3.8e, the concrete slab extends 1.2 m past the edge of the W12X16 steel sections, as such, there is considerable bending moment in these edges where they meet the W12X16 beam. While the specimen is designed to support this force under standard loading, it was feared that shock during the installation process would cause the unsupported edges to fracture. To remedy this problem, wooden beams were placed on the top of the slab and used to support the otherwise unsupported edges during placement as seen in Fig. 3.12b.

The beam slab assembly was brought into the proximity of the furnace utilizing an overhead crane system. Due to the geometric constraints of the furnace and the overhead crane, it was not possible for the specimen to be placed directly in the furnace. Rather, the specimen had to be transferred to a four point, cantilevered, overhead roller system. Once transferred onto the roller system, a forklift was used to push the assembly into the testing furnace as shown in Fig. 3.12c. The specimen was then lowed onto support points such that the entire assembly was level and very near the top of the furnace as shown in Fig. 3.12d. Sufficient distance was maintained between the furnace and the assembly as to eliminate the possibility of the furnace offering any structural support to the specimen as it defected due to the effects of fire exposure.

a) Beam-slab lifting mechanism

b) Lifting of test specimen for placement in the furnace

c) Placing of specimen on top of the testing furnace

d) Final position of the beam-slab assembly atop the testing furnace

Fig. 3.12: Procedure used for placing of the beam-slab assembly atop the testing furnace

3.3.5 Test Conditions

Loading on the beam-slab assemblies was applied via hydraulic actuators at the 5 points indicated by arrows in Fig. 3.13. Different point load magnitudes were applied to the center of the different assemblies (PC-1, PC-2, PC-3, and SFRC) while the four perimeter point loads were held constant at 22.5 kN for all tests. For test PC-1, the loading on the central actuator was 133.4 kN and the load was split to two point loads separated by 304 mm. For assemblies PC-2 and PC-3, the central actuator applied a load of 111.2 kN. For the SFRC slab, the central actuator applied a load of 90 kN. The loading was calculated as per AISC provisions (2005), and represented a load ratio of 30-45% on the central unprotected beam, 40-55% on the connections between the central unprotected beam and the girders, and 50-65% on the protected girders for the various assemblies. This loading was applied 30 minutes prior to the initiation of testing to ensure that the deflections reached a steady condition before initiating fire exposure. The slab was supported on steel supports 152 mm from each end of the W12X16 girders. Support conditions were such that vertical displacement of the specimen was completely restrained, horizontal translation of the slab was restrained by the friction between the girders and the supports, and rotation was completely unrestrained.

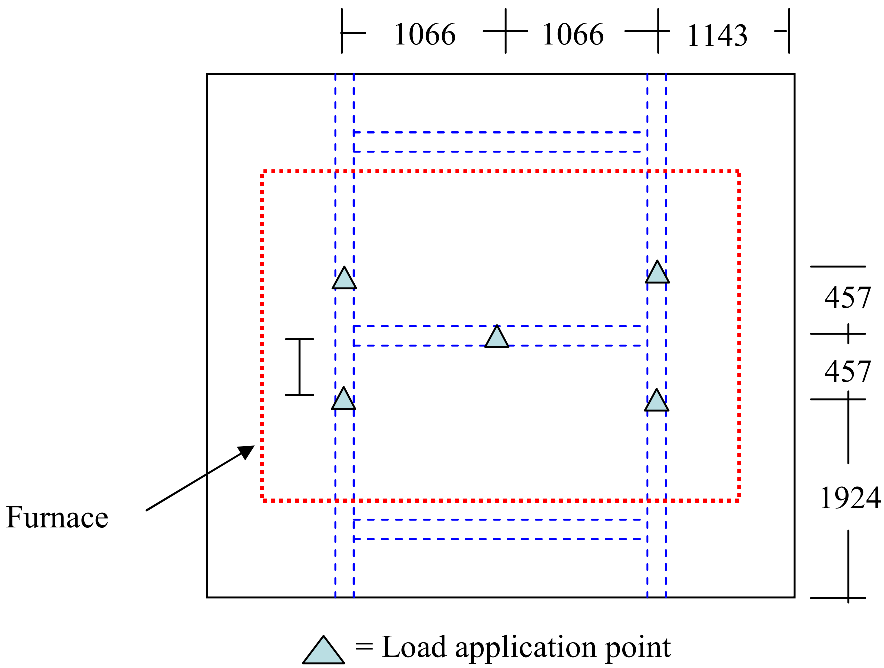

Fig. 3.13: Schematic of loading on the beam slab assembly (mm)

The non-standard fire exposure chosen was composed of a growth phase for the first 90 minutes, followed by a decay phase such that the total fire exposure lasted approximately 4 hours to simulate a realistic yet severe office fire scenario. The growth phase of the fire followed ASTM E-119 (2007) fire exposure for 90 minutes, while in the decay phase the temperatures decreased at 5.6 °C/min to ambient temperature as shown in Fig. 3.14. This cooling rate, which is 0.5 °C/min less than specified in Eurocode, was selected to achieve conservative test results by increasing the duration of the fire exposure. During the fire test, temperatures, deflections, and strains were recorded at five second intervals, and manual visual observations were recorded at five minute intervals or when significant events such as spalling or cracking occurred.

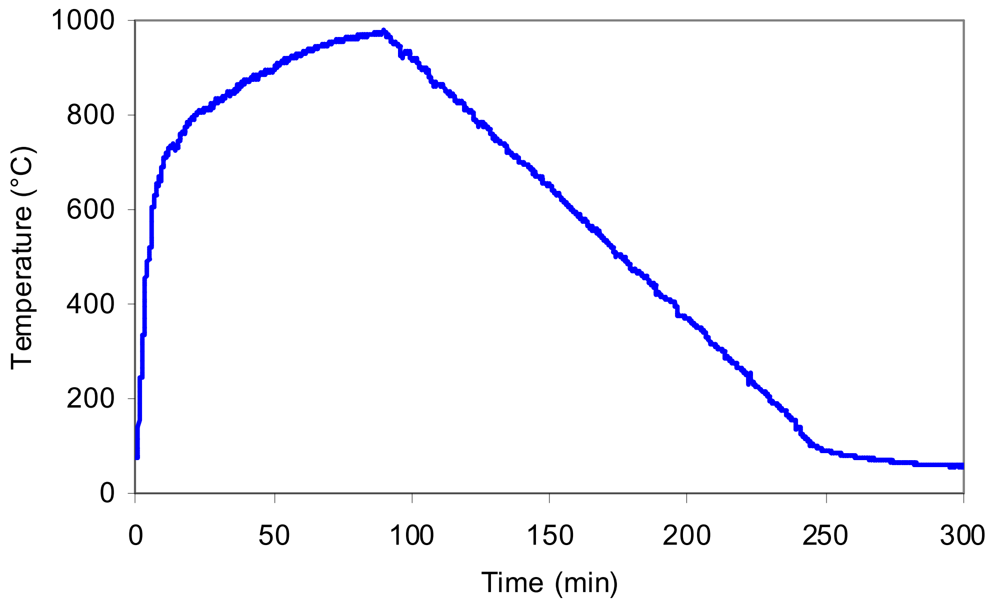

Fig. 3.14: Time temperature curve used in fire resistance test

3.3.6 Test Results

Initially, the three plain lightweight concrete slabs were tested under fire exposure, based on the results from these tests it was decided to conduct an additional test on a similar beam-slab assembly made with SFRC as described above. As such, the following discussion is divided between the plain concrete assemblies that were initially tested, and the SFRC assembly tested later.

Visual Observations - Plain Concrete

During the fire test, visual observations of the assembly were made every five minutes, or when a significant event occurred. Where practical, these events were documented via photographs as well.

For assembly PC-1, popping noises were heard almost immediately upon initiation of the heating process. Approximately 10 minutes after initial heating, cracks were becoming visible on the surface of the assembly with steam and boiling water being emitted from these cracks as shown in Fig. 3.15. At approximately 26 minutes, it was observed that the large deflection in the beams was causing the fireproofing to de-bond from the surface of the beams. The test continued with deflections increasing and moderate levels of cracking until the large deflections of the slab were sufficient to cause instability in the load splitter, at which point, it failed as shown in Fig. 3.16, this point was taken as failure of the assembly for the purposes of this research.

Fig. 3.15: Steam coming out of longitudinal crack in slab.

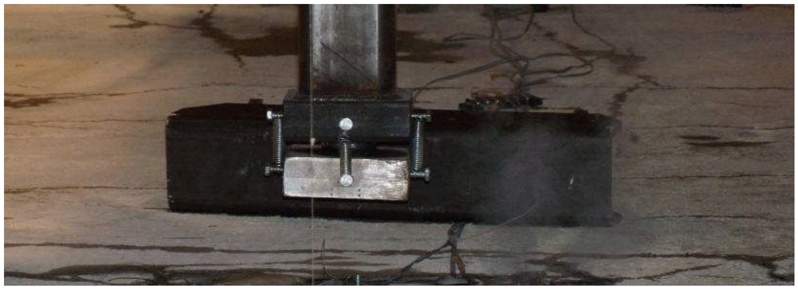

Fig. 3.16: Failure of load splitter during testing of assembly PC-1

Similar to the first lightweight concrete assembly, popping was heard early in the fire exposure for assembly PC-2 with the first sounds being heard at approximately 11 minutes. As the fire progressed, cracks began to form on the surface of the assembly with steam and boiling water being emitted from these cracks. After about 15 minutes of fire exposure, cracks were observed to form and grow parallel to the W12X16 beams. These cracks grew in length and depth similarly to those shown in Fig. 3.17. Finally at 27 minutes, the central unprotected beam was observed to fail as it could not longer support the load. Failure of the unprotected beam was accompanied by a punching failure of the concrete slab as seen in Fig. 3.18.

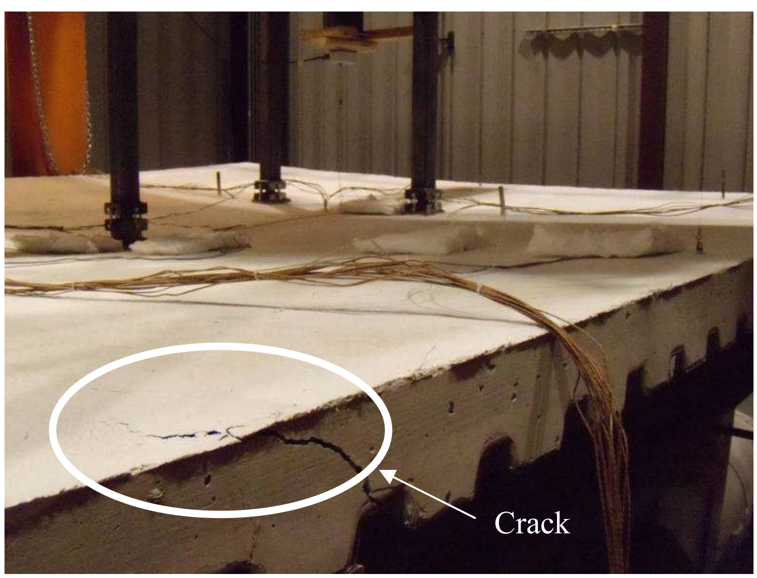

Fig. 3.17: Longitudinal crack at 90 minutes into fire resistance test

Fig. 3.18: Punching shear accompanying failure of the central beam in PC-2

Visual observations recorded during the testing of assembly PC-3 follow the same trend as those observed for assembly PC-2. Popping was heard in assembly PC-3 starting at approximately seven minutes, and was accompanied by the formation of cracks appearing on the surface of the specimen. It was observed, as was the case in the previous tests, that cracks formed parallel to the W12X16 beams at approximately 15 minutes. These cracks continued to grow in both length and depth as the fire exposure time increased. This trend continued until 31 minutes at which point the beam could no longer support the applied load, and the specimen failed. As was the case of assembly PC-2, failure of the beam in assembly PC-3 was accompanied by a punching failure of the slab as shown in Fig. 3.19.

Fig. 3.19: Punching shear accompanying failure of the central beam in PC-3

Post Fire Observations – Plain Concrete

Due to the extreme temperatures achieved during fire testing, it was not possible to trace the development of cracks during the tests. After the tests, observations were made on the fire exposed specimen regarding the deflected shape, the cracking pattern on the top of the slab, and the integrity of the beam network and connections.

The primary post fire observation is that the fire resistance achieved though composite beam-slab assemblies made with plain concrete is insufficient to meet the levels required in codes and standards. Assembly PC-1 failed at 51 minutes, PC-2 failed at 27 minutes, and assembly PC-3 failed at 31 minutes, all slabs developed a deflection basin similar to that shown in Fig. 3.20.

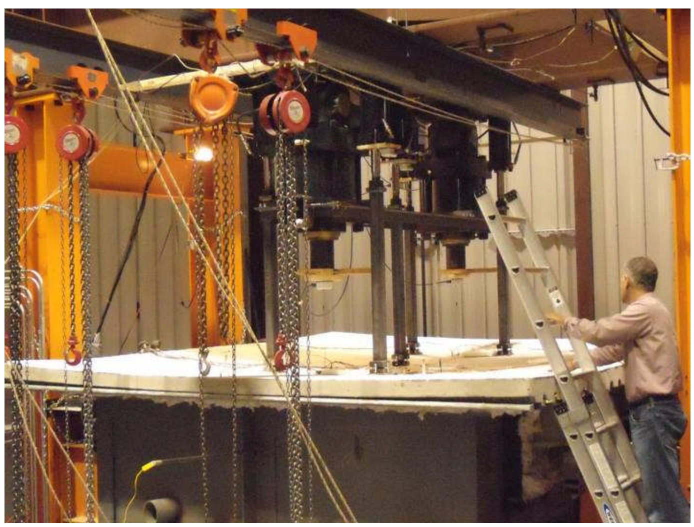

Fig. 3.20: Post fire deflected shape of the beam-slab assembly

Considerable insight can be gained on the response of the assemblies to fire exposure through examination of the cracking pattern on the top of the assembly. In all of the plane concrete assemblies, cracking was observed to follow the traditional yield line pattern until just prior to failure of the assembly. When the specimens failed due to softening of the heated central beam, a multitude of radial cracks rapidly formed from the central actuator to the perimeter of the heated region as observed in Figs. 3.21a-c. It should be noted in reference specifically to Fig. 3.21a that failure of this specimen occurred due to instability in the load splitter, as such, the same extent of cracking was not observed Fig. 3.21a as in the other specimens.

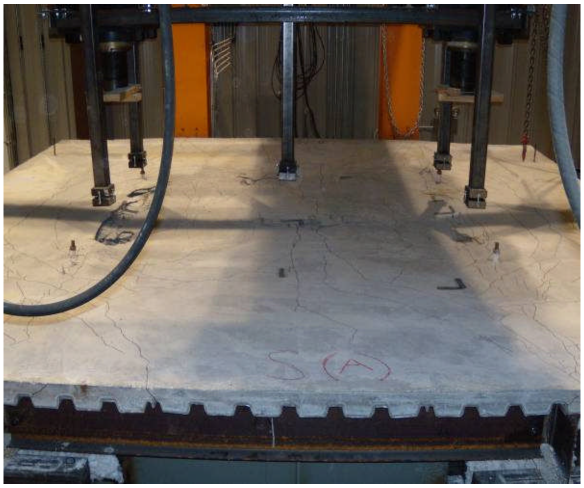

a) PC-1

b) PC-2

c) PC-3

Fig. 3.21: Cracking pattern on the top of the tested plain concrete assemblies after exposure to fire

Upon cooling of the specimens, they were removed from the furnace and the post fire condition of the assembly assessed. For assembly PC-1, due to the presence of one hour of fire protection on the surface of the central beam and failure being attributed to instability in the load splitting system, only minor deflections were observed in the central beam. Assemblies PC-2 and PC-3 however sustained appreciable damage as shown in Fig. 3.22, due however to the similarities between the post fire conditions of the specimens, only one figure is shown. From Fig. 3.22 it can be seen that significant yielding occurred in the unprotected W10X15 beam. This deformation is attributed to the inability of the slab to carry the entire load from the central actuator, as such, a high stress state existed in the unprotected beam causing considerable yielding of the section. Due however to the continual lateral support provided to the top flange of the section by the composite deck, no local or global instabilities were observed to develop in the beam.

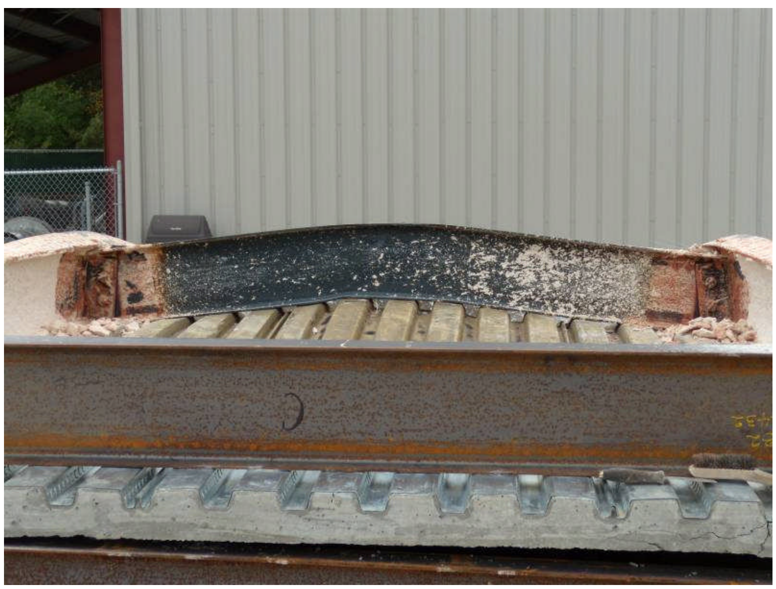

Fig. 3.22: Post fire condition of central beam in PC-2

Conditions observed in the connections following fire exposure are consistent with the deformations observed in the central beam. For assembly PC-1, only minor rotations were observed in the fin plate connections, and the bolts were observed to be fully functional with no damage to either the bolts or the holes through which the bolts pass. Assemblies PC-2 and PC-3 however revealed a different behavior as compared to assembly PC-1. The large deformations observed in Fig. 3.22 caused significant rotations in the fin plate connections (PC-2) and double angle connections (PC-3). These rotations were sufficient to cause shear deformations in the top bolts of the connections as shown in Fig. 3.23. For more detailed information on the response of the connections in these tests to fire exposure, the reader is directed to the literature (Wellman 2010).

Fig. 3.23: Post fire condition of connection bolts

Shear studs were observed to have no perceivable deformations at any location (on protected or unprotected beams) following the fire tests. A maximum temperature of 400 °C was observed in the shear studs. Even at these temperatures, no deformation of the shear studs was observed. This is of critical importance as it indicates that there was no slip between the steel and the concrete at any point during the fire exposure.

In all of the assemblies, the protected W12X16 girders sustained large deflections, but were not observed to fail. There was no indication of local or global failure of the W12X16 sections in any of the tests, though there were rotations observed in the W12X16 sections resulting from the forces generated through thermal expansion of the heated central beam.

For all of the tested plain concrete assemblies, the composite deck was observed to have almost completely delaminated from the concrete slab. It is assumed that the excessive pressure caused by steam escaping from the heated region of the test caused the decking to delaminate. While the decking was significantly discolored and delaminated from the concrete, there were no points where the deck ruptured, thus, the deck helped to protect the concrete from direct fire exposure.

Thermal Response – Plain Concrete

The temperature measurements recorded at various points throughout the thermocouple network can be used to illustrate the thermal response of the beam-slab assemblies. The three main components for consideration in the thermal analysis are the protected beam, the unprotected beam, and the slab. These components will be discussed separately in the following sub-sections.

<u>Protected Beam – Plain Concrete</u>

For all of the lightweight concrete assemblies, the W12X16 beams were provided with one hour of fire protection, and in assembly PC-1, the central beam was provided with the same protection. Temperatures were monitored on the top and bottom flanges as well as on the web of these beams at several cross sections. Due to the ASTM fire exposure being used in all of the PC cases, and the assemblies failing prior to reaching the prescribed decay phase, the thermal results from all of these cross sections in all of the tests are appreciably similar, and as such, the following discussion should be assumed to apply to all of the beams provided with one hour of fire protection.

From Fig. 3.24, it can be seen that the temperatures in the bottom flange of the beam are the hottest followed by the web then the top flange. When the central protected beam failed in assembly PC-1, the temperature in the bottom flange of the beam was approximately 600 °C as indicated in Fig. 3.24. As such, the beam had approximately 55% of its ambient temperature capacity remaining when the deflection of the slab caused instabilities in the load splitter and it failed to support the applied load. For assemblies PC-2 and PC-3, the one hour fire protection applied to the W12X16 girders provided sufficient strength that failure was observed in the unprotected central beam.

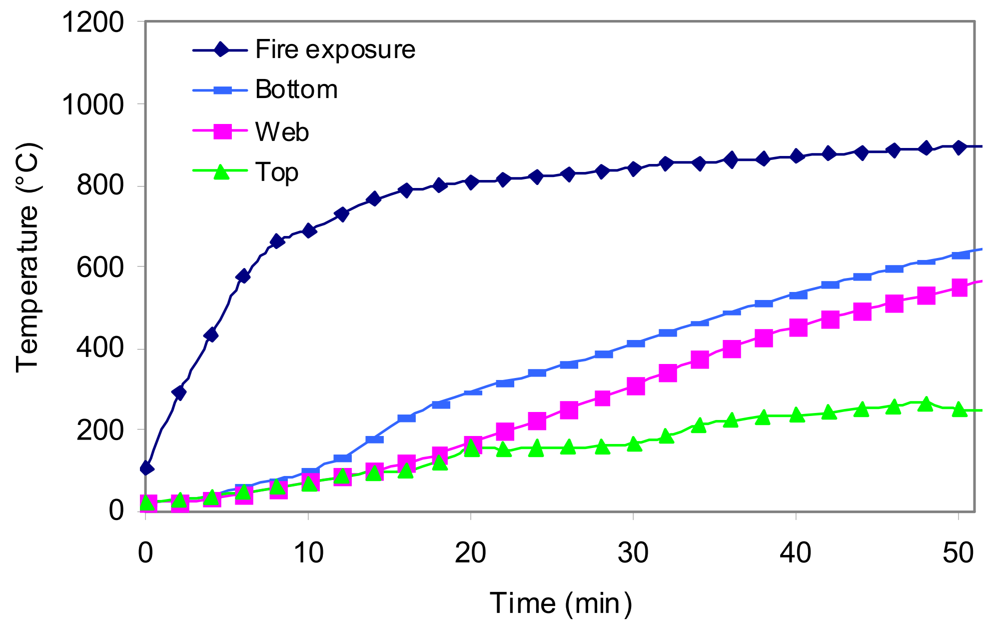

Fig. 3.24: Temperatures in the one hour protected (W12X16) beam with fire exposure time

Unprotected Beam – Plain Concrete

As was the case with the protected beam, temperatures were monitored in the bottom flange, web, and top flange of the unprotected beam, these temperatures are plotted in Fig. 3.25. Fig. 3.25 shows temperatures recorded for assembly PC-3 due to the similarities between the thermal response for the unprotected beam in assemblies PC-2 and PC-3 only one figure is provided. It is observed from Fig. 3.25 that the temperatures in the unprotected beam follow those of the fire closely (reaching a maximum temperature of 700 °C) due to the high fire exposed surface area to the weight ratio (W/D) of the section. This W/D ratio causes a slight "lag" in temperature between the fire exposure and the steel temperatures. At failure of assemblies, PC-2 and PC-3 had approximately 17% of their ambient temperature strength remaining.

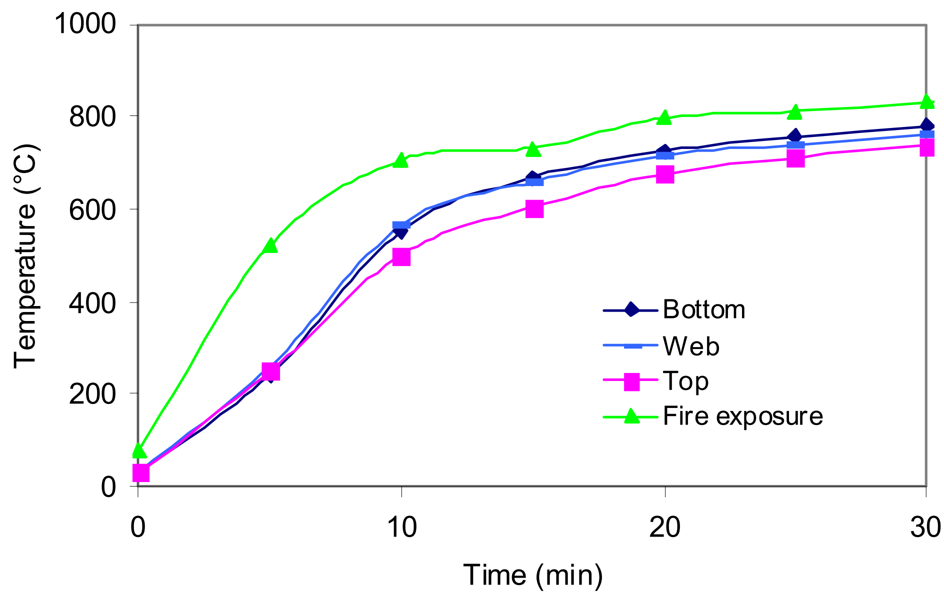

Fig. 3.25: Temperatures in the unprotected beam as a function of fire exposure time

<u>Slab Temperatures – Plain Concrete</u>

Temperatures at the bottom, mid-depth, and top of the plain concrete slab as recorded for assembly PC-1 are shown in Fig. 3.26. Only results for PC-1 are presented since the thermal results from assemblies PC-2 and PC-3 are similar with the exception of the shorted fire duration time, as such, this discussion applies to all of the plain concrete assemblies. Of particular note from Fig. 3.26 is the observation that temperatures on the unexposed surface are sufficiently low that they do not control failure of the specimen. It can also be seen in Fig. 3.26 that the temperatures at the bottom and mid-depth of the slab experience a rapid increase at about 30 minutes. This is attributed to the extensive cracking of the slab permitting the heat from fire to penetrate the slab more readily as deflections increase.

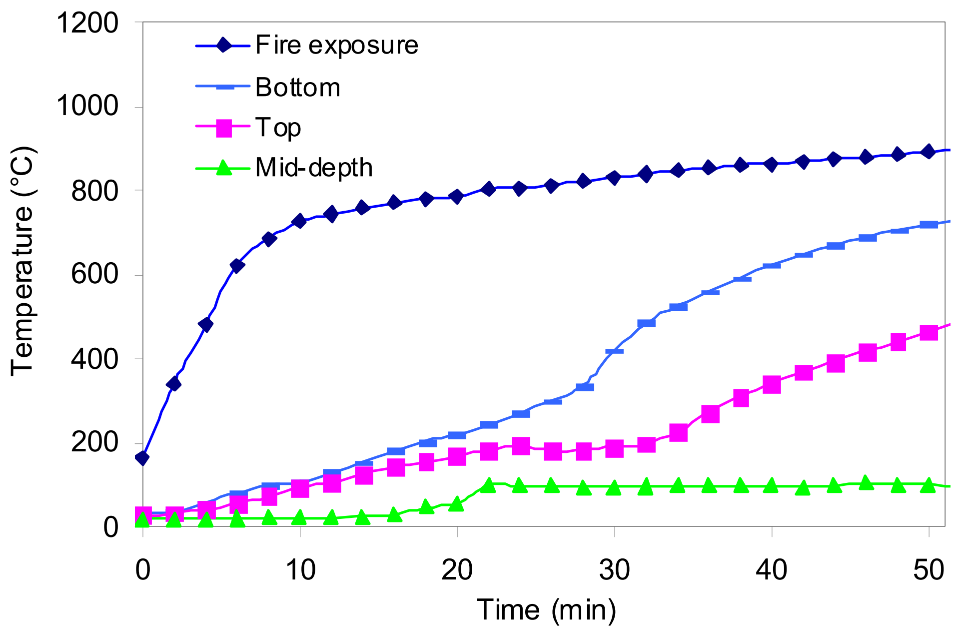

Fig. 3.26: Temperatures at various depths of the lightweight slab as a function of fire exposure time

Structural Response – Plain Concrete

Monitored structural responses consisted of strains and deflections on the top surface of the assemblies at the locations noted previously. Due to the poor response of the plain concrete assemblies (short fire resistance), it was necessary to test advanced material systems (SFRC) in a similar assembly to develop practical alternatives for achieving fire resistance. As such, the structural response of the plain concrete assemblies will be presented only briefly here, for a full description of the test results, the interested readier is directed to the literature (Wellman 2010).

Strains – Plain Concrete

Fire exposure is one of the most severe conditions to be duplicated in a laboratory environment, as such, accurate measuring of sensitive data such as strains is inherently difficult. To further complicate the issue, the adhesives used to attach strain gages to the top surface of the assembly fail to adhere above 80 °C. In the case of the 101.6 mm lightweight aggregate slabs, temperatures above 80 °C are achieved in approximately 15 minutes as seen in Fig. 3.26. The rapid failure of the strain gages in the fire exposure severely limits the information available from this portion of the data network, and as such, only a brief discussion on strains can be presented.

During the initial part of the fire exposure, compression resulting from application of the mechanical loading is observed over the surface of the assembly. The magnitude of the compressive strains decreases as fire exposure time increases (presumably due to thermal expansion of the central beam), however, the strain gages fail prior to transitioning to the tension regime, thus little information can be gained from further examination of strains.

Deflections – Plain Concrete

A significant deflection rate is observed at the center of the plain concrete assemblies, and all three of the assemblies fail in less that one hour as shown in Fig. 3.27. Assembly PC-1 was observed to withstand the fire exposure for the longest time supporting the applied load for 51 minutes with an ultimate deflection of 78 mm at failure. Assemblies PC-2 and PC-3 did not perform as well due to the absence of fire protection on the central beam in these assemblies. Failure was observed in assembly PC-2 at 27 minutes with an ultimate deflection of 133 mm. Assembly PC-3 was observed to fail at 31 minutes with a total deflection of 132 mm as seen in Fig. 3.27.

Upon inception of the fire exposure, the assemblies are all observed to start deflecting as seen in Fig. 3.27. These deflections are attributed to the thermal expansion of the supporting steel sections for the initial portion (15 minutes) of the fire exposure. As the temperatures continue to increase in the case of PC-2 and PC-3, the unprotected beam continues to lose strength, and significant yielding of the section is observed. This continued until failure of the assembly at the respective times indicated above.

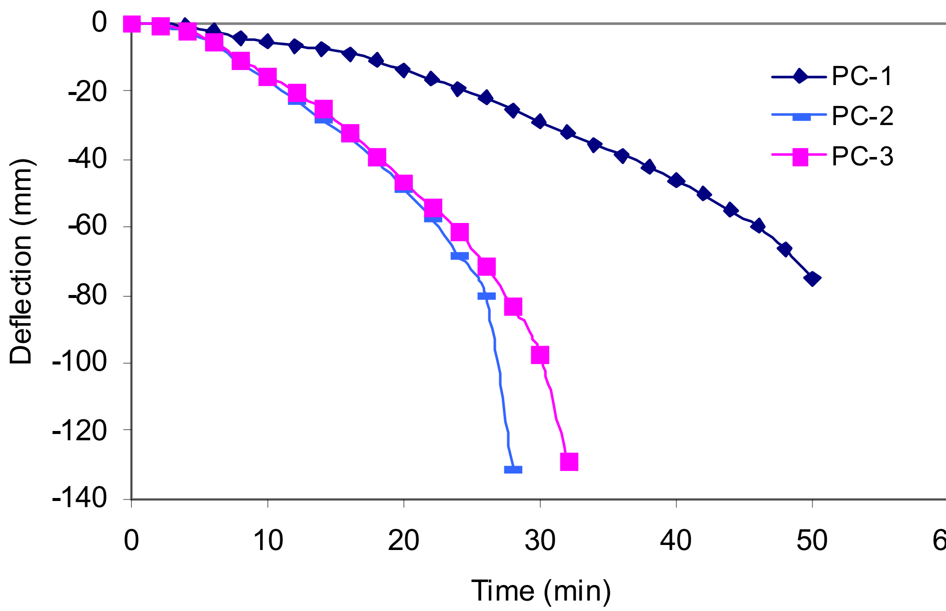

Fig. 3.27: Center point deflections recorded during testing for assemblies made with plain concrete

Failure of specimen PC-1 was observed to differ slightly from that of either PC-2 or PC-3 as observed from Fig. 3.27. Due to the presence of fire protection on the central beam for assembly PC-1, the heating rate of the beam was significantly slower than in the other tests. As such, it takes more time (25-30 minutes) for the supporting steel beam to be sufficiently weakened that yielding begins to dominate the response of the assembly. For the period from 25 minutes to the end of the fire exposure, the beam is slowly increasing in temperature and composite action is developed in the assembly as it deflects. This permitted the assembly to withstand fire exposure for 51 minutes prior to developing an instability in the load splitter which lead to termination of the test.

Overall, from the fire resistance tests on composite beam slab assemblies made with plain lightweight concrete, it was observed that composite action with plain concrete enhances fire resistance over that observed for structural steel elements tested individually. However, it was further observed that the fire resistance achieved though this composite action is insufficient to meet the levels required in codes and standards. As such, an alternative material system (SFRC) was considered in a similar beam slab assembly and exposed to the same fire exposure shown in Fig. 3.14. The response of the SFRC assembly including visual observations, post fire analysis, and thermal and structural responses are presented in the following section.

Visual Observations - SFRC

During the heating portion of the fire exposure, significant popping was heard starting at about 5 minutes as the steel deck de-bonded from the concrete. Often times, the deboning and popping was accompanied by bursts of steam coming out from around the perimeter of the slab between the deck and the concrete.

After forty minutes of fire exposure, the unsupported edge of the slab was observed to lift vertically by a significant amount as seen in Fig. 3.28. This is attributed to thermal expansion and curvature of the supporting steel sections as mentioned previously.

After approximately 50 minutes of fire exposure, as was observed in the plain concrete slabs, a crack formed through the thickness of the slab next to the W12X16 beam on both edges as shown in Fig. 3.29.

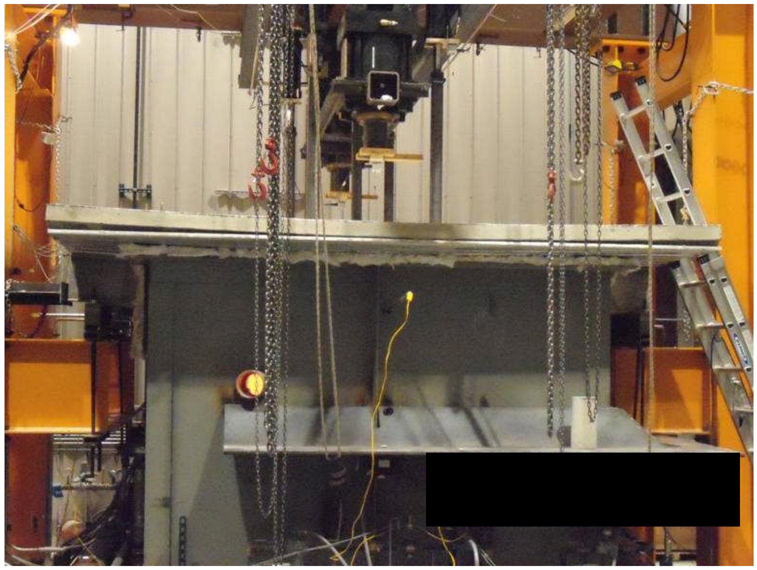

Fig. 3.28: Lifting of unsupported edge from the furnace and separation from the deck

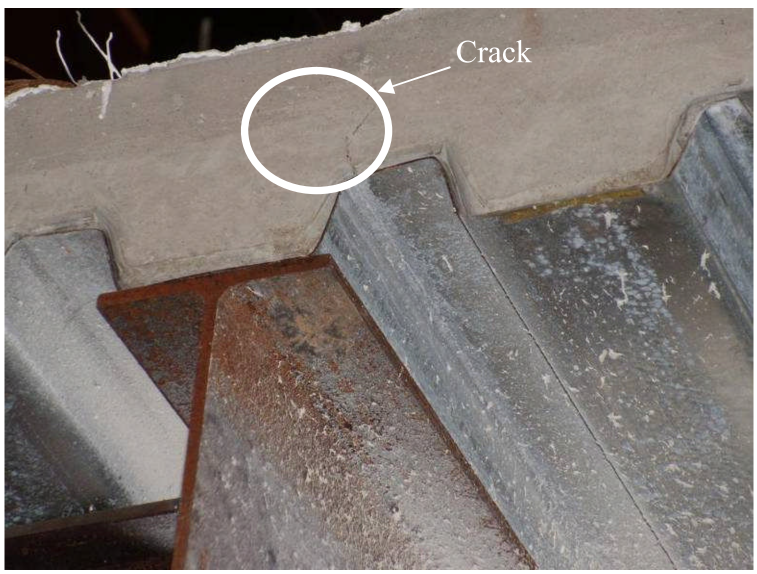

Fig. 3.29: Crack formation next to W12X16 section

Following formation of the crack shown in Fig. 3.29, the crack began to grow rapidly until approximately 90 minutes of fire exposure, at which point the crack reached steady state. During this time, significant amounts of steam (as in Fig. 3.15) was observed to be coming out of the crack as additional popping occurred in the slab. After the steam had finished coming out of the crack, it was observed that the crack was significantly larger than when the steam first began

Following propagation of the crack over the entire length of the assembly (parallel to the W12X16 beam) a discontinuity in the curvature of the slab was observed as shown in Fig. 3.30. This corresponds to the point when the slab fractured, the edge deflections returned to zero, and the unsupported edge was resting on the furnace.

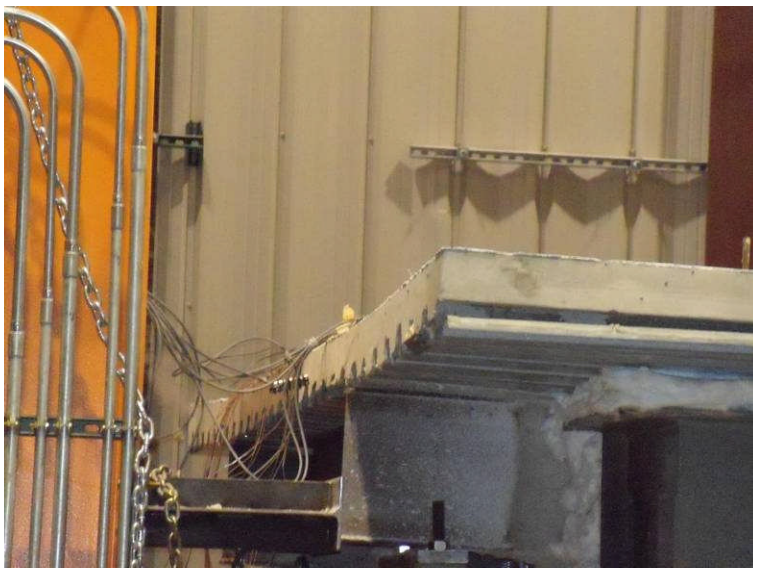

Fig. 3.30: Discontinuous curvature along slab edge

Post Fire Observations - SFRC

The primary post fire observation is that the assembly was able to support the applied load for the entire fire exposure, including the decay phase, with no failures or signs of failure. At no point did deflections increase rapidly (as seen from the recorded deflection data), or the assembly show signs of eminent failure. The deflected shape of the specimen is shown in Fig. 3.20 from which it can be seen that the slab deflected downward causing a deflection basin to form in the center of the assembly. This deflection basin recovered to a total deflection of approximately 95 mm.

Given that the unprotected beam reached temperatures in excess of 900 °C, it can be assumed that the beam offered relatively little support to the assembly during the peak of the heating phase. This would cause the central portion of the slab to essentially behave as a two way slab. Under this postulate, it is reasonable to assume that the central portion of the slab would crack according to the traditional yield line failure pattern as was the case with the plain concrete slabs. This cracking pattern was however not observed in the post-fire test assessment due to the high tensile strength of SFRC. The cracking pattern observed on the top of the beam-slab assembly is shown in Fig. 3.31 (cracks highlighted to enhance visibility).

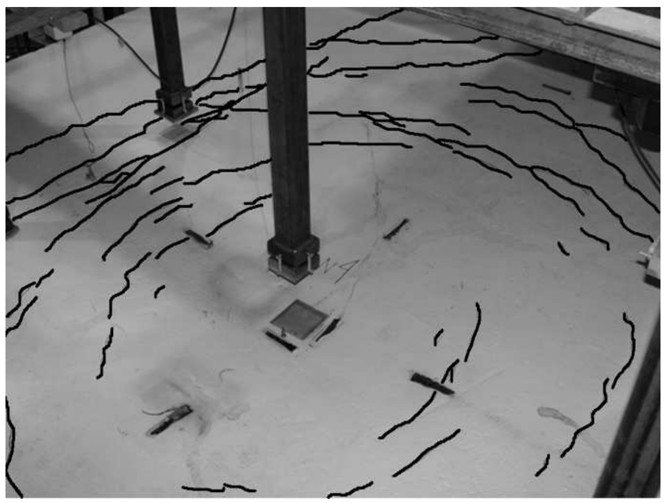

Fig. 3.31: Cracking pattern on the top of the tested SFRC beam slab assembly after exposure to fire

Critical in Fig. 3.31 is the observation that the cracks take the form of concentric circles around the central load actuator. This cracking pattern is consistent with the development of tensile membrane action. The deflection of the slab, causing a deflection basin, caused cracks to form in concentric circles as the tensile strains developed in a radial pattern outward from the center of the slab. These cracks were quickly arrested by the steel fibers that bridged the cracks, allowing the assembly to survive complete design fire burnout.

After the assembly had cooled sufficiently, one of the unsupported edges was removed to allow entry to the furnace and subsequent assessment of the steel beam network. It was found during this inspection that the assembly sustained relatively little damage considering the extreme temperatures and loading to which it was subjected. As seen in Fig. 3.32, the unprotected beam underwent considerable deflection, but never lost stability as indicated by the absence of local or global buckling.

Fig. 3.32: Post fire condition of central unprotected beam

In the same manner, only minor damage was observed in the connections between the beams. While minor rotations were observed in the fin plate connections, the bolts were observed to be fully functional with no damage to either the bolts or the holes through which the bolts pass. Fig. 3.33 shows the condition of one connection following the fire exposure (both were similar thus only one is shown).

Fig. 3.33: Post fire condition of fin plate connection

As was the case with the unprotected beam and the connection, only minor damage was observed in the protected beam. The center of the beam had deflected downward and retained some deflections as residuals from the fire exposure. There was however no indication of imminent failure in the protected beam in the form of either local or global buckling.

As was the case with the plain concrete assemblies, the composite deck was observed to have almost completely delaminated from the concrete slab. It is assumed that the excessive pressure cause by steam escaping from the heated region of the test caused the decking to delaminate. While the decking was significantly discolored and delaminated from the concrete, there were no points where the deck ruptured, thus, the deck helped to protect the concrete from direct fire exposure.

Lastly, as was the case with the plain concrete slabs, the shear studs were observed to have no perceivable deformations at any location (on protected or unprotected beams) following the fire tests. This is of critical importance as it indicates that there was no slip between the steel and the concrete at any point during the fire exposure.

The observation that the assembly withstood the effects of fire and load while sustaining relatively little damage led to the development of the postulate that the use of SFRC in composite floor assemblies can significantly enhance their fire resistance. In this experiment, the behavior of the floor assembly was enhanced to the point where an unprotected steel beam, which is commonly assumed to have fire resistance on the order of 15-20 minutes, was able to survive burnout under a design fire exposure.

Thermal Response – SFRC

The temperature measurements recorded at various points throughout the thermocouple network can be used to illustrate the thermal response of the beam-slab assembly. The three main components for consideration in the thermal analysis are the protected beam, the unprotected beam, and the slab. These components will be discussed separately in the following sub-sections.

<u>Protected Beam – SFRC</u>

Temperatures were monitored in the bottom flange, top flange, and the web of the protected W12X16 beam at a total of 6 locations (see Fig. 3.8a). The temperatures in the respective components were significantly similar at each of the cross sections monitored. As such, only one temperature is plotted for each of the protected beam components (bottom flange, top flange, and web) as well as the furnace temperature in Fig. 3.34.

From Fig. 3.34 it is clear that the temperatures experienced by the top flange are lower than those in the bottom flange and web of the beam, this is primarily due to the cooling effect of the slab to the top portion of the beam. In addition to cooling the top flange of the beam, the concrete slab also limits the fire exposure on the beam to three-sided exposure. This causes the top flange to experience notably lower temperatures than the rest of the beam. On the contrary, the bottom flange of the beam being exposed on all sides and not being directly connected to the slab experiences the highest temperatures observed in the cross section. Lastly, the web temperatures are between those in the top and bottom flanges. In large part this is due to the heating and cooling effects of the bottom and top flanges on the web respectively.

It can also be seen from Fig. 3.34 that the temperatures in the protected beam reach their maximum of 700 °C approximately 30 minutes after the fire enters the decay phase. This is attributed to the fact that though in the decay phase, the fire is still hotter than the steel section, thus, the section keeps increasing in temperature until the fire temperature drops below that of the steel section. As the beam temperatures decrease, it is observed that temperatures in the beam cross-section begin to converge. This is due to the slow rate of cooling allowing sufficient time for the section to reach relative equilibrium, facilitated by the high thermal conductivity of steel.

Peak temperatures in the protected beam were sufficient to cause the bottom flange of the beam to lose approximately 75% of it yield strength, and the web to lose approximately 60% of it yield strength. Due to the cooling effect of the slab, the top flange of the beam experienced no loss of strength.

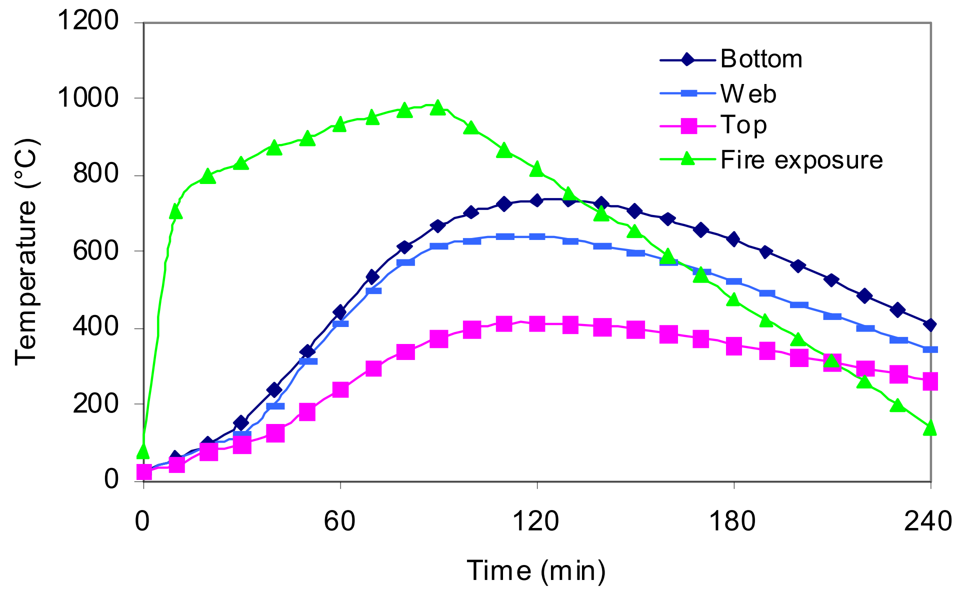

Fig. 3.34: Temperatures in the protected (W12X16) beam with fire exposure time

<u>Unprotected Beam – SFRC</u>

As was the case with the protected beam, temperatures were monitored in the bottom flange, web, and top flange of the unprotected beam, these temperatures are plotted in Fig. 3.35. This instrumentation layout was used only in the center of the beam and no duplicate thermal results were recorded due to the limited availability of data acquisition channels.

Temperatures in the unprotected beam follow those of the fire closely (reaching a maximum temperature of 950 °C) due to the high fire exposed surface area to the weight ratio (W/D) of the section. This W/D ratio causes a slight "lag" in temperature between the fire exposure and the steel temperatures. Thermal lag is also responsible for the temperatures in the steel beam in the cooling phase exceeding the fire temperatures. Additionally, in the cooling phase, the temperature in the top flange of the beam exceeds those in the rest of the beam. This is attributed to the fact that the slab, which keeps the top flange cooler in the heating phase, heats the top flange of the beam during the cooling phase, keeping it warmer than the fire temperature.

At peak temperature, the entire unprotected cross-section had about 5% of its ambient yield strength remaining based on the strength-temperature relationships for steel. Yet, as will be seen in the discussion on structural response, the assembly did not fail despite losing almost all of the strength in the central (loaded) beam.

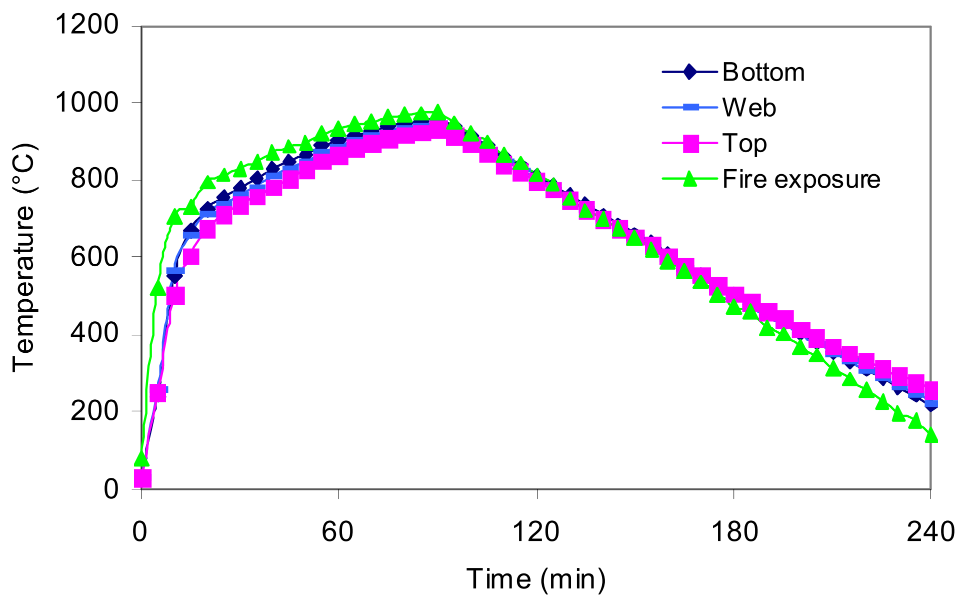

Fig. 3.35: Temperatures in the unprotected beam as a function of fire exposure time

Slab Temperatures – SFRC

Temperatures in the slab were monitored in the thick part of the ribbing as presented in Fig. 3.8b. Thermocouples were located on the steel decking, the shrinkage steel, and on the top surface of the slab. While four points in the slab were instrumented in similar fashion, again, the same trends were observed in all of the locations, and as such, only one location will be presented. Fig. 3.36 shows the temperatures across the depth of the slab as a function of fire exposure time. Intuitively, the temperatures decreases with increasing distance from the fire exposed surface. The temperature at the steel-concrete interface in the deck experienced the highest temperatures, with a peak temperature of 800 °C that roughly coincided with the peak fire temperature. The thermocouples located on the shrinkage reinforcing experienced temperatures in excess of 400 °C with a peak temperature occurring approximately 45 minutes after the peak fire temperature, while the top surface of the slab reached a maximum temperature of 180 °C approximately three hours after the peak fire temperature. The delay in peak temperatures associated with increasing depth is due to the low thermal conductivity of concrete.

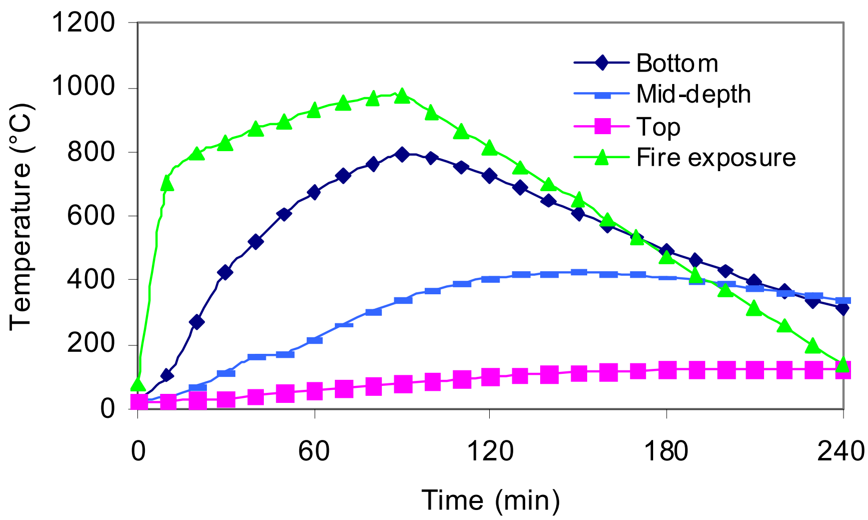

Fig. 3.36: Temperatures at various depths of the slab as a function of fire exposure time

Temperatures at the deck-concrete interface are observed in Fig. 3.36 to lag the fire exposure temperature with a plateau occurring at approximately 100 °C which lasted approximately 20 minutes. This is attributed to the presence of water in the concrete. When the concrete reaches 100 °C, the temperature stabilizes until all of the free water is driven out of the concrete. This results in the temperature profile seen in Fig. 3.36.

Structural Response – SFRC

Instrumentation to capture the structural response of the assembly consisted of strain gages and displacement transducers. The recorded data is utilized to trace the structural response of the beam slab assembly.

<u>Strains - SFRC</u>

For the same reasons state in regard to the plain concrete slabs, it is difficult to acquire accurate strain information under fire exposure conditions. As such, the following sections analyze the strain data from a qualitative stance as the thicker concrete slab permitted the strain gages to return data for an extended period of time as compared to the plain concrete slabs. The strain data is divided into three sections, the center point strain gages which were located 76 mm from the central load application point, the mid-slab strain gages which were located 610 mm from the center of the slab, and the outside strain gages which were inset 305 mm from the edge of the slab. The location of these strain gages can be more clearly seen in Fig. 3.8d. In the following discussion, when a strain gage no longer returned coherent readings, the channel is terminated in the respective plots.

Due to the need to accommodate a spreading plate for the loading actuator, the strain gages at the center of the specimen were located 76 mm from the center of the slab, and were oriented at 90° from each other. Data from these gages is plotted as a function of fire exposure time in Fig. 3.37

below, strain gage 135 is oriented parallel to the unprotected steel beam, while strain gage 136 is perpendicular to the unprotected beam. Both strain gages are slightly under compression at the beginning of the test due to the mechanical loading. As the test continues, the strain gages register considerably more compression, then compression starts to decrease and strain gage 136 enters tension before the gage fails. Gage 136 approaches zero strain, but just prior to failure again goes into compression.

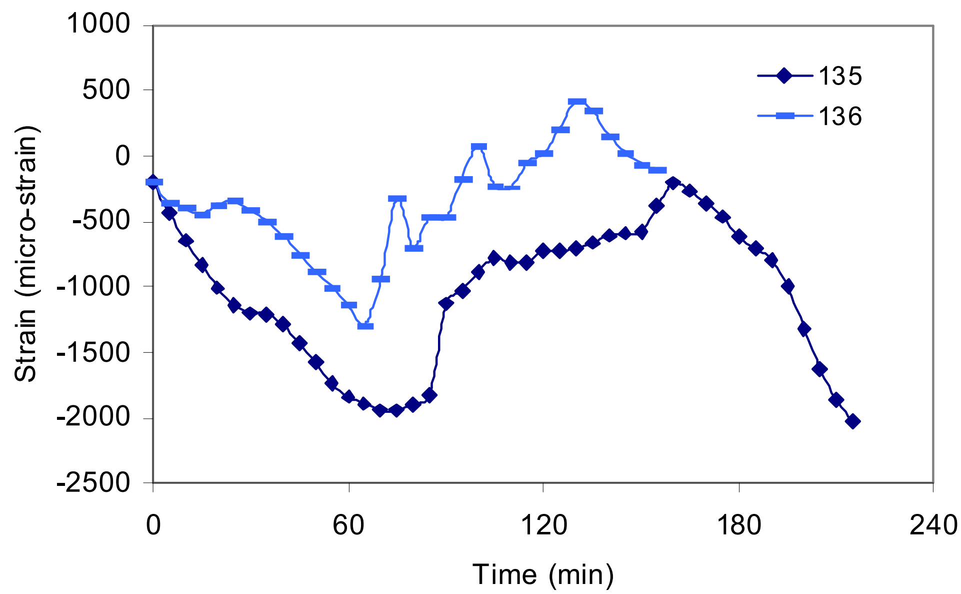

Fig. 3.37: Strains at central strain gages (76 mm offset) as a function of fire exposure time

Initially, the strain gages are in compression due to the mechanical loading being transferred across the slab via bending. This compression on the top of the slab is observed until the slab is sufficiently weakened that it can no longer support the slab via bending. At this point, tensile membrane action begins to carry a portion of the load. As the slab develops tensile membrane behavior, the compression decreases at both strain monitoring locations with one gage entering into tension while compression decreases at the other. At the end of the fire exposure, when the entire specimen is cooling, both strain gages show an increase in compressive strain; this can be attributed to the cooling of the specimen and the relative thermal shrinkage of the assembly.

Of particular interest in Fig. 3.37, is the observation that the strain gages though very close in proximity, and having similar initial readings, register significantly different results during the fire test. This is attributed to the orientation of the strain gages relative to the unprotected steel beam. Strain gage 135, being parallel to the rapidly expanding and contracting steel beam experiences stresses caused by the relative thermal expansion difference between steel and concrete. Strain gage 136 is relatively immune from this thermal expansion incompatibility being oriented perpendicular to the steel beam, and hence, the different strains observed in Fig. 3.37 result.

The second group of strain gages that can be readily separated for discussion purposes are those located 610 mm from the center of the slab. These strain gages are all oriented radially from the center of the slab. Strain gages 132 and 134 are located on top of (and parallel to) the unprotected W10X15 section, while strain gages 138 and 140 are located away from any steel members as seen in Fig. 3.8d above. Strain as a function of fire exposure time for these gages is shown in Fig. 3.38 below.

While all of the gages start at relatively the same point in compression due to the mechanical loading, the two gages (132 and 134) located over the steel beam respond differently than those away from the steel beam, this is attributed to the difference in thermal expansion between steel and concrete as discussed previously. Early in the fire exposure, all of the strain gages begin to register increasing compressive strains. This trend is continued until approximately 60 minutes of fire exposure, at which point all of the gages show a rapid decrease in compression strain with three of the four gages transitioning to the tensile region as seen in Fig. 3.38. At this transition point, there is a disconnect appearing in the data for gage 134, this is due to the strain gage failing to register strain readings during this time period. After the transition from compression to tension, the strain gages stay in the tensile region for as long as data is available with the exception of gage 140 which transitions back into the compression region in the cooling phase of the fire due to the decrease in thermally induced strains.

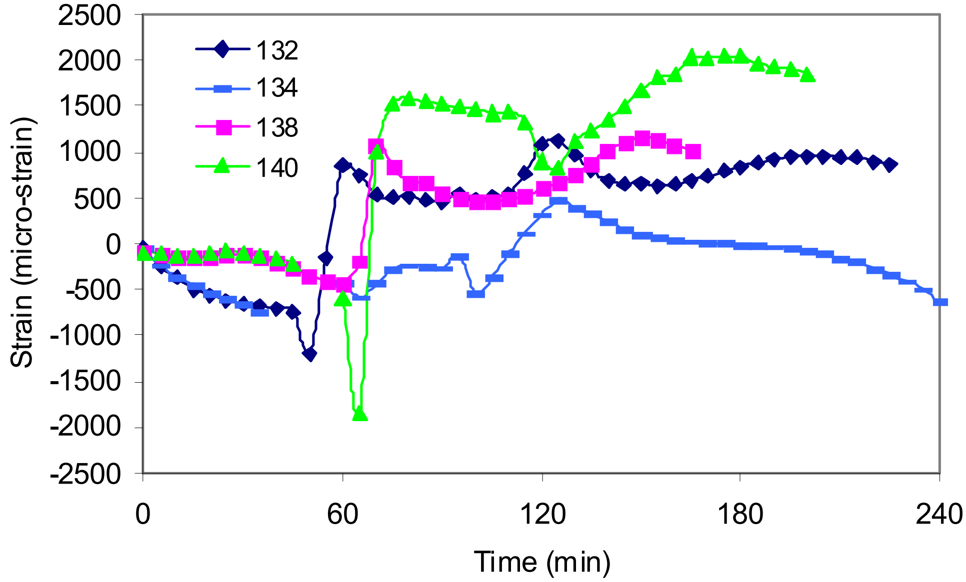

Fig. 3.38: Strains observed at the middle of the slab as a function of fire exposure time.

Considering that the strain gages are located on the top of the slab, the only way for the strain gages to experience tension in the given loading configuration, is if the entire depth of the slab is experiencing tension. As such, the existence of tensile forces as indicated by three of the four strain gages indicates that the slab has developed tensile membrane behavior.

The final group of strain gages to be discussed is those inset 305 mm from the edge of the slab as shown in Fig. 3.8d. As observed in Fig. 3.8d, these strain gages are oriented parallel to the edge to which they are closest. Strain gages 131 and 133 are on the unsupported edges of the slab, while gages 139 and 137 are located almost over the edge W10X15 beams (which were not exposed to fire). Fig. 3.39 shows the strain at the edge of the slab recorded by these strain gages as a function of fire exposure time.

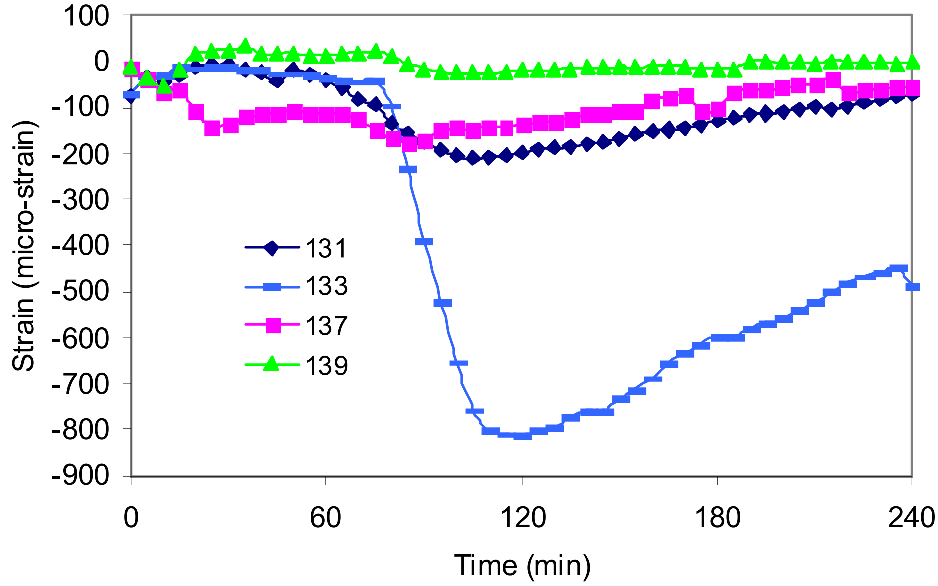

Fig. 3.39: Strains recorded at the edge of the slab (305 mm inset) as a function of fire exposure time

Strain gages 137 and 139 being located above the unheated steel beam show relatively little change during the course of the fire exposure due to the high strength at that location relative to other locations on the slab (due to the presence of the steel beam below the strain gages). Strain gages 133 and 131 however show comparatively interesting results. At one hour, strain gage 131 begins to develop compressive forces while strain gage 133 does not develop these forces until approximately 80 minutes of fire exposure. These times roughly coincide with the times at which the mid-slab strain gages transition to tension. Compression in the perimeter of the slab being an indicator of tensile membrane behavior, serves to reinforce the observation that tensile membrane action was developed and helped to transfer the load to the cooler parts of the structure at this time.

In Fig. 3.39, it is clear that while strain gages 131 and 133 transition into the compression zone, gage 133 developed far more compressive strain than gage 131. Given the symmetry of the specimen there should not be such a discrepancy between similarly placed gages. As discussed in the visual observations section, a large crack formed along the outside edge of the W12X16 next to strain gage 131. This crack occurring over the full depth and length of the specimen, is believed to have significantly altered the force transfer across that section. Hence, the compressive forces could not be transferred across that discontinuity, causing gage 133 to register significantly higher compressive forces as shown in Fig. 3.39.

Strain data being inherently volatile in fire resistance experiments should be used with considerable caution. The preceding qualitative assessment of the strains recorded during the describe fire resistance test indicate that the slab developed tensile membrane action, with tensile forces in the center of the slab and compressive force around the perimeter. This hypothesis is further reinforced by the cracking pattern discussed in the post fire exposure assessment presented in previous sections.

Deflections – SFRC

As discussed in the instrumentation section, vertical displacements were recorded at a total of nine locations over the unexposed surface of the slab (Fig. 3.8e). Due to the critical nature of displacements for the validation of computational models, five of the displacement transducers were redundant, and as such, the results obtained are not unique, and hence, will not be discussed. The four unique data sets are those corresponding to the supported edge (over the unheated 10X15), the center of the slab, the connection of the W10X15 to the W12X16, and the center of the unsupported edge. The deflection time history recorded by these four displacement transducers is presented in Fig. 3.40 and will be discussed independently below.

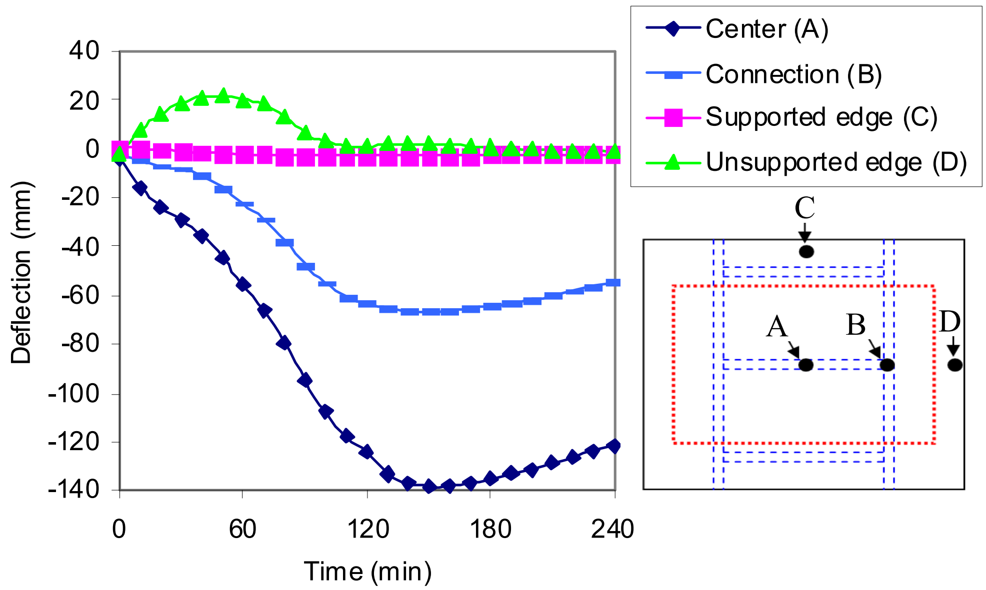

Fig. 3.40: Deflection time history in a beam slab assembly exposed to fire

Early into the fire exposure, the deflections of the slab over the connection between the beam and girder are relatively small, and remain essentially constant due to the insulation protecting the girder from the effects of fire. The deflections at the center of the slab however increase rapidly during this time. This can be attributed to the thermal expansion of, and loss of stiffness properties in, the unprotected W10X15 beam. Due to the heat from fire, the unprotected steel beam undergoes thermal expansion which caused the beam-slab assembly to deflect downward. In addition to the thermally induced downward deflection, the unprotected steel beam is losing strength and stiffness due to the increasing temperatures in steel from fire.

Between 20 and 90 minutes of fire exposure, the deflections increase slowly at both the center of the slab, and above the connection between the beam and the girder. The deflections at the connection between the beam and the girder are primarily caused by the slow heating of the protected W12X16 girder weakening the member, and allowing it to deflect under the load. The deflection at the center of the slab however, is due to further weakening of the unprotected beam and the weakening of the concrete due to the heat from fire. The temperatures reached in the steel beam by 90 minutes are in excess of 900 °C, thus, the remaining stiffness in the steel beam is relatively insignificant (about 6.7% of ambient temperature). The loss of stiffness from the unprotected beam causes the slab to deflect downward more than 100 mm until the majority of the load from the central actuator (90 kN) is transferred through the slab via TMA.

After 90 minutes of fire exposure, the fire temperatures begin to decrease due to the presence of a decay phase. At this time, the temperatures in the unprotected steel beam are in excess of 900 °C. As the fire temperatures start to decrease, the temperatures in the unprotected steel beam decrease at the same rate. The decreasing temperatures allow the steel beam to recover its strength and stiffness. As the steel beam re-gains its strength, it again begins to contribute to the strength capacity of the assembly. The strength contribution from the unprotected beam in combination with the thermal contraction of the unprotected beam causes the deflections in the assembly to stabilize at 130 mm by 150 minutes of fire exposure.

After 150 minutes of fire exposure, all parts of the assembly are cooling and subsequently regaining strength. The combination of increasing strength and thermal contraction due to cooling causes the assembly to rebound through out the duration of the fire exposure.

Supported edge displacement is relatively constant for the entire duration of the fire exposure. A maximum downward deflection of 2 mm was reached during the fire exposure at this location. This deflection is due to the downward deflection in the center of the slab causing the perimeter of the slab to rotate on the supports, resulting in a minor deflection of the supported section.

The unsupported edge however, shows a very unique response compared to the rest of the assembly. It is observed in Fig. 3.40 that the unsupported edge of the specimen rises vertically early in the fire exposure. This behavior is confirmed by observations taken during the test, both the direction and magnitude of this deflection was visually confirmed at the time of testing. The upward translation observed at this location is due to the thermal expansion of the bottom of the slab, combined with the displacement caused by the mechanical loading. When the slab is initially heated, the bottom of the slab expands relative to the top. Inside the network of steel beams, this causes the slab to deflect downward and place the central strain gages in compression as noted previously. On the unrestrained edges however, the thermal expansion of the concrete on the bottom of the slab just causes the unsupported edge to curve up and avoid stress development from thermally induced strains. In addition to the thermal strains, the center of the assembly deflects downward in the center relative to the connection as discussed in the preceding section. These deflections cause the assembly to be sloped at the connection between the beams. This slope, in combination with the thermal expansion on the bottom of the slab outside the steel beam network, causes the unsupported edge to translate vertically upward as observed in the test. Between 20 and 90 minutes of fire exposure, the unsupported edge is observed to relax downward again until reaching its original location, where it remains essentially unmoved for the remainder of the test. This behavior corresponds to the time at which large cracks began to develop along the outside edge of the W12X16 sections. These cracks started in the slab at the ends of the beam then slowly propagated toward the center of the specimen, joining in the center at approximately 90 minutes. This crack formation caused a discontinuity in the slab, and resulted in an inability to transfer forces to the unsupported edge, thus allowing it to return to its original location. For the remainder of the test, the unsupported edge of the slab rested on the edge of the furnace and offered little support to the remainder of the assembly.

3.3.7 Summary

Due to the absence of experimental data on the response of composite floor assemblies to fire exposure, it was necessary to conduct four novel assembly level fire resistance tests to acquire data for numerical model calibration. In the fire resistance tests discussed in this section, three lightweight slabs and a SFRC slab were compositely cast atop networks of 5 steel beams, some of which were unprotected, and exposed to ASTM E-119 fire exposure for 90 minutes followed by a 5.6 °C/min decay phase. For the full duration of the fire tests, temperatures, strains, and deflections were recorded at various locations over the specimen. These data indicate that the SFRC assembly survived the complete fire exposure reaching a maximum deflection of 137 mm in the center of the specimen, while the lightweight concrete assemblies all failed in less than an hour. During the post fire assessment, it was observed that the cracking pattern on the top surface of the SFRC specimen was one of concentric circles around the central actuator while those observed on the top of the lightweight concrete assemblies initially followed the yield line pattern transitioning to radial cracks by the end of the fire test. As such, it is believed that tensile membrane action was developed in the SFRC slab, and contributed to the fire resistance of the assembly despite the presence of unprotected steel beams, this belief is further validated by the recorded data as discussed in the preceding sections, and the early failure times observed in the lightweight concrete assemblies. Due to the poor response of the lightweight aggregate assemblies to fire exposure, it was decided that this material system would not be pursued as a means of achieving fire resistance through composite construction. Rather, the SFRC system was selected as the primary focus for the current research, and results from the respective test are utilized in Chapter 4 for validation of numerical models for use in parametric studies.

3.4 System Level – Full-Scale Building

A review of the literature, as conducted in Chapter 2, indicates that several system level studies on fire resistance of steel framed structures have been conducted. The most comprehensive of these research programs is that conducted by the Large Building Research Establishment in its large building test facility in Cardington UK (British Steel 1998). In these tests, collectively known as the Cardington tests, an eight story steel frame building was subjected to a series of fires. A total of 8 fire resistance tests were conducted at this facility. Results from the Cardington tests are used in this research to calibrate numerical models of a structural system's response to fire exposure. Reviewing the different tests that were conducted at the Cardington facility, it was determined that the most relevant test to the behavior of system level composite floor assemblies was the restrained beam test as described below.

The restrained beam test consisted of monitoring the fire response in a compartment of the eight story braced-frame steel structure where an unprotected UB 305x40 (W12x26 equivalent) beam spanned between two UC 254 columns. The beam spanned 9 m between the two columns and was designed to be simply supported while acting compositely with the concrete floor slab. The floor slab was an in place lightweight concrete floor on a ribbed metal deck, with a maximum thickness of 130 mm and incorporating A142 anti-crack mesh. The connections of the beam to the column were typical fin plate connections as seen in Fig. 3.41.

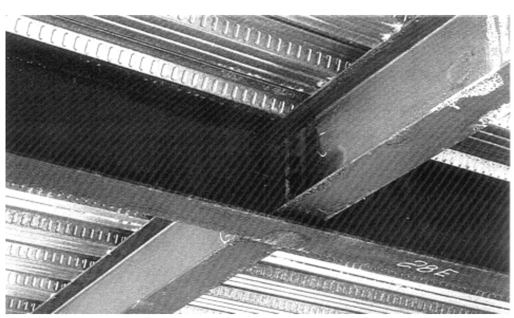

Fig. 3.41: Fin plate connections used in Cardington building

A furnace 8 m long and 3 m wide was constructed around a composite beam-slab assembly supporting the seventh floor of the structure (as seen in Fig. 3.42) to simulate fire exposure. Loading on the seventh floor of the structure (above the heated beam) was accomplished by placing sand bags over the floor (also seen in Fig. 3.42) such that the applied load during fire exposure was 4.94 kN/m^2. The central 8 m of the beam was exposed to fire leaving 500 mm on each end of the beam, including the connections, outside the fire exposure. The objective of leaving the connections outside the furnace area was to keep the connections as close as possible to ambient temperature. The furnace was constructed in such a fashion that it offered no structural support to the assembly as it deflected.

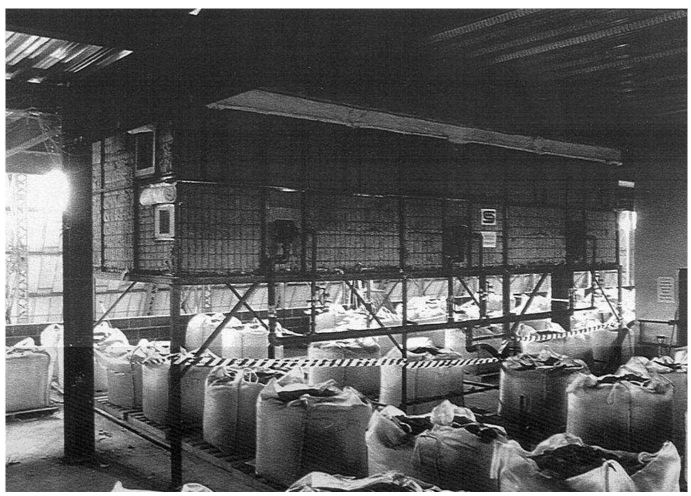

Fig. 3.42: Furnace constructed around the composite beam for restrained beam test

The assembly was exposed to fire for approximately 2.5 hours, though the time temperature curve as per ISO 834 (ISO 1975) was to be simulated, the curve designated as “Cardington test” in Fig. 3.43 resulted. The temperatures attained in the steel beam were in excess of 800 °C, thus, the steel beam lost approximately 90% of its strength. However, the assembly did not collapse in spite of recorded deflections as high as 231 mm in the center of the span as seen in Fig. 3.44. Even when the fire was terminated, there was no sign of runaway deflections in the composite beam. Following the test, the deflection of the beam recovered more than 100 mm to a final deflection of 113 mm. It was observed that during the test (after about 70 minutes of fire exposure) local buckling occurred at both ends of the beam just inside the edge of the furnace as shown in Fig. 3.45. Additionally, there was a slight distortion of the beam bottom flange as thermal expansion caused the beam to push into the web of the column. It was also observed that during the cooling phase, the fin plate connection on both ends of the beam fractured as shown in Fig. 3.46. The fracture of the connections was presumably due to the development of high thermally induced forces in both the heating and cooling phase of the fire. The main reason for avoidance of collapse was attributed to the contribution of the concrete slab to load transfer through TMA (Huang et al. 2001, Alkawakhiri et al. 2004) and the beam-slab interactions both during the fire exposure and during the cooling phase when the connections failed.

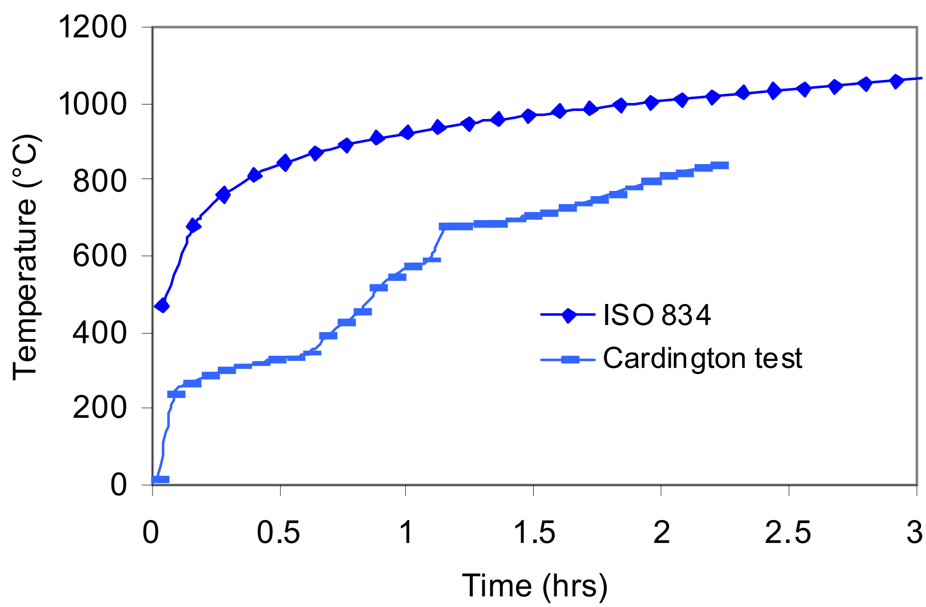

Fig. 3.43: Time temperature relationship achieved during the Cardington restrained beam test and ISO 834 fire exposure for comparison

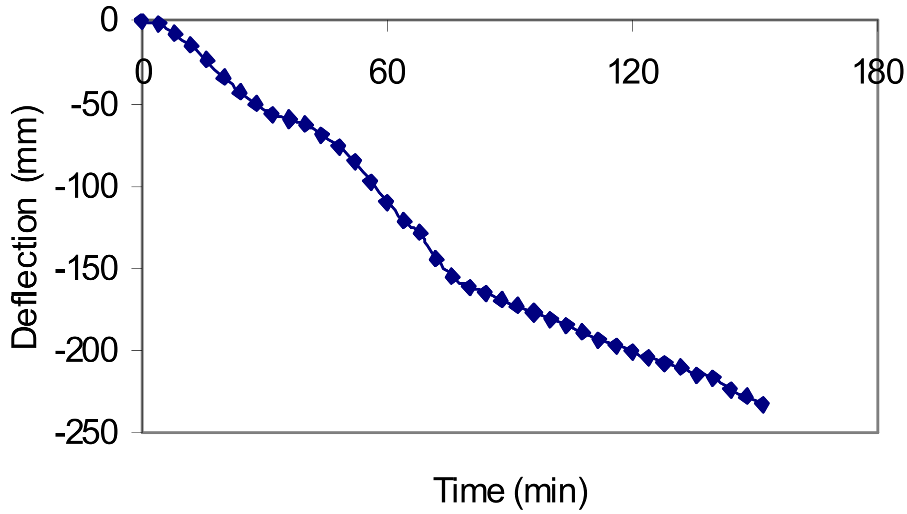

Fig. 3.44: Measured mid-span deflections for the restrained beam

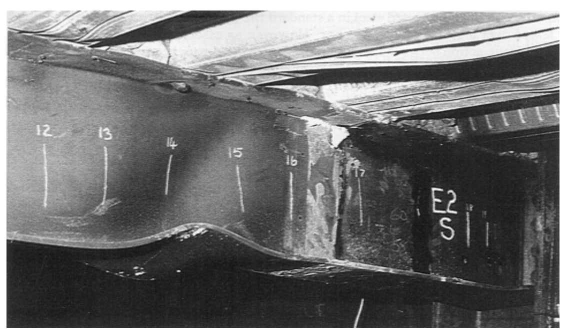

Fig. 3.45: Local buckling of beam ends in restrained beam test

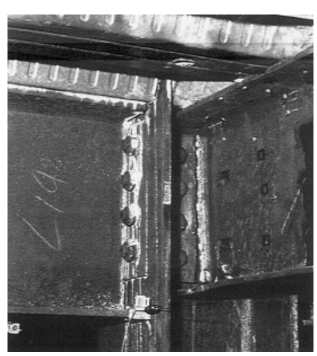

Fig. 3.46: Fractured fin plate connections in restrained beam after cooling phase of fire

3.5 Summary

A large number of fire resistance tests on CFHSS columns have been conducted at NRCC in Canada. A total of 85 CFHSS columns were tested under exposure to ASTM E-119 fire exposure. Detailed results from these tests are available through NRCC internal reports, and through journal publications on the test results. Given the level of detail in the results as discussed in Section 3.2 of this chapter, and full details on the construction of the assemblies, this data will be used for the calibration of the element level numerical models necessary in this research program.

Since there is limited information available on the fire response of composite floor assemblies under fire exposure, fire resistance tests were carried out on four composite floor assemblies, three made with lightweight concrete, and one made with SFRC. The test assemblies consisted of three W10X15 beams and 2 W12X16 beams with the concrete deck on top. To assess the response of the assemblies to fire exposure, various fire resistance schemes were applied to the steel beams and the assemblies were subjected to loading under a design fire exposure.

Results from the fire resistance test indicated that the steel beam-SFRC slab assembly, which incorporated an unprotected steel beam, withstood the full duration of the fire exposure with no signs of failure while the assemblies made with lightweight concrete did not. Data from the instrumentation network, which included thermocouples, LVDT's, and strain gages, indicates that the SFRC assembly developed tensile membrane action in the composite SFRC slab. This observation is reinforced by the presence of cracking in concentric circles above the unprotected steel beam not seen in the lightweight concrete slabs. Results from this test are used in subsequent chapters for the validation and calibration of numerical models.

A comprehensive series of tests were conducted on an eight story steel frame building at the Cardington test facility in the UK. Data from these tests including temperatures, displacements, and construction details is available to the research community. Given the ready availability of these detailed test results, it is not prudent to conduct additional system level tests, as such, data from the Cardington tests will be utilized for validation of the system level models created and employed in this research.

CHAPTER 4

4 NUMERICAL MODEL

4.1 General

Recent advances in computational ability and numerical modeling codes offer an attractive alternative to conducting costly fire resistance tests. Numerical modeling allows the user to economically investigate the effect of altering a single parameter while holding others factors constant. This allows the generation of a large data pool for use in statistical regression, trend identification, and methodology development. Given the need for such data pools in this research, not just at the element level, but also at the assembly and system levels, it is necessary to develop and validate a series of numerical models.

There are several computational models that can be applied for simulating structural response under fire conditions. These models which are based on finite element formulations include, ABAQUS, ANSYS, VULCAN, and SAFIR. Of these, ABAQUS and ANSYS are general purpose finite element programs, while VULCAN and SAFIR were specifically developed for the analysis of structures exposed to fire. Though general purpose finite element codes can be employed for analysis of structures under fire exposure, SAFIR was selected for this research study because it has undergone extensive validation, and predictions from SAFIR have been shown to closely match fire test data and predictions from other more detailed numerical models (Franssen, 2005, Gilvary and Dexter, 1997, Talamona, 2005).

4.2 Analysis Procedure

The computer program SAFIR, developed at the University of Liege in Belgium, is capable of accounting for multiple materials in a cross section, both heating and cooling phase of fire exposure, large displacements, different strain components, non-linear material properties according to Eurocode 3 (Eurocode, 2005), and residual stresses. Additionally, SAFIR allows the user to input any time-temperature relationship to facilitate the use of design fire scenarios. For tracing structural response under fire exposure, the basic equation utilized in SAFIR is:

$$\{F\} = [K]\{U\} \qquad [4.1]$$

where {F} is the force vector and [K] is the stiffness matrix. In traditional finite element analysis, the force vector {F} is changing as a function of time, and, if material non-linearity is taken into consideration the stiffness matrix [K] changes according to a predefine constitutive model. For the analysis of structures exposed to fire, additional complexity is added in that thermal expansion and material degradation due to the effect of fire must be taken into account both in the stiffness matrix [K], and the force vector {F}. However, before the modified force vector and stiffness matrix can be determined, it is necessary to determine the temperature at each node in the assembly. The procedure employed by SAFIR to accomplish this is outlined below, followed by a description of how SAFIR carries out structural analysis.

4.2.1 Development of Fire Scenarios

The design fire scenario for the desired structural analysis can be established either through the use of parametric fires (time-temperature curves) specified in Eurocode (2005a) or through design tables (Magnusson and Thelandersson 1970) based on ventilation, fuel load, and surface lining characteristics. Once the design fire time-temperature profile is identified (an example using the Eurocode procedure is presented in Section 6.2.4) this relationship is input into SAFIR though a *.FCT file. This file is read by the thermal analysis routine, and utilized to determine the temperatures in the member cross-section according to the following procedure.

4.2.2 Thermal Analysis

In the thermal analysis, SAFIR utilizes the general form of the three dimensional heat transfer (conduction) equation which is:

$$k\left(\frac{\partial^2 T}{\partial x^2}+\frac{\partial^2 T}{\partial y^2}+\frac{\partial^2 T}{\partial z^2}\right)+Q-C\rho\frac{\partial T}{\partial t}=0 \qquad [4.2]$$

where:

k = thermal conductivity

T = temperature

x,y,z = coordinates

Q = internally generated heat

C = specific heat

ρ = Specific mass density

t = time

The traditional shape functions as shown in Eqs. 4.3 and 4.4 for triangular and square elements respectively are used. In Eqs 4.3 and 4.4 ξ and η are the coordinates used to define the reference elements.

$$N=\left\langle 1-\xi-\eta;\xi;\eta\right\rangle \qquad [4.3]$$

$$N=\frac{1}{4}\left\langle\begin{matrix}(1-\xi)(1-\eta); & (1+\xi)(1-\eta)\\ (1+\xi)(1+\eta); & (1-\xi)(1+\eta)\end{matrix}\right\rangle \qquad [4.4]$$

Utilizing these shaped functions, the geometry of the element can be described as a function of the nodal coordinates as:

$$x=N_i x_i;\, y=N_i y_i;\, z=N_i z_i \qquad [4.5]$$

And the temperatures at any location in the element can be written as a function of the nodal temperatures as:

$$T = N_i T_i \qquad [4.6]$$

Since Eq. 4.2 is not in differential form, it is necessary to transform it prior to implementation in the finite element method. SAFIR accomplishes this by first replacing the temperatures in Eq. 4.2 by the approximation given in Eq. 4.6. After this substitution, the shape functions are used to weight the function according to the Galerkin method, and then it is integrated over the surface. Following this integration, the first term in this equation is transformed into a definite integral through the use of Greens equation. Finally, the system is subjected to the boundary condition of Eq. 4.7, and Eq. 4.8 is obtained.

$$q_n = -k\nabla T_j N_j \qquad [4.7]$$

$$\int_{el} k\{\nabla N_i\}\langle\nabla N_j\rangle dV T_i + \int_{el} C\rho N_i N_j dV \dot{T}_i + \int_{el} Q N_j dV = -\int_{boundary} N_j q_n dS \qquad [4.8]$$

where:

$$\nabla = \left\langle \frac{\partial}{\partial x}; \frac{\partial}{\partial y}; \frac{\partial}{\partial z} \right\rangle$$

q_n = heat flux at the boundary of the element

when all of the contributions from the elements are summed the following is obtained:

$$[K]\{T\} + [C]\{\dot{T}\} = \{g\} \qquad [4.9]$$

where:

[K] is the thermal conductivity matrix

[C] is the heat capacity matrix

$\{\dot{T}\}$ is a vector of the nodal temperatures {g} is a vector accounting for the heat exchange at the boundaries

The heat flux across the boundary accounts for convection and radiation according to Eurocode 1 (1995) and is given by Eq. 4.10. If no exposure is specified for a given surface it is assumed that the surface is adiabatic.

$$q_n = h\left(T_g - T_s\right) + \sigma\varepsilon\left(T_g^4 - T_S^4\right) \qquad [4.10]$$

where

T_g is the gas temperature

T_s is the surface temperature

h is the convection coefficient

ε is the emissivity

σ is the Stefan Boltzmann constant

For generating matrices [K] and [C] in Eq. 4.9, the integration over the volume of the element is done according to a Gaussian procedure with the number if integration points being specified by the user. The integration scheme takes into account that the properties of the material are temperature dependent and can change over the volume of the element.

For thermal analysis, 2D solid elements are used where the fire exposed sides and the exposure types are specified by the user. The thermal model in SAFIR neglects heat transfer in the longitudinal direction, and assumes that every longitudinal cross-section has the same temperature profile unless otherwise specified. The energy consumed for evaporation of water present in the concrete is included, but that associated with hydraulic migration within the cross-section is neglected.

4.2.3 Structural Analysis

For structural analysis, SAFIR utilizes the incremental form of the principal of virtual work. Assuming a co-rotational configuration, the incremental form of the principal of virtual work can be written as:

$$\int_V (\overline{D}_{ijkl} d\overline{E}_{kl} \delta\overline{E}_{ij} + S_{ij} \delta d\overline{E}_{ij}) dV = \int_V (d\bar{f}_i \delta\overline{u}_i + \bar{f}_i \delta d\overline{u}_i) dV \qquad [4.11]$$

The presence of a bar indicates that the variable is evaluated from a rotated position obtained such that the rigid body rotation matches the deformed shape as closely as possible.

Where:

$V = \overline{V}$ = the un-deformed volume of the element

S_{ij} = tensor of the second Piola-Kirchoff stress

$D_{ijkl} = \overline{D}_{ijkl}$ = tensor defining the incremental constitutive law of the material (see Eq below)

$\delta\overline{E}_{ij}$ = Tensor of the green field of virtual displacement, see equation below

$\bar{f}_i$ = Volume forces

$\delta\overline{u}_i$ = virtual field of displacement from the deformed position of the element

Since the temperatures change during the simulation, the constitutive law can be written as:

$$dS_{ij} = D_{ijkl}\left(dE_{kl} - dE_{kl}^{Th}\right) = D_{ijkl} dE_{kl}^{m} \qquad [4.12]$$

where

dE_{kl}^{th} = tensor of incremental strain

dE_{kl}^{m} = tensor of mechanical or stress related strains where the tensor of the virtual displacement field is given as:

$$\delta E_{ij} = \frac{1}{2}\left(\delta u_{i,j} + \delta u_{j,i} + u_{k,i}\delta u_{k,j} + \delta u_{k,i}u_{k,j}\right) \qquad [4.13]$$

Utilizing a discretized field to represent the displacement field allows the incremental tensor strains to be derived as a function of nodal displacements, when this is done, Eq. 4.13 can be rewritten as:

$$\int_{v} B^{T} DBdVdp + \int_{v} S^{T} \delta dedVdp = \left(K_{u} + K_{s}\right)dp = f^{ext} - f^{\text{int}} \qquad [4.14]$$

where

K_u is the linear elastic and the geometric stiffness matrices

K_s is the stress generated stiffness matrix

f^{ext} is the nodal forces which are energetically equivalent to the applied force

f^{int} are the nodal forces resulting form the integration of internal force.

For structural analysis, SAFIR uses a fiber-based approach wherein each of the solid elements in the thermal model is considered as a fiber in the structural model. A stress and temperature dependent stiffness matrix is established that incorporates all of the fibers.

4.3 Program Features

The capabilities of SAFIR for thermal analysis include:

- Thermal gradients in two and three dimensional structures, including those with internal voids, can be determined
- For determining the thermal gradients in a structural member, SAFIR considers both radiation and convection from the fire to the member, and conduction within the member

- Thermal analysis can be conducted on members incorporating multiple materials in the cross-section
- SAFIR can simulate any time temperature profile including those with a cooling phase

Following completion of the thermal analysis, the thermal information is stored in a text file, which is then utilized by the structural model. Capabilities of the structural model include:

- Deformations in two and three dimensional structures can be determined
- Members with pre-stressing forces can be considered
- Consideration is given to both thermal and mechanical strains the structural analysis
- Both static or dynamic structural analysis can be performed in SAFIR
- An arc length convergence criterion is utilized by SAFIR to achieve convergence

Lastly, SAFIR uses some common computational features for both thermal and structural analysis, they are as follows:

- Internal numbering of nodes, SAFIR can automatically re-numbers the nodes to optimize the matrix bandwidth reducing storage and computational time requirements.
- Imposing the same temperature or displacement at two different nodes can be accomplished using master-slave relations
- Thermal and mechanical properties of steel and concrete according to Eurocode 2, 3, and 4 are pre-programmed
- All post processing applications are completed with the post processor Diamond

4.3.1 General

As mentioned previously, SAFIR conducts calculations in two steps, the first is a thermal analysis and the second is a structural analysis. Each of these steps requires the use of independent input files, which can be written either by the SAFIR Wizard or manually with text editing software. A schematic of the analysis procedure as reproduced from (Franssen et al. 2000) is shown as Fig. 4.1 below. The link between the thermal and the structural analysis is the use of a *.tem file produced by the thermal analysis. This file contains all of the nodal temperatures in the discretized cross-section. These temperatures are used to determine the temperature dependent material (structural) properties in the structural analysis procedure. Both the thermal and the structural analysis produce a *.out file which contains the results from the respective analysis. This file is opened and viewed by the user via the SAFIR post processor Diamond as indicated in Fig. 4.1 A brief description of the data in the respective input (*.in) files is presented for the thermal and structural models in the following sections respectively.

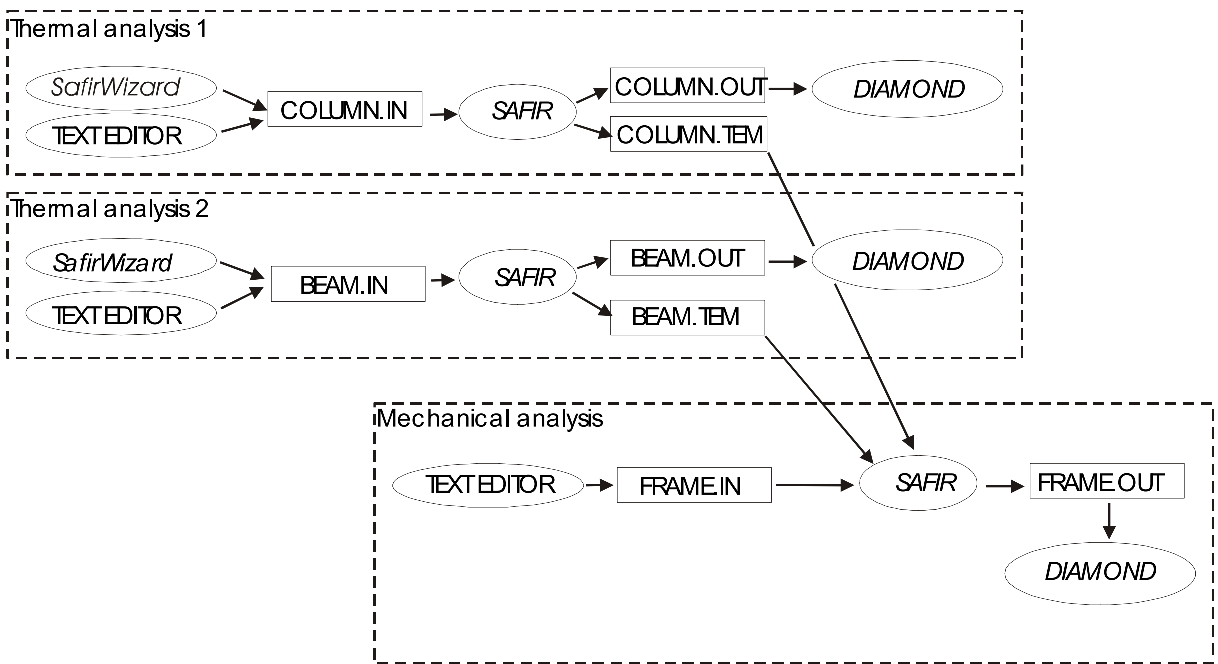

Fig. 4.1: Schematic of SAFIR operational procedure (Franssen et. al 2000)

4.3.2 Thermal Input

While the SAFIR Wizard is capable of writing input files for structural steel members with or without protection, it is unable to write thermal input files for CFHSS columns or concrete members, and has no capability to write structural input files. The primary information contained in the thermal input file is the location of the nodes that compose the member cross-section, the ordering of these nodes to define the elements, and the thermal properties of the constituent materials such as thermal conductivity, specific heat, emissivity, convection coefficients, and water content (where applicable). Also defined in the thermal input file are the materials in the cross section, the fire exposure conditions, and any symmetry in the member. A detailed summary of the specific format used in the thermal input file is provided in Appendix C.

4.3.3 Structural Input

Once the temperatures in the cross-section(s) are determined, the geometry of the simulated structure is defined in the structural input file. As there is no pre-processor available for the structural model, all of the nodes must be manually written in the text input file. A sample of the input file with descriptions of each line is included as Appendix D. The primary information contained in the structural input file is the location of the nodes, the ordering of these nodes to define beam shell or truss elements, and the mechanical properties of the constituent materials such as Poisson's ratio, yield strength, compressive strength, tensile strength, and elastic modulus. For each of the elements in the structural model an associated *.tem file is specified by the user. SAFIR uses the temperatures in the *.tem file to establish the temperature depended stiffness matrix for the element under consideration. Composite action between steel and concrete is accounted for in SAFIR through the use of the "SAMEALL" or "SAME" commands. These force nodes at the same location to have the same displacements. The output from the structural analysis includes the stresses in elements, bending and axial forces, (where applicable) displacements, and reaction forces. There are however several assumptions employed in the structural model as enumerated by Kodur et al. (1999) they are:

- Plane sections are assumed to remain plane under bending

- Shear energy is not considered in the analysis in accordance with Bernoulli's hypothesis
- Plastic strain energy is assumed to be temperature independent
- The non-linear part of the strain is averaged over the length of the element to avoid numerical locking
- In case of strain unloading, material behavior is elastic with the modulus of elasticity equal to the Young's modulus at the origin of the curve
- Plastification is only considered in the longitudinal direction of the member

4.3.4 Material Models in SAFIR

The high temperature thermal and mechanical relationships for several common materials are pre-programmed into SAFIR according to the relations specified in Eurocode (2004, 2005). Of particular interest for this research are the high temperature constitutive models for steel and concrete. Appendix B contains the material models for steel and concrete as specified in Eurocode (2004) and ASCE (1992) for comparison purposes. The pre-programmed thermal properties in SAFIR included thermal conductivity, specific heat, and thermal expansion for both steel and concrete. The pre-programmed mechanical properties in SAFIR include yield strength, elastic modulus, and ductility for steel, compressive strength, strain at peak stress, and ductility for concrete.

4.3.5 Modifications to SAFIR

SAFIR has several advantages and pre-programmed material properties as discussed previously. However, SAFIR lacks a material model for steel fiber reinforced concrete which is paramount to this research. Therefore, a temperature dependent constitutive material model for SFRC was implemented in the SAFIR source code.

Due to the similarities in thermal properties observed between plain and steel fiber reinforced concrete (Lie and Kodur, 1995b), only high temperature strength relations for SFRC as found in Appendix B were added to SAFIR as outlined below. For the thermal analysis, the pre-programmed high temperature models for either carbonate or siliceous aggregate should be used, and the mechanical properties of SFRC is to be specified only for the structural analysis.

Compressive strength of concrete, like other properties, deteriorates with fire exposure time due to increasing temperature. The normalized (with respect to the ambient temperature compressive strength of plain concrete) compressive strength of plain concrete (PC) and SFRC are shown as a function of temperature in Fig. 4.2 below (SFPE 2002, Eurocode 2004, Lie and Kodur 1994, 1995). Plain concrete behaves as expected in that the strength starts to deteriorate at approximately 100 °C and the strength deterioration continues in a nearly linear fashion from 200 °C to 800 °C at which point the compressive strength is about 10% of the ambient temperature strength. SFRC on the other hand behaves markedly differently as seen in Fig. 4.2. The compressive strength of SFRC increases by about 10% at 200 °C, and this trend is continued to 400 °C due to the effect of the steel fibers as they help to confine the concrete, and allow it to act as though under tri-axial compression. This advantage is not fully realized until about 200 °C due to the need for the concrete to become slightly more ductile before the full advantage of the steel fibers can be realized. Above 400 °C, the compressive strength of SFRC deteriorates linearly to zero at 850 °C due to the degradation of the mechanical properties of the steel fibers. Of particular note is the observation that above 800 °C the compressive strength of PC is higher than that of SFRC. This, however, is not postulated to adversely affect the performance of structural members due to the relatively small depth of concrete that would be exposed to temperatures in excess of 800 °C in most realistic (design) fires.

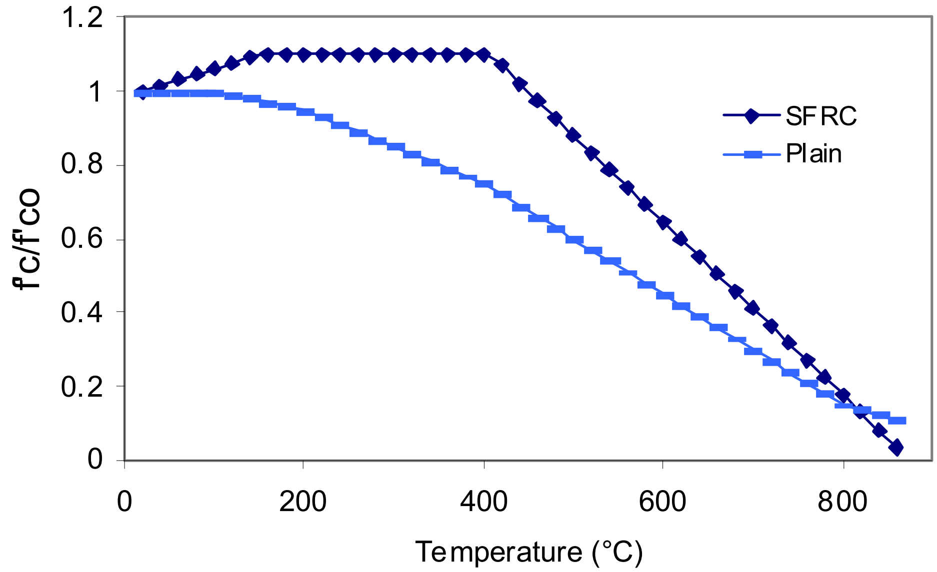

Fig. 4.2: Compressive strength of PC and SFRC as a function of temperature

The addition of steel fibers also significantly enhances ductility of SFRC as compared to PC. Fig. 4.3 shows the normalized stress strain relationships for PC and SFRC in compression for different temperatures ranging from ambient to 600 °C as specified by Lie and Kodur (1995b). From Fig. 4.3, it can be seen that SFRC is more ductile than PC as indicated by the higher ultimate strain of SFRC at all temperatures plotted. The enhancement that can be achieved through the inclusion of steel fibers is to such and extent that at 400 °C, the ductility of SFRC is 83% higher than that of PC. This trend is continued such that at 600 °C, the ductility of SFRC is approximately 3.5 times that of PC. Ductility is enhanced through the inclusion of steel fibers, not just in terms of the ultimate strain that can be reached, but also in the strain at peak stress. At all temperatures, the strain at peak stress in the SFRC is considerably higher than that in the PC. The enhanced ductility of SFRC is critical to the development of TMA. As such, SFRC being more ductile and at the same time having higher tensile strength, should enhance the development of TMA. This enhancement of TMA should subsequently significantly improve the fire resistance of floor systems when SFRC is used as part of a composite beam slab assembly.

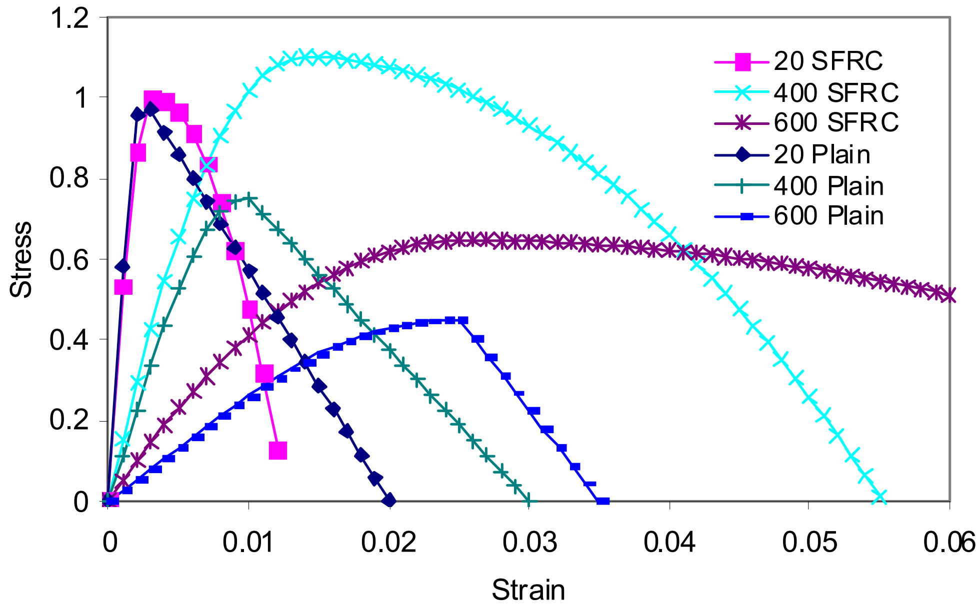

Fig. 4.3: Stress-strain relationships for plain and SFRC concrete at various temperatures

An additional benefit of adding steel fibers to concrete is the enhanced the tensile strength of concrete throughout the full temperature range practically achieved under fire exposure. Fig. 4.4 (SFPE 2002, Eurocode 2004, Lie and Kodur 1994, 1995) shows the normalized (with respect to ambient temperature tensile strength) tensile strength of PC and SFRC as a function of temperature. The increase in tensile strength through the inclusion of steel fibers is approximately 38% at ambient temperature, and is continued to temperatures in excess of 800 °C as seen in Fig. 4.4. The increased tensile strength of SFRC is attributed to the steel fibers arresting cracks as they propagate across the cement matrix. This causes the cracks to have to take a more tortuous path to cause failure of the concrete. This enhanced tensile strength from SFRC facilitates the development of tensile membrane action in the concrete slab, thus enhancing the fire resistance of composite floor slab assemblies.

To aid in achieving convergence of the structural models, some modifications were made to the material models shown in the previous sections, they are as follows. The compressive strength while zero above 850 °C, was granted nominal (0.1%) strength up to 1200 °C to avoid the stiffness matrix arbitrarily becoming zero above 850 °C and causing numerical failure of the structure. Likewise, the tensile strength model due to an absence of data above 800 °C was assumed to decay linearly to zero at 1200 °C to avoid numerical instability in the model.

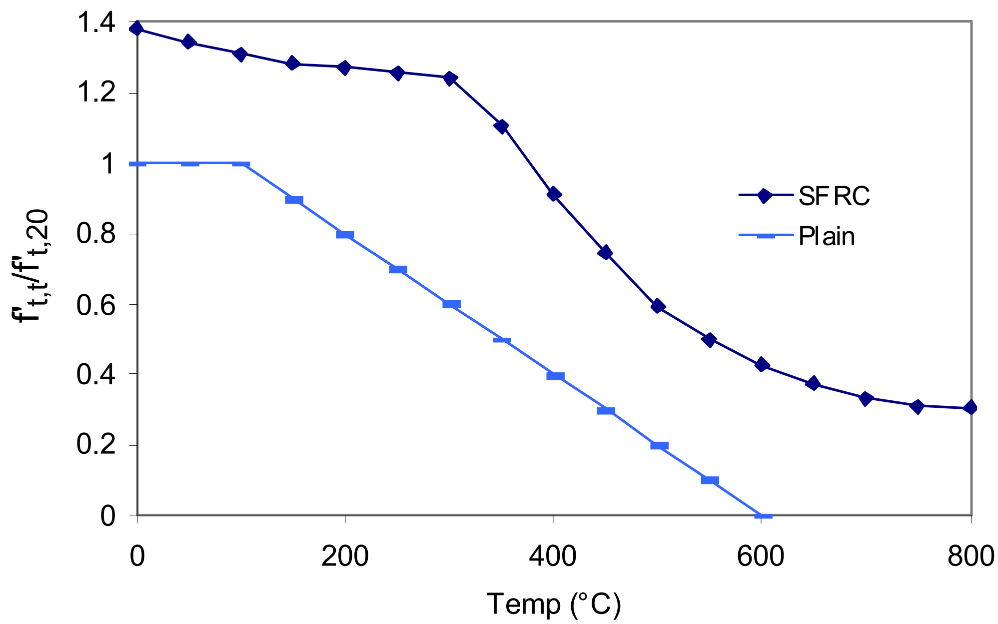

Fig. 4.4: Tensile strength of PC and SFRC as a function of temperature

Validation of the material model for SFRC was accomplished by comparing deflection prediction from SAFIR with those recorded during the novel fire tests conducted on an SFRC floor system at MSU. A description of the validation of the material model for SFRC, as well as the use of SAFIR for element, assembly, and system level parametric studies is presented below.

4.4 Validation of SAFIR Computer Program

The applicability of SAFIR to trace the response of structural members under fire exposure is well validated in the literature (Franssen, 2005, Gilvary, 1997, Talamona, 2005). However, there is a lack of validation for the use of SAFIR to capture the effects of composite construction and tensile membrane action under fire exposure, particularly for SFRC. As such, for use in parametric studies, numerical models of the experimental setups described in the respective sections of Chapter 3 were created in SAFIR and subsequently validated. For the validation of these models, and to ensure that they account as closely as possible for the conditions present in the respective fire tests, thermal and structural results from SAFIR were compared with those from testing. The following sections present these comparisons for the element, assembly, and system level models independently.

4.4.1 Element Level – CFHSS Columns

The modeling of CFHSS columns differs significantly from the modeling of typical steel columns (HSS or W-flange sections) due to the development of composite action. Composite action in CFHSS columns serves to reinforce the wall of the section against crippling, and reduce the risk of local bucking. As such, it is possible to accurately model the behavior of these sections under fire utilizing beam elements. Beam elements are capable of accounting for composite action between the steel and concrete, and capturing both crushing and global column buckling.

For the thermal analysis in SAFIR, full advantage was taken of the symmetry in both circular and square CFHSS columns. Only a quarter section of each column was modeled with double symmetry to reduce computational requirements. The steel section and rebar were modeled as having perfect thermal and structural contact with the concrete core. The rebar was included as square elements with an area equivalent to that of the rebar designated in the testing details. As an illustration of a typical CFHSS column model, an image of the material composition including discretization for a circular bar reinforced CFHSS columns is presented in Fig. 4.5 below.

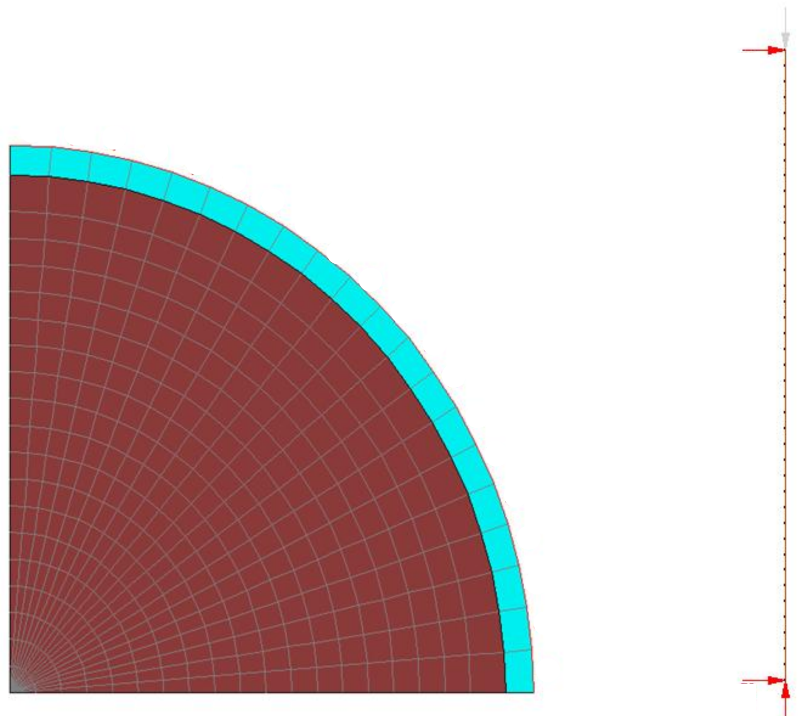

Fig. 4.5: CFHSS column cross section and elevation discretization in SAFIR

Beam elements with a length of 150 mm were used for discretization along the length of the column as shown in Fig. 4.5. End nodes of the beam elements were assumed to have six degrees of freedom (three translations and three rotations) while the center node of the three nodded beam elements was assumed to have one degree of freedom. End conditions were provided to simulate as closely as possible those used in testing, pinned-pinned, pinned-fixed, and fixed-fixed conditions were all considered in various simulations. For steel and plain concrete, high temperature material models according to Eurocode were utilized, for SFRC, the high temperature material model presented in section 4.3.4 was used.

To validate SAFIR for use in modeling the fire response of CFHSS columns including PC, FC, and RC filling, the fourteen columns in Table 3.1 were analyzed under ASTM E-119 (ASTM, 2007) and the SAFIR predicts compared with the test data. Fig. 4.6 shows a graphical representation of the columns considered in the validation, while Table 4.1 presents the critical mechanical properties for the columns as reported, and Table 4.2 shows thermal and mechanical properties assumed in the simulations. The thermal and structural response, and ultimate failure times generated by SAFIR were compared with the measured test data for all of the columns. All of the columns for which test data was available underwent the same level of scrutiny as the single column used to illustrate the validation below. However, only a sample validation is presented below.

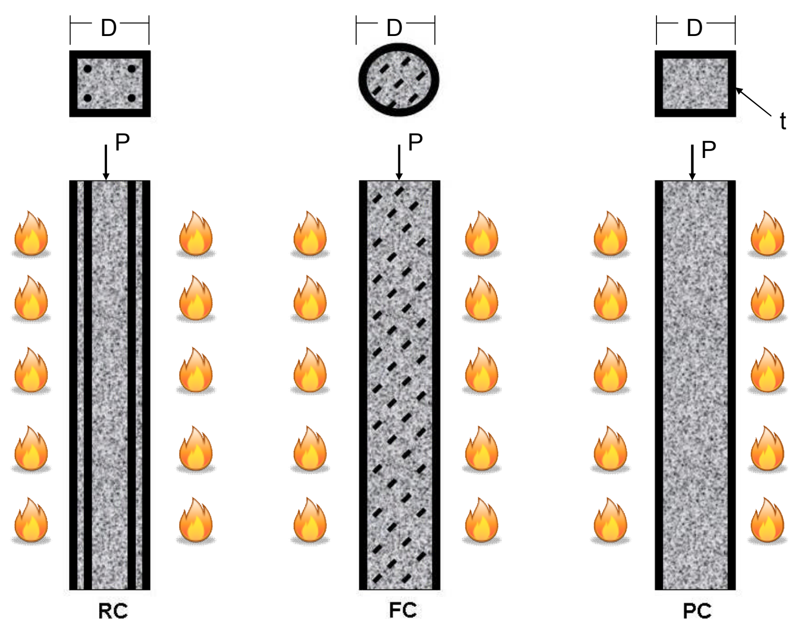

Fig. 4.6: Typical RC, FC, and PC square and round column cross-sections used for validation of SAFIR

Table 4.1: Characteristics of CFHSS columns used for validation of SAFIR

Column Designation	Dia. or Width (mm)	Load (kN)	f'c	Fire Resistance (min)	Concrete Filling	Agg. Type
RP-168	168.3	150	35.4	81	Plain	Sil.
RP-273	273.1	525	27.4	143	Plain	Sil.
RP-355	355.6	1050	25.4	170	Plain	Sil.
SP-152	152.4	286	46.5	86	Plain	Carb.
SP-178	177.8	549	57.0	80	Plain	Sil.
RF-324	323.9	1600	57.0	199	Fiber	Carb.
RF-356	355.6	1500	53.5	227	Fiber	Carb.
SF-203	203.2	900	90.1	128	Fiber	Carb.
SF-219	219.1	600	90.1	174	Fiber	Carb.
RB-273a	273.1	1050	46.7	188	Bar	Carb.
RB-273b	273.1	1900	47.0	96	Bar	Carb.
SB-203	203.2	500	47.0	150	Bar	Carb.
SB-254a	254	1440	48.1	113	Bar	Carb.
SB-254b	254	2200	48.1	70	Bar	Carb.

Table 4.2: Assumed thermal and mechanical properties

Steel			
Heat transfer coefficients		Mechanical properties (HSS/Rebar)	
Hot convection coefficient	25	Young's modulus (GPa)	210/210
Cold convection coefficient	9	Poisson's ratio	0.3/0.3
Relative emissivity	0.5	Yield strength (MPa)	350/413
Concrete			
Heat transfer coefficients		Mechanical properties	
Hot convection coefficient	25	Poisson's ratio	.25
Cold convection coefficient	9	Compressive strength (MPa)	Variable
Relative emissivity	0.5	Tensile strength (MPa)	Variable

A comparison of the temperatures predicted by SAFIR and those measured in a fire test at the steel surface (HSS section), and at the center of the concrete core, is shown in Fig. 4.7 for Column SP-178. Of note from Fig. 4.7 is the observation that it takes almost 30 minutes to reach

600 °C in the steel section. In unprotected HSS columns this temperature is achieved in approximately 15-20. The delayed heating in the CFHSS columns can be attributed to the mass of the concrete in the composite column that absorbs heat from the exposed steel section, thus limiting the temperature rise in steel. The contribution of the concrete to the thermal response of the column is observed in both the SAFIR analysis and the test data. Good agreement between predicted and measured temperatures is observed in Fig 4.7 for the concrete core after 100 °C, at which point free water is driven off. The steel temperatures initially deviate such that temperatures observed in the test are hotter than those predicted by SAFIR. This can be attributed to the assumption in SAFIR that there is perfect thermal contact between the steel and the concrete. When however, the steel approaches the critical phase transformation temperature of 700-750 °C, at which point the bonded water in the concrete is also driven off, SAFIR begins to over predict the temperature in the steel. This is mainly due to the assumption in SAFIR that hydraulic migration in concrete can be neglected. Toward the end of the test, the temperatures compare reasonably well such that there is only a 30 °C temperature difference between the test data and the SAFIR simulation. Overall, the temperature predictions from SAFIR are in reasonable agreement with data measured from tests.

The structural response predicted by SAFIR was validated by comparing the axial deformations (at the loaded end of the column) for Column SP-178 with those measured during tests (Fig. 4.8). The column initially expands as a result of the quick rise in steel temperatures. This increased temperature leads to eventual loss of strength and yielding of steel, at which point the benefits of composite construction are observed in the column as the concrete starts to take over most of the load bearing function, causing the column to contract slightly. A peak deflection (expansion) of 18.3 mm was observed in the tests, while the corresponding peak deflection from SAFIR was

17.9 mm. These two maximum deflections show good agreement occurring at 20 and 23 minutes respectively. The differences in deflection between SAFIR data and test data are a result of the temperature discrepancies seen in Fig. 4.7. The initially higher temperatures in the steel shell produces higher expansion of the column in the fire test than in SAFIR, as seen in Fig. 4.8. After peak deflections are reached, the temperatures in the steel shell, as predicted by SAFIR, are hotter than those observed in tests. This results in the steel retaining slightly higher strength in tests than in the SAFIR simulation, thus, there is a slightly larger contraction of the column in the SAFIR simulation than observed in the test. Overall, the predicted deformations compare well with those measured during the fire test.

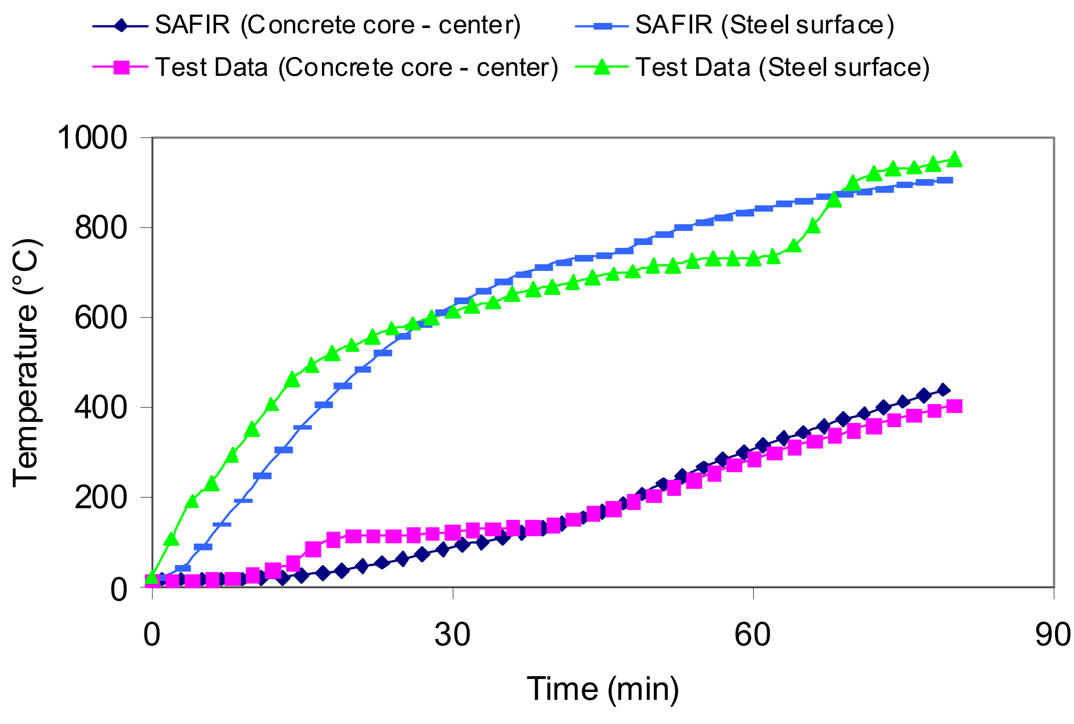

Fig. 4.7: Comparison of predicted temperatures from SAFIR with test data for Column SP-178

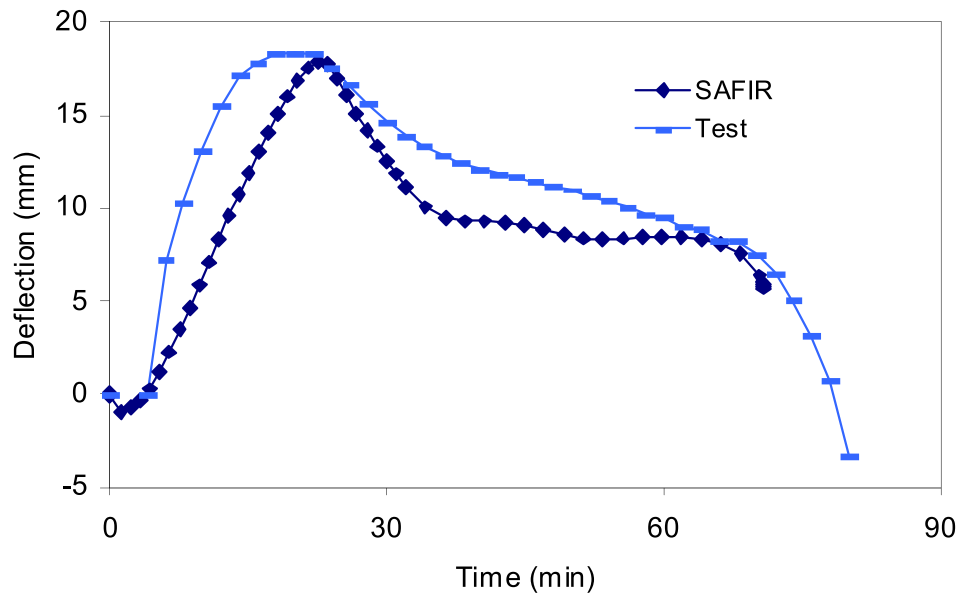

Fig. 4.8: Comparison of predicted axial deformations from SAFIR with test data for Column SP-178

All of the columns were simulated with axial loads and support conditions that matched those in testing as closely as possible with vertical translation (under loading) permitted at the top. The failure times in fire tests shown in Table 4.1 correspond to the point at which the column could not sustain the applied load as indicated by SAFIR through a failure to achieve convergence. The time to reach that point is defined as the fire resistance of the column. A comparison of the fire resistance values indicates that the SAFIR predictions are in good agreement with measured fire resistance values and that SAFIR can accurately model composite construction in the CFHSS columns. In 5 of the 14 columns modeled, SAFIR predicts a higher fire resistance than observed in testing, thus representing the un-conservative case as illustrated in Fig. 4.9. For the 9 remaining cases, SAFIR predicts a lower fire resistance than observed in testing, this corresponds to the conservative case as indicated in Fig. 4.9. The maximum error on the conservative side was 16% with the maximum error on the un-conservative side being 6%. This small (6%) error on the un-conservative side indicates that there is good agreement between test results and results from the constructed numerical models. Given this good agreement between the tests and simulation results, the models, (both the thermal and structural) constructed here are deemed acceptably conservative for use in parametric studies.

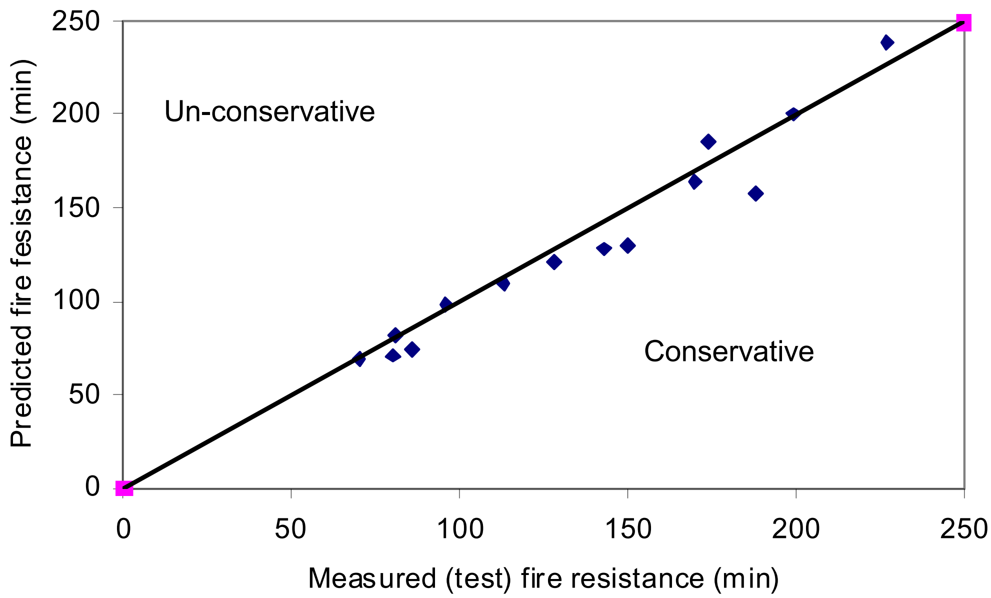

Fig. 4.9: Comparison of predicted (SAFIR) and measured fire resistance times

4.4.2 Assembly Level – SFRC Floor Slab

SAFIR has been shown to accurately model the response of floor assemblies exposed to fire (Talamona 2005). However, the validity of SAFIR for modeling the response of SFRC to fire exposure has not yet been validated. To that end, the steel beam-SFRC slab structural assembly described in Chapter 3 and tested at the MSU structural fire testing facility was modeled using SAFIR, and the response of the assembly as predicted by SAFIR compared to data recorded in the fire resistance test. The validation of both the material model and the model of the constructed assembly are presented in the following sections. No consideration is given to the use of lightweight concrete in the development of validated computational models as presented in this chapter. Plain lightweight concrete as discussed in Chapter 3 does not enhance fire resistance to the levels required in codes and standards, as such, it is not a practical alternative and will be given no further consideration.

In order to minimize the computational time required for fire resistance analysis, full advantage was taken of symmetry conditions of the beam-slab assembly. A quarter-section of the floor slab and supporting steel beams was modeled in SAFIR as shown in Fig. 4.10, where the fire exposed zone is indicated in light gray. In this region, thermal input files consistent with the fire exposure were used to capture the temperature evolution in both the concrete slab and the steel beams. Outside this region, the slab and supporting beams were assumed to be at ambient temperature. This assumption of a distinct line separating the fire exposed and the unexposed regions of the test assembly generate considerable stress concentrations at the interface. These stresses could presumably influence the structural response of the assembly. Given that these stresses will make the structural analysis more conservative, no further attention was given to the thermal gradients at this interface.

Given the assumption of a doubly symmetric condition, particular attention was given to the boundary conditions assumed in the model. Along the symmetric edge, the boundary conditions were implemented such that vertical translation was allowed, and rotation about the symmetric axis was restrained. The horizontal restraints were implemented at the symmetric edges to ensure that any deformations, whether thermal or mechanical, generated in the quarter section impact only the modeled section.

Supports where the assembly rested on the steel bearing plates were equipped with half rounds to minimize the friction at the support; these supports were modeled as a vertical support with no restriction to horizontal movement in SAFIR. This support condition neglects the contribution of friction between the steel bearing plate and the bottom of the protected W12X16 beam. This assumption is conservative since horizontal restraint at the bottom of the W12X16 should enhance the response of the assembly to fire by decreasing vertical defection. As such, neglecting this restraint is conservative.

The concrete slab was modeled as a series of four nodded 150 mm square shell elements (with minor geometric alterations to accommodate the geometry of the assembly) with each node having six degrees of freedom. As has been assumed in previous studies (Bailey 2000, Fike and Kodur 2009a,b) the slab was assumed to be of uniform thickness equal to the maximum thickness of the composite deck. Additionally, the strength contribution of the conform steel decking was neglected under fire exposure. The shrinkage reinforcing previously described was incorporated in the form of a smeared model. This means that the steel and the concrete were assumed to exist in the same location, and the steel was assumed to be uniformly distributed over the cross-section of the slab. The supporting beams were modeled as 150 mm long three nodded beam elements; the two end nodes each had seven degrees of freedom, while the center node had one degree of freedom.

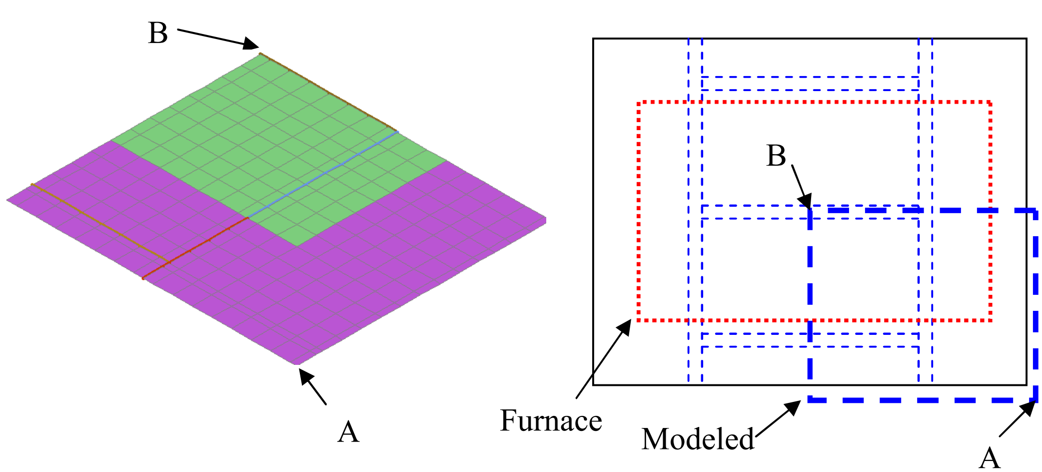

Fig. 4.10: Discretization of the tested steel beam-SFRC slab assembly for SAFIR analysis

The assumed symmetric condition causes one of the lines of symmetry to run down the length of the unprotected W10X15 beam in the center of the assembly. Two options exist for modeling this condition, first, only half of the beam could be modeled, or second, the entire beam could be modeled and the elastic modulus and yield strength reduced to 50% for the duration of the fire exposure to simulate the response of the partial section in the symmetric condition. The first option causes instability in the model due to a non-symmetric beam element about its own axis and SAFIR has a difficult time converging on a solution, as such, the later option was chosen, and the entire beam was modeled with a yield strength and elastic modulus of 50%. In addition to this concern, the bending stiffness of the section is proportional to the elastic modulus multiplied by the moment of inertia, either of these can be reduced and the effect is the same, as such, the assumption should not influence the response of the structure to fire exposure. To establish the validity of this approach, parallel simulations were run for the full assembly and the reduced assembly with the material properties of the central beam reduced by 50%. Deflections predicted by the two models almost coincided, having less than a 5% discrepancy at any point during the simulation. As such, this assumption of reduced material properties is deemed a reasonable, and in light of the computational savings, a necessary assumption.

In SAFIR, the user must specify the node line or line of action for beams, and the plane of action for shell elements. The plane of action was assumed to be at the bottom surface of the shell elements, and the line of action was assumed to be at the top of the top flange in the beam elements. When the composite action between the steel beams and the concrete slab is modeled, the selection of these lines of action causes SAFIR to model the interaction at the correct location on both the shell and beam elements. As described previously, the composite action between the steel beam and the concrete slab is modeled through the use of master-slave node relations via the "SAMEALL" command.

For validation, the actual temperatures measured in the slab and the beams during the fire test were input directly into the structural model in SAFIR. This was done to eliminate errors that can accumulate from thermal analysis. The ability of SAFIR to simulate temperatures produced by real fire exposure is presented in the literature for plain concrete (Alfwakhiri et. al 2004). Additionally, the similarities between the thermal response of plain and SFRC has been established in the literature (Lie and Kodur 1995b) thus no further discussion on the thermal validation will be presented here.

Due to the inherent instability associated with strains recorded during fire testing as discussed previously, only deflections are used for calibration of the model discussed in this section. The two most critical points for use in calibration are the center of the slab, and the connection between the beams in the heated region. As shown in Fig. 3.31 and discussed in the respective section, deflections over the supported edge are minor in comparison to these two, and hence, of little use for calibration purposes. While the deflection of the unsupported edge offers a unique set of data, the presence of extensive cracking next to the W12X16 beam makes this behavior intrinsically difficult to simulate. As such, only the center point and the connection deflections will be used for model validation. The mechanical properties utilized in the analysis are summarized in Table 4.3 below.

Table 4.3: Mechanical properties utilized in steel beam-SFRC slab analysis simulations

Steel		SFRC	
Young's modulus (GPa)	210	Poisson's ratio	0.25
Poisson's ratio	0.3	Compressive strength (MPa)	46.6
Yield strength (MPa)	350	Tensile strength (MPa)	5.34

Fig. 4.11 shows the comparison of deflections predicted by SAFIR and those measured during the fire test at the center of the slab, and over the center of the W12X16 beam (see Figs. 3.1 and 3.8 for layout of the test assembly). The predicted and measured deflections at the center of the W12X16 beam compare well for most of the fire duration. The peak deflections from SAFIR and test were 61.8 mm at 135 min and 63.8 mm at 145 min respectively, thus showing close agreement. There is however a slight divergence between measured and predicted data starting at around 130 minutes. This may be partially attributed to the slight variations between the actual high temperature stress-strain relationships for SFRC and those used in SAFIR.

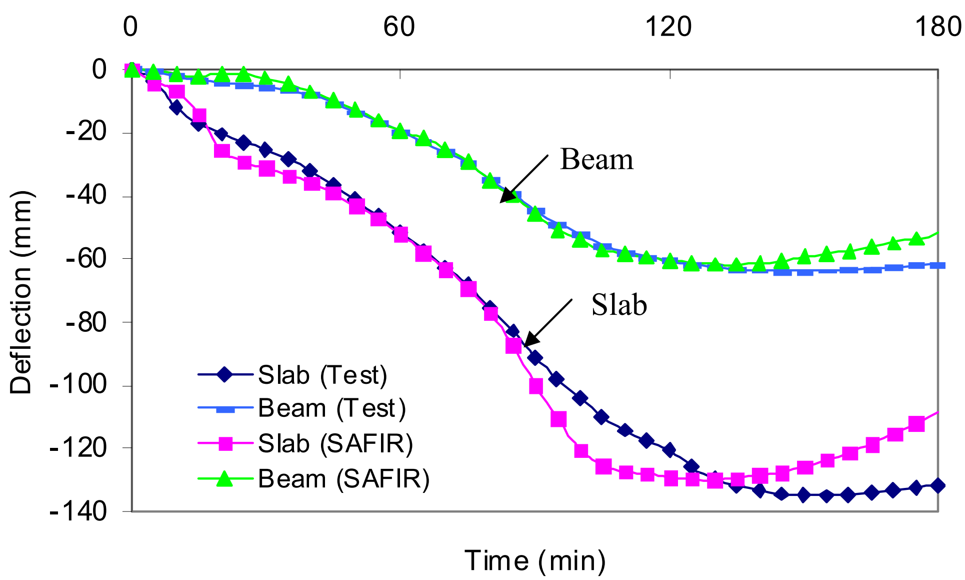

Fig. 4.11: Comparison of predicted and measured deflections at the center of the slab and at the center of the beam in the fire exposed beam slab assembly

The predicted deflections from SAFIR are also close to measured deflections at the center of the slab for the duration of the test as can be seen in Fig. 4.11. However, after about 80 minutes, the predicted deflections from SAFIR diverge from the measured deflections. The differences between the predicted and the actual response are such that the peak defection at the center of the slab predicted by SAFIR is 130 mm at 130 min, and that measured in the fire test was 135 mm at 155 min. At this point of fire exposure, the unprotected steel beam is offering little strength to the assembly due to the high steel temperatures. Additionally, the deflection at the center of the W12X16 beam is accurately predicted as seen in Fig. 4.11. Given these observations, the difference in deformations between the SAFIR simulation and the test results can be attributed to the discrepancies between assumed and actual properties of the SFRC used in the test.

From the above discussion, it is believed that SAFIR is fully capable of simulating the structural response of the tested assembly with SFRC under design fire exposure. This validation indicates that SAFIR is fully capable of simulating the structural response of SFRC at elevated temperatures. As such, the material model input into SAFIR as discussed previously is assumed to be accurate and correctly programmed in SAFIR. Secondly, the model of the tested assembly is sufficiently accurate to warrant its use in parametric studies to identify the factors affecting the response of a composite floor assembly made with SFRC to fire exposure.

4.4.3 System Level-Steel Framed Building

The validity of SAFIR in predicting the system level response of structural systems under fire exposure has been established previously (Lim at. al 2004, Lamont and Lane 2006). As such, it is only necessary to validate SAFIR for use with the specific model constructed for this research. To that end, the test conditions for the Cardington restrained beam test as described in the previous chapter were modeled as closely as possible in SAFIR. Following completion of the numerical model, the deflection time history for select locations as predicted by SAFIR, were compared to those recorded during the fire resistance test.

Due to the symmetry within the structure, only a portion of the structure was modeled in SAFIR. Fig. 4.12a and 4.12b (British Steel 1998) show the elevation and plan views of the steel framed building respectively, with the location of the restrained beam highlighted, and the portion of the building that was modeled in this simulation indicated. Due to the complexities that are associated with modeling a ribbed composite floor slab, it was decided to use a slab represented by shell elements of uniform thickness as has been done in other studies (Zhang et al. 2008, Cashell et al. 2008). The thickness chosen for the slab was that of the thickest part of the ribbed flooring system, 130 mm. Fig. 4.13 shows the portion of the structure as modeled in the SAFIR computer program.

In the numerical model shown in Fig. 4.13, the concrete slab was modeled using four nodded shell elements with six degrees of freedom at each of the nodes. The beams and columns were modeled using three nodded beam elements with seven degrees of freedom at the end nodes and one degree of freedom at the center node. To simulate the composite action between the steel beam and the floor slab, the "SAMEALL" command was used for the nodes where the beam and shell elements coincide. This caused all of the translations and rotations at these points to be the same for the beam and slab, thus simulating the fully composite condition.

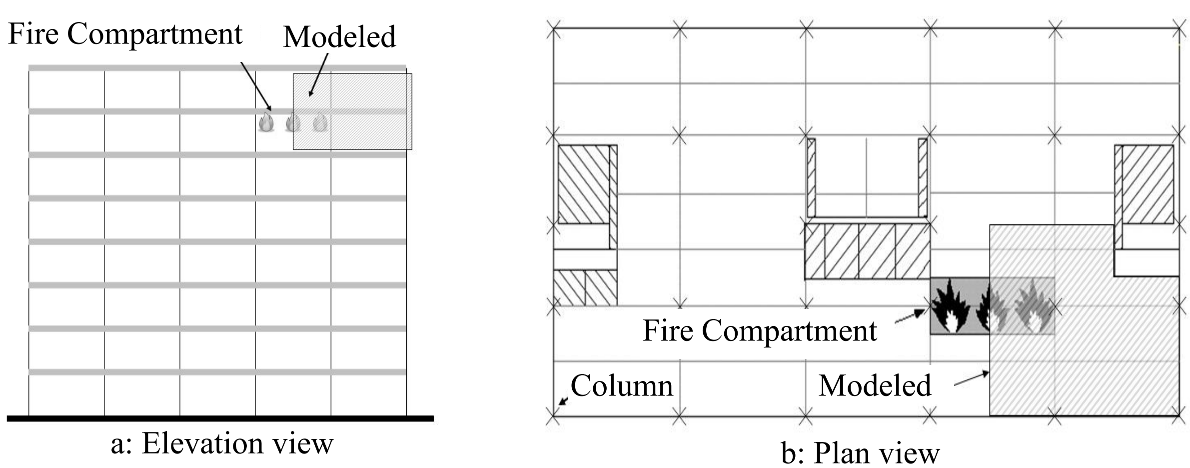

Fig. 4.12: Model of the steel framed Cardington steel framed building used for numerical studies

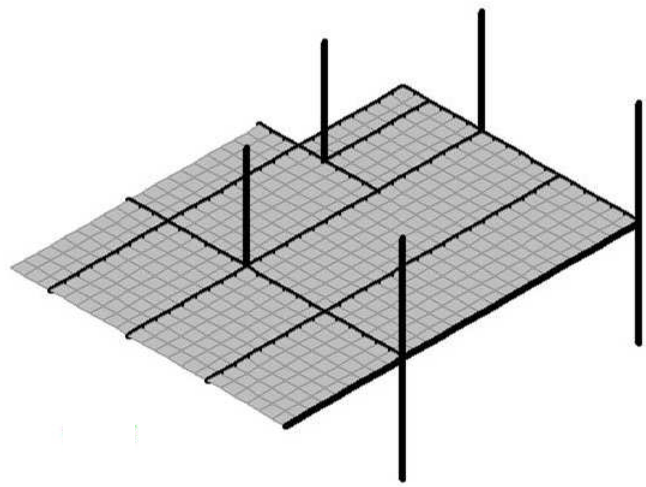

Fig. 4.13: Idealization of substructure modeled from the Cardington steel framed building for fire resistance analysis

Particular attention was given to the boundary conditions used in the simulation. It was assumed that the ends of the columns where they pass though the adjacent floors acted as fixed supports with all degrees of freedom being fully restrained. It was also assumed that the portion of the structure which was not modeled, being significantly larger than the modeled potion, was essentially rigid compared to the modeled portion. As such, the horizontal translation on the continuous edges was fully restrained in both directions. Due to the continuity of the slab over these points, the rotation about the length of the edge was assumed to be restrained, thus simulating the realist defection at the center of an unsupported slab. Lastly, the vertical translation was completely unrestrained, thus allowing the continuous edges of the modeled portion to deflect with realistic restraint. The validity of these assumptions of symmetry will be discussed in the following section.

For validation of the SAFIR model, the above depicted portion of the steel framed building was modeled under the time-temperature curve used in the restrained beam test (shown in Fig. 4.14) and under the test load of 4.94 kN/m^2 (British Steel 1998). For the analysis, the thermal and mechanical properties shown in Table 4.4 were utilized in SAFIR.

Table 4.4: Thermal and mechanical properties assumed in simulations

Steel			
Heat transfer coefficients		Mechanical parameters	
Hot convection coefficient	25	Young's modulus (GPa)	210
Cold convection coefficient	9	Poisson's ratio	0.3
Relative emissivity	0.5	Yield strength (MPa)	350
Concrete			
Heat transfer coefficients		Mechanical parameters	
Moisture content (kg/m^3)	46	Poisson's ratio	.25
Hot convection coefficient	25	Compressive strength (MPa)	35.4
Cold convection coefficient	9	Tensile strength (MPa)	1.78
Relative emissivity	0.5	-	-

Fig. 4.14 shows a comparison of the temperatures predicted by SAFIR with those observed during fire tests in the bottom corner of the heated beam. It can be seen that the temperatures predicted by SAFIR closely match those measured during the test. Toward the end of the simulation period there is a divergence in the temperatures, this is mainly due to ventilation issues inside the furnace causing the beam to cool differently, which could not be capture in the SAFIR analysis. The temperatures at several points in the unprotected steel beam and in the concrete floor slab were compared with predictions from SAFIR, and similarly good agreement was found at all locations. Overall, there is good agreement in the temperatures measured during testing and those predicted by SAFIR.

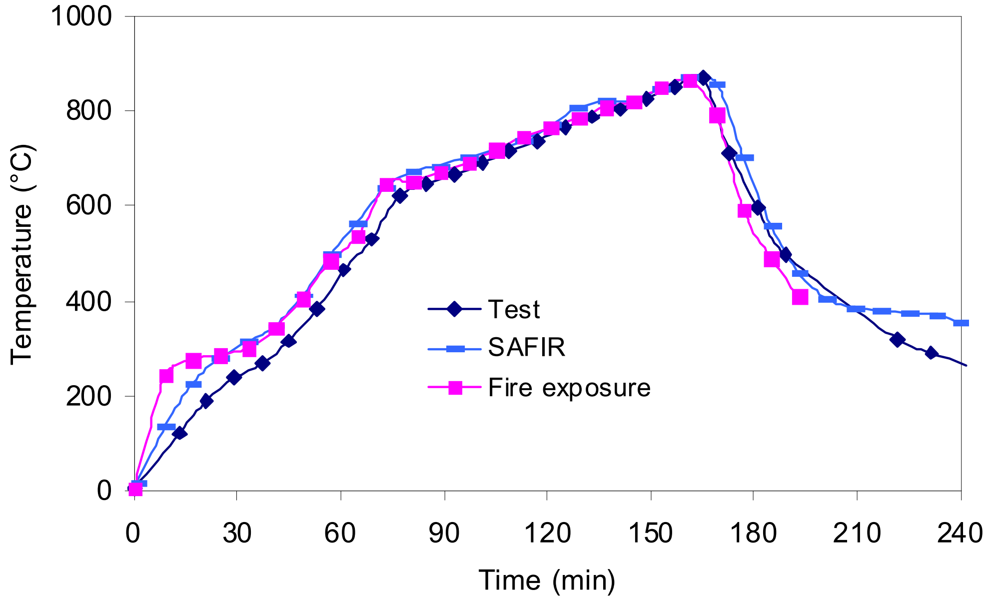

Fig. 4.14: Comparison of measured and predicted temperatures in the steel beam

The structural response from SAFIR was validated by comparing the measured mid-span deflection of the heated beam-slab assembly with that predicted by SAFIR (Fig. 4.15). As seen in Fig. 4.15, there is good agreement between the test data and the predictions from the SAFIR model in the heating phase. This indicates that SAFIR is able to accurately capture the effect of composite construction and the development of tensile membrane action during fire exposure. Due however to the unavailability of the test data beyond 150 minutes, it is not possible to validate the response of the model during the cooling phase of the fire. During testing, it was observed that the center of the heated beam rebounded such that a total deflection of 113 mm remained after the cooling phase. From Fig. 4.15 it can be seen that the same degree of rebound is not observed from the SAFIR model as 180 mm of deflection remain after the structure has completely cooled. This discrepancy is due to the material models used in SAFIR. It is assumed within SAFIR that both steel and concrete have the same mechanical properties at a specific temperature in both the heating and cooling phase of fire. Thus SAFIR neglects any damage that occurred to the constitutive materials due to the heat from fire.

The existence of only slight variations in the heating phase indicates that the SAFIR model accurately accounts for the contribution of composite and tensile membrane action during the heating phase of fire exposure. Ultimate deflections after fire exposure however cannot be accurately assessed using the validated model. As such, the following discussion deals with survival of the structure and maximum deflections, not the residual deflections after the structure has completely cooled. Any variation between the predicted and observed deflections in the heating phase can be attributed to assumptions made in the structural model constructed in SAFIR. These assumptions include the boundary conditions as discussed previously and the assumption that the steel beam and the slab act in complete composite action.

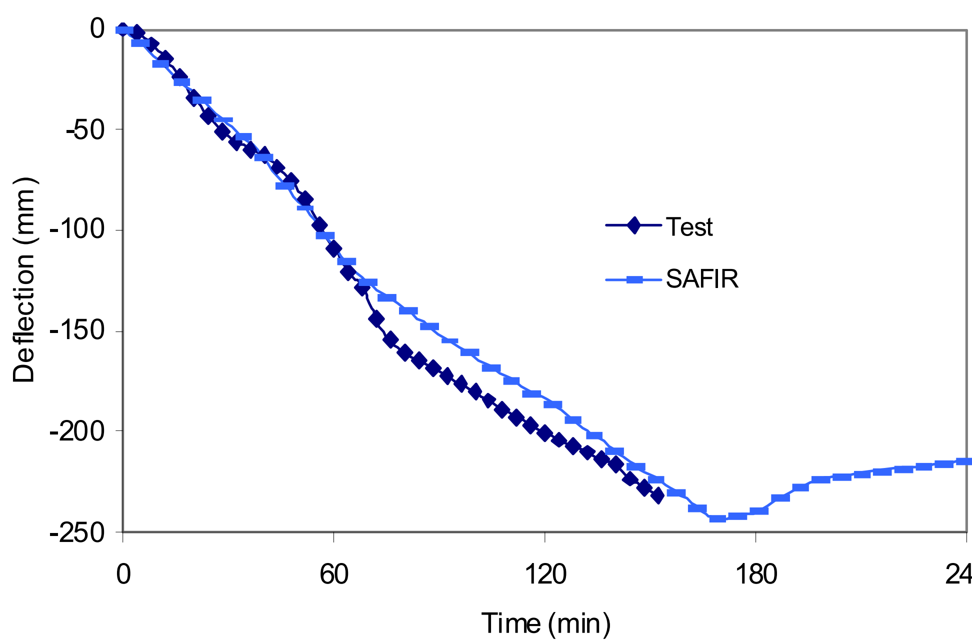

Fig. 4.15: Comparison of measured and predicted mid-span deflections for the beam

Given the thermal and structural model validations presented above, it was concluded that the models were sufficiently accurate to be used in parametric studies.

4.5 Summary

SAFIR was selected as the computational model of choice for use in the numerical studies conducted as part of this research program. Use of SAFIR to trace the response of structural members under fire exposure is well validated in the literature. However, there is a lack of validation for the use of SAFIR to capture the effects of composite construction and tensile membrane action under fire exposure, particularly for SFRC.

In order to validate the ability of SAFIR to accurately capture the effect of composite action under fire exposure, the assemblies tested at the element, assembly, and system levels as discussed in Chapter 3 were modeled using SAFIR. Results, (both thermal and structural) from the SAFIR simulations were compared with those recorded in fire tests. It was seen that in all cases, SAFIR predictions closely match the behavior of the specimen during the heating phase of fire exposure and not in the cooling phase. Thus, SAFIR is capable of capturing the contribution of composite construction to fire resistance only during the heating phase of fire exposure. Additionally, through validation of the tested steel beam-SFRC slab assembly, SAFIR was shown to accurately predict the behavior of steel fiber reinforced concrete under fire exposure, thus, the high temperature constitutive model implemented in SAFIR is deemed to be acceptable.

CHAPTER 5

5 PARAMETRIC STUDIES

5.1 General

For developing a methodology for fire resistant design of steel frame structures, the influence of critical factors on fire resistance is to be quantified. To that end, the numerical models discussed in the previous chapter were applied to conduct a series of parametric studies. These studies were conducted at the element, assembly, and system levels to quantify the influence of various factors on fire resistance of steel framed structures incorporating composite construction. At the element level, the effect of fire scenario, length, concrete filling type, load ratio, cross sectional size, and failure criterion were considered. For the assembly level, the effect of fire scenario, load level, slab thickness, and concrete type were studied. Finally, at the system level, the effect member interactions including composite construction and tensile membrane action were studied. These parameters were selected based on the previous studies in literature where the key parameters having an influence on structural fire resistance were identified. Further details on the range of variables selected and the full results from the parametric studies are provided in each section for the respective level of analysis.

5.2 Element Level – CFHSS Columns

To study the factors influencing the response of CFHSS columns exposed to fire, the calibrated SAFIR model discussed in Chapter 4 was applied to conduct a series of parametric studies. Data from these studies was used to identify trends on the response of CFHSS columns under fire exposure over a wide range of variables, details of which are presented below.

5.2.1 Column Characteristics

For the parametric studies, 20 CFHSS columns were selected. Fourteen of these were columns tested at NRCC (Table 3.1), while the remaining six are typical CFHSS columns specifically selected to cover a wider range of sectional sizes. The columns consisted of round and square sections filled with plain, steel fiber, and bar reinforced concrete as shown in Fig. 5.1.

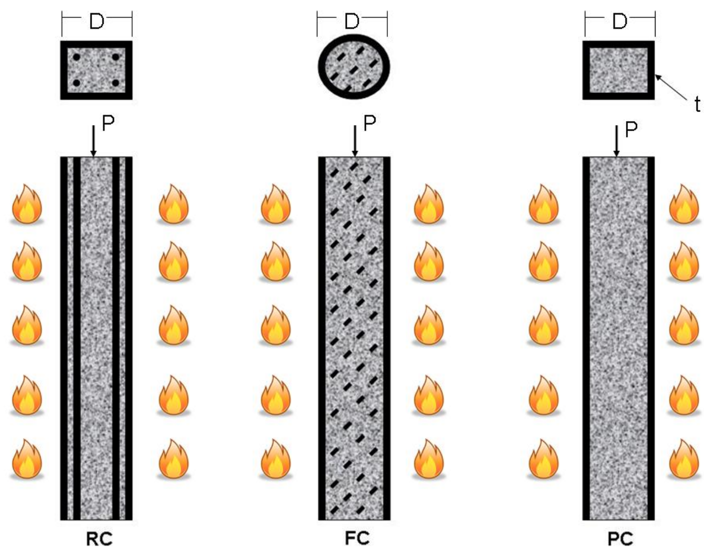

Fig. 5.1: Elevation and cross-section of RC, FC, and PC filled HSS columns used in parametric studies

For thermal analysis, the columns were modeled using two dimensional shell elements as shown in Fig. 5.2. For structural analysis, the columns were discretized along their length using three-node beam elements with an average length of 150 mm. The beam elements were assumed to have six degrees of freedom (three translations and three rotations) at the end nodes, and one degree of freedom at the middle nodes. Both the thermal and structural models used material properties according to Eurocode (2005a,b) for both steel and concrete. The specific material properties input into SAFIR for the thermal and structural analyses are presented in Table 5.1.

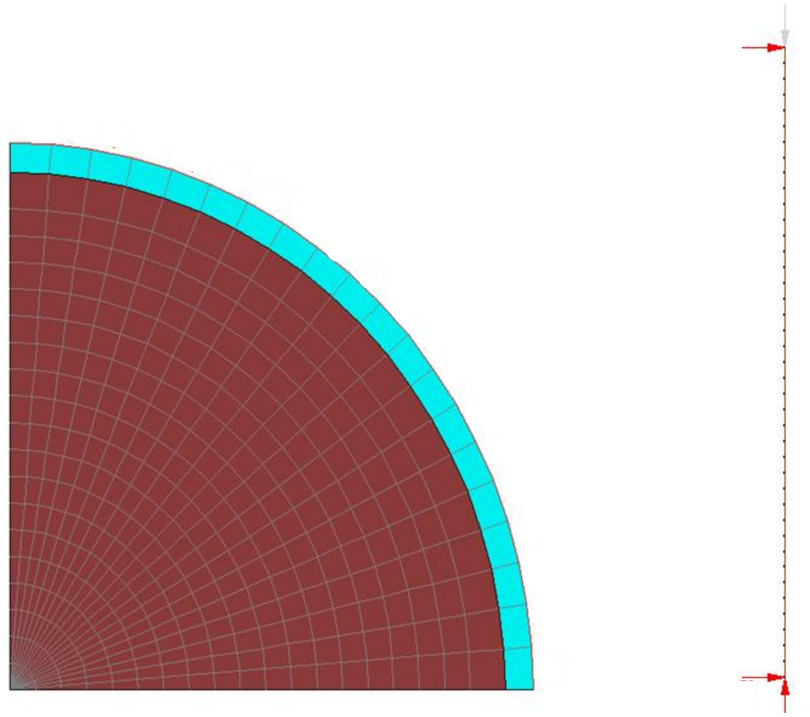

Fig. 5.2: Discretization of CFHSS columns for SAFIR analysis

Table 5.1: Thermal and mechanical properties assumed in simulations

Steel			
Heat transfer coefficients		Mechanical parameters (HSS/Rebar)	
Hot convection coefficient	25	Young's modulus (GPa)	210/210
Cold convection coefficient	9	Poisson's ratio	0.3/0.3
Relative emissivity	0.5	Yield strength (MPa)	350/413
Concrete			
Heat transfer coefficients		Mechanical parameters	
Moisture content (kg/m^3)	46	Poisson's ratio	.25
Hot convection coefficient	25	Compressive strength (MPa)	Variable
Cold convection coefficient	9	Tensile strength (MPa)	Variable
Relative emissivity	0.5	-	-

5.2.2 Critical Factors

Utilizing the SAFIR computer program, the 20 columns employed in the parametric study were exposed to a wide range of fire scenarios, lengths, loads, concrete strengths/composition, and failure criterion. These parameters were selected because their influence on the fire resistance of CFHSS columns in a performance-based environment has yet to be quantified. As such, a total of seven fire scenarios, five of which are shown in Fig. 5.3, were considered in the analysis. These fires were selected to represent the full range of fire exposures that would be practically experienced in typical medium rise office buildings. Fire exposure was assumed on all four sides (or around) of the column with the bottom and top 5% of the column unexposed to fire. It should be noted that the analysis was continued until the column attained failure or 240 minutes of exposure to fire. As such, if a fire resistance of 240 minutes is reached, it is indicative of the column withstanding compartment burnout, not that the column failed at 240 minutes unless specifically noted.

In addition to fire exposure, column length has been identified in the literature as a factor that can have a significant influence on the fire resistance of CFHSS columns that is yet to be investigated. To address this factor, columns ranging from 3.81 to 10 meters were considered under all fire exposures and load ratios to cover the practical range of columns that would be used in construction. To account for the fact that longer columns typically have lower load capacities that shorter columns, the load ratio was maintained constant in all analysis regardless of the length. That is to say, shorter columns had a higher (magnitude) load than longer columns.

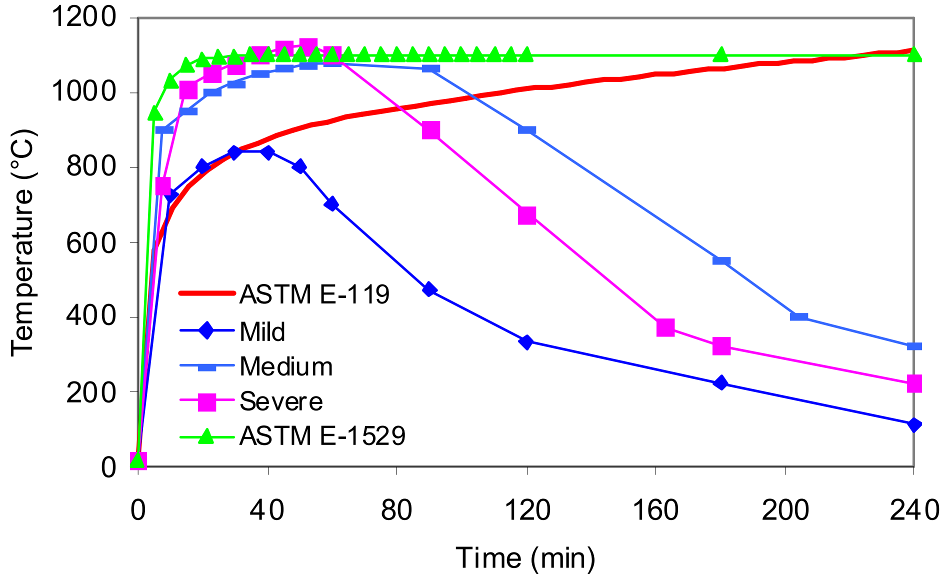

Fig. 5.3: Time-temperature relationships for various fire scenarios

As alluded to in the previous paragraph, load is also assumed to have a considerable influence on the fire resistance of CFHSS columns. To that end, the full range of columns was considered under different load levels to quantify the effect of load on fire resistance. Loads were modified to maintain a constant load ratio for all of the lengths modeled for a specific cross-section according to the AISC analysis procedure (AISC 2005). The applied loads on the columns were also modified to take into account the effect that the type of concrete filling has on fire resistance, accounting for the fact that steel fiber and bar reinforced concrete-filled HSS columns have a higher load capacity than columns filled with plain concrete.

Clearly, the type and strength of concrete will also have an influence on the fire resistance of CFHSS columns. As such, a wide range of concrete compressive strengths, the three primary filling types (PC, FC, and RC), and two primary types of concrete (siliceous and carbonate) were considered in the parametric study.

Lastly, failure criterion was considered as a factor influencing the fire resistance of CFHSS columns. In the physical domain, there are two ways in which a column can fail, the column can crush or buckle, i.e. material or stability failure. Often the provisions in codes and standards apply simplified criterion such as critical temperature to evaluate failure of a column, and these criterion do not take into account the beneficial effects of composite action on fire resistance. The presence of the concrete core serves to cool the steel shell and carry a portion of the load, and as such needs to be taken into consideration when evaluating the fire resistance of CFHSS columns. The effect of failure limit states on fire resistance for the full range of columns is presented in the respective section below.

5.2.3 Analysis Procedure

To study the effect of each variable outlined in the previous section, a series of parametric studies were carried out using the validated models. For each study, only one variable was changed at a time so the effect of that variable could be quantified. The primary output used to establish the effect of each parameter on fire resistance was the failure time of the column under fire exposure. No consideration was given to deflection in the analysis, only the failure time of the column as indicated by the inability of SAFIR to converge on a solution was used as a means for comparison.

5.2.4 Results and Discussion

This parametric study generated a total of 980 numerical simulations. The results (trends) discussed in the following sections apply to all three types of columns considered (PC, FC, RC) unless otherwise noted. To reduce redundancy however, only one column type is used to illustrate each point.

Effect of Fire Exposure

The effect of fire severity on fire resistance is illustrated in Fig. 5.4 by plotting the fire resistance as a function of length for column RP-273 under different fire scenarios. As is intuitive, as the fire severity decreases, the fire resistance of the column increases. It can be seen in Fig. 5.4 that fire resistance of four hours or more can be obtained for columns up to 10 m long under mild fire conditions. However, for other fire exposures, fire resistance decreases with an increase in length. A closer look at Fig. 5.4 indicates that fire resistance of a 5 m long CFHSS column ranges from 240 minutes for medium and mild fire exposure, to 68 minutes under severe exposure, with ASTM exposure yielding 100 minutes. The reason for this decreased fire resistance with increased fire severity can be attributed to the higher internal temperatures attained under severe fire exposure. Consequently, the column loses its strength and stiffness at a faster rate leading to early failure. Figs. 5.5 and 5.5 show the difference in internal temperatures observed in the steel shell and at the center of the concrete core for the fire exposures shown in Fig. 5.3.

It can be seen in Fig. 5.5 that two of the three design fires produce higher initial temperatures in steel than the ASTM E-119 (ASTM, 2007) fire. This effect is continued in concrete temperatures also, (Fig. 5.6) though to a lesser extent. The presence of the decay phase in the design fires causes the temperature in all locations of the column to be less (cooler) than that for the ASTM E-119 (ASTM, 2007) fire at the end of the simulation period. Column stability is maintained under design fires, despite the more severe initial temperatures, due to the decay phase of the fire allowing cooling of the steel before significant loss of strength in the concrete core occurs, as discussed in the following sections.

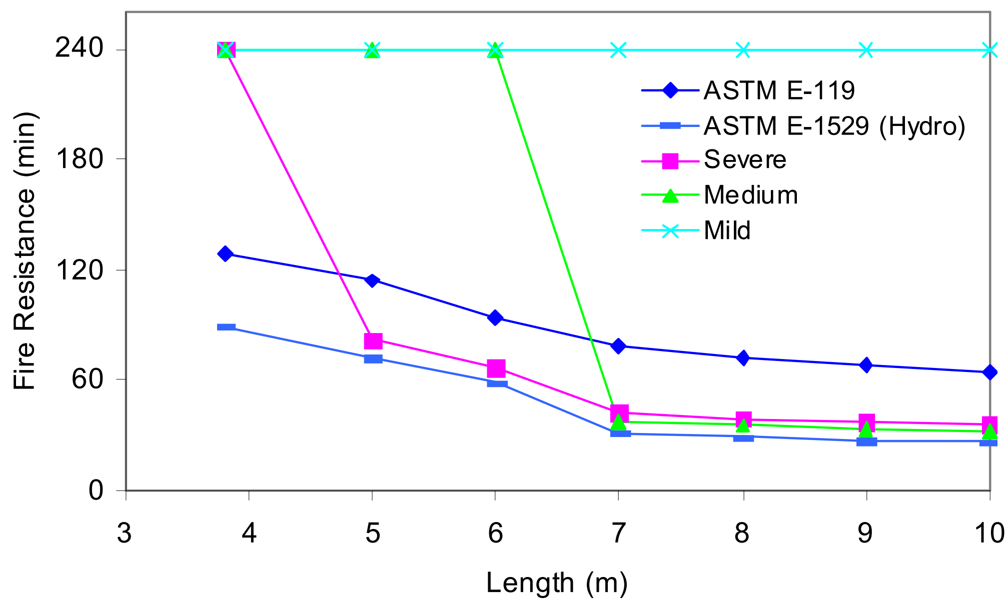

Fig. 5.4: Fire resistance as a function of length for column (RP-273) under different fire scenarios

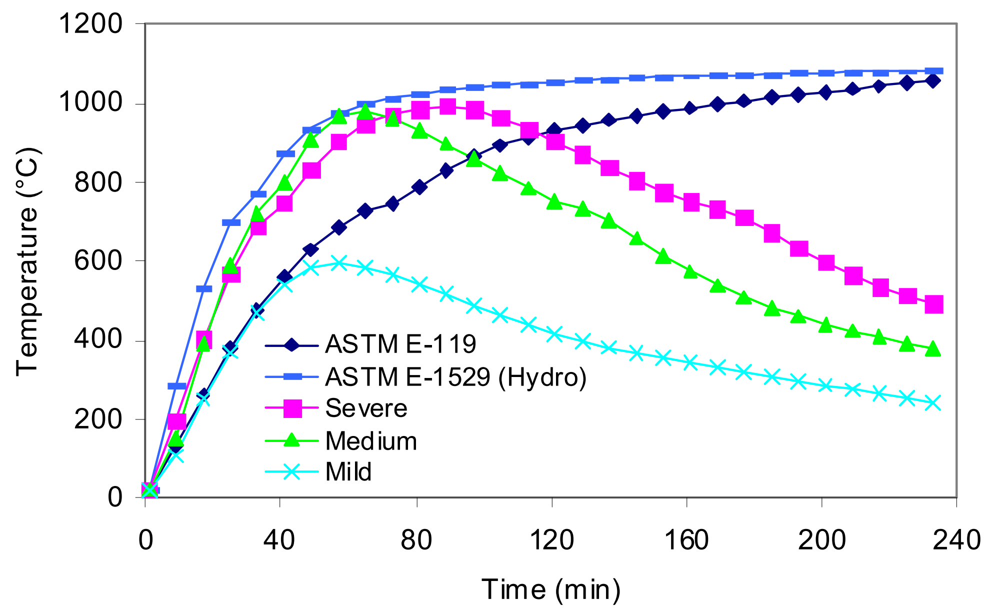

Fig. 5.5: Steel temperatures for column RP-273 exposed to different fire scenarios

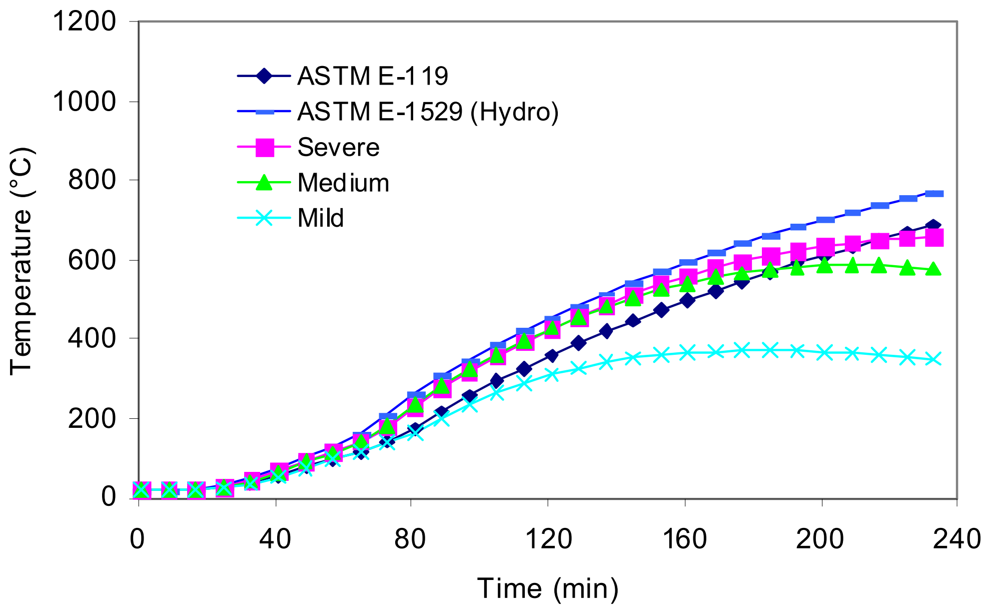

Fig. 5.6: Temperatures at the center of concrete core for column RP-273 exposed to different fire scenarios

To illustrate the effect of fire scenario on the structural response, Fig. 5.7 displays the axial deformation of column RP-273 resulting from ASTM E-119 (ASTM, 2007), severe, medium, and mild fire exposure. In all simulations, the column initially expanded due to the increasing steel temperatures. After this initial expansion, the response of the column is significantly influenced by the type of fire exposure. In the case of severe and medium fire scenarios, significant contraction occurs though the column does survive compartment burnout. The residual shortening of the column is attributed to residual damage from the heating phase of fire. During the heating phase of the fire, the column sustains damage in the form of steel yielding and some loss of concrete strength. When the column enters the cooling phase, the HSS section is in its damaged (shorter) condition. Hence, when the shorter damaged column cools, additional contraction (thermal shrinkage) is observed and the combined effect of cooling and the mechanical damage to the column results in the column suffering axial shortening by the end of the fire exposure period. However, under ASTM E-119 (ASTM, 2007) fire exposure, the column failed in 32 minutes without much contraction due to the absence of a cooling phase. Under the mild fire exposure, the temperatures achieved in the column are insufficient to cause failure of the HSS section and the subsequent load transfer to the concrete core. As such, there is minimal damage to the column and no residual deformation is observed.

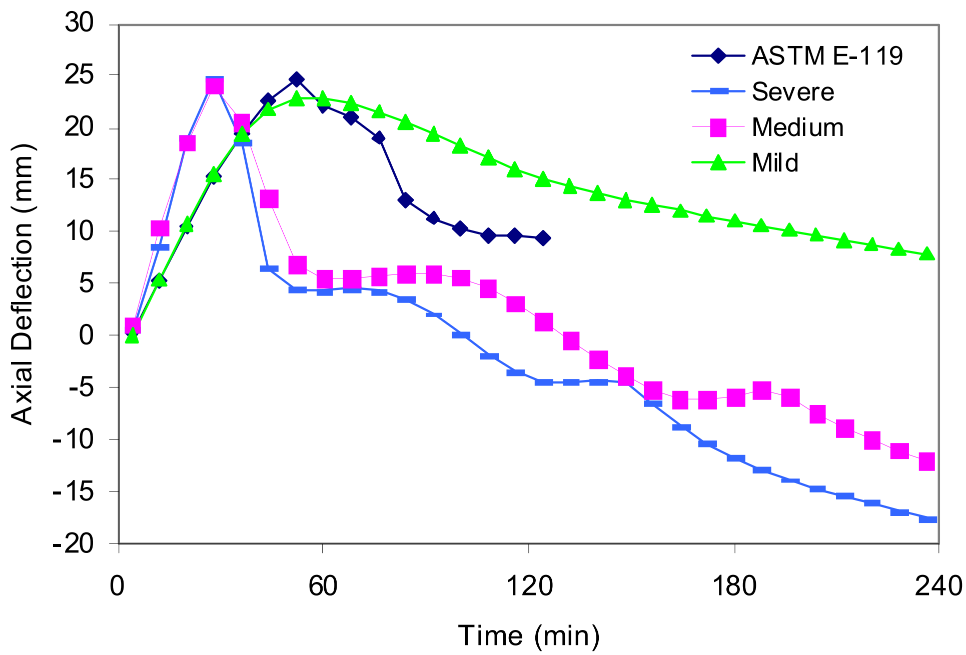

Fig. 5.7: Axial deformation of column RP-273 under different fire scenarios

Effect of Length

The results presented in Fig. 5.4 can be used to demonstrate the effect of length on the fire resistance of CFHSS columns. In the analysis, the load on the column was reduced as the length was increased, such that the load ratio on a single column was kept constant through all of the simulations. As would be expected, fire resistance for a given fire exposure decreases with an increase in column length. This is due to the increase in slenderness that accompanies the increase in length. Fire resistance is drastically reduced when the failure mode switches from crushing to buckling with increased length. This is most pronounced for the "medium" and "severe" fire exposure as can be seen in Fig. 5.4. Fire resistance under the medium fire drops from 240 to 45 minutes when length is increased from 5 to 7 m. Under severe fire exposure, the fire resistance decreases from 240 to 75 minutes for an increase in length from 3.81 to 5 m. However, under mild fire exposure, fire resistance remains high for all cases, and the length does not have any influence. The reason for such a drastic reduction in fire resistance with increased length in PC-filled HSS columns (not observed for RC and FC-filled columns as described in the next section) for more severe fire exposures is attributed to the weakening of the HSS section due to the heat from fire. PC-filled columns do not have sufficient strength (mainly tensile) in the concrete core to resist buckling when the heat from fire reduces the structural contribution of the HSS section. The composite columns that experience a rapid rise in temperature fail at a much shorter time when the dominant mode of failure switches from crushing to buckling. Based on the results and discussion presented here, it is clear that length has a significant influence on column fire resistance, specifically under severe fire exposures and for PC-filled HSS column.

Effect of Concrete Filling

The effect of concrete filling type on fire resistance is illustrated by analyzing HSS columns with different concrete filling types under ASTM E-119 (ASTM, 2007) fire exposure. As was the case with the effect of length, the applied load was modified according to AISC analysis procedures (AISC, 2005) to account for the different types of concrete filling in these cases. The fire resistance is plotted as a function of length for three similar CFHSS columns (Fig. 5.8), each with a different type (plain, steel fiber reinforced, bar reinforced) of concrete filling, columns selected for this comparison are RP 355, RF 356, and RB 406 respectively. The fire resistance decreases with an increase in length for all of the filling types. However, columns filled with bar or steel fiber reinforced concrete demonstrate higher fire resistance than the plain concrete-filled HSS column for all lengths. This can be attributed to the increased load carrying capacity and the increased resistance to buckling provided by the inclusion of reinforcement, and also due to the slower loss of strength in columns filled with RC and FC. These results indicate that it is possible to significantly enhance the fire resistance of CFHSS columns by changing the type of concrete filling.

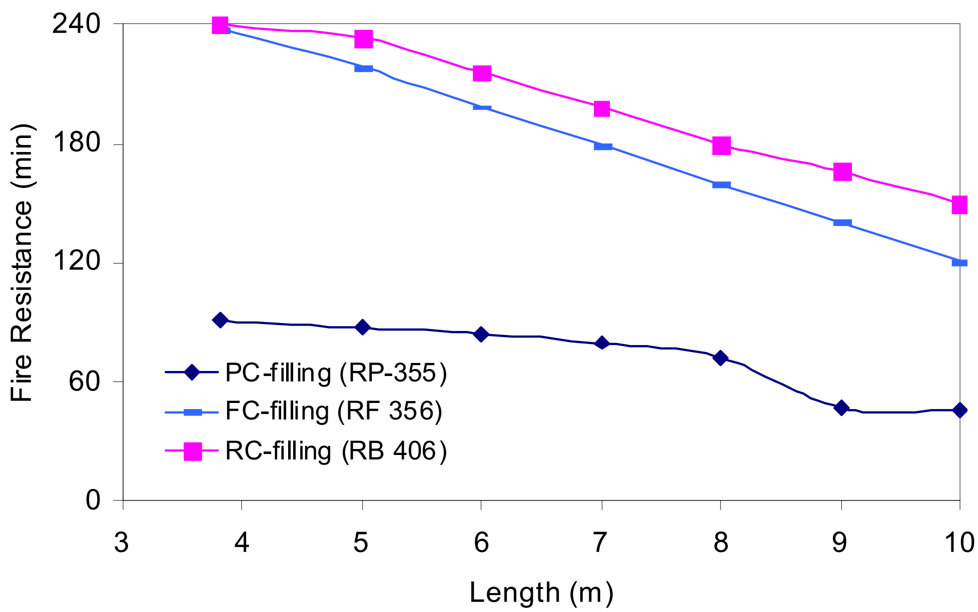

Fig. 5.8: Effect of length and concrete filling on fire resistance of CFHSS columns

Effect of Load Ratio

The effect of load ratio on fire resistance was investigated by analyzing three columns under ASTM E-119 (ASTM, 2007) fire, with load ratios ranging from 0.1 to 1.0 (10% to 100%). The analysis was carried out for three types of concrete filling, namely: plain (RP 273), steel fiber reinforced (SF 219), and bar reinforced (RB 273) filling. It can be seen in Fig. 5.9 that only the bar reinforced concrete-filled HSS column withstood the ASTM E-119 (ASTM, 2007) fire for

240 minutes with a load ratio of 10% (0.1). Columns SF-219 and RP-273 lasted for 234 and 170 minutes respectively. The fire resistance decreases rapidly with an increase in load ratio up to 0.4. After which point the rate of decrease in fire resistance is slower. This can be attributed to the fact that concrete filling generally provides a load bearing contribution of about 30%-40% of the overall composite column capacity. In a fire scenario, the steel shell looses its strength very quickly, and concrete carries most of the load. Thus, for load ratios higher than 40%, the concrete filling has to be strengthened either through the use of bar-reinforcement, or through the use of steel fibers to achieve higher fire resistance. In design fires, the same trend is observed as in the ASTM E-119 (ASTM, 2007) fire, with the exception that the times to reach failure are increased depending on the type of design fire considered. Design fires allow the use of load ratios in the range of 40-50%, while still achieving the required fire resistance

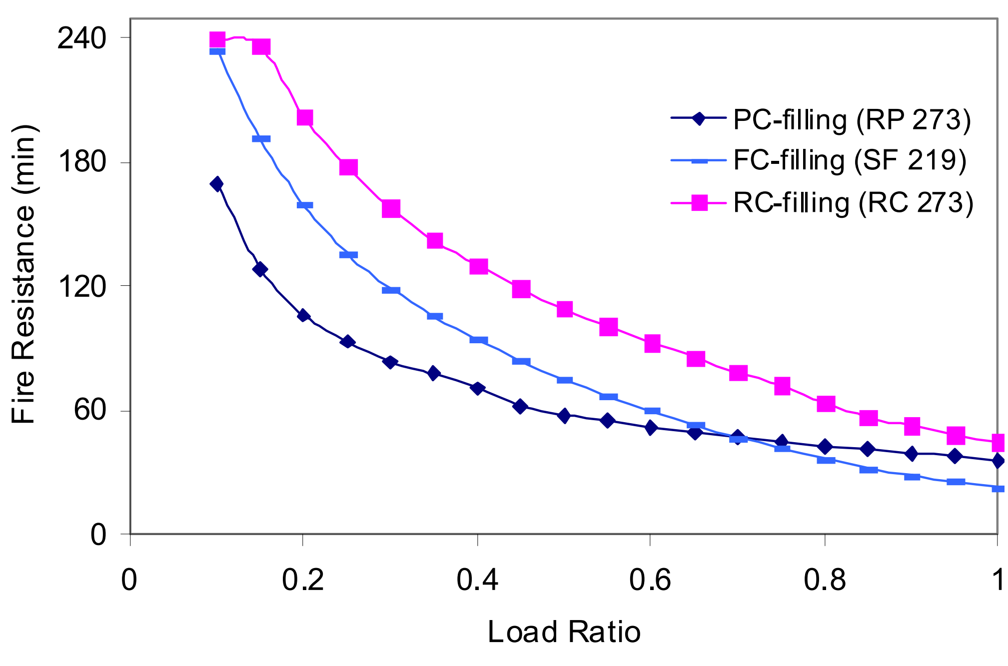

Fig. 5.9: Effect of load ratio on fire resistance of CFHSS columns

Effect of Cross-section Size

Results from the analysis indicate that the fire resistance of CFHSS columns increases with an increase in cross-sectional size. This is due to the increased contribution of the concrete core to the column strength. When cross-section size is increased, the concrete core comprises a larger percentage of the load bearing capacity of the section. When a CFHSS column is exposed to fire, the steel section loses its strength quickly and transfers the load to the concrete core. The core in turn being larger, is capable of providing longer fire resistance times. The strength loss in the concrete core is slower than in the HSS section, allowing the column to achieve enhanced fire resistance. The increased cross-sectional size also enhances stiffness, and thus, resistance to buckling of the column, allowing higher fire resistances to be achieved in longer columns. Columns filled with plain concrete however, realize no additional advantage from cross-section increases beyond 400 mm. This is due to high-temperature instability of the concrete core causing premature failure for larger cross-sectional sizes when plain concrete is used.

Effect of Aggregate Type

Results from the SAFIR analyses indicate that aggregate type has a moderate influence on the fire resistance of CFHSS columns. The two common types of aggregate used in CFHSS columns are: carbonate (mainly consisting of limestone) and siliceous (mainly consisting of quartz) aggregate. Carbonate aggregate concrete typically demonstrates higher fire resistance than siliceous aggregate concrete (Kodur and Lie, 1996, Kodur and Lie, 1997). This is due to an endothermic reaction occurring in carbonate aggregate at 600-800 °C, in which the dolomite within the aggregate dissociates. Consequently, the heat capacity of carbonate aggregate increases significantly and is approximately 10 times higher than siliceous aggregate in the same temperature range. As a result, there is a slower increase in temperature in the carbonate aggregate concrete, and thus, a slower loss of strength. Therefore, the fire resistance of CFHSS columns filled with carbonate aggregate concrete is about 10% higher than siliceous aggregate concrete-filled HSS columns.

Effect of Failure Criterion

The two limit states considered in codes and standards for defining failure of steel columns under fire conditions are: limiting temperature, and stability retention. ASTM E-119 (ASTM, 2007) defines fire resistance as the time it takes to reach a maximum average section temperature of 538 °C, or a maximum single point temperature of 649 °C. On the contrary, stability-based failure criterion are based on the duration of time during which a column maintains structural stability (strength) during fire exposure. In the case of CFHSS (composite) columns, using the limiting temperature criterion for steel does not reflect realistic fire resistance performance due to the significant structural contribution from concrete through composite action. As an illustration, column RP-273 achieved fire resistance of 143 minutes in testing, and 128 minutes in the SAFIR simulation, thermal failure criterion however would only yield a resistance of 38 minutes for this column. Clearly, thermal failure criteria do not reflect the contribution of the concrete filling to the fire resistance of CFHSS columns. As such, it is necessary to employ stability-based failure criterion in the evaluation of the fire resistance of CFHSS columns.

5.2.5 Summary

Based on the above analysis, the following points can be summarized with respect to critical factors influencing the fire resistance of CFHSS columns:

- Type of fire exposure has a significant influence on the fire resistance of CFHSS columns. The fire resistance of CFHSS columns under most design fire scenarios is higher than that under ASTM E-119 (ASTM, 2007) standard fire exposure.

- Apart from fire exposure, the other significant factors that affect the fire resistance of CFHSS columns are length, type of concrete filling, load ratio, and failure criterion.
- It is possible to obtain unprotected CFHSS columns up to 10 m in length capable of withstanding complete compartment burnout through the use of different types of concrete filling.
- The limiting criterion, used for determining failure, has a significant influence on the fire resistance of CFHSS columns. The conventional failure criterion, such as limiting steel temperature can not be applied to CFHSS columns. Strength and deformation failure criteria should be considered for evaluating fire resistance of CFHSS columns.

In the following Chapter, these factors will be utilized to develop relevant design methodologies for enhancing the fire resistance of CFHSS columns.

5.3 Assembly Level – Composite Floor Assemblies

To study the factors influencing the response of composite floors incorporating SFRC to fire exposure, the calibrated assembly level model of the tested steel beam-SFRC slab assembly was applied to conduct a series of parametric studies. Data from the parametric studies was utilized to identify trends in the response of composite floors incorporating SFRC under fire exposure over a wide range of variables, details of which are presented below.

5.3.1 Assembly Characteristics

For all of the simulations, the beam-slab assembly had the same geometric configuration as the validated model discussed in Chapter 4. A quarter-section of the floor slab and supporting steel beams was modeled in SAFIR as shown in Fig. 5.10. The concrete slab was modeled as a series of four nodded 150 mm square shell elements (with minor geometric alterations to accommodate the geometry of the assembly) with each node having six degrees of freedom. The supporting beams were modeled as 150 mm long three nodded beam elements; the two end nodes each had seven degrees of freedom, while the center node had one degree of freedom. The mechanical properties as input in SAFIR for the steel and concrete are summarized in Table 5.2.

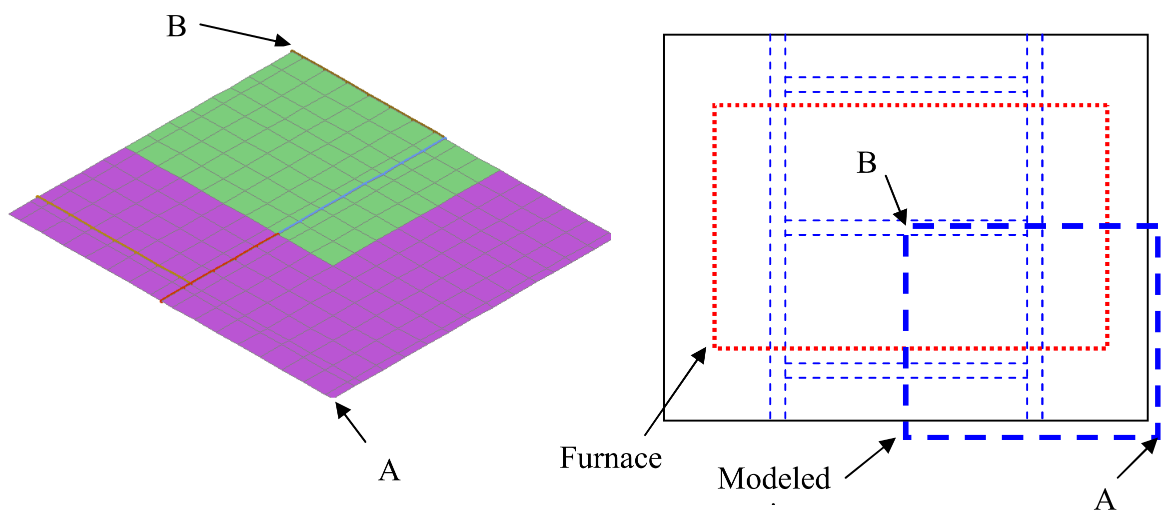

Fig. 5.10: Dicretization of the steel beam-SFRC slab assembly used in parametric studies

Table 5.2: Mechanical properties utilized in analysis simulations

Steel		Concrete	
Young's modulus (GPa)	210	Poisson's ratio	0.25
Poisson's ratio	0.3	Compressive strength (MPa)	46.6
Yield strength (MPa)	350	Tensile strength (MPa)	5.34

The assumed symmetric condition causes one of the lines of symmetry to run down the length of the unprotected W10X15 beam in the center of the assembly. Two options exist for modeling this condition, first, only half of the beam could be modeled, or second, the entire beam could be modeled and the elastic modulus and yield strength reduced to 50% for the duration of the fire exposure to simulate the response of the partial section in the symmetric condition. The first option causes instability in the model due to a non-symmetric beam element about its own axis and SAFIR has a difficult time converging on a solution, as such, the later option was chosen, and the entire beam was modeled with a yield strength and elastic modulus of 50%. In addition to this concern, the bending stiffness of the section is proportional to the elastic modulus multiplied by the moment of inertia, either of these can be reduced and the effect is the same, as such, the assumption should not influence the response of the structure to fire exposure. To establish the validity of this approach, parallel simulations were run for the full assembly and the reduced assembly with the material properties of the central beam reduced by 50%. Deflections predicted by the two models almost coincided, having less than a 5% discrepancy at any point during the simulation. As such, this assumption of reduced material properties is deemed a reasonable, and in light of the computational savings, a necessary assumption.

5.3.2 Critical Factors

Utilizing the SAFIR computer program the effect of fire exposure, load level, slab thickness, and concrete type (SFRC) on the fire resistance of composite floor assemblies was studied. These parameters were selected because their influence on the fire resistance of steel beam-concrete slab assemblies in a performance-based environment has yet to be quantified. As such, to investigate the effect of fire exposure, ASTM E-119 fire exposure and four levels of design fires were considered as shown in Fig. 5.11. The design fires utilized in this study are an extreme fire representing a large open workspace, a severe case representing a small more compartmentalized workspace, and a medium fire representing a storage area in which the fuel load is considerable but ventilation is poor. In addition, the analysis was also carried out under the fire scenario used in the fire test (Fig. 3.14). A mild fire case was not considered in these simulations since very few failures occur as a result of mild fire exposure. The effect of each of these parameters is discussed independently in the following sections.

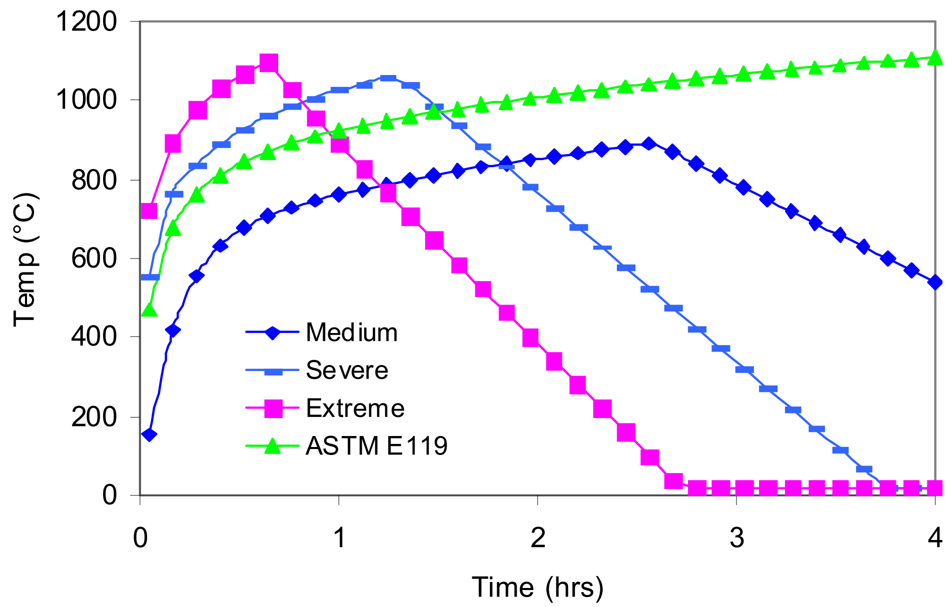

Fig. 5.11: Standard and design fire scenarios used in parametric studies on beam-slab assemblies

In addition to fire exposure, load level was considered as a primary factor influencing fire resistance of the composite floor assemblies. To investigate the influence that load has on the structure, three load levels were considered, a high, medium, and low load level. It should be noted that the load was not adjusted for changes in slab thickness or concrete strength, as such, the load refers to an absolute magnitude value load rather than a load ratio as was the case with CFHSS columns.

From the literature, it was determined that slab thickness also plays a significant role on fire resistance of floor systems, as such, slab thickness was investigated as part of this research study. Slab thicknesses ranging from 110 to 150 mm were considered atop the steel beam network previously described, and the effect of slab thickness on fire resistance was determined.

Lastly, the effect of concrete type, namely, plain and steel fiber reinforced concrete, on the fire response of beam-slab assemblies was studied to quantify the influence of SFRC as presented in the following sections.

5.3.3 Analysis Procedure

To study the effect of each variable outlined in the previous section, a series of parametric studies were carried out using the validated model. For each study, only one variable was changed at a time so the effect of that variable could be clearly isolated. The primary output used to establish the effect of each parameter was the failure time of the assembly under fire exposure. Failure of the assembly was said to occur in the analysis at the time when SAFIR failed to converge on a solution.

5.3.4 Results and Discussion

The parametric study generated a total of 81 numerical simulations under different parameters. It should be noted that only the significant trends are discussed, and that the discussion applies to all of the assembly models unless otherwise noted.

Effect of Fire Exposure

Fig. 5.12 illustrates the effect of different fire exposures on the fire resistance of the beam-slab assembly. It can be seen in Fig. 5.12 that both beam slab assemblies (with plain concrete and SFRC) survive complete compartment burnout under the medium fire exposure. This can be attributed to the relatively low temperatures achieved in the medium fire exposure being insufficient to substantially reduce the structural capacity and stiffness of the assembly. Under the test (Fig. 3.14) and severe (Fig. 5.12) fire exposures, only the assembly with the SFRC slab survives compartment burnout. Though the temperatures in the severe fire case are more severe than in the medium case, the enhanced tensile strength and ductility properties of SFRC, coupled with the early onset of the cooling phase in the severe fire exposure, help the steel beam-SFRC assembly to survive compartment burnout. In the case of the steel beam-PC slab, the structural contribution of the concrete is insufficient, and the assembly fails in the simulation. This serves to highlight the effect of tensile membrane action on fire resistance under different fire exposure conditions. The superior tensile strength of SFRC as compared to PC enhances the fire resistance of the assembly sufficiently, through the development of TMA, for the assembly to reach burnout conditions and survive the severe fire exposure.

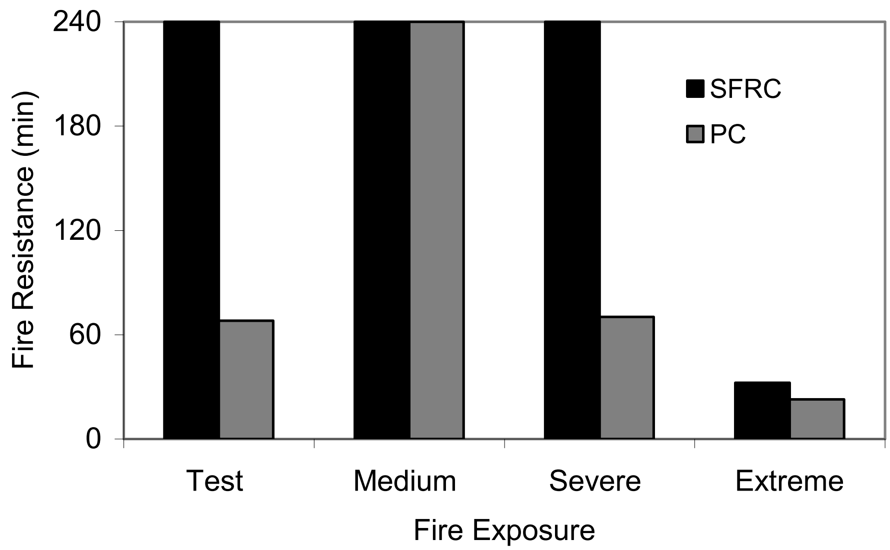

Fig. 5.12: Fire resistance of beam-slab assemblies under various fire exposures

Lastly, under extreme fire exposure, neither the plain concrete nor the SFRC concrete slab assemblies achieved one hour fire resistance. This can be attributed to very high temperatures (in excess of 1100 °C) reached in the beam early in the fire exposure. The high early temperatures in the beam do not allow sufficient heating of the slab for the benefits of composite construction to be realized. For the development of TMA, significant deflections need to be achieved in the slab, under the fire exposure, failure occurs before these defections can develop. In typical office building compartments however, it is highly unlikely that such extreme temperatures would be achieved, and the “medium” and “severe” fire exposures (where temperatures are in the range of 700-1000 °C) are far more representative fire scenarios. Under such fire conditions, the beam-slab assembly made with SFRC (despite reaching large deflections) can withstand complete compartment burnout. This is attributed to the enhanced properties of SFRC (tensile strength) allowing the assembly to survive until the cooling phase of the fire, at which point the assembly begins to regain strength and stiffness. As such, it is possible under design fire exposure, for beam-slab assemblies made with SFRC and utilizing unprotected steel beams to provide 1-2 hours of fire resistance.

Effect of Load

The fire response of the beam slab assembly was investigated under three (high, medium, and low) load levels representing a range of load ratios of 24-36% in the central unprotected beam, 32-48% in the connections of the central beam to the protected girders, and 40 to 60% in the protected girders. This range of load levels was selected because it represents the realistic (reduced) load levels that would be on the floor system of a typical office building under fire exposure when load factors for fire conditions as specified in ASCE-07 (1.2DL + 0.5LL) are applied. Fig. 5.13 shows SAFIR predictions for the mid-span deflections in the beam under the high and low load ratios for an assembly with a 130 mm thick SFRC slab exposed to the "severe" fire. While a total of 81 simulations were conducted under different combinations of fire exposure, loading, slab thickness, and concrete type, Fig. 5.13 presents only two cases to illustrate the typical response of the assembly. From Fig. 5.13 it can be seen that under the high load ratio, the assembly demonstrates approximately 70 minutes of fire resistance, while in the case of the low load ratio, the assembly survives compartment burnout.

Of particular interest from Fig. 5.13 is the observation that the deflection profiles in both cases follow a similar trend for the first 20 minutes of fire exposure, with deflections under the high load ratio being only slightly greater than those under the low load ratio. This can be attributed to the response of the beam-slab assembly being controlled by the strength of the unprotected steel beam early in fire exposure. As the temperatures in the unprotected beam continue to increase as a result of fire exposure, the strength contribution of the beam is reduced, and the benefit of composite action is utilized. Under the low load ratio, the strength contribution achieved through composite action and SFRC is sufficient to transfer the entire load from the failing unprotected beam to the protected girders, thus leading to the beam-slab assembly surviving compartment burnout. Under the high load ratio however the slab is unable to transfer the full load from the failing unprotected beam through TMA, so the beam fails after approximately 70 minutes of fire exposure.

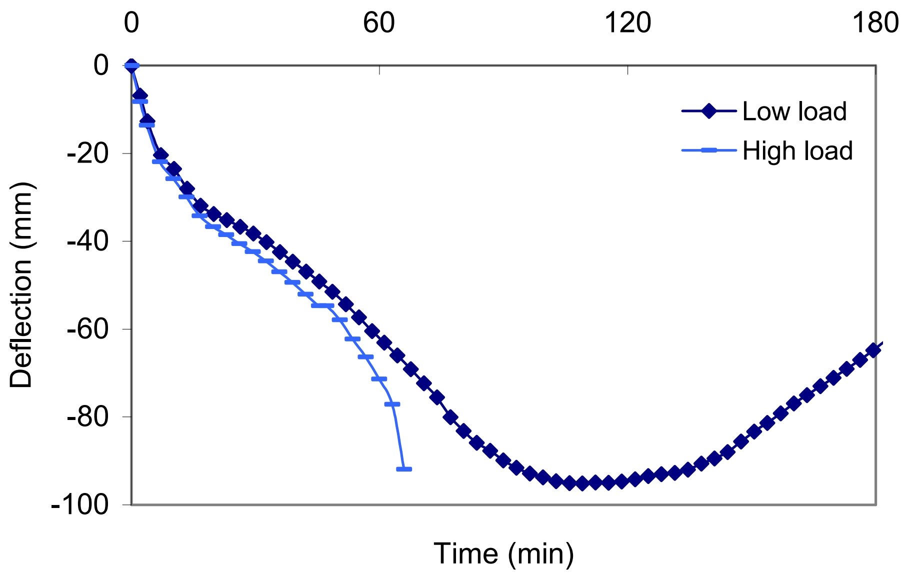

Fig. 5.13: Variation of mid-span (beam) deflection as a function of fire exposure time for different load levels

Effect of Slab Thickness

The effect of slab thickness on fire resistance of the assembly was evaluated by simulating three different thicknesses of slab (110, 130, and 150 mm) under different combinations of loading, fire exposure, and concrete type (PC and SFRC) previously discussed. The limit state used to determine failure in these analyses is that of structural integrity, though temperatures on the unexposed surface were monitored, they did not govern. Though a total of 81 simulations were conducted, two cases are potted in Fig. 5.14 that correspond to an assembly with a SFRC slab of 110 mm and 150 mm (thin and thick respectively) exposed to a severe fire and subjected to a medium load level to illustrate the typical response observed in the simulations. For the first fifteen minutes of fire exposure, both slabs produce similar deflection trends and at the same rate, this can be attributed to the structural contribution of the unprotected steel beam early in the fire exposure. As the steel beam weakens later in the fire exposure due to increasing temperatures, the thin slab due to higher temperatures and the inability of the slab to develop TMA starts to deflect rapidly until failure of the assembly. The thicker slab however, experiences lower temperatures (due to the increased thermal capacity of the thicker slab) and is able to develop higher TMA (due to the thicker slab). This benefit of composite construction slows the deflection rate of the slab and allows the thick assembly to survive until the cooling stage of the fire, and hence, survive compartment burnout.

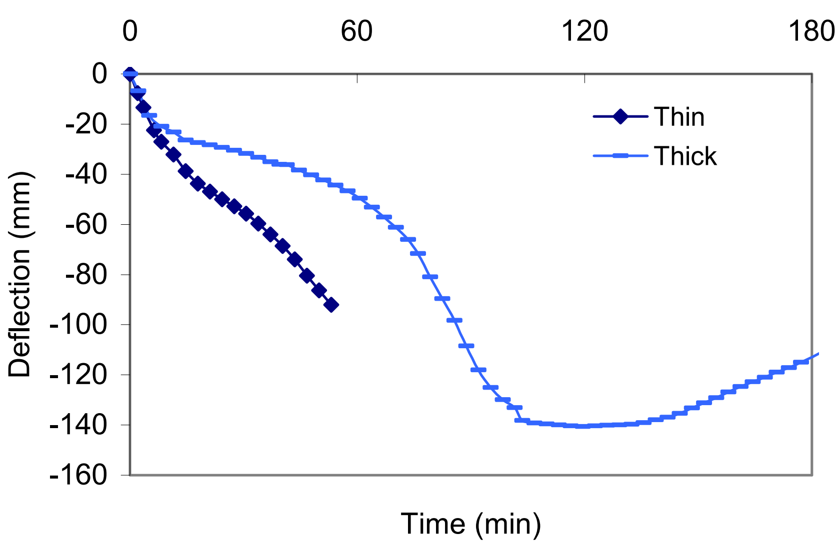

Fig. 5.14: Fire resistance of beam-slab assembly as a function of slab thickness

Effect of Concrete Type

Results presented in Fig. 5.12 can also be used to illustrate the effect of concrete type used in the slab on the fire response of beam-slab assemblies. Under “test” fire conditions (Fig. 3.14), the beam-slab assembly with SFRC attained more than four hours of fire resistance, (survived compartment burnout) while plain concrete slab assembly achieved only about a hour of fire resistance as seen in Fig. 5.12. The ability of the steel beam-SFRC slab assembly to survive compartment burnout in this condition can be attributed to several factors, the most significant of which is the development of TMA. The stress distribution as predicted by SAFIR was markedly different for assemblies with SFRC and plain concrete slabs. The SFRC specimen had a tensile field develop in the center of the slab consistent with a tensile membrane action mechanism, while the plain concrete slab did not develop TMA. The development of this tensile field helped redistributed loads from the failing unprotected W10X15 beam to the cooler insulated W12X16 beams that supported the specimen (see Fig. 3.13 for the structural layout). This load redistribution allowed the assembly to withstand the heating phase of the fire and enter the cooling regime (decay phase) in which the beam slabs could regain their strength and stiffness properties.

The structural response of two beam slab assemblies (PC and SFRC) is plotted in Fig. 5.15 which shows that both assemblies behave similarly early in the fire exposure (prior to failure of the W10X15 beam at about 20 minutes). However, when the unprotected W10X15 beam begins to fail, due to increasing steel temperatures, the slab starts to carry an increasing portion of the load in both cases. At this point, the response of the respective slab begins to differ. The rate of deflection did not significantly change for the plain concrete slab, thus indicating that the plain concrete slab was unable to support the additional load being transferred to it by the failing

W10X15 beam. In the plain concrete slab specimen, the rate of deflection remained relatively unchanged until a deflection of approximately 80 mm was achieved in the center of the slab. At this point, the rate of deflection changed because the plain concrete slab failed to develop tensile membrane action. This contribution increased the fire resistance by about 10 minutes with the specimen ultimately failing at about an hour.

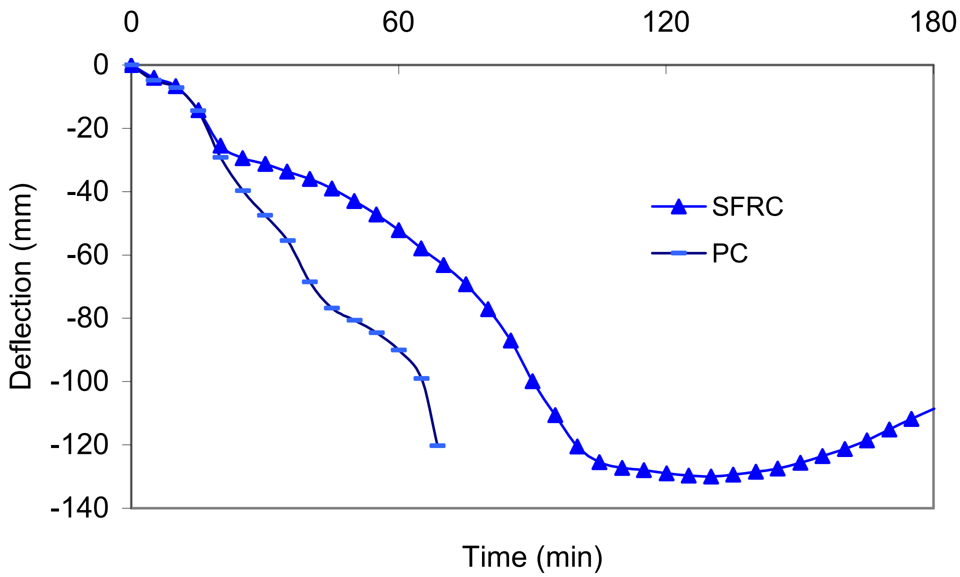

Fig. 5.15: Mid-span deflection in secondary beam as a function of time for PC and SFRC slabs

The behavior of the SFRC assembly, however, is markedly different as can be seen in Fig. 5.15. When the unprotected W10X15 beam looses its strength capacity, the SFRC slab due to enhanced tensile and ductility properties of SFRC was able to transfer the load to the cooler parts of the assembly through TMA. This load transfer significantly lowered the deflection rate after approximately 25 minutes. Between 25 and 90 minutes, deflections increased gradually (due to increasing slab temperatures) until the fire entered the decay phase. During the initial stages of the decay phase, the deflections were steady and the load was carried by the SFRC slab through

TMA. When the unprotected W10X15 steel beam starts to cool and re-gain strength and stiffness, the beam starts to carry some portion of the load. This contribution of the W10X15 to load transfer, combined with the thermal shrinkage of the deck and supporting steel beams caused the slab to rebound as seen in Fig. 5.15. This markedly different behavior is made possible by the better tensile and ductility properties of SFRC that enhanced the beneficial effects of TMA.

5.3.5 Summary

Based on the above analysis, the following points can be summarized with respect to critical factors influencing the fire resistance of composite floor assemblies:

- Composite floor assemblies under fire exposure develop significant tensile forces through tensile membrane action; this facilitates load transfer from fire weakened steel beams to other cooler parts of the slab. The extent of load transfer achieved though tensile membrane action is dependent on the fire exposure, slab thickness, and concrete type.
- Through the utilization of composite action, fire resistance can be significantly enhanced in steel beam-concrete slab assemblies. Unprotected steel beams that have fire resistance of only 20-25 minutes can survive compartment burnout under most low to moderate fire exposure scenarios when part of a composite beam-slab assembly.
- The use of SFRC in slabs, in place of plain concrete, further enhances the fire resistance of the beam-slab assembly even under medium to high fire scenarios. This is attributed to the high tensile strength of SFRC facilitating the development of tensile membrane action. Thus, no consideration is given to the use of plain concrete for achieving fire resistance in composite beam slab assemblies in the following chapters

- Through the use of SFRC, in place of plain concrete, in composite beam-slab assemblies, it is possible to achieve fully unprotected secondary steel beams even under medium to high fire scenarios.

In the following Chapter, these conclusions will be utilized to develop relevant design methodologies for enhancing the fire resistance of composite beam slab assemblies.

5.4 System Level – Steel Framed Structural Systems

To study the factors influencing the response of a full-scale composite steel framed structure to fire exposure, the calibrated model of the Cardington Restrained beam test was applied to conduct a series of parametric studies. Results from these parametric studies were used to identify trends in the response of composite steel framed structures under fire exposure over a range of variables, details of which are presented below.

5.4.1 System Characteristics

For all of the simulations, the validated model of the Cardington restrained beam test as described in Chapter 4 was utilized. Fig. 5.16a and 5.16b show the elevation and plan views of the steel framed building respectively, with the location of the restrained beam highlighted, and the portion of the building that was modeled in these simulations indicated.

In the numerical model shown in Fig. 5.17, the concrete slab was modeled using four nodded shell elements with six degrees of freedom at each of the nodes. The beams and columns were modeled using three nodded beam elements with seven degrees of freedom at the end nodes and one degree of freedom at the center node. To simulate the composite action between the steel beam and the floor slab, the "SAMEALL" command was used for the nodes where the beam and shell elements coincide.

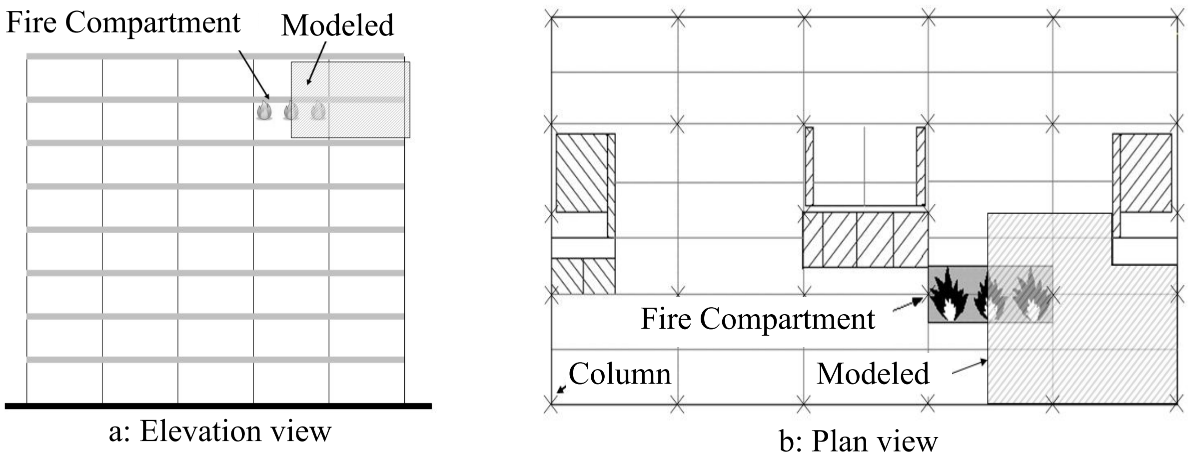

Fig. 5.16: Elevation and plan view of the simulated steel framed building (used in Cardington tests)

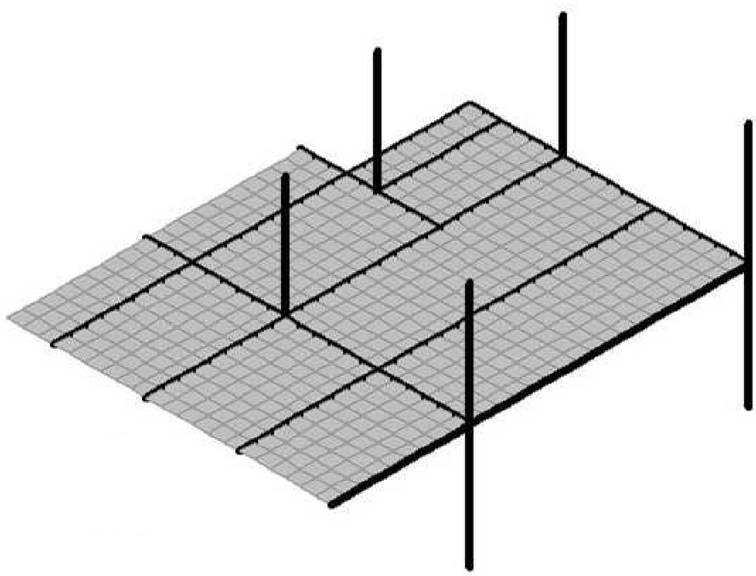

Fig. 5.17: Discritazation of the steel framed building (used in Cardington tests) for use in parametric studies

To aid in achieving convergence of the numerical model, it was assumed that the steel decking on the bottom of the slab did not contribute to the strength of the slab at elevated temperature, as was assumed by Bailey et al. (2000). Therefore, the ribbed steel deck was omitted from the model used in the parametric studies. High temperate material models as specified in Eurocode were utilized with the thermal and mechanical input parameters shown in Table 5.3.

Table 5.3: Thermal and mechanical properties assumed in simulations

Steel			
Heat transfer coefficients		Mechanical properties (beams/reinforcement.)	
Hot convection coefficient	25	Young's modulus (GPa)	210/210
Cold convection coefficient	9	Poisson's ratio	0.3/0.3
Relative emissivity	0.5	Yield strength (MPa)	350/413
Concrete			
Heat transfer coefficients		Mechanical properties	
Moisture content (kg/m^3)	46	Poisson's ratio	.25
Hot convection coefficient	25	Compressive strength (MPa)	35.4
Cold convection coefficient	9	Tensile strength (MPa)	1.78
Relative emissivity	0.5	-	-

5.4.2 Critical Factors

Based on a review of the literature, the primary factor influencing fire resistance that is unique to system level analysis is the effect of member interactions (including the effect of composite construction and tensile membrane action). As such, the effect of member interactions on structural fire resistance at the system level was studied as part of this research.

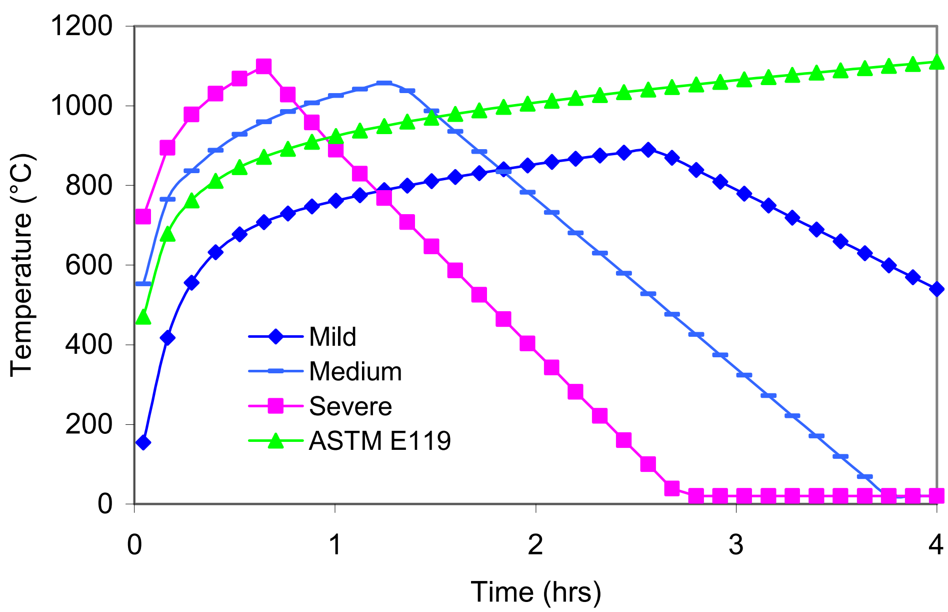

Fig. 5.18: Standard and design fire exposures considered for system

5.4.3 Analysis Procedure

To study the effect of member interactions on the fire response of a steel framed structure, the validated model of the Cardington restrained beam test was applied to conduct parametric studies. The response of the structure under the design fire exposures shown in Fig. 5.18 was simulated and evaluated, the results are presented below. It should be noted that the simulations were run for 180 minutes (as opposed to 240 minutes as was done for the element and assembly level simulations) to reduce computational time. As such, if an end time of 180 minutes is observed, that is indicative of the simulation surviving compartment burnout rather than the simulation failing, unless otherwise noted.

5.4.4 Results and Discussion

The parametric study generated a total of 68 numerical simulations under different parameters. It should be noted that many of the trends discussed at the element and assembly levels were also studied at the system level, since these factors have been presented previously, no further discussion on them will be presented here. The following discussion presents only those results unique to the system level response. For a discussion on all of the parameters investigated at the system level utilizing this model, the interested reader is directed to the respective literature (Fike and Kodur 2009b).

Effect of Member Interactions

Fig. 5.19 plots the deflection time history predicted by SAFIR for the center of the heated beam for each of the fire exposures shown in Fig. 5.18. As seen in Fig. 5.19, failure is observed in each of the simulations when the unprotected beam reaches approximately 750 °C (+/- 30 °C). This can be attributed to the combined strength of the steel beam and the plain concrete slab dropping below the applied load at this point. Intuitively, since the fire exposures take different lengths of time to reach this temperature in the unprotected steel beam, the failure time of the system will vary depending on the fire exposure modeled. Of interest however are the different deflections achieved as shown in Fig. 5.19. The longer the fire resistance, the greater the deflection achieved, this is in spite of the fact that the steel beam is almost the same temperature (750 °C) at failure in each of the simulations. While the steel beam is at the same temperature at failure in each simulation, the average concrete temperature in the mild fire exposure is approximately 100 °C higher than in either of the other simulations. This results in the combined strength of the steel beam-plain concrete slab being significantly less in the mild fire scenario that in the other three fires. Yet, the slab is observed to achieve the highest fire resistance under the mild fire exposure. This is attributed to the redistribution of forces that is achieved though member interactions. Though the system is weaker at failure in the mild fire exposure, the slower heating rate allows sufficient deflections to be developed for the redistribution of the applied load though member interactions and TMA. Thus, a higher fire resistance time is achieved.

The beneficial effect of member interactions at the system level has been clearly shown to enhance fire resistance by permitting larger deflections. However, the current models are not capable of the detailed analysis that would be required to develop a methodology for enhancing fire resistance though member interactions. As such, the knowledge gained though these simulations will be used to illustrate the use of the design methodologies developed at the element level for CFHSS columns and at the assembly level for composite SFRC floor assemblies.

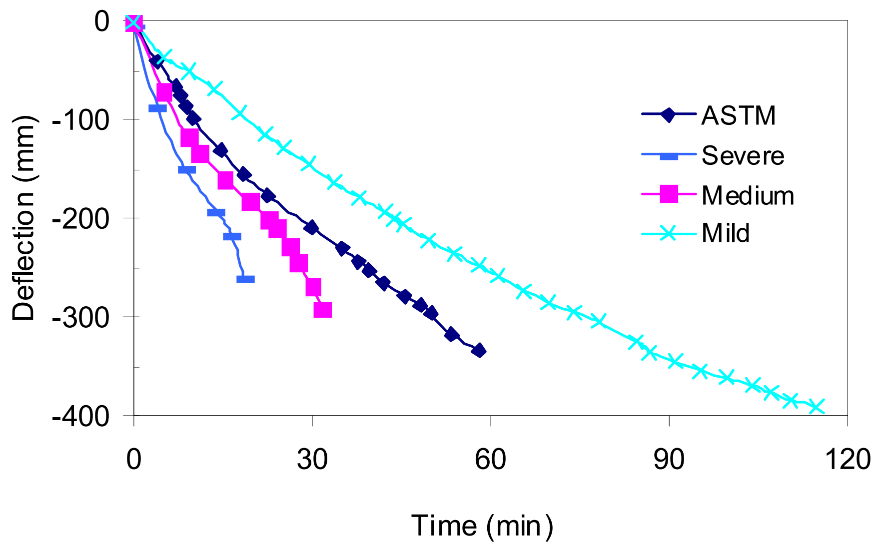

Fig. 5.19: Mid-span deflection of slab-beam assembly for various fire exposures

5.4.5 Summary

Based on the above analysis, the main factor influencing fire resistance that is unique to the system level is the effect of member interactions including composite construction and tensile membrane action. It was observed that member interactions serve to enhance the fire resistance of composite steel framed structures by redistributing forces from fire weakened members to other cooler parts of the structure. Given the complex nature of member interactions at the system level, it is not practical to develop simplified system level evaluation techniques at this time. Rather, system level analysis taking into account the beneficial effects of member interactions will be used in subsequent chapters to illustrate the use of the design methodologies developed for CFHSS columns and composite beam-slab assemblies.

5.5 Summary

In order to develop design methodologies for evaluating the fire resistance of steel framed structures, a set of parametric studies were conducted at the element, assembly, and system levels. At the element level, the effect of fire scenario, length, concrete filling type, load ratio, cross sectional size, and failure criterion on the fire resistance of CFHSS columns was investigated. For the assembly level, the effect of fire scenario, load level, slab thickness, and concrete type on the fire resistance of a composite beam slab assembly was studied. Finally, at the system level, the effect of member interactions on the fire resistance of a full-scale composite steel framed building was studied. Based on these parametric studies, the following conclusions can be drawn:

- It is possible to achieve unprotected structural members through the use of composite construction.
- Type of fire exposure and failure criterion has a significant influence on the fire resistance of composite construction.
- At the element level, the effect of fire scenario, length, concrete filling type, load ratio, cross sectional size, and failure criterion were identified as influencing fire resistance.
- At the assembly level, the effect of fire scenario, load level, slab thickness, and concrete type were identified has influencing fire resistance.
- At the system level, the effect of member interactions was identified as having a significant influencing on fire performance of the structure.

In the following chapter, the information gained in the parametric studies of this chapter will be utilized for the development of simplified design methodologies for achieving fire resistance in CFHSS columns and composite steel beam-SFRC slab assemblies.

CHAPTER 6

6 DEVELOPMENT OF DESIGN APPROACH

6.1 General

Data generated from the experimental and numerical studies is utilized to developed relevant, simplified design methodologies for evaluating fire resistance. As noted in the previous chapters, CFHSS columns offer a practical means for achieving the required fire resistance without the need for external fire protection. However, at the present there is no simplified approach for their use under design fire exposures. Based on the data from parametric studies, a simplified method to determine the fire resistance of CHFSS columns under non-standard fire exposure is proposed.

Similarly, composite steel beam-SFRC floor systems offer an attractive method of achieving fire resistance without the need for applied fire protection, and there is no design methodology for their use in any capacity. Based on the results from the experimental and numerical studies, a simplified design methodology to determine the load carrying capacity of composite steel beam-SFRC slab assemblies under fire exposure is proposed. Finally, an overview of fire resistance evaluation at the system level is presented.

6.2 Design Methodology for CFHSS Columns

At the present, a design equation exists wherein the fire resistance of a specific column can be determined under standard fire exposure. It is therefore practical extend this equation to account for design fire exposures. To accomplish this, all factors affecting fire resistance need to be taken into account in the analysis used as the basis for development of the correlation methodology. To that end, a brief review of the factor affecting fire resistance of CFHSS columns is presented in the following section.

6.2.1 Factors Governing Fire Resistance of CFHSS Columns

Based on the parametric studies conducted in the previous chapter, fire exposure was identified as a primary factor influencing fire resistance. Additionally, column length, concrete filling type, load ratio and failure criterion influence the fire resistance of CFHSS columns. Given however the importance of fire exposure on fire resistance, it is necessary to compile additional information on the effect of fire exposure on fire resistance of CFHSS columns. To that end, the 14 columns presented in Table 3.2 were analyzed by exposing them to 75 design fires. For all analyses, the factors identified in chapter five as having an influence on fire resistance were taken into account. The result was 1050 fire-column combinations being simulated, thus providing the wide range of data necessary to establish an approach for determining fire resistance equivalency. The time-temperature curves for each of these design fires were selected by assessing different compartment characteristics. The selected fire scenarios ranged from severe fire, representing a library room or records storage area, to a mild fire scenario, representing an average office room in a typical building. Five of these fires, including the most severe fire and the most mild fire are shown in Fig. 6.1 along with 2 standard fires (ASTM E-119 and ASTM E-1529). All of the design fires used in this study were taken from Magnusson and Thelandersson (1970).

Load ratio on the columns was maintained at the same levels noted in Table 3.2. This allowed the influence of other inherent properties of the column to be investigated without the added ambiguity of varying loads. All of the loads were applied as a concentric load on the top of the column (including the self weight). The point load was applied along the longitudinal axis such that no eccentricity resulted from the load application. This was done to simulate the conditions believed to be present during testing. In order however to simulate the constructional imperfections present in any structure, the columns were assumed to have an out of straightness of H/500 at the center of the column, where H is the height of the column.

Failure was said to occur based in the strength limit state when the column can no longer support the applied load. In SAFIR, this point generally corresponds to the time at which the stiffness matrix is no longer positive. Failure of the column can occur due to either local failure within the beam elements used for the column cross section, or it can be due to global buckling of the column.

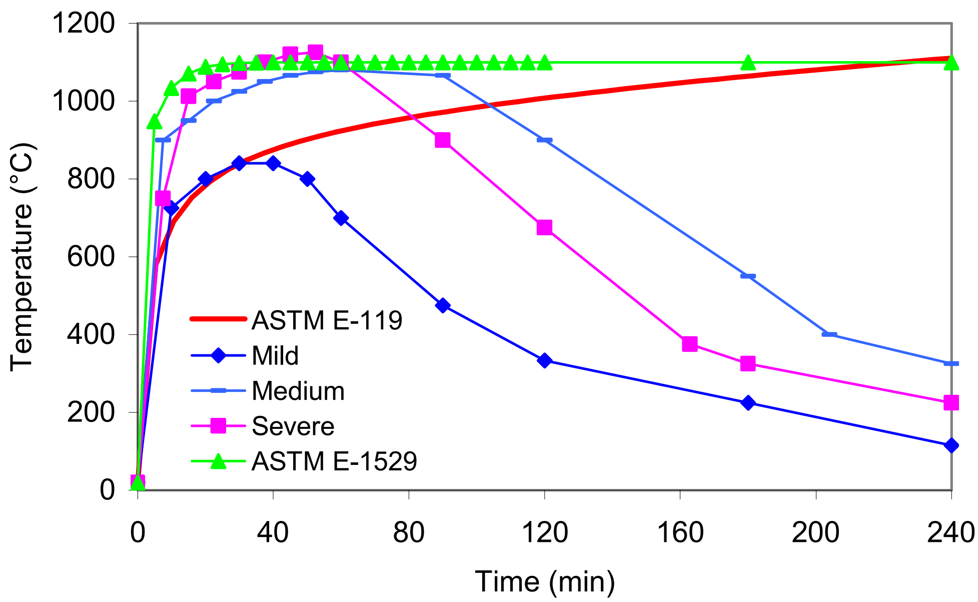

Fig. 6.1: Range of fire exposures considered in the development of a design methodology for CFHSS columns

6.2.2 Development of an Approach for Evaluating Fire Resistance

As pointed out in previous sections, available methods for equivalent fire severity were developed for traditionally protected steel members, failure of which is based on a limited temperature rise in steel. When these methods (equivalent area, maximum temperature, and minimum load) discussed above were applied to the CFHSS columns presented in Table 3.2, it was quickly determined that none of the methods can accurately predict the failure time of CFHSS columns under design fire exposure based on the ASTM E-119 fire resistance. The main reason for this is that CFHSS columns derive their fire resistance from the strength contribution of the concrete core, and thus determining the fire resistance based on critical steel temperature does not indicate true failure.

In the process of checking each of the equivalent fire severity concepts for CFHSS columns, it was observed that CFHSS columns either fail in less time in the design fire than the standard fire, or they survive complete compartment burnout. Further scrutiny revealed that a modification to the equal area concept produced a method by which failure of a column in a design fire can be predicted with a high degree of reliability by considering only the initial fire severity. Since a CFHSS column will either fail in less time in a design fire than in standard fire, or will survive complete compartment burnout, only the severity of the fire up to the time of column failure under standard fire exposure needs to be compared. It should however be pointed out that determining the time of failure for the column in a design fire is not the objective, it is rather to determine if the column will fail in the design fire or withstand complete compartment burnout.

The proposed approach can be applied to establish equivalency (survival of a column) between a standard and design fire. As a first step, the fire resistance of the CFHSS column under standard fire is evaluated using Eq. 2.1.

$$R = f\,\frac{(f'_c + 20)}{(KL - 1000)}\,D^2\sqrt{\frac{D}{C}} \qquad [2.1]$$

To determine the survivability of the column under a design fire exposure, the equivalency can be established by comparing the area under the standard time temperature curve to that under the design fire time temperature curve.

To determine if the column will fail in a design fire, the area under both the standard and the design fire time temperature curves is determined at the time the column fails in the standard fire. If the area under the standard fire curve is greater than the area under the design fire curve, the column will not fail in the design fire, that is to say the column will survive complete compartment burnout. If however, the area under the standard fire curve is less than that under the design fire curve, the column will fail in the design fire. Most notably, in the latter case, the column will fail in less time in the design fire than in the standard fire.

The application of this approach is illustrated in Fig. 6.2 which shows the time temperature curves corresponding to the standard (ASTM E-119) and a design fire exposure. Knowing the basic details of the column, the fire resistance of the column under standard fire exposure can be estimated by applying Eq. 2.1. Once both the design fire and the failure time of the column under standard fire exposure are known, the area under the standard fire time temperature curve (Area A in Fig. 6.2) and the area under the design fire time temperature curve (Area B in Fig. 6.2) can be determined at the time of column failure under standard fire exposure. The areas A and B are now compared: if the area under the standard fire curve (Area A) is less than the area under the design fire curve (Area B) the column is said to have failed in the design fire, and most notably in less time than in the standard fire. If however, the area under the standard fire curve (Area A) is greater than that under the design fire curve (Area B) the column is said to not have failed in the design fire, that is to say the column will survive complete compartment burnout (Fike and Kodur 2009a).

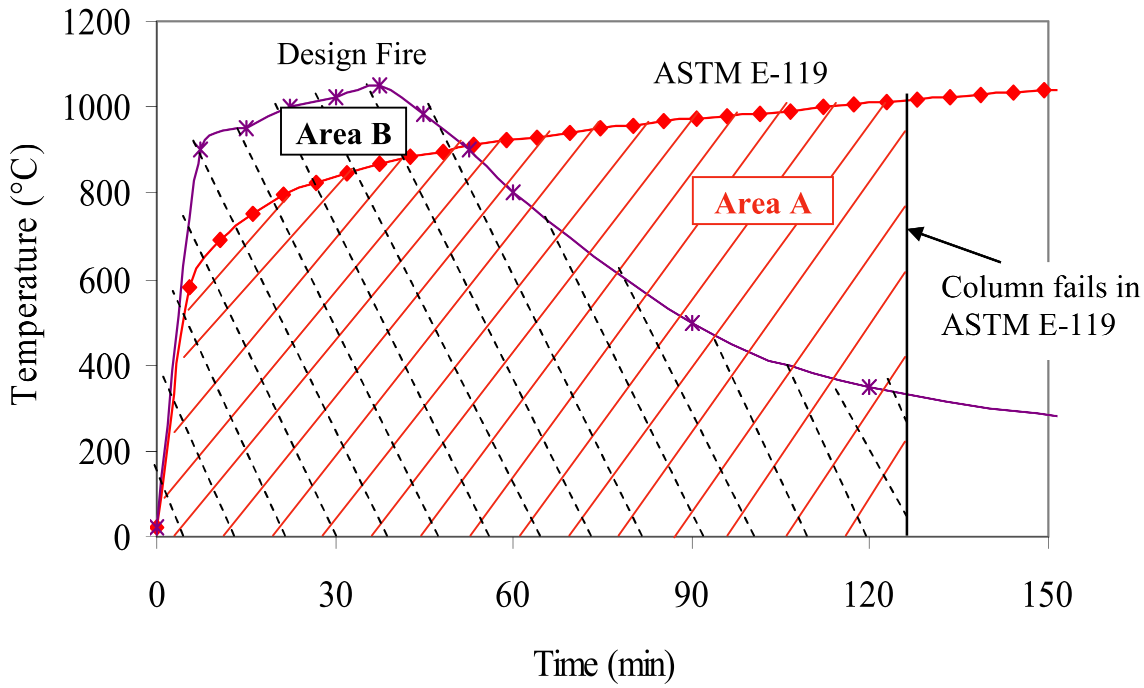

Fig. 6.2: Illustration of proposed approach for a CFHSS column

The approach proposed here is predicated on the concept that design fires have a similar initial rate of temperature increase, and most design fires achieve higher initial temperatures than the standard fire exposure, as seen in Fig. 6.1. It should be noted that the proposed method is not applicable for design fires that do not have a similar initial temperature rise as that of the ASTM E-119 fire exposure (up to ten minutes of fire exposure). Since the failure time of the column under standard (ASTM E-119 or ISO 834) fire exposure is known (using Eq. 2.1), only the fire severity up to this point needs to be compared with that of the design fire. Given the previous observation that the initial temperatures in most design fires are higher than in the standard fire, the only way for the design fire to be less severe than the standard fire over the same time period is if the design fire enters the cooling phase (in which the column regains strength) prior to the end of the time period (defined as column fire resistance under standard fire exposure). The area under the respective time-temperature relationships serves as a ready means for comparing the relative fire severity. Since only the initial portion of the fires is being compared, the problem of drastically different fire exposures is avoided, and an accurate comparison is possible. Hence the conclusion that if the area under the standard fire curve (Area A in Fig. 6.2) is greater than the area under design fire curve (area B in Fig. 6.2), the column will not fail in the design fire. On the contrary, if the area under the standard fire curve (Area A in Fig. 6.2) is less than that under the design fire curve (Area B in Fig. 6.2), the column will fail in the design fire.

6.2.3 Validation of the Proposed Approach

The proposed approach was applied to the 1050 column-fire combinations analyzed using SAFIR to determine if the columns fail or survive complete compartment burnout. In 761 out of the 1050 column-fire combinations analyzed, both SAFIR and the proposed approach indicated that no failure occurs in the column. This high percentage of survivability can be attributed to the fact that the decay phase of the fire allows the column to regain part of its strength, resulting in a fire exposure that is less severe than the "standard" fire exposure. The agreement in failure predictions between SAFIR and the proposed approach for a large number of columns illustrates the strength of the proposed approach.

Of the 289 remaining column-fire combinations, both SAFIR and the proposed approach predicted failure in 182 of them. The failure of CHFSS column can be attributed to the high severity of fires encountered in these cases. Again, the agreement between the actual (SAFIR) failure and that predicted by the proposed approach indicates the validity of the proposed approach. Further, for another 90 column-fire combinations while failure was not observed in SAFIR, the proposed approach predicted failure. This can be attributed to fires that are similar to ASTM E-119 for the considered time period, entering the decay phase possibly only minutes before the column failed under ASTM E-119 fire exposure. This can however be taken as conservative for design purposes. For the remaining 17 column-fire combinations, SAFIR predicted that the columns would fail while the proposed approach does not. This can be attributed to fires with a low ventilation coefficient and a comparatively large fuel load. The resulting long duration cool fire imparts more heat to the columns than short duration fires that are hotter causing them to fail much later in the simulation.

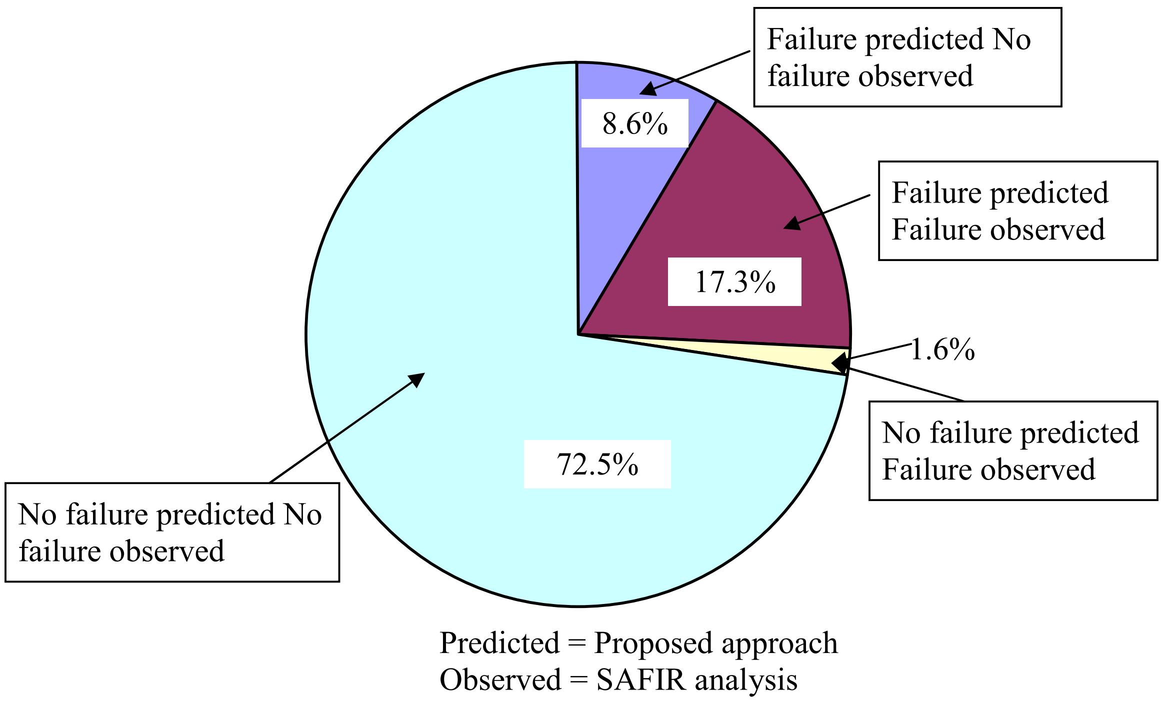

Fig. 6.3: Graphical illustration of the effectiveness of the proposed approach

To illustrate the effectiveness of the proposed approach, a statistical representation of the 1050 numerical simulations is presented in Fig. 6.3. In 72.5% (761) of the column-fire combinations, both the SAFIR and proposed approach indicated that the column would not fail. In 17.3% (182) of the cases both SAFIR and the proposed approach indicate that the column-fire combination will result in failure of the column. SAFIR predicts that failure will not occur while the proposed approach indicated that failure will occur in 8.6% (90) of the column-fire combinations, thus being a conservative prediction. In the remaining 1.6% (17) of the column-fire combinations, SAFIR indicates the column will fail while the proposed method indicated that the column will not. This low (1.6%) probability of an un-conservative estimation of column failure for the selected range of fire exposures serves to further reinforce the strength of the proposed method.

A subset of the data is presented in Table 6.1 to illustrate the results from analysis. For each of the column-fire combinations, Table 6.1 presents the failure time as determined by SAFIR where applicable, and whether or not the column is determined to fail using the proposed method. Boxes occupied by a "-" in the "SAFIR Failure" column indicate that no failure was observed in SAFIR analysis under that design fire exposure. Of the 252 column-fire combinations in Table 6.1, both SAFIR and the proposed approach indicate that the column will not fail in 131 of them. Of the 121 remaining column-fire combinations, both SAFIR and the proposed approach predicted failure in 86 of them. For another 31 column-fire combinations while failure was not observed in SAFIR, the proposed approach predicted failure. In the remaining 4 column-fire combinations, SAFIR predicted that the columns would fail while the proposed approach does not. Reasons for the observed results are the same for this subset as for the entire data set, as such, the reasons given above will not be reiterated here, though this data subset serves to further reinforce the validity of the proposed approach.

As an example from Table 6.1, SAFIR analysis of CFHSS column RP 168 under standard fire exposure yielded a failure time of 82 minutes, while no failure was observed for "FIRE 1" through "FIRE 5" with failure occurring in "FIRE 6". The proposed approach also predicts no failure for "FIRE 1" through "FIRE 4", predicting failure for "FIRE 5" and "FIRE 6" though failure is not observed in "FIRE 5"

Table 6.1: Fire resistance equivalency as predicted by SAFIR and the proposed approach

	RP 168		SP 152		RF 324		SF 203		RB 273b		SB 203	
Type of Fire Exposure ↓	Failure (min)	Predicted Failure	Failure (min)	Predicted Failure	Failure (min)	Predicted Failure	Failure (min)	Predicted Failure	Failure (min)	Predicted Failure	Failure (min)	Predicted Failure
ASTM	82	NA	74	NA	204	NA	121	NA	98	NA	130	NA
FIRE 1	-	N	-	N	-	N	-	N	-	N	-	N
FIRE 2	-	N	-	N	-	N	-	N	-	N	-	N
FIRE 3	-	N	-	N	-	N	-	N	-	N	-	N
FIRE 4	-	N	-	N	-	N	-	N	-	N	-	N
FIRE 5	-	Y	70	Y	-	N	-	N	-	Y	-	N
FIRE 6	77	Y	70	Y	-	N	123	Y	94	Y	-	Y
FIRE 7	-	Y	47	Y	-	N	-	N	-	Y	-	N
FIRE 8	49	Y	47	Y	-	N	85	Y	67	Y	-	Y
FIRE 9	49	Y	47	Y	-	Y	83	Y	67	Y	88	Y
FIRE 10	42	Y	40	Y	-	N	-	N	-	Y	-	N
FIRE 11	42	Y	40	Y	-	N	74	Y	58	Y	-	Y
FIRE 12	42	Y	40	Y	-	Y	73	Y	58	Y	77	Y
FIRE 13	-	N	-	N	-	N	-	N	-	N	-	N
FIRE 14	-	N	-	N	-	N	-	N	-	N	-	N
FIRE 15	-	N	-	N	-	N	-	N	-	N	-	N
FIRE 16	-	N	-	N	-	N	-	N	-	N	-	N
FIRE 17	-	N	-	N	-	N	-	N	-	N	-	N
FIRE 18	-	Y	-	Y	-	N	-	N	-	N	-	N
FIRE 19	54	Y	52	Y	-	N	94	Y	72	Y	-	Y
FIRE 20	54	Y	52	Y	-	Y	89	Y	72	Y	94	Y
FIRE 21	45	Y	43	Y	-	N	-	N	-	Y	-	N
FIRE 22	45	Y	43	Y	-	N	77	Y	62	Y	-	Y
FIRE 23	45	Y	43	Y	-	Y	77	Y	62	Y	80	Y
FIRE 24	-	N	-	N	-	N	-	N	-	N	-	N
FIRE 25	-	N	-	N	-	N	-	N	-	N	-	N
FIRE 26	-	N	-	N	-	N	-	N	139	N	-	N
FIRE 27	-	Y	-	Y	-	N	-	N	-	N	-	N
FIRE 28	59	Y	58	Y	-	N	-	Y	82	Y	-	Y
FIRE 29	59	Y	58	Y	-	N	99	Y	81	Y	-	Y
FIRE 30	44	Y	42	Y	-	N	-	N	-	Y	-	N
FIRE 31	44	Y	42	Y	-	N	76	Y	61	Y	-	Y
FIRE 32	44	Y	42	Y	-	Y	76	Y	61	Y	80	Y
FIRE 33	39	Y	37	Y	-	N	-	N	67	Y	-	N
FIRE 34	39	Y	37	Y	-	N	69	Y	54	Y	72	Y
FIRE 35	39	Y	37	Y	-	Y	69	Y	54	Y	72	Y
FIRE 36	-	N	-	N	-	N	-	N	-	N	-	N
FIRE 37	-	N	-	N	-	N	-	N	-	N	-	N
FIRE 38	178	N	178	N	-	N	-	N	146	N	-	N
FIRE 39	-	Y	-	Y	-	N	-	N	-	N	-	N
FIRE 40	63	Y	60	Y	-	N	-	Y	88	Y	-	N
FIRE 41	63	Y	60	Y	-	N	110	Y	85	Y	-	Y
FIRE 42	45	Y	43	Y	-	N	-	N	-	Y	-	N

It should be reiterated that this method does not determine the fire resistance of CFHSS columns in design fires in a quantified manner, rather, it predicts whether or not the column will survive the design fire exposure. If it is determined that the column does not survive the fire exposure, that is all the information available, the duration of survival is not known from this method. As such, there is a built in factor of safety in that all columns designed according to this method will have sufficient fire resistance to withstand complete burnout of the probabilistic fires to which the column would be exposed, rather than satisfying specific fire resistance requirements. It might be possible to achieve more deterministic results using more sophisticated methods, but that would increase the complexity of the calculations and make the approach less practical for use in design. To illustrate the use of the proposed approach, a design example is presented below followed by the limitations to the proposed approach.

6.2.4 Illustration of the proposed approach

Application of the proposed equivalent area approach for a design situation is illustrated through a numerical example. Detailed calculations for this example are presented in Appendix E.

A CFHSS column located in a room 3 m high with a 6 m by 4 m floor that has a fuel load of 550 MJ/m^2 (of floor area) is to be designed. The room has one window opening 3 m wide by 2 m high. In this compartment, the architect has proposed a 273 mm diameter circular HSS column filled with plain concrete made with siliceous aggregate. The height of the column needs to be 3.81 m (to accommodate the drop ceiling and utilities) with fixed connections on both ends. The building code requires the column to have a 2-hour fire resistance rating. Now it is desired to know if this column will satisfy the code requirements by withstanding complete burnout of the fire that would occur within the compartment.

The first step is to determine the design fire that is most likely to occur within the compartment. The fire scenario can be determined using the Eurocode (2005a) method. The detailed calculations associated with this example are presented in Appendix E, along with further details on the compartment characteristics. The ventilation factor for this example is 0.079 $m^{1/2}$ and the burning duration is 0.79 hours. The time temperature curve determined using this method and the standard (ASTM E-119) time temperature curve are shown in Fig. 6.4.

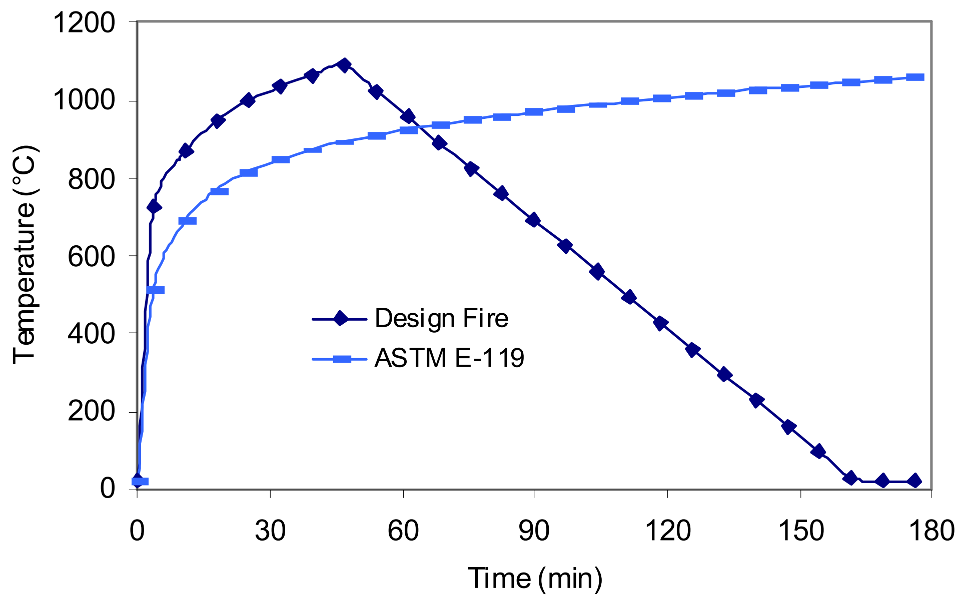

Fig. 6.4: Comparison of standard and design fire exposure

The second step is to determine the fire resistance of the column under standard fire exposure (ASTM E-119 or ISO 834). Applying Eq. 2.1, the fire resistance of the column is determined to be 101 minutes. The area under the standard time temperature curve at 101 minutes is 1462 min*°C. The corresponding area under the design fire curve at 101 minutes is 1503 min*°C. Since the area under the design fire time temperature curve is greater than that under the standard time temperature curve, the column will fail in less time in the design fire than when exposed to standard fire, as such, practical alternatives need to be developed.

The most practical alternative is to simply change the type of aggregate used in the concrete. By switching to carbonate aggregate, according to Eq. 2.1 the fire resistance of the column increases from 101 to 116 minutes under standard fire exposure. At 116 minutes, the area under the standard (ASTM E-119) time temperature curve is 1701 min*°C, while that under the design fire time temperature curve is 1626 min*°C. As such, since the area under the design fire curve is less than that under the standard fire curve, the column will survive complete compartment burnout, thus, the column is safe for use in this building because it has the highest fire resistance rating possible, surviving complete compartment burnout when carbonate aggregate is used in the concrete. Thus, the proposed approach facilitates the use of CFHSS columns in buildings where traditional prescriptive design would not utilize these columns.

6.2.5 Application and Limitations

The proposed method offers a practical approach for evaluating the fire resistance of CFHSS columns exposed to design (real) fires. However, the applicability of this method is limited to the range of parameters that were considered in the numerical study which formed the basis for developing this approach. The explicit limitations for the proposed methods are as follows:

- The initial temperature rise (in the first 5-10 minutes) in the design fire must be similar to the ASTM E-119 temperature rise
- The maximum fire temperature reached must be greater than that of ASTM E-119 during the first 20 minutes.
- This method is not applicable for the ASTM E-1529 hydrocarbon fire exposure due to the absence of a decay phase

- The approach is only applicable for unprotected CFHSS columns (i.e. no insulation provided on the steel
- Since the approach makes use of Eq. 2.1, all of the limitations that apply to Eq. 2.1 (length, concrete compressive strength, end conditions, and cross section) also apply to this method
- This method is applicable for bar, steel fiber, and plain concrete filled HSS columns

It should be noted that the above limitations are specified due to a lack of validation for these conditions. Through further validation, it should be possible to extend this method to overcome some of these limitations.

6.3 Design Methodology for Composite Beam-Slab Assemblies

The state-of-the-art review presented in Chapter 2 indicated that composite construction, and considering assemblies rather than single elements in fire resistance tests has a significant influence on the observed fire resistance. At the present however, the fire resistance that can be achieved through composite floor systems is insufficient to meet the levels required in codes and standards, without the application of external fire protection to the supporting steel beams. To overcome this limitation, a novel material system (SFRC) was tested in composite floor assemblies under fire exposure as outlined in Chapter 3. Following the experimental program, a computational model was constructed and the factors influencing fire resistance of the assembly identified in Chapter 4 and Chapter 5 respectively. Based on these findings, a design methodology for determining the fire resistance of composite steel beam SFRC slab floor assemblies under any fire exposure is presented below. As was the case with CFHSS columns, all factors identified as influencing the fire resistance of composite steel beam-SFRC floor slabs were taken into account in all relevant simulations. A review of the factors influencing the fire resistance of composite steel-beam-SFRC floor systems under fire exposure is presented in the following section.

6.3.1 Factors Affecting the Fire Resistance of Composite Floor Assemblies

The primary factors influencing the development of TMA in composite floor assemblies under fire exposure are fire scenario, load level, slab thickness, span, and concrete type. Through the novel experimental program and numerical studies presented in this research, it has been shown that concrete type, namely the use of SFRC significantly enhances the response of composite construction to fire exposure under realistic conditions. This is attributed to the enhanced tensile strength of SFRC as compared to plain concrete facilitating the development of tensile membrane action. To illustrate the beneficial effects of using SFRC in floor slabs, the following section presents a derivation of the effect that concrete tensile strength has on the development of TMA, and consequently enhancing fire resistance. Once having established the beneficial effect of SFRC in composite floor assemblies, a design methodology for predicting the response of SFRC floor systems to fire exposure will be presented.

6.3.2 Development of Tensile Membrane Action in SFRC Slabs

The mechanics associated with the contribution of SFRC to fire performance of a beam slab assembly are derived by expanding Bailey's (2000) approach. For a typical concrete slab experiencing two-way bending, the failure patterns as determined by yield line analysis are shown in Fig. 6.5a. The slab is considered to be comprised of four zones. Equilibrium principals can be applied to these zones to quantify to define an upper bound for the contribution of SFRC to overall fire resistance. Due to symmetry, only two zones defined by yield line failure theory as shown in Fig. 6.5b are considered. Based on the geometry of the elliptical tensile region shown in Fig. 6.5b, Fig. 6.5c gives the location of the forces C and T_2 in terms of the slab lengths L and D. The primary difference between the derivation shown below and that originally published by Bailey (2000) is that the tensile strength (f'_t) contribution of SFRC is accounted for in this derivation.

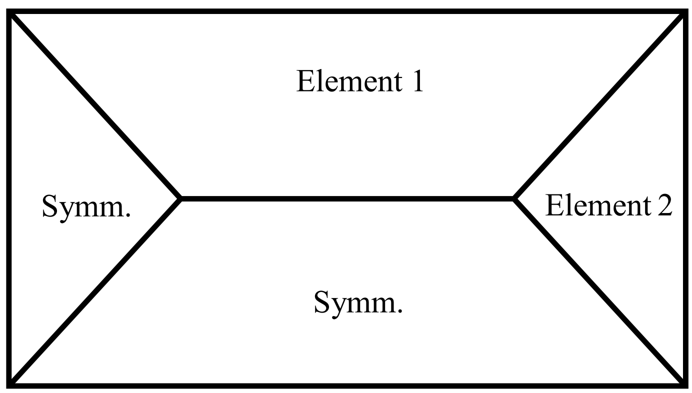

(a): Failure patterns for a two-way slab based on yield line theory.

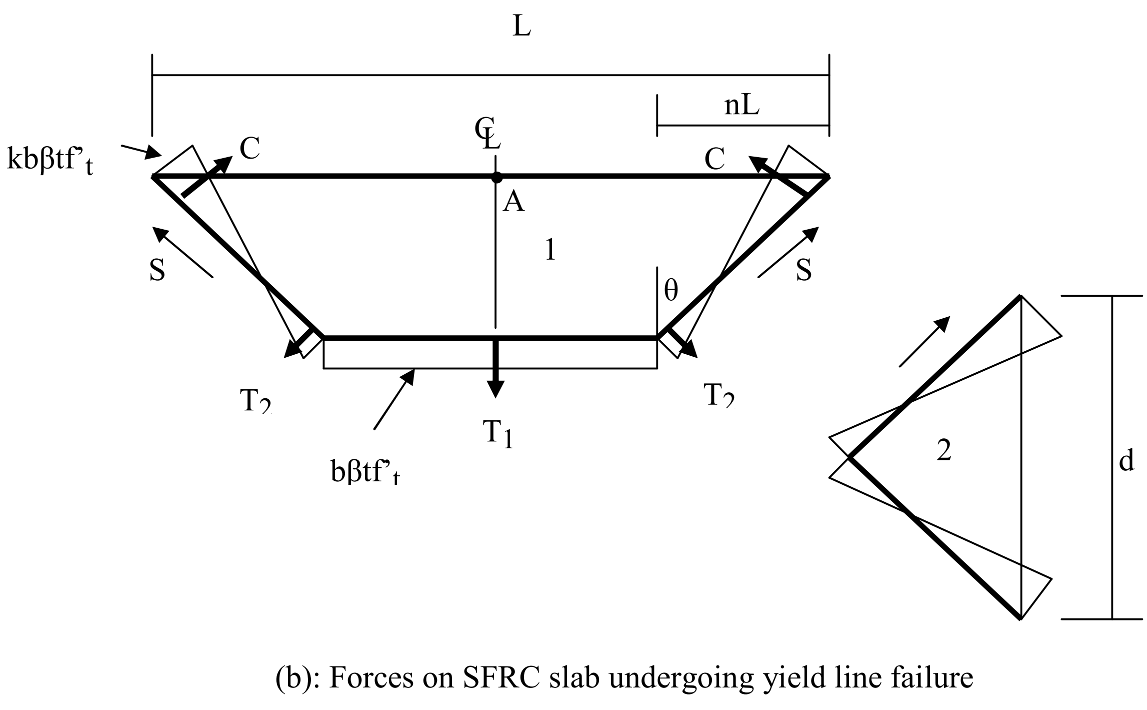

(b): Forces on SFRC slab undergoing yield line failure

Fig. 6.5: Illustration of forces developed in a beam-slab assembly under fire exposure

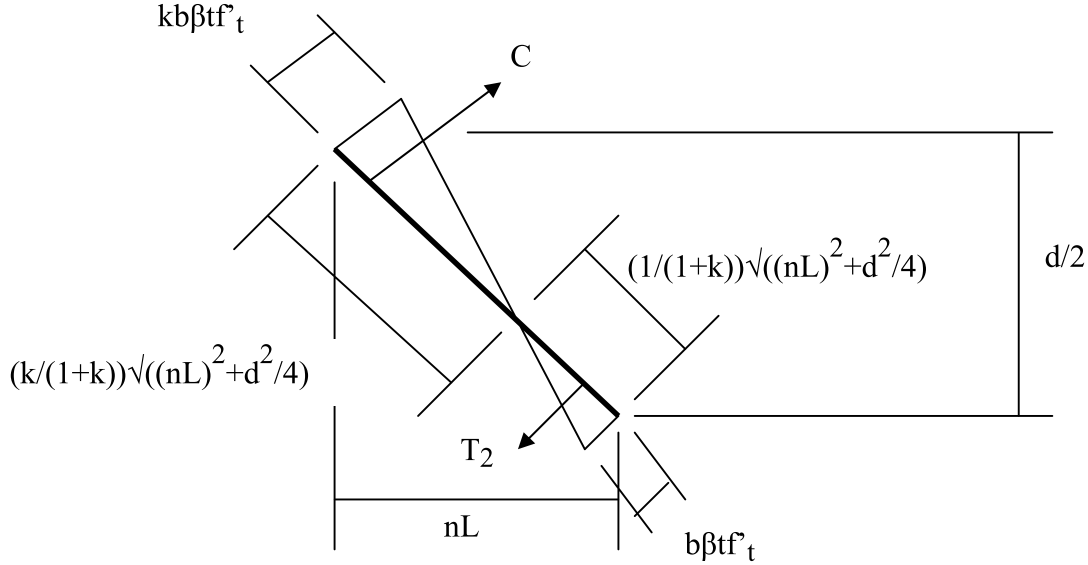

(c): Dimensions of yield line based on geometry

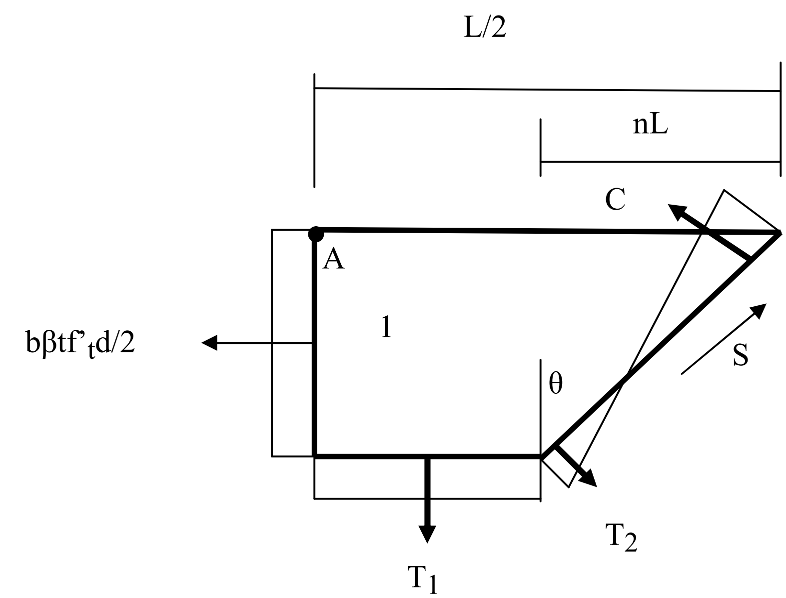

(d): Fracture equilibrium at failure

Fig. 6.5 (Continued): Illustration of forces developed in a beam-slab assembly under fire exposure

where k and b are modification factors of the SFRC tensile force, L and d are the length and width of the slab respectively, f'_t is the tensile strength of SFRC, t is the thickness of the slab, β is a correction factor to account for the strain distribution through the thickness of the slab ($0<\beta<1$), and C, T_1, T_2, and S are the compressive, tensile, and shear forces on the elements respectively.

by applying force equilibrium (Fig. 6.5b), the relationship between forces C, T_1, and T_2 can be shown to be:

$$\frac{T_1}{2}\sin(\theta)=(C-T_2) \qquad [6.1]$$

from further consideration of Figs. 6.5b and 6.5c the forces T_1, T_2, and C can be determined to be the following:

$$T_1 = b\beta t f'_t(L-2nL) \qquad [6.2]$$

$$T_2 = \frac{b\beta t f'_t}{2}\left(\frac{1}{1+k}\right)\sqrt{(nd)^2+\frac{d^2}{4}} \qquad [6.3]$$

$$C = \frac{kb\beta t f'_t}{2}\left(\frac{k}{1+k}\right)\sqrt{(nd)^2+\frac{d^2}{4}} \qquad [6.4]$$

by substituting Eqs. [6.2-6.4] into Eq. [6.11] k can be expressed as:

$$k = \frac{4n\left(\frac{L}{d}\right)^2(1-2n)}{4n^2\left(\frac{L}{d}\right)^2+1}+1 \qquad [6.5]$$

Lastly, the geometry of element 1 as shown in Fig. 6.5b can be used to define the angle of the yield lines relative to the long axis of the slab as:

$$\sin(\theta) = \frac{nL}{\sqrt{(nd)^2 + \frac{d^2}{4}}} \qquad [6.6]$$

Assuming that failure occurs due to the formation of a full depth crack along the centerline of element 1 in the short direction, the force distribution shown in Fig. 6.5d can be assumed. The primary difference between the equilibrium shown in Fig. 6.5d and that assumed by Bailey (2000) is that only tensile strength of SFRC is considered to contribute to the fracture resistance of element 1 whereas Bailey (2000) considered the contribution of the shrinkage steel only.

Taking equilibrium of the fractured element 1 shown in Fig. 6.5d about point A yields the following:

$$T_2\left[\left(\cos\theta\frac{L}{2} - \frac{(L/2 - nL)}{\cos(\theta)}\right)\frac{1}{\tan(\theta)} - \frac{1}{3}\left(\frac{1}{1+k}\right)\sqrt{(nd)^2 + \frac{d^2}{4}}\right]$$

$$+C\left[\sin\theta\frac{L}{2} - \frac{1}{3}\left(\frac{k}{1+k}\right)\sqrt{(nd)^2 + \frac{d^2}{4}}\right]$$

$$+S\cos(\theta)\frac{L}{2} - \frac{T_1}{2}\left[\frac{1}{2}\left(\frac{L}{2} - nd\right)\right] = \frac{\beta t f' t d^2}{8} \qquad [6.7]$$

By substitution and re-arranging b can be expressed as:

$$b = \frac{d^2}{8(A + B + C + D)} \qquad [6.8]$$

where A, B, C, D are given as:

$$A = \frac{1}{2}\left(\frac{1}{1+k}\right)\left[\frac{d^2}{8n} - \frac{(L/2 - nL}{nL}\left((nL)^2 + \frac{d^2}{4}\right) - \frac{1}{3}\left(\frac{1}{1+k}\right)\left((nL)^2 + \frac{d^2}{4}\right)\right] \qquad [6.9]$$

$$B = \frac{1}{2}\left(\frac{k^2}{1+k}\right)\left[\frac{nL^2}{2} - \frac{k}{3(1+k)}\left((nL)^2 + \frac{d^2}{4}\right)\right] \quad [6.10]$$

$$C = \frac{d^2}{16n}(k-1) \quad [6.11]$$

$$D = \left(\frac{L}{2} - nL\right)\left(\frac{L}{4} - \frac{nL}{2}\right) \quad [6.12]$$

Taking the moment for element 1 about the support at an arbitrary deflection Δ yields the following expression for the contribution of SFRC to load bearing capacity of element 1:

$$M = \beta t f'_t\, Lbw\left((1-2n) + \frac{n(3k+2)}{3(1+k)^2} - \frac{nk^3}{3(1+k)^2}\right) \quad [6.13]$$

where b and k are as derived above, n, t, f'_t, and L are based on the geometry of the assembly and material properties, and β is an assumed value between 0 and 1 based on test results. This equation being intrinsically positive (assuming downward deflection Δ to be positive) illustrates that the tensile strength of concrete contributes to the moment capacity of a concrete slab. SFRC having superior tensile strength properties as compared to normal strength concrete will maximize this benefit well into fire exposure.

6.3.3 Development of an Approach for Evaluating Fire Resistance

Through the fire test, parametric studies, and derivation presented previously, it has been demonstrated that the use of SFRC in the floor slab can enhance the fire resistance of composite beam slab assemblies. The fire resistance enhancement that can be achieved through the use of composite construction with SFRC is to such an extent, that it may by possible to eliminate the need for fire protection on secondary steel beams, while still achieving the required fire resistance rating. It is therefore desirable to determine if such a level of fire resistance can be practically achieved through the inclusion of steel fibers in the slab. If so, it is desirable to develop a design equation that will allow practitioners to readily use SFRC for achieving fire resistance in practical design applications.

Fire exposure, thickness, and load were identified in the previous section as factors that have a significant influence on the fire resistance of SFRC floor assemblies. In addition to these factors, the secondary beam section and the secondary beam spacing can significantly impact the fire resistance of the floor assembly. While related to the loading on the floor system, the network of supporting beams is a relatively independent variable which depends not only on structural considerations, but on geometric and architectural considerations. This added variability makes the number of simulations that would be required to evaluate the response of composite floor assemblies under the full range of variables untenably large.

To reduce the size of the parametric study, and to enhance the applicability of the developed design methodology, observations made from SAFIR analysis can be utilized to make relevant simplifying assumptions. The first observation made was that the load capacity of the composite beam slab assembly under fire exposure longer than 20 minutes is relatively independent of the supporting secondary steel beam section. This trend is attributed to the extreme temperatures that are rapidly reached in the unprotected steel section reducing its structural contribution to a nominal value. As such, after 20 minutes of fire exposure the SFRC slab dominates the response of the section, and there is no need to model the steel section in the structural models, only the floor slab.

The second observation made, is that the load capacity of the composite floor system does not monotonically decrease as a function of fire exposure time, rather, it follows the trend shown in

Fig. 6.6. This trend is presumably due to the relative heating rates of the constituent materials in the assembly. At ambient temperatures, the capacity of the composite section is dominated by the steel section contributing considerable load bearing capacity. As the fire exposure time increases, the temperatures in the unprotected beam increase, this causes the steel beam to weaken and much of the load is transferred to the SFRC slab. The SFRC slab being cool and at relatively low deflections can not develop TMA, as such, a minimum is observed in the load capacity. As the SFRC slab is slowly heated, the slab becomes more ductile and deflections in the slab increase. These increasing deflections provide the geometry necessary to develop TMA in the slab. As the load which can be carried through TMA in the slab increases, the load capacity of the system is observed to increase as seen in Fig. 6.6. Later in fire exposure, (after 150 minutes for the case shown in Fig. 6.6) the tensile strength of SFRC begins to deteriorate due to increasing concrete temperatures.

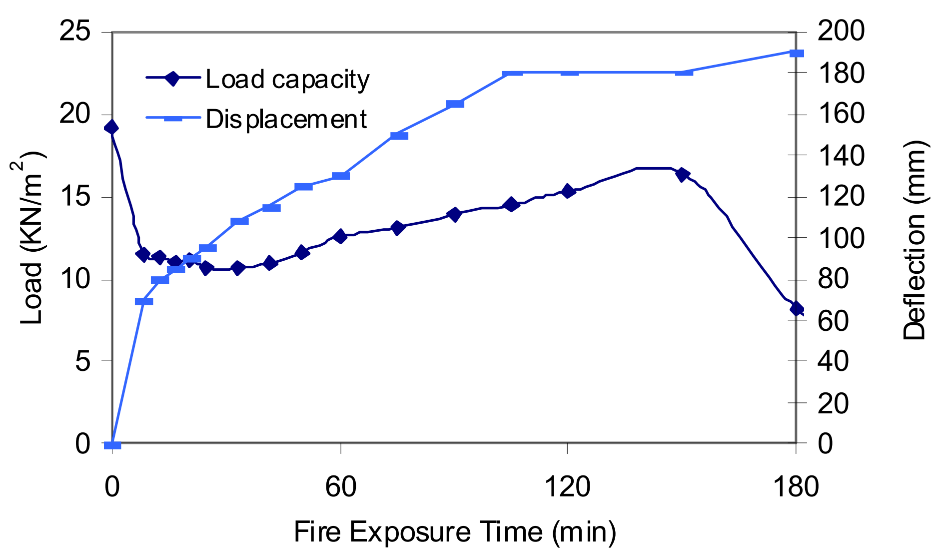

Fig. 6.6: Load carrying capacity and deflection as a function of fire exposure time for a SFRC floor assembly

Ultimately, the tensile strength of the concrete deteriorates to a point where the load which can be transferred through TMA decreases to a nominal and impractical value, and the assembly fails. Based on this, if the assembly can survive past the local minimum in load capacity, it is highly likely that the assembly will reach compartment burnout in most design fires.

Based on the above observations, the two simplifications that can be made to the approach used for the development of a design methodology for composite SFRC floor system under fire exposure are as follows

- The contribution of the unprotected secondary beam was neglected in the simulations, and only the SFRC floor slab was simulated under fire exposure. This is justified by the observation that for fire exposures longer than 20 minutes, the response of the composite floor system is independent of the steel section utilized.
- Rather then trying to determine the load capacity of the floor system exposed to design fires, the maximum applied load under which the assembly can survive compartment burnout is desired.

To determine the maximum load that would allow the assembly to survive compartment burnout, without consideration being given to the supporting secondary beams, beam elements were used to model a strip of the SFRC floor slab (here unto referred to as a strip slab) exposed to fire. The beam elements employed were fiber based elements which had been discretized to represent the SFRC floor slab as shown in Fig. 6.7 below. Beam elements offer several advantages over shell elements for the type of analysis being conducted. Stability of the simulated strip slab is considerably easier to achieve, and the need to apply boundary conditions over the length of the strip slab is eliminated. Lastly, computational time is also reduced through the use of beam elements as compared to a larger number of shell elements.

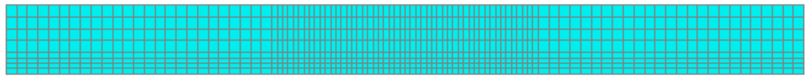

Fig. 6.7: Discretization of beam elements used in the parametric study for evaluating the response of composite SFRC floor slabs exposed to fire

Having simplified the models using the information gathered in the parametric studies described above, an additional data pool is necessary for the development of a practical engineering design methodology. To that end, numerical models were constructed to simulate a strip of SFRC floor slab 1.5 m wide with different spans and thicknesses exposed to different design and standard fires. A slab width of 1.5 m was selected to ensure that the thickness was no more than 10% of the slab width in any of the simulations, and to avoid lateral torsional buckling of the strip slab. Simulated spans ranged from 4.6 to 12.2 m, thicknesses from 100 to 150 mm, and the range of fire exposures considered are shown in Fig. 6.8. It should be noted that the span referred to in the following discussion is that corresponding to the short direction of the slab, i.e. in the direction of the secondary beams. The floor strip was assumed to be fully supported at the ends with all rotations and translations restrained. In all simulations, the compressive strength of the SFRC was assumed to be 28 MPa and the steel fiber content 42 kg/m^3 (1.75% by mass).

In order to evaluate the load carrying capacity of the flooring strips as a function of time, traditional analysis methods could not be employed. Given the presence of a local minimum in load capacity of the floor system exposed to fire as seen in Fig. 6.6, were a specified load to be applied to the system and the analysis run, the system will either fail in a very short period of time, or survive compartment burnout. As such, alternate methods to evaluate the load capacity of the system under increasing temperatures had to be employed.

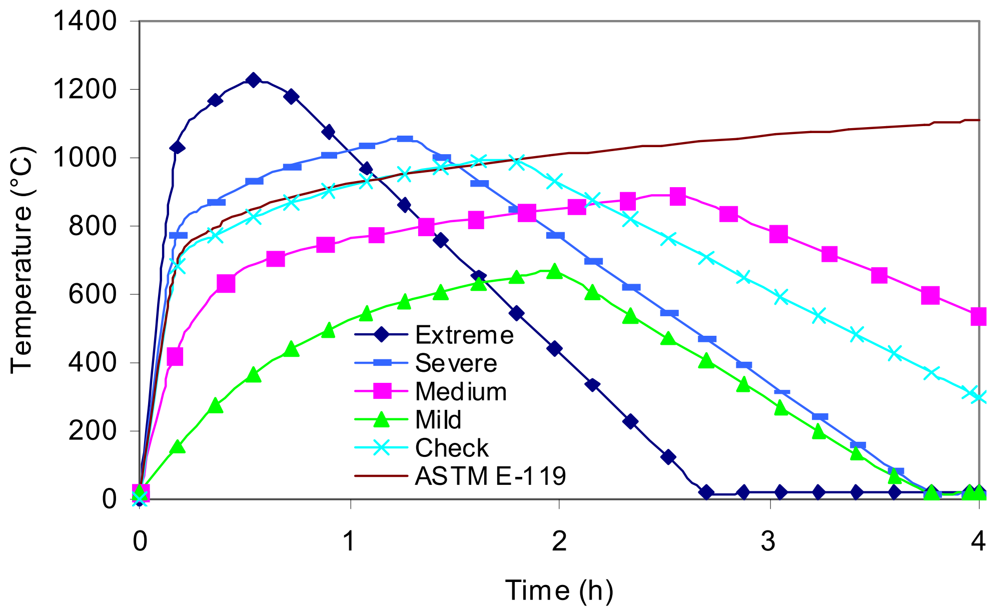

Fig. 6.8: Design (real) fires considered in parametric study on composite beam slab assembly

SAFIR was used to determine the thermal profiles in the floor system over the entire duration of fire. This data was then used to determine the cross-section temperatures in the floor system at each desired time. This temperature profile was then assumed static at the time of the structural analysis, and the loads applied to the system were increased. From this structural analysis, the failure load of the beam-slab assembly could be determined based on the time at which instability (failure) occurs in the slab.

For the results presented in the following sections, the load capacity of the system was determined every 10 minutes until the fire was well into the decay phase (compartment burnout). This approach resulted in more than 1200 simulations being conducted for the six fire exposures shown in Fig. 6.8. Table 6.2 shows a summary of the load capacity for the different sections considered under the full range of design fires.

Table 6.2: Load capacity of strip floors considered in numerical simulations

Slab thickness (mm)	Span (m)	ASTM 1 hour (kN/m^2)	ASTM 2 hour (kN/m^2)	Extreme (kN/m^2)	Severe (kN/m^2)	Medium (kN/m^2)
100	4.57	7.26	7.26	6.41	7.05	8.10
	6.10	5.23	5.23	4.74	5.12	5.63
	7.62	4.12	4.12	3.52	4.07	4.34
	9.15	3.42	3.42	2.99	3.39	3.53
	10.67	2.93	2.93	2.03	2.91	2.98
	12.20	2.57	2.57	1.44	2.24	2.57
125	4.57	16.48	16.48	14.17	16.06	12.54
	6.10	11.18	11.18	10.68	11.22	10.88
	7.62	8.39	8.39	6.57	8.34	8.57
	9.15	6.72	6.59	4.90	5.68	6.76
	10.67	5.54	4.69	2.81	3.73	5.46
	12.20	4.44	3.55	1.86	2.77	4.49
150	4.57	15.45	15.45	13.01	14.82	9.83
	6.10	12.38	12.38	10.37	12.00	11.60
	7.62	10.24	10.24	9.83	10.91	8.85
	9.15	9.29	9.29	8.37	9.29	8.35
	10.67	8.71	6.86	5.32	5.73	7.66
	12.20	7.12	5.35	3.51	4.03	5.35

6.3.4 Development of Design Methodology

For development of a design methodology, results from only three of the fires shown in Fig. 6.8 were used. This was done to provide two distinct data sets, one (three cases) to develop the design methodology, and the second (remaining two cases) for validation of the methodology. The fire exposures selected were extreme, severe, and medium, the load capacity of the floor strips under these fire exposures as determined by SAFIR simulations can be seen in Table 6.2.

Based on results from the numerical investigations discussed in the previous section, a correlation was developed between the load capacity of a specific slab able to survive two hours of ASTM E-119 fire exposure (hereunto referred to as the two hour ASTM load capacity), and the load capacity of the same slab able to survive burnout of a design fire (hereunto referred to as burnout load capacity). Given the complex nature of fire design, and the wide range of floor systems that can be represented with a single figure, a design equation to determine load capacity under ASTM E-119 fire exposure was not developed. Rather, Fig. 6.9 which shows the load capacity of a floor that survives two hours of ASTM E-119 fire exposure is referenced to determine the two hour ASTM load capacity of a specific slab spanning a specific length. Also, of note, is that the method presented here only determines the load capacity of the slab which will allow it to reach compartment burnout, not the specific fire resistance duration (time to failure) of the slab under a given load.

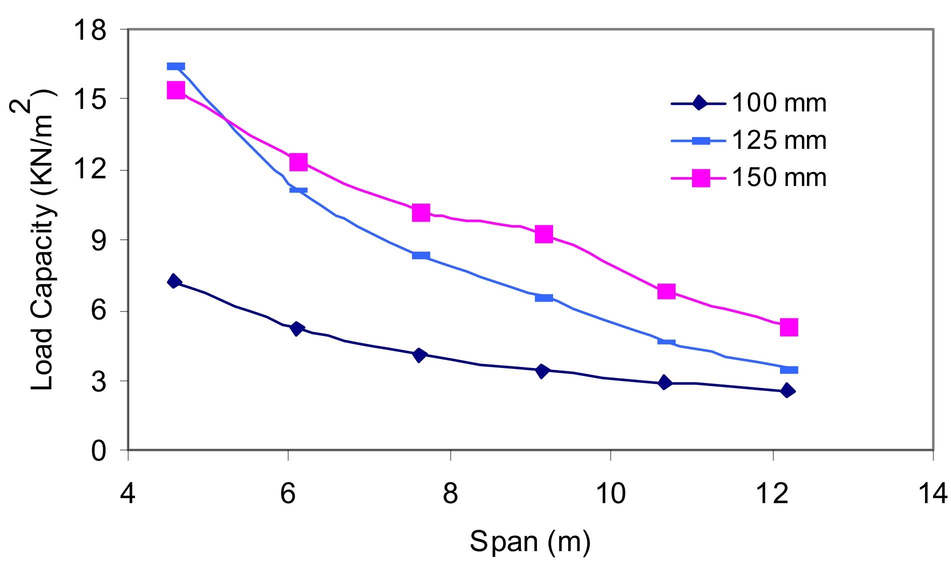

Fig. 6.9: Load capacity of strip floor able to achieve two hour fire resistance rating under ASTM E-119 fire exposure

It is assumed at this point that the designer is familiar with the procedure to develop a probabilistic design fire time-temperature curve based on the compartment characteristics (if this is not the case, the reader is referred to Eurocode (2002)). Having the design time-temperature curve based on compartment characteristics, the peak temperature of the design fire is recorded. Having this value, Eq. 6.14 is used to determine the load capacity of the SFRC slab that will allow it to reach compartment burnout under the design fire exposure.

$$Design\,Load\,Capacity = \frac{ASTM\,Two\,Hour\,Load\,Capacity}{\alpha \dfrac{t}{101.6}} \qquad [6.14]$$

where the *ASTM Two Hour Load Capacity* is read from Fig. 6.9, α is equal to the maximum design fire temperature divided by the ASTM E-119 temperature at two hours (1006 °C) and must be greater than or equal to 1, and t is the thickness of the slab in mm. Units of load capacity are unimportant in the equation.

From Fig. 6.9 it can be seen that load capacity of a concrete slab increases with slab thickness, contrary to this, Eq. 6.14 shows thickness of the slab in the denominator of the equation, thus indicating that increasing thickness decreases load capacity of the slab. Upon closer inspection, it is observed that the ASTM load capacity (as seen in Fig. 6.9) increases with increasing thickness, and this is taken into consideration in the numerator of Eq. 6.14. Therefore, thickness being in the denominator indicates that the design fire burnout capacity does not increase as much with thickness as the two-hour ASTM E-119 load capacity. As an example, under ASTM fire, the load capacity for a 100 mm slab spanning 7.62 m is 4.12 kN/m^2. If this thickness of slab is increased to 125 mm, the load carrying capacity of the section increases to 8.39 kN/m^2. Using Eq. 6.14 and the peak fire temperature for the extreme fire case (1224 °C), the load capacity of the 100 mm thick slab is 3.38 kN/m^2 and the load capacity of the 125 mm thick slab is 5.52 kN/m^2. In this example, increasing floor thickness from 100 to 125 mm increases the load capacity under ASTM fire by 100%, and under the design fire by only 73%. As such, despite the fact that thickness is in the denominator of Eq. 6.14, the load capacity of the slab does increase with an increase in slab thickness under design fire exposure. This increase is just not as large as the increase realized when the ASTM E-119 fire is simulated.

The proposed approach was first used to predict the burnout load capacity of the 18 span-thickness combinations shown in Table 6.2 which correspond to the three design fires used in the development of the approach. The results from this comparison are shown in Fig. 6.10 with conservative and un-conservative predictions appropriately indicated. A total of 54 simulations and corresponding predictions are shown in Fig. 6.10. Of those 54 simulations, an un-conservative prediction of load capacity of the floor system is returned only once by the proposed method. This un-conservative prediction corresponds to the 100 mm slab spanning 12.2 m and exposed to the extreme fire condition. Because this configuration is outside the practical range, the un-conservative prediction is not believed to indicate a fundamental failure of the developed method. Based on the data set shown in Fig. 6.10 (that which was use in the development of the equation) the proposed approach accurately predicts the load capacity of the floor system 98% of the time.

From Fig. 6.10 it can also be seen that the proposed design equation is quite conservative when SAFIR predicts a load capacity greater than 15 kN/m^2. This does result in some economic advantage being lost due to the conservative nature of the proposed approach. Considering however the use of reduced loads in fire as per ASCE (2005), and the lack of any other safety factor in the proposed approach, this level of conservatism is not believed to be excessive.

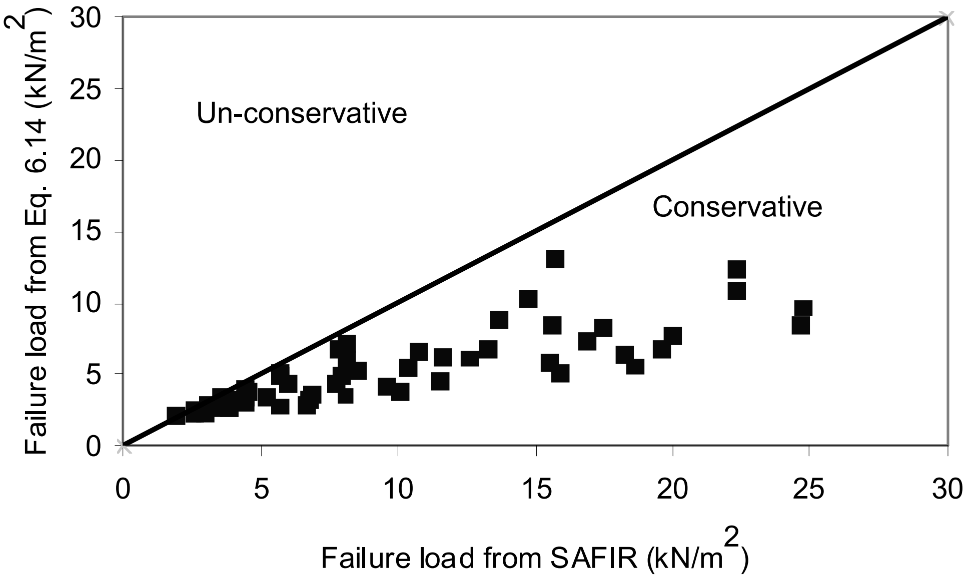

Fig. 6.10: Comparison of failure load of slab as predicted by SAFIR and the proposed equation (6.14)

While the proposed approach predicts the burnout load capacity for the data set used to develop the approach very accurately (<2% un-conservative predictions), it is necessary to consider an independent data set to fully check the validity of the approach. To that end, two additional fires were simulated and the burnout load capacities determined. The two additional fires correspond to the “mild” and “check” fire shown in Fig. 6.8. A comparison of the burnout load capacity predictions from SAFIR and those from the proposed design methodology are presented in Fig. 6.11 below. Again in Fig. 6.11, a line indicating safety of the proposed approach is included with the conservative and un-conservative regions indicated.

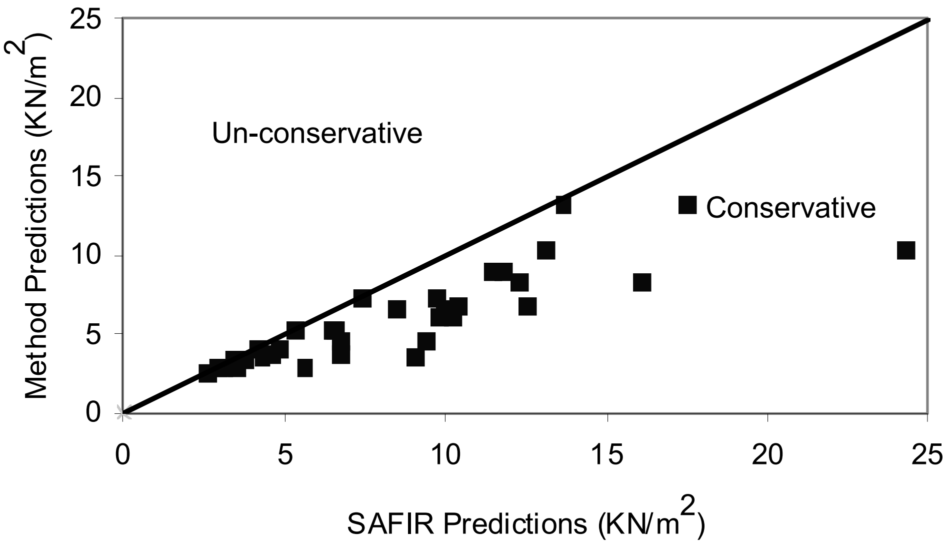

Fig. 6.11: SAFIR and equation predictions for additional data set

The same trend is observed in Fig. 6.11, as was noticed in Fig. 6.10, in that the proposed method is conservative in the vast majority of cases. Of the 36 simulations represented in Fig. 6.11, the proposed method predicts the burnout load capacity of the floor system un-conservatively once, and conservatively 35 times. The un-conservative data point corresponds to the 100 mm thick slab spanning 10.67 m and exposed to the "check" fire exposure. As was the case with the previous data set, the parameters are outside the practical range, and as such, are not believed to indicate a fundamental weakness in the proposed design methodology. Considering only the data used for validation, and excluding that in Fig. 6.10 (which was used in the development of the proposed approach), the proposed approach predicts the burnout load capacity of the floor conservatively 97% of the time. Considering the entire data set, (represented in Figs. 6.10 and 6.11) the proposed approach predicts the burnout load capacity conservatively 97.8% of the time. Based on the comparisons of SAFIR predictions and those from the proposed approach, it is reasonable to conclude that the proposed approach can accurately predict the burnout load capacity of a floor exposed to design fires base on the two hour ASTM E-119 load capacity. To illustrate the applicability of the proposed approach in design situations, an example is presented below followed by the limitations to the proposed approach.

6.3.5 Illustration of the Proposed Approach

Applicability of the proposed approach for fire resistance design of a SFRC floor system is illustrated through a numerical example. Detailed calculations for this problem are presented in Appendix F.

A room 3 m high with a 6 m by 4 m floor (with secondary beams spanning in the 6 m direction) and a fire load of 5.25 kN/m^2 is to be designed. The room has one window opening 3 m wide by 2 m high. The architect has indicated that the room below the considered compartment has the same dimensions and will have a fuel load of 550 MJ/m^2 (of floor area). Now, it is desired to know what thickness the floor needs to be to satisfy the code requirements by withstanding complete burnout of the probabilistic fire that would occur within the compartment.

The first step is to determine the design fire that is most likely to occur within the compartment. The fire scenario can be determined using the Eurocode (2005a) method. The detailed calculations associated with this example are presented in Appendix F, along with further details on the compartment characteristics. The ventilation factor for this example is 0.079 m$^{1/2}$ and the burning duration is 0.79 hours. The time temperature curve of the possible fire determined using this method, and the standard (ASTM E-119) time temperature curve are shown in Fig. 6.12.

The second step is to assume a floor thickness and check that thickness using Fig. 6.9 and Eq. 6.14 to determine if the floor will meet the specified fire resistance requirements and support the applied load until compartment burnout. For this example, the assumed floor slab thickness will be 100 mm, with this information Fig. 6.9 is referenced as done in Appendix F, and the limit load capacity of the floor at 2-hours of standard fire exposure is found to be 5.5 kN/m^2. The second step it to determine the maximum design fire temperature which is 1089 °C for the example given (see Appendix F). Having this information, Eq. 6.14 is applied and the burnout load capacity of the floor is found to be 5.08 kN/m^2

The burnout load capacity of the floor is found to be less than the applied load on the slab during a fire event, as such, it is necessary to enhance the fire resistance of the floor slab. The most practical way to accomplish this is to increase the thickness of the floor system. A second thickness of 112.5 mm is selected and the process repeated as detailed in Appendix F. The result of the thicker floor slab is a burnout capacity of 6.98 kN/m^2 which is sufficient to withstand the applied load of 5.25 kN/m^2, thus, the SFRC floor is capable of sustaining burnout conditions, and there is no need for applied fire protection on the secondary beams.

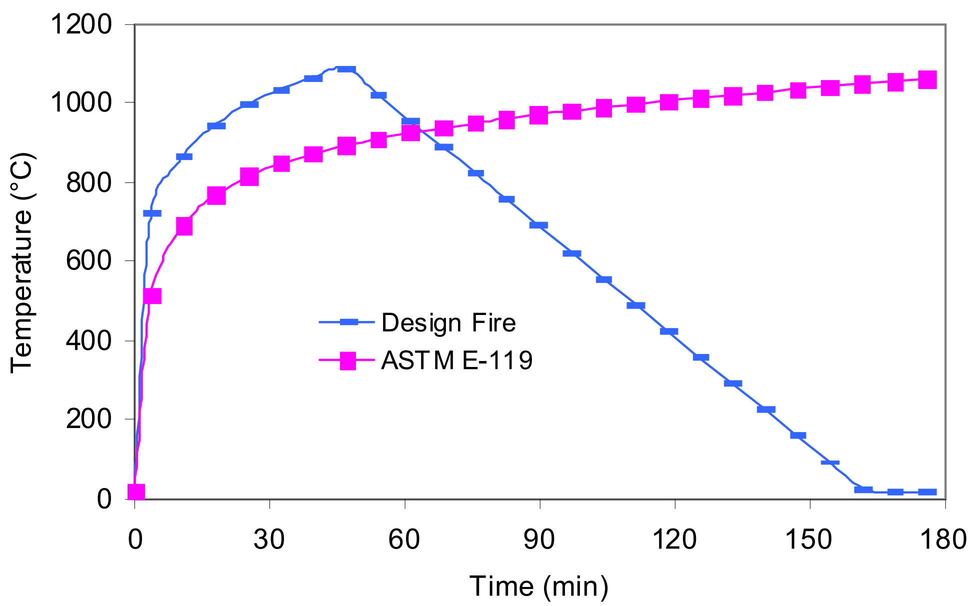

Fig. 6.12: Comparison of standard and design fire exposure

6.3.6 *Application and Limitations*

The proposed method offers a practical approach for evaluating the fire resistance of floor systems exposed to design (real) fires. However, the applicability of this method is limited to the range of parameters that were considered in the numerical study which formed the basis for development of the approach. The explicit limitations for the proposed methods are as follows:

- This method is applicable for standard fire exposure up to two hours, and design fires that have a similar temperature rise in the first 20 minutes as ASTM E119 followed by a cooling phase.
- The approach is only applicable for slabs ranging from 100 to 150 mm thick, and spanning between 4.57 and 12.2 m in the short direction.
- Slabs must be supported on the edge by protected beams that provide vertical, horizontal, and rotational support to the slab during the entirety of the fire exposure.
- Slabs must be supported by unprotected secondary beams, the presence of protection on the secondary beams will significantly alter the load capacities determined in the above simulations, and hence, Eq. 6.14 may not be valid.
- The approach is valid only for SFRC made with carbonate or siliceous aggregate, and having a specified compressive strength of between 25 and 30 MPa and a steel fiber content between 1.75 and 2.25% by mass.
- One and two-way slabs can be designed using the proposed approach since the development was conservatively done considering only one-way slabs.

It should be noted that the above limitations are specified due to a lack of validation for these conditions. Through further validation, it should be possible to extend this method to overcome some, if not all, of these limitations.

6.4 Methodology for System Level Evaluation of Fire Resistance

The contribution of composite construction and tensile membrane action to fire resistance is best considered at the system level. In order however to account for all relevant design variables, the complexity associated with analysis is compounded as compared to element or assembly level analysis and the models are excessively large. It is therefore not practical or feasible to develop simplified design methodologies that can include all relevant factors as for system level analysis. Any such approach would have to account for a significant number of variables, and as such, would cease to be either simplified or rational.

System level fire resistance evaluation is far better suited for specific applications, and to investigate the effect of specific parameters on fire resistance. The system level simulations conducted for this research, as presented in Chapter 5, served to identify the factors affecting fire resistance at the system level. In addition to the factors that influence fire resistance at the element and assembly level, composite action, the development of tensile membrane action, and member interactions enhance fire resistance at the system level. These factors enhance fire resistance by providing alternate load paths to transfer loads from fire weakened members to other cooler parts of the structure.

Thus far in this research, numerical models have been employed to identify factors that influence fire resistance, and for the development of rational design methodologies. Due however to the complexities involved in evaluating system level fire resistance, system level models will henceforth be utilized to study the applicability of the design methodologies developed for enhancing fire resistance through composite construction. In all simulations conducted at the system level, the factors affecting the fire resistance at the system level, namely, composite construction, development of tensile membrane action, fire exposure, member interactions, and failure criterion, are taken into account. The detailed procedure for assessing fire resistance at the system level is outlined in Chapter 7, and as such will not be presented here.

6.5 Summary

Rational design methodologies for the fire resistant design of CFHSS columns and composite steel beam-SFRC slab assemblies are presented in this chapter. In the development of these methodologies, the beneficial effects arising from composite construction, realistic fire scenarios, loading, and restraint conditions are taken into consideration. Through extensive validation, these design methodologies are deemed conservative for use in practical applications.

For CFHSS columns, the developed methodology allows the survivability of a CFHSS column under design fire exposure to be determined. The methodology capitalizes on the previous research on CFHSS column to establish the fire resistance of a column under standard fire exposure. This fire resistance time evaluated under standard fire exposure is then used with an equivalent area approach to determine with a high degree of accuracy if the column will fail under the specified fire exposure, or survive compartment burnout.

Similar to the case of CFHSS columns, based on an equivalent fire severity approach, a correlation between structural performance under standard fire and design fire exposure is presented. The design methodology allows the limit load capacity under which an SFRC floor system can survive complete compartment burnout to be determined based on the load capacity under standard fire exposure. In this approach, the developed figure is referenced for a specific slab thickness and span to determine the two hour load capacity of the floor system under standard fire exposure. The proposed correlation methodology is then applied to the two hour load capacity of the system, and the load limit for the slab to survive complete burnout of the specified design fire exposure is obtained.

CHAPTER 7

7 IMPLEMENTATION OF DESIGN METHODOLOGIES

7.1 General

Concrete is utilized in almost all steel framed buildings due to the advantages composite construction offers over other types of construction. For fire resistance evaluation however, the beneficial effects of composite construction are not taken into consideration. For evaluating fire resistance, current provisions in codes and standards apply a critical temperature criterion in steel members to define failure. Thus, the contribution of concrete in enhancing the fire resistance is steel framed structures is not taken into consideration. This prescriptive approach continues to be used due to the lack of design methodologies for evaluating fire resistance based on all significant factors including composite construction.

To overcome these drawbacks, this chapter presents guidance on the two possibilities for utilizing composite construction to enhance fire resistance, the first is a detailed finite element analysis procedure, while the second utilizes the design methodologies developed in Chapter 6. Following the discussion on performance-based design, a case study is presented to illustrate the implementation of the design methodologies for evaluating the fire resistance of steel frames incorporating composite construction.

7.2 Performance-Based Fire Resistance Design

In recent years, performance-based approach to fire safety design is becoming popular since cost-effective and rational fire safety solutions that can be developed using such an approach (Kodur, 1999). One of the key aspects in any performance-based fire safety design is the fire resistance design of structural members. Currently, to evaluate the fire resistance of structural members, numerical models that can simulate the response of the member under realistic fire, loading, and restraint scenarios must be used. The main steps needed to undertake performance-based design of structural members at the present are:

1. Developing proper design (realistic) fire scenarios
2. Developing realistic design parameters such as loading, restraint, and other structural parameters
3. Carrying out detailed thermal and structural analysis by subjecting the structural member to specified fire conditions; and
4. Developing relevant practical solutions to achieve the required fire resistance.

Each of these steps will be elaborated upon in the following sections, following this discussion, a simplified approach utilizing the design methodologies of this research will be presented.

7.2.1 Development of Fire Scenario

When evaluating fire resistance in a performance-based environment, it is paramount that realistic (design) fires be used. Real fires generally have a cooling phase after the initial growth and combustion phase. This cooling phase limits the temperature rise in structural members, and is followed by a reduction in temperatures that allow the members to regain strength and stiffness. As the materials regain strength and stiffness, they contribute to the load bearing capacity of the system and serve to enhance the fire resistance of the entire structure. In addition, the use of design fires permits the beneficial effects of fire suppression systems to be accounted for in the modelled fire exposure.

The design fire scenarios for any given situation should be established either through the use of parametric fires (time-temperature curves) specified in Eurocode (2005a) or through design tables (Magnusson and Thelandersson 1970). These methods take into consideration critical factors influencing fire resistance by accounting for compartment size, ventilation characteristics (compartment openings), room use (fuel load), and the decay phase is based on the duration of combustion prior to cooling. An example is provided in Section 6.2.4 in which the Eurocode procedure is utilized to developed a design fire for a specific compartment, as such, it will not be reiterated here.

7.2.2 Development of Design Parameters and Loading

For evaluating fire realistic fire resistance, it is necessary to account for the actual conditions the structural system would experience under fire conditions. These factors include composite construction, restraint levels (boundary conditions), and load levels. Composite construction and restraint levels are implicitly taken into consideration when the numerical model is established; load level on the other hand needs to be explicitly taken into consideration. As discussed in Chapter 2, during fire exposure, structural members are assumed to experience reduced loading due to the low probability of a fire event. The reduced load levels to be considered in the analysis can be evaluated by using the provisions presented in ASCE or Eurocode namely 1.2DL + 0.5LL (ASCE 2005) or 1.2DL + 0.4LL (Eurocode 2002) should be used.

7.2.3 Conducting Thermal and Structural Analysis

Once the fire scenarios and structural parameters are established, fire resistance analysis can be carried out using computer programs that are capable of conducting the thermal and structural analysis. Computational programs such as SAFIR, ABAQUS, and ANSYS can be used to undertake fire resistance analysis. Once the computational program is selected, a detailed discretized model is to be constructed that takes into consideration the high temperature material properties of the constituent materials. Given however the large scale of these models, it is necessary to consider a wide range of practical fire exposures as the entire structure is not necessarily exposed to fire at the same time. This last factor of fire size results in there being hundreds if not thousands of simulations that need to be conducted. It is critical that in all of these simulations the effect of composite action, fire scenarios, load levels, restrain, high temperature properties of constituent materials, and realistic failure limit states.

7.2.4 Development of Practical Alternatives

Results generated by the fire resistance analysis can be utilized to develop alternate strategies for achieving the required fire resistance levels. This can be accomplished by altering design parameters such as the thickness of a floor system, the concrete type used in the floor system, or the type of columns utilized. The method adopted to achieve the practical alternatives is dependent on the weak link in the structure as identified by the numerical simulations. This iterative process should be repeated and additional factors changed until the desired fire resistance level is achieved. When developing the practical alternatives, the fire resistance benefits must be considered in light of economics and sound engineering principles. In this chapter, a case study is presented which illustrates the development and implementation of practical alternatives for achieving fire resistance through composite construction. Specific methods implemented in this chapter include optimizing the concrete type utilized in CFHSS columns, and optimizing the type of concrete used in composite floor systems.

7.2.5 Use of Performance-Based Design Methodology

The process outlined for detailed fire resistance analysis requires significant time, effort, advanced skills and expensive computational software. As an alternative, simplified design methodologies can be applied for evaluating fire resistance of CFHSS columns or composite floor assemblies.

For fire resistance analysis utilizing simplified design methodologies, the first two steps in section 7.2 remain the same, the design time-temperature curve and loading on the respective member/system must be determined. The design methodologies can then be applied to assess the fire resistance of the structural member and to develop practical alternatives. For enhancing fire resistance, practical alternative can include increasing the thickness of floor system, altering the concrete type, developing alternate design fire exposure, changing the filling in CFHSS columns, or reducing load levels on the assembly. After implementation of a practical alternative, the developed methodologies are reapplied to assess the fire resistance. This iterative procedure is repeated until the desired level of fire resistance is achieved in the structure.

The case study presented in this chapter illustrates use of the simplified design methodologies developed in this research. To carry out this example, a typical steel framed building is modeled in SAFIR, and a series of simulations undertaken to illustrate the effectiveness of both the proposed structural components (CFHSS columns and composite floor slabs made with SFRC) to achieve fire resistance, and to illustrate the use of the respective design methodologies. In each of the cases, the structural geometry or the fire exposure is altered to illustrate the effect that each change has on fire resistance of the structure.

7.3 System Level Fire Resistance Evaluation

To illustrate the effectiveness of the simplified methodologies developed as part of this thesis, it is necessary to compare fire resistance evaluated through the simplified approach with that obtained from detailed analysis utilizing finite clement models of a building constructed according to recent (AISC 2005) U.S. design standards exposed to fire. To that end, a numerical model of a typical eight story steel framed building is constructed in SAFIR, and the proposed design methodologies applied in evaluating fire resistance. Utilizing results from the numerical simulations and proposed design methodologies, the feasibility of achieving the required levels of fire resistance in steel framed structures utilizing composite construction is explored under different fire scenarios.

7.3.1 Building Description

The building selected for the fire resistance evaluation is the William Beaumont West Bed Tower in Troy, Michigan. This is an eight story steel framed building constructed in 2008, and represents typical office and heath care facilities built according to current construction practices in the United States. Though the building represents typical construction for hospital and office buildings, the methods developed in this research are only sufficient to satisfy fire resistance requirements as they pertain to office buildings. This is because typical sprinklered office buildings generally require less fire resistance (1-2 hours) that health care facilities (3-4 hours), henceforth, for this reason, the building will be referred to as an office building.

The structural framing details of this building were acquired from Douglas Steel, the design firm responsible for the design and construction of the structure. A partial structural framing plan for the 5th story is shown as Fig. 7.1. The secondary beams used are W16x26 and the primary beams spanning on line C and D in the middle of the structure are W21x57 sections, the edge beams are W30X124. In plan, the building is 56.7 m by 29.3 m, each of the bays is 10 m by 10 m. Emergency evacuation stairs are located in two of the corners with a third set of stairs located in the center of the building as seen in Fig. 7.1.

Connections used in the structural frame consist of both shear and moment connections. Moment connections are provided in the exterior frames to provide resistance to lateral (wind) force. All connections on the interior of the structure, including those on the ends of secondary beams, are shear connections.

The floor slab in the buildings comprised of a composite deck, shear studs, and shrinkage reinforcement. The deck in each story of the structure was poured in one continuous pour without shoring to the floor beams.

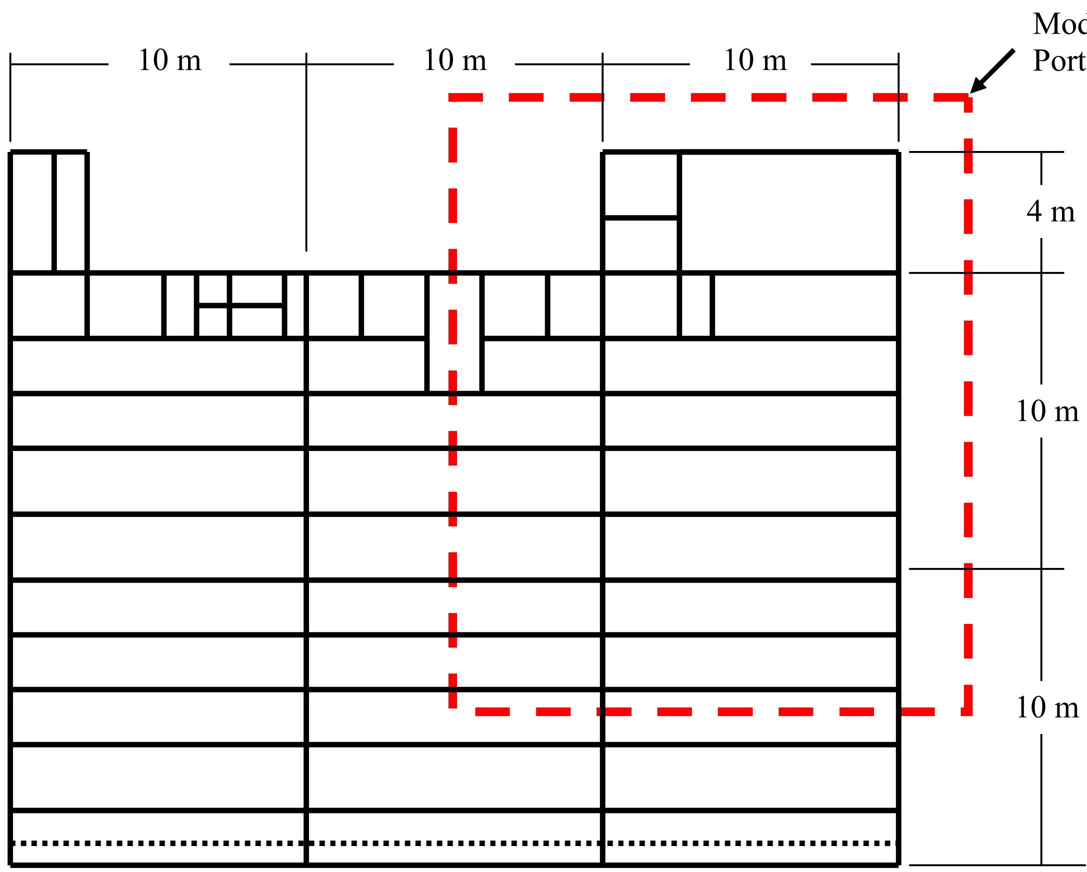

Fig. 7.1: Framing plan for the steel framed building used to illustrate application of the developed methodologies

The first four stories of the structure are larger in plan to accommodate other service functionalities. As such, the fifth floor was selected for fire resistance analysis to eliminate the interaction of multiple functions on the same floor, and to reduce the size of the structure being modeled.

7.3.2 Numerical Model

Having selected a typical building to be used in the fire resistance analysis, it was necessary to construct a numerical model of the building. While a model of the entire building would be most desirable in terms of simulation results, this is impractical due to the many simulations (case scenarios) desired. It was therefore decided that two levels of analysis would be conducted. As such, a one story model was created to assess the practicality in application of the proposed design methods, and a three story model was constructed to assess the ability of the proposed methods to create a design capable of withstanding a multi-story fully developed fire including a cooling phase. As described in the following section, great care was taken in constructing the model to accurately reflect the system level behavior of the structure, and to capture the contribution of composite construction and tensile membrane action to the fire resistance of the steel framed structure.

7.3.3 Discretization

Due to the complexities that are associated with modeling a ribbed composite floor slab, it was decided to use a slab represented by a shell element of uniform thickness as has been done in previous studies (Zhang et al. 2008, Cashell et al. 2008). The thickness chosen for the slab was that of the thickest part of the ribbed flooring system, 130 mm. This slab was modeled using four nodded shell elements with six degrees of freedom at each of the nodes. The beams supporting the slab and the columns were modeled using three nodded beam elements with seven degrees of freedom at the end nodes, and one degree of freedom at the center node. To simulate the composite action between the steel beam and the floor slab, the "SAMEALL" command was used for the nodes where the beam and shell elements coincide. This caused all of the translations and rotations at these points to be the same for the beam and slab, thus simulating the fully composite condition.

Due to the large floor plan for the entire structure, and the computational time associated with such a large model, only the portion of the building indicated in Fig. 7.1 was modeled. This section was modeled as a single story (5^{th} story) as shown in Fig. 7.2 and a three story model (5^{th}, 6^{th}, 7^{th} stories) as shown in Fig. 7.3. Modeling only the portion of the structure indicated in Fig. 7.1 requires that particular attention be given to the boundary conditions used in the simulation. It was assumed that the column ends where they pass though the adjacent floors acted as fixed connections with all degrees of freedom being fully restrained. It was also assumed that the portion of the structure that was not modeled, being significantly larger than the modeled potion, was essentially rigid compared to the modeled portion. As such, the horizontal translation on the continuous edges was fully restrained perpendicular to the modeled edge. Due to the continuity of the slab over these points, the rotation about the length of the edge was assumed to be restrained, thus simulating the realistic support offered by the portion of the structure which was not modeled.

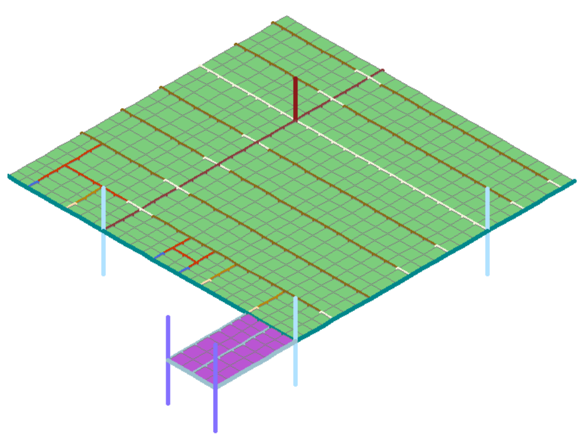

Fig. 7.2: One story numerical model of selected building

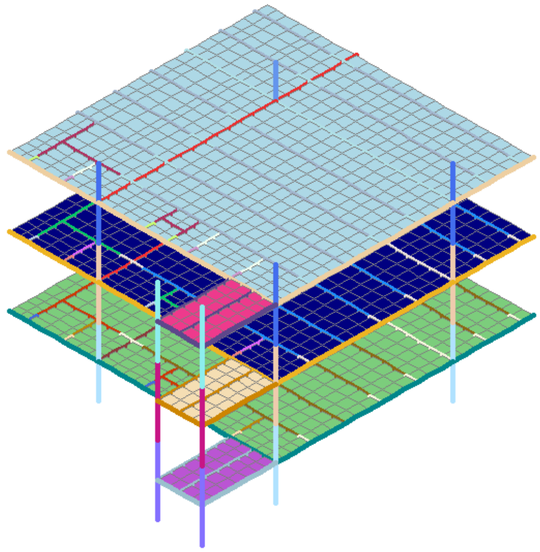

Fig. 7.3: Three story numerical model of selected building

It was assumed in the models that the full floor area with the exception of the stair area was exposed to fire. The stair area was designated in the plans as a fire escape rout, thus, the walls separating the stairs from the rest of the structure provided a 3-hour fire resistance rating. Loading on the structure was taken to be 4.5 kN/m^2 based on the reduced loads present during fire exposure, and the loads used in the Cardington test. This is a typical load for office buildings and is based on 1.2DL + 0.5LL. It was assumed that the fire exposure was the same to all parts of the fire exposed member. That is to say that the ends of beam that would be protected from direct fire exposure in a real structure, were modeled as being fully exposed to the same severity of fire as experienced by the center of the beam span. Beams and columns on the perimeter of the structure were assumed to be supplied with fire protection. It was assumed that secondary beams which attach to protected structural members were also supplied with fire protection for 150 mm past the connection, thus allowing the connection to remain cool enough that its structural integrity was not compromised. This assumption was invoked to eliminate the need to consider the complex behavior of the connection at elevated temperatures. Due to the continuity in the concrete slab and the relatively high tensile strength of SFRC, it was assumed that all of the connections acted as moment connections. This assumption is predicated on the assumption that the concrete slab will not fracture over the supporting beams, and as such, will maintain moment restraint throughout the course of fire exposure.

Four design fire scenarios and ASTM E-119 fire exposure were considered in the analyses, these fires were developed to represent firs that could occur in a typical steel framed office building. In the development of these fires, structural geometry and typical fuel loads are taken into consideration. The developed fire exposures are shown in Fig. 7.4. All one story simulations were run for 3 hours, or until the structure became unstable and the simulation indicated failure of the structure. For the three story models, it was assumed that it took one hour from ignition of the first floor until the second floor was exposed to fire, and subsequently it took another hour for the third floor to be exposed to fire. As such, in all three story cases, the first floor was experiencing a fully developed fire when the second floor was ignited, when the third floor ignited, the second floor was fully developed and the first floor was in the cooling phase. The simulations were continued until the third floor had been exposed to three hours of fire exposure (for total fire duration of 5 hours) or until SAFIR indicated that the structure was unstable and failure of the simulation occurred.

The fire resistance analysis was carried out for a total of 11 cases which correspond to different fire scenarios, column configurations, and floor slab types. The analysis matrix corresponding to these cases is presented in Table 7.1. The analysis with Case 1 was conducted to assess the performance of the structural frame without any fire protection on the columns or secondary beams to determine the "weak link" in the structural system under fire conditions. Case 2 analysis was conducted to assess the beneficial effects of composite construction on the fire performance of the structure if the wide flange columns in Case 1 were replaced with equivalent CFHSS sections designed as per AISC provisions (AISC 2005). For the remaining cases (Case 9 through Case 11), the columns and floor system were replaced with CFHSS columns and SFRC floor systems (respectively) designed according AISC provisions. One and three story models of this modified structural system were exposed to all of the design fires shown in Fig. 7.4 to assess the applicability of the developed design equations. For each of these cases, fire resistance is evaluated using the developed finite element analysis and also by applying the simplified approach proposed in chapter 6. Failure times and location of failure for each case are presented in Table 7.1, and a more detailed discussion for each case is presented in the following sections. In each of the simulations, the constitutive models from Eurocode are utilized and the parameters shown in Table 5.3 were input into SAFIR.

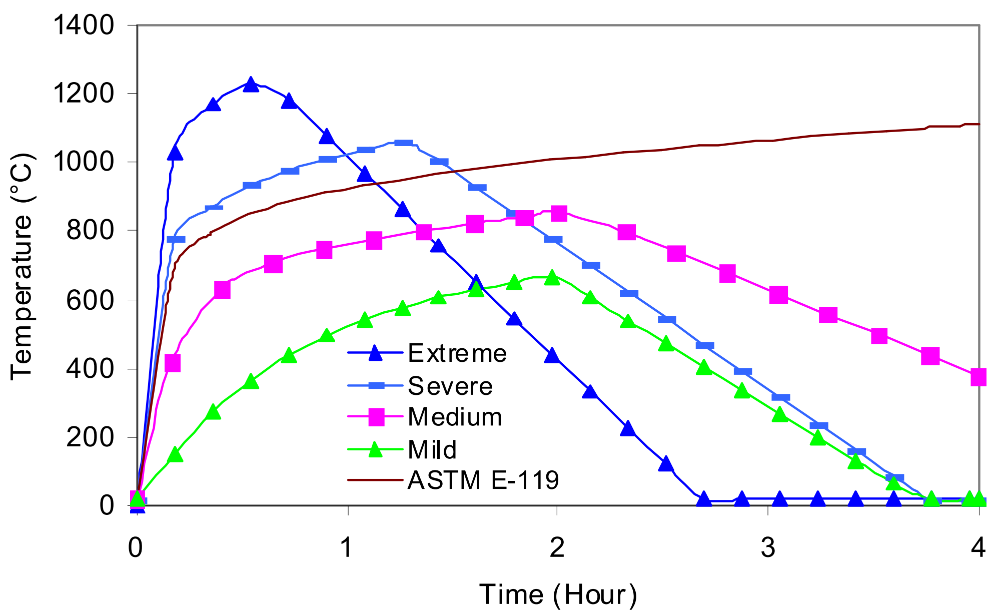

Fig. 7.4: Possible fire scenarios used in the fire resistance analysis

Table 7.1: Various structural configurations and fire scenarios simulated in the building

	Fire exposure	# of stories under fire	Column configuration	Floor slab configuration	Fire resistance (min)	Failure zone/member
Case 1	ASTM E-119	1	W	Plain	16.5	W-column
Case 2	ASTM E-119	1	CFHSS	Plain	58	Floor slab
Case 3	ASTM E-119	1	CFHSS	SFRC	118	Floor slab
Case 4	Extreme	1	CFHSS	SFRC	12.5	Floor slab
Case 5	Extreme	3	CFHSS	SFRC	13	Floor slab
Case 6	Severe	1	CFHSS	SFRC	37	Floor slab
Case 7	Severe	3	CFHSS	SFRC	39	Floor slab
Case 8	Medium	1	CFHSS	SFRC	No failure	None
Case 9	Mild	1	CFHSS	SFRC	No failure	None
Case 10	Medium	3	CFHSS	SFRC	No failure	None
Case 11	Mild	3	CFHSS	SFRC	No failure	None

7.3.4 Model Validation

For validation of the numerical model, due to the lack of information on the response of the considered structure to fire exposure, it is necessary to consider the structural response of the building at ambient temperatures. To accomplish this, structural analysis on the 8-story building under ambient temperature was conducted utilizing SAFIR with a design load of 9.8 kN/m^2 to represent a typical ambient temperature design load on the structure. Deflection predictions from SAFIR were then compared with deflection limits specified in codes and standards. A maximum deflection of 19.9 mm was observed in the center of the secondary W16x26 beams. By considering the deflection limit to be L/480 for a structural element supporting a structural element that could be damage by deflections, the allowable deflection of the beam is 20.8 mm, thus, the deflection limit is satisfied. Additionally, the deflected shape of the structure returned from the simulation as shown in Fig. 7.5 is intuitively correct based on elementary structural principals.

Given that the deflection limit is satisfied by predictions from the numerical model, and that the deflected shape of the structure is intuitively correct, it is concluded that the structural model of the eight story steel framed building is realistically constructed in SAFIR. While full validation cannot be completed for the structure due to a lack of fire response data, it should be noted that the same model will be used in all of the simulations. As such, any error in model construction would be applied to all of the models. Thus, any error resulting from the numerical idealization of the structure will exist in all cases, and thus be self-canceling.

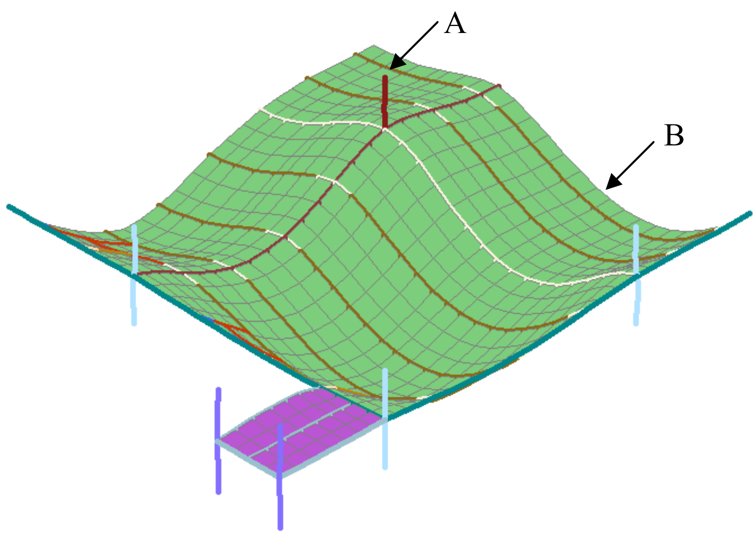

Fig. 7.5: Deflected shape under service loads and ambient temperature (125x)

7.3.5 ParametricSstudy

Using the models described and validated above, the simulations corresponding to the 11 cases shown in Table 7.1 were conducted. Each of these simulations is addressed separately in the following sections.

Case 1

To form a baseline for the study, the structural frame was simulated under ASTM E-119 fire exposure assuming that the primary and exterior beams, and the exterior columns had 2-hour fire protection, while the interior columns and secondary beams had no protection. Failure occurred in this simulation at 16.5 minutes due to failure of the central unprotected W14x61 column, which is marked with an "A" in Fig. 7.5. Failure is achieved early in the fire exposure due to the elevated temperature rapidly achieved in the unprotected steel section. Axial deflection at the top of the column is plotted as a function of fire exposure time in Fig. 7.6. From Fig. 7.6, it can be seen that the column failed suddenly at 16.5 minutes. Results from this simulation indicate that failure of the column which was loaded to approximately 40% of its design strength occurred at an average section temperature of 625 °C due to global buckling of the section.

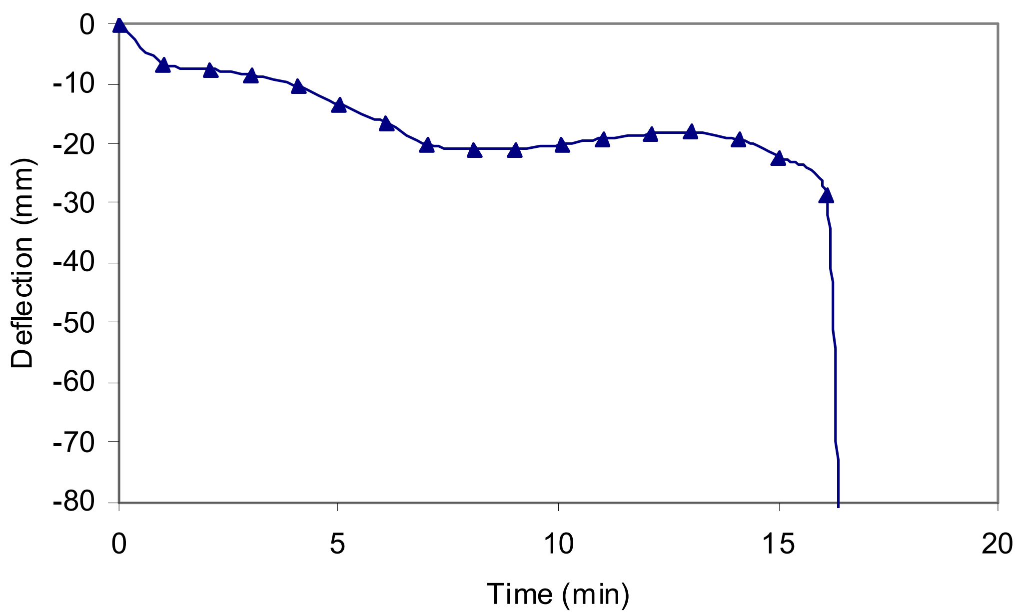

Fig. 7.6: Variation of central column axial deflection with time corresponding to for Case 1 analysis

Case 2

Results from Case 1 indicate that the weak link in the simulated building was the W-shape column. To explore the possibility of improving fire resistance through the use of composite construction, an equivalent CFHSS column was selected to replace the W14x61 section used in Case 1. Design of the column was conducted according to AISC (AISC 2005) ambient temperature trength design, and the fire resistance of the column checked via the design methodology proposed in this research. It was found that a 254 mm square HSS column with 12.5 mm thick walls and filled with carbonate aggregate concrete with a compressive strength of 35 MPa will provide equivalent load capacity at ambient temperatures, and a two hour fire resistance rating.

The structure, with CFHSS columns was analyzed using SAFIR, results from the simulation indicate that the structure fails at approximately 58 minutes due to instability in the plain concrete floor system. Failure of the system initiated at point B indicated in Fig. 7.5. Mid-span deflection in the slab at this location is plotted as a function of fire exposure time in Fig. 7.7. From Fig. 7.7, and it can be seen that the floor system undergoes a sudden increase in the defection rate at 58 minutes. Also of note from Fig. 7.7, is the observation that the deflection in the center of the composite beam utilizing plain concrete reached a maximum of 650 mm before failure of the floor system. This large deflection can be attributed to the composite action that develops between the concrete slab and the beams. The composite action from the floor slab was however insufficient to achieve the two hour fire resistance rating required for this building.

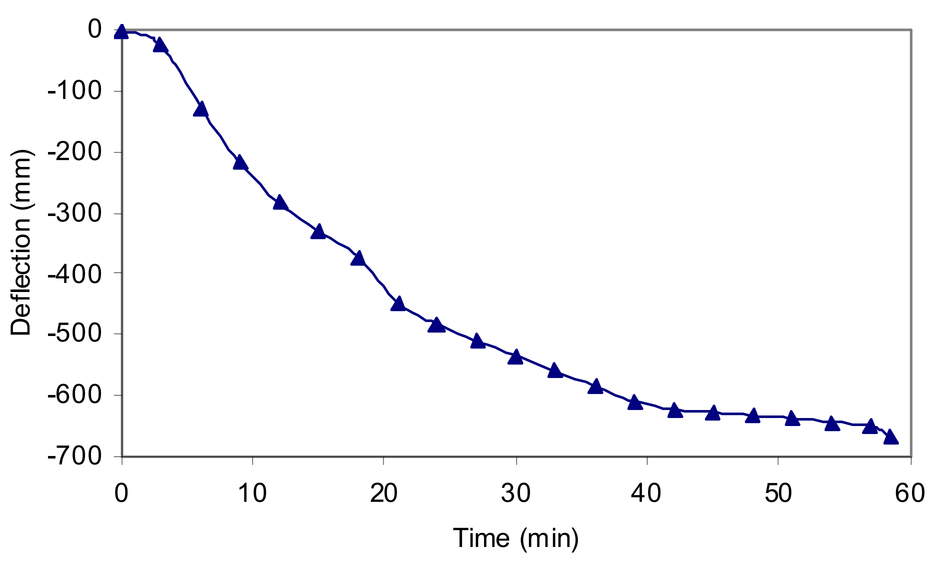

Fig. 7.7: Secondary beam mid-span deflection with time corresponding to Case 2 analysis

Case 3

In order to enhance the fire resistance of the floor system analyzed in Case 2, the floor system was redesigned with SFRC in place of plain concrete. Fire resistant design of the SFRC floor system was carried out according to the developed methodology, and the fire resistance analysis carried out on the reconfigured structural system using SAFIR. Results from the SAFIR analysis show that the use of SFRC in the floor system in place of plain concrete increased the fire resistance to 118 minutes under ASTM E-119 fire exposure. The maximum deflection of the SFRC slab prior to failure was 688 mm as observed in Fig. 7.8 (which plots floor deflections for point B in Fig. 7.5).

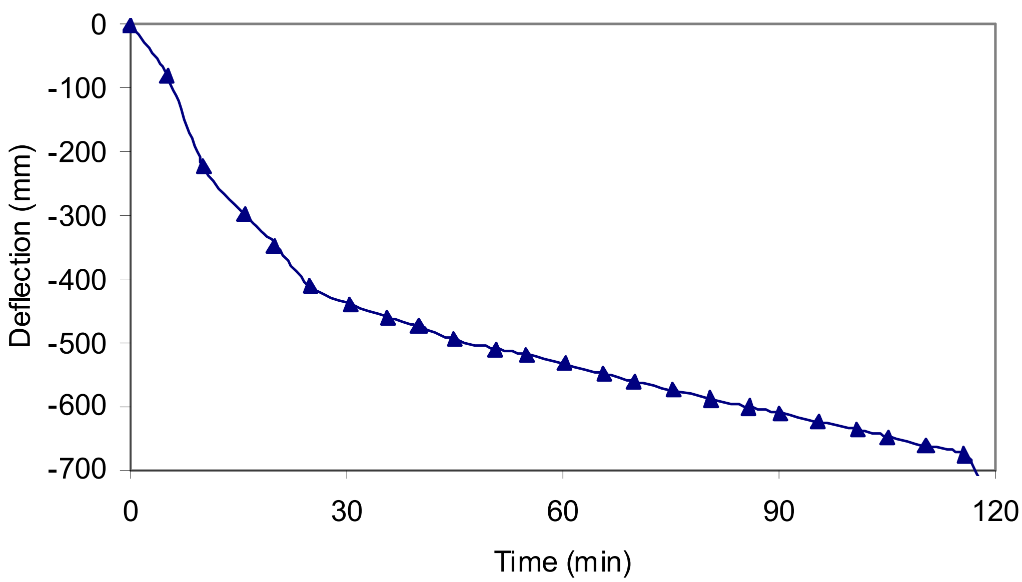

Fig. 7.8: Mid-span deflection in the secondary beam as a function of fire exposure time corresponding to Case 3 analysis

While this deflection is not significantly more than the deflection reached with plain concrete, it should be noted that the failure (fire resistance) time is more than doubled through the use of SFRC. This can be attributed to tensile membrane action in the floor slab that is facilitated by the increased tensile strength of SFRC. Despite the significant increase in fire resistance, this is still insufficient to provide the two hour fire resistance rating required for this type of building. As such, consideration needs to be given to design fires to achieve fire resistance in a performance-based environment

Cases 4 and 5

In order to assess the response of the structure under design fire exposure, alternate fire exposures were developed and the fire resistance analysis carried out on the reconfigured structural system. To that end, the model used in Case 3 was analyzed under the extreme design fire shown in Fig. 7.4. Prior to conducting this analysis, the design methodologies developed above were applied to the column and the SFRC floor system, and it was predicted that the floor system would fail in the analysis. Results from the SAFIR analysis confirm this postulate, fire resistance under the extreme fire exposure was observed to be 12.5 minutes. The maximum deflection observed in the slab prior to failure was 450 mm as shown in Fig. 7.9. The early failure in the floor system can be attributed to the local minimum in floor load capacity as shown in Fig. 6.6. This local minimum is sufficiently below the applied load on the floor, that the simulation returns failure very early in the fire exposure, never allowing the fire to reach the decay phase, thus no advantage of modeling a design fire is realized.

Following completion of this analysis, a three story model of the structure was exposed to the extreme fire scenario. Results of the one story model were confirmed in that the three story model failed at 13 minutes due to a floor failure. The low failure time for the three story model is attributed to the same factors indicated for the one story model.

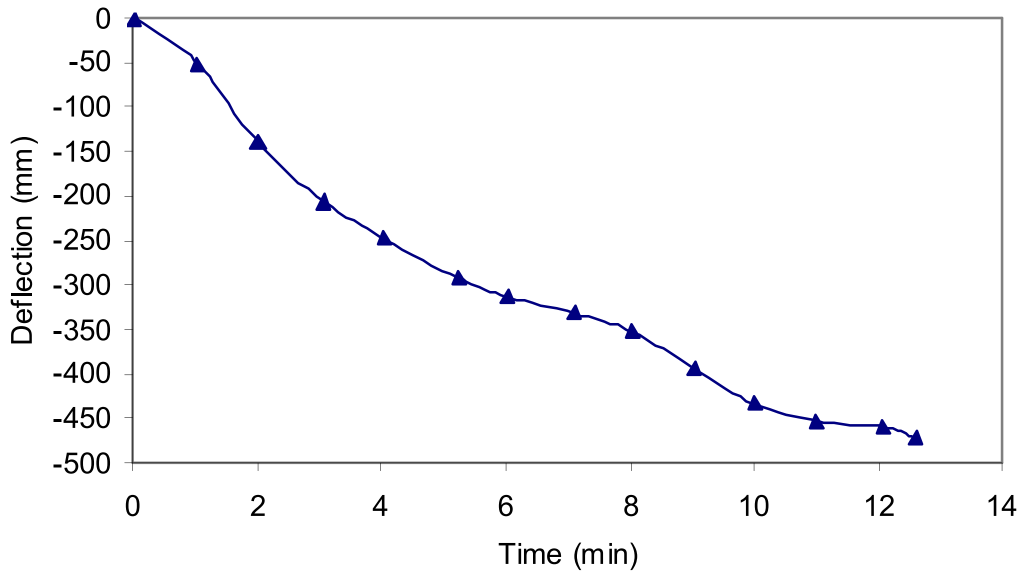

Fig. 7.9: Mid-span deflection in the secondary beam as a function of fire exposure time corresponding to Case 4 analysis

Cases 6 and 7

The analysis corresponding to the structural configuration of Case 4 was repeated under the severe fire exposure shown in Fig. 7.4. As in Case 4, the developed design methodologies indicate that failure will occur in the SFRC floor system, results from the SAFIR analysis confirm this postulate. Under severe fire exposure, the structure was able to withstand the severe fire exposure for 37 minutes, reaching a maximum deflection of 510 mm prior to failure as shown in Fig. 7.10. While failure of the floor system still occurs in a relatively short period of time, fire resistance is enhanced appreciably as compared to Case 4. This enhanced fire resistance is attributed to the development of tensile membrane action in the SFRC slab. Due however to the extreme temperatures reached early in the fire exposure, the extent of tensile membrane action is insufficient for the structure to reach the decay phase of the fire exposure, thus the structure fails in the simulation.

As was the case under the extreme fire exposure, a three story model of the structure was simulated under the severe fire exposure. This simulation failed at 39 minutes due to failure of the floor system as compared to the 37 minutes in the one story model, thus confirming the results from the one story case.

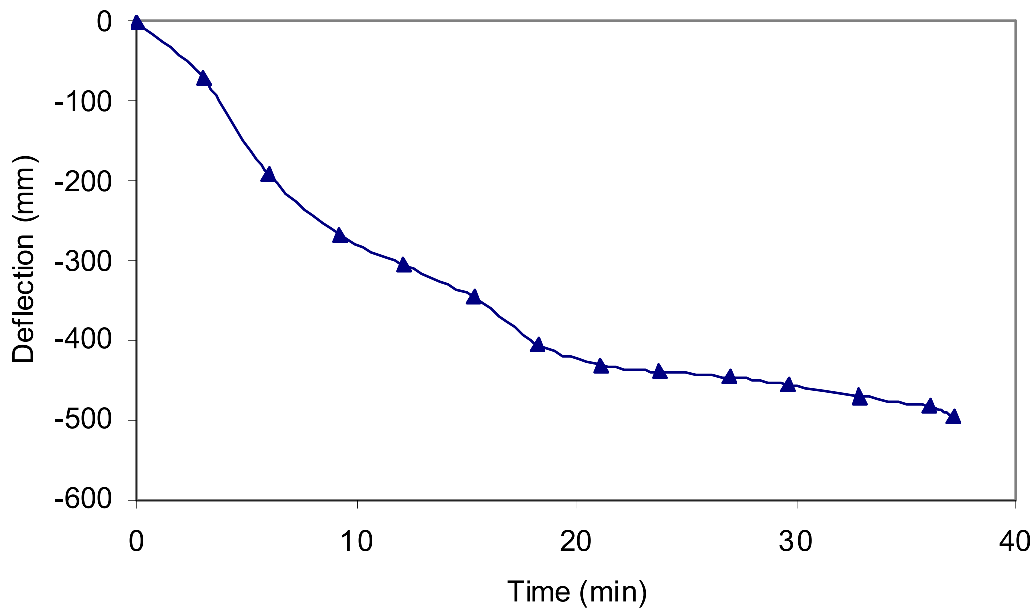

Fig. 7.10: Mid-span deflection in the secondary beam as a function of fire exposure time corresponding to Case 6 analysis

Case 8

To further enhance the fire resistance of the assembly beyond that observed in Case 6, a medium design fire was developed and the fire resistance analysis carried out. As was done in previous cases, prior to conducting the analysis, the developed methodologies were applied to the structure, and in this case, the prediction was made that both the CFHSS columns and the SFRC floor slab would be able to survive the entirety of the design fire exposure, results from the SAFIR analysis confirm this postulate. A maximum deflection of 566 mm was reached in the floor slab at 160 minutes, approximately 40 minutes after the peak fire temperatures as seen in

Fig. 7.11. The ability of the floor system to survive the medium fire exposure is attributed to the development of tensile membrane forces and composite action between the SFRC slab and the steel beam facilitated by the development of large displacements. From this case, it can be seen that composite construction can provide sufficient fire resistance for a structure to reach compartment burnout in a performance-based environment. Additionally, the design methodologies here developed are shown to accurately predict the survival of a structure utilizing composite construction under the medium design fire exposure.

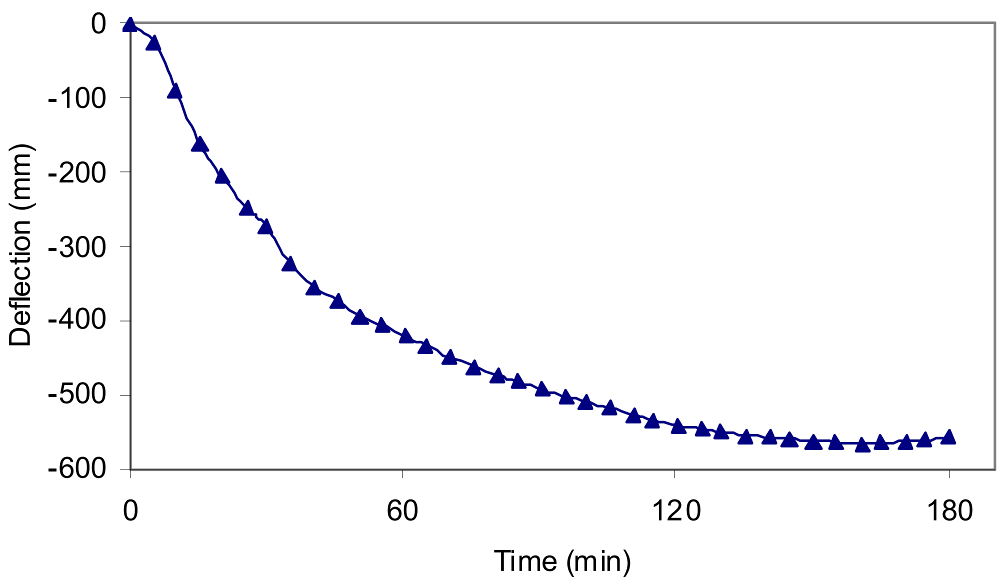

Fig. 7.11: Mid-span deflection in the secondary beam as a function of fire exposure time corresponding to Case 8 analysis

Case 9

To illustrate the ability of composite construction to enhance fire resistance through the development of composite and tensile membrane action, an additional case was analyzed using SAFIR under the mild fire exposure shown in Fig. 7.4. Results from the SAFIR analysis confirm the predictions of the developed methodologies as the structure is able to survive complete compartment burnout under the mild design fire exposure. A maximum deflection of 390 mm was observed in the floor system as seen in Fig. 7.12. While survival of the structure is attributed to the development of composite and tensile membrane action, the lesser deflections under the mild fire exposure as compared to the medium fire are attributed to the lower fire temperatures. The lower fire temperatures result in lower steel and concrete temperatures as well as lower thermal gradients in the materials, as such, thermal and mechanical deflections are reduced. The end result is overall lower deflections under the mild fire case as compared to the medium fire case.

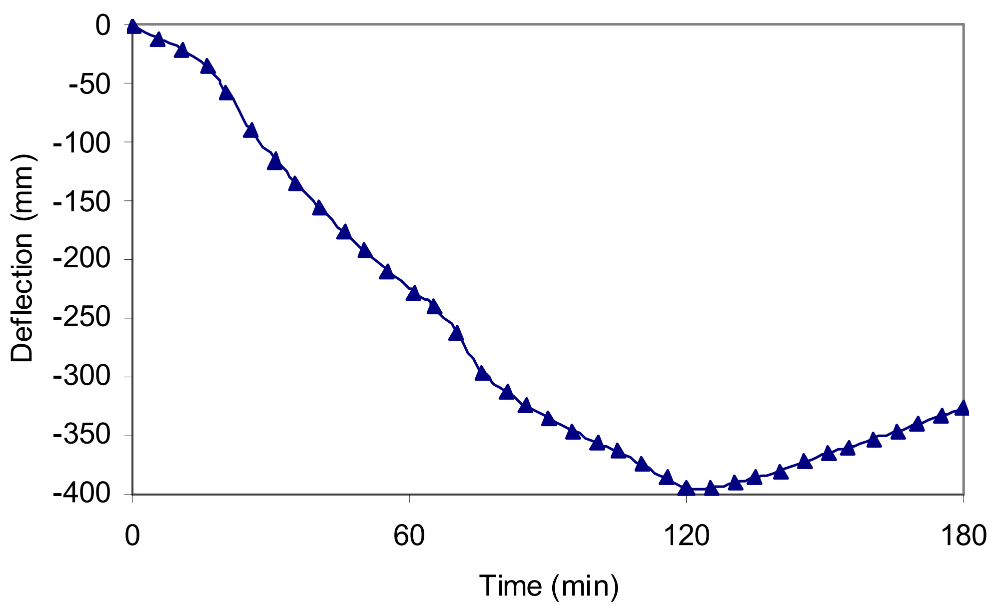

Fig. 7.12: Mid-span deflection in the secondary beam as a function of fire exposure time corresponding to Case 9 analysis

Cases 10 and 11

To illustrate the full capability of composite construction to enhance structural fire resistance without the need for applied fire protection on columns of secondary beams, the three-story case with CFHSS columns and SFRC floor systems was simulated under the medium and mild fire exposures of Fig. 7.4. In both cases, a one hour delay in ignition for one story to the next was assumed. The result is a 5 hour fire exposure time in place of the 3 hour fire exposures considered in the one story models. Due to similarities between results from both the medium and mild fire simulations, only the mild fire will be used to illustrate the behavior of the structure, though the discussion applies to both fire exposures.

Results from the SAFIR simulations indicate that the structure was able to survive burnout of three consecutive stories under both of the design fire exposures. Maximum deflections ranging from 375 to 425 mm were observed in the floor system as shown in Fig. 7.13. Overall survival of the structure is attributed to the development of composite and tensile membrane action, both in the CFHSS columns and the SFRC floor slab. There are however two key observations that can be made from Fig. 7.13. The primary observation is that the first floor of the structure is noted to deflect more (~40 mm) than the subsequent stories. This is attributed the difference in the column end conditions of the three floors. The bottom floor has assumed boundary conditions on the bottom of the columns; the second floor has a simulated floor on both sides while the third floor has assumed boundary conditions at the top of the columns. The second observation from Fig. 7.13 is that the second and third stories in the simulation "rebound" between 20 and 60 minutes. This is attributed to the slow thermal expansion of the supporting columns below these stories. As these columns elongate, they lift the structure above them, thus causing the "rebound" of these stories prior to their experiencing fire exposure.

From the different cases presented above, it can be seen that the development of composite and tensile membrane action contributes to overall fire resistance. Additional consideration of design fires further enhances fire resistance such that elimination of applied fire protection from columns and secondary beams can be achieved. Both of these factors are taken into consideration in the developed design methodologies, and the methodologies have been shown to accurately predict the fire resistance of composite construction under a wide range of configurations and design fires.

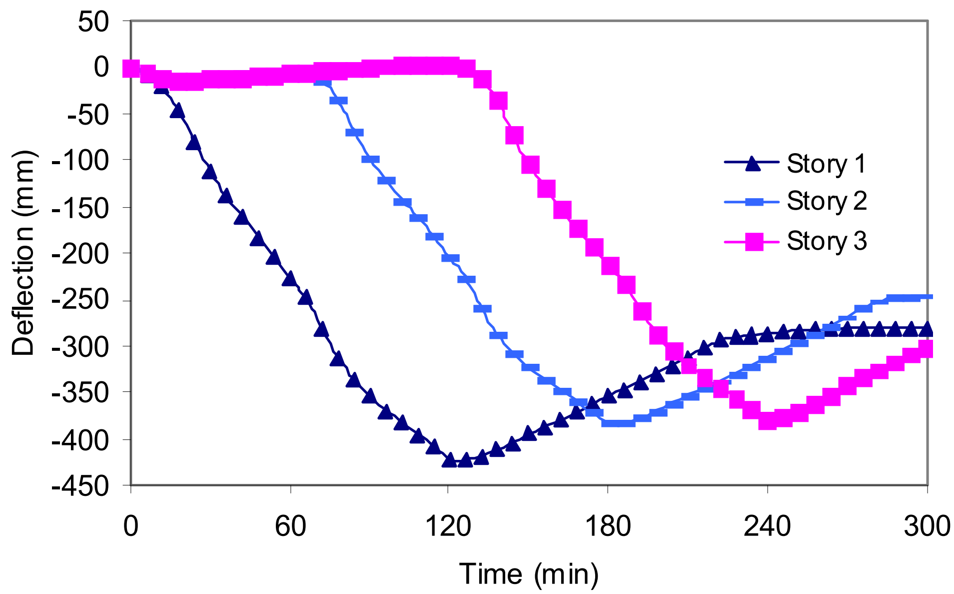

Fig. 7.13: Mid-span deflection in the secondary beam as a function of fire exposure time corresponding to Case 10 analysis

7.4 Summary

The case study presented in this chapter illustrates the use of the proposed simplified approaches for developing alternate fire resistance strategies for steel framed structures. Through consideration of composite construction in a performance-based design environment, it is illustrated that the required levels of fire resistance can be achieved in steel framed structures without the need for applied fire protection to columns or secondary beams through the use of CFHSS columns and SFRC floor systems and the subsequent development of composite action. In addition to providing a cost effective alternative to applied fire protection, the fire resistance provided through composite construction is inherent to the structure, and not easily damaged, thus increasing the reliability of structures under fire exposure.

Performance-based design of structural members for fire resistance facilitated by the fire resistance evaluation methodologies developed above. These methodologies provide a means for practitioners to rapidly and accurately assess the fire resistance of composite structures without the need for costly computational or time resources, thus saving further resources in the design process.

CHAPTER 8

8 CONCLUSIONS AND RECOMMENDATIONS

8.1 General

Steel framed structures often utilize composite construction due to several advantages composite structural systems offer over other types of construction. The composite action that develops between steel and concrete significantly enhances structural performance under ambient and fire conditions. However, the beneficial effects of composite action are not taken into consideration in evaluating fire response of structures due to a lack of understanding and design methodologies. With the aim of developing this comprehensive understanding and rational design methodologies, both experimental and numerical studies were carried out as part of this research. The experimental studies consisted of analyzing concrete filled HSS columns, and evaluating the response of a steel beam-steel fiber reinforced concrete slab assembly to fire exposure. In the experimental study on beam-slab assemblies, special attention was given to monitor the development of composite action and tensile membrane action under realistic loading, fire, and restraint conditions.

Data from the fire resistance experiments were used to validate composite column, beam slab assembly, and full-scale steel framed structural models created in SAFIR computer program. These validated models were applied to study the influence that several factors have on the fire response of composite structural systems at the element, assembly, and system levels. Factors investigated include the effect of fire exposure, load level, concrete properties, failure limit states, member interaction, and development of tensile membrane action. Results from these parametric studies are utilized to quantify the influence of various factors and to develop rational design methodologies. At the element level, a methodology for predicting the survivability of

CFHSS columns under design fire exposure was developed. At the assembly level, a methodology was developed that allows the maximum load a composite steel beam-SFRC slab can carry while surviving design fire exposure to be determined. At the system level, the various factors to be considered in undertaking detailed fire resistance analysis of composite structures are laid out.

The methodologies developed above were incrementally applied to an 8-story office building, and the fire resistance of the building was evaluated at each increment and under different fire scenarios. When the as-constructed building was considered without external fire protection on the columns and secondary beams, the columns failed in less than 20 minutes. When the beneficial effects of composite construction, tensile membrane action, design fire exposure, realistic load levels, and structural failure limit states were accounted for according to the above developed methodologies, the fire resistance of the structure was significantly enhanced. Further, when the inherent fire resistance derived through composite construction was accounted for, the fire response of the structure was sufficient to eliminate external fire protection from columns and secondary beams.

8.2 Key Findings

Based on the information presented in this study, the following key conclusions can be drawn:

- There is very limited information on the response of composite floor assemblies under realistic fire scenarios, loading, and restraint conditions.
- The current fire resistance provisions in codes and standards are prescriptive in nature and do not facilitate the use of rational methods that accurately account for the beneficial effects of composite action in evaluating fire resistance. The use of composite

construction enhances fire resistance through the development of composite action and tensile membrane behavior.

- The main factors that influence the fire resistance of concrete filled HSS columns are concrete type, fire exposure, column size, load level, length (slenderness), and failure limit states. CFHSS columns made with bar and steel fiber reinforced concrete have significantly higher fire resistance than those made with plain concrete, mainly due to higher load carrying capacity and higher confinement effect provided by the presence of reinforcement in the concrete core. Through the use of bar or fiber reinforced concrete, it is possible to achieve three hours of fire resistance.
- The main factors that influence the fire response of composite floor assemblies are the development of tensile membrane action, concrete type, fire exposure, slab geometry, and failure limit states. The use of SFRC in floor slabs in place of plain concrete leads to the development of significant tensile membrane forces and this in turn enhances the fire resistance of the floor slab. Through the use of SFRC in slabs, it is possible to achieve two hours of fire resistance without any applied fire protection to secondary beams under ASTM E-119 fire exposure.
- The use of plain concrete in composite beam slab assemblies enhances fire resistance above that of unprotected steel beams tested individually. The enhanced fire resistance however does not meet the required levels, and alternate approaches for enhancing fire resistance (SFRC) must be utilized.
- The fire resistance of steel framed structures is further enhanced if a system level approach is applied for evaluating fire resistance. The main factors that are to be

considered in evaluating system level fire response are member interactions, composite and tensile action, and type of fire exposure.

- A simplified approach based on equivalent fire severity principals has been proposed for evaluating fire resistance of CFHSS columns under design fire exposure.
- A simplified approach based on equivalent fire severity principals has been developed for evaluating the load carrying capacity of a composite SFRC slab under design fire exposure has been proposed.
- The methodologies developed to evaluate the fire resistance of CFHSS columns and steel beam-SFRC slab assemblies are capable of predicting their survivability under design fire exposures. For the data pools used in this research, the developed methodologies predict an un-conservative response less than three percent of the time.
- In steel framed office buildings, it is possible to eliminate external fire protection to columns and secondary beams (and possibly primary beams under low level fires) by taking into consideration the beneficial effects of composite construction and through the application of a performance-based fire design.

8.3 Recommendations for Future Research

While this research has served to advance the state-of-the-art with respect to the response of composite construction to fire exposure, there is still a considerable need for further research to extend the concepts to other situations encountered in typical steel framed buildings. The following are some of the key requirements for further research in this area:

- The current models for design fire scenarios are based on limited experimental results, thus, the applicability of these fire scenarios for a wider range of compartments needs to be further validated. Computational fluid dynamics based modes should be utilized to investigate probable fire exposures in a compartment, and results utilized to validate the simplified approaches for design fire development.

- The conventional approach of evaluating fire resistance of CFHSS columns under standard fire exposure has a number of limitations with respect geometry, load eccentricity, and load magnitude. These limitations need to be overcome and a comprehensive design methodology developed that can be readily utilized for a wider range of column parameters.
- Normal weight steel fiber reinforced concrete was used in the experimental and numerical studies on CFHSS columns and beam slab assemblies. Consideration should be given to the use of light weight steel fiber reinforced concrete to maximize the benefits achieve through this higher weight system.
- At the present, it is assumed that a ribbed composite deck can be modeled structurally as a deck of uniform (average) thickness, this assumption and the influence of connections on structural behavior need to be given consideration.
- Slip between steel and concrete whether it be between the walls and the core of a CFHSS column, or between the concrete slab and deck of a floor system, is not taken into account in the current analyses due to the complexity of this interaction and the lack of data to accurately model it. This interaction should be given further attention in future research by modeling the components individually, joined at the interface through the use of frictional elements.
- Very limited information is available on the mechanical properties of SFRC at elevated temperatures. Studies should be undertaken to establish sound, statistically based,

constitutive models for SFRC over the full range of temperatures practically experienced under fire exposure.

- Currently, building information management (BIM) software is widely used in practice, and contains all of the information regarding a structures geometry. Software should be developed assess structural fire resistance utilizing the data in the BIM models.

8.4 Research Impact

The current prescriptive based fire design approach for steel framed structures is expensive, time consuming, and has a number of drawbacks. The methods do not take into account critical factors like composite construction, realistic loading, restraint, and fire exposure. Rather, fire resistance is achieved through the provision of external fire protection on structural steel members. Thickness of this protection is not based on sound engineering principals as they neglect the inherent fire resistance achieved though composite construction. Thus, modern steel structures do not utilize the inherent fire resistance within the structural system, thereby reducing their cost effectiveness and life safety.

Use of composite construction offers a practical alternative to the current prescriptive methods of achieving fire resistance. Through the use of composite construction in the form of steel fiber reinforced concrete in floor slab assemblies and concrete filled HSS columns, fire resistance can be achieved without the need for external fire protection. Composite systems exist in almost all steel framed structures and would require only minor engineering alterations to attain the required level of fire resistance in most cases. In addition to being a simple means of satisfying fire resistance requirements, altering existing structural components in the design process is a cost effective means of enhancing fire resistance both in terms of labor and material savings. Such a rational approach to fire safety design, through the elimination of external fire protection from secondary beams and columns, will make steel framed buildings more cost effective and contribute to reduced loss of life and property damage in fire incidents.

APPENDICES

APPENDIX A

E-mail Permission for Use of Copyrighted Cardington Figures

From: colin.bailey@manchester.ac.uk
Sent: Tuesday, December 14, 2010 2:16 AM
To: Rustin S. Fike
Subject: Re: Cardington Test Picture Permission

Yes of course
Colin

Sent from my BlackBerry® wireless device

From: "Rustin S. Fike" <Fikerust@msu.edu>
Date: Mon, 13 Dec 2010 21:04:59 -0500
To: <colin.bailey@manchester.ac.uk>
Subject: Cardington Test Picture Permission

Dr. Bailey,

I am currently completing my Ph.D. in structural fire engineering at Michigan State University under Dr. Venkatesh Kodur. I have a section in my thesis about the tests conducted at Cardington and would like to include some figures from the Cardington tests that are on your website. Pursuant to copyright policy, I need you permission to use these figures in my thesis, may I use the figures from your website in my thesis? If you would like I can indicate the exact pictures.

Thank you,
Kind regards,
Rustin

____
Michigan State University
Civil and Environmental Engineering
3558 Engineering Building
E. Lansing, MI 48824
PH: (517) 423-1529
Cell: (402) 418 2263

APPENDIX B

High Temperature Material Relationships

Table B.1: High temperature constitutive relationships for concrete

	ASCE Manual (1992)
Stress-strain relationships	$\sigma_c = \begin{cases} f'_{c,T}\left[1-\left(\dfrac{\varepsilon-\varepsilon_{\max,T}}{\varepsilon_{\max,T}}\right)^2\right], & \varepsilon \le \varepsilon_{\max,T} \\ f'_{c,T}\left[1-\left(\dfrac{\varepsilon_{\max,T}-\varepsilon}{3\varepsilon_{\max,T}}\right)^2\right], & \varepsilon > \varepsilon_{\max,T} \end{cases}$ $\varepsilon_{\max,T} = 0.0025+\left(6.0T+0.04T^2\right)\times 10^{-6}$ $f'_{c,T} = \begin{cases} f'_c & ,20\ {}^\circ C \le T \le 450\ {}^\circ C \\ f'_c\left[2.011-2.353\left(\dfrac{T-20}{1000}\right)\right] & ,450\ {}^\circ C < T \le 874\ {}^\circ C \\ 0 & ,\ 874\ {}^\circ C < T \end{cases}$
Thermal Capacity	Siliceous Aggregate Concrete $\rho c = \begin{cases} 0.005T+1.7 & 20\ {}^\circ C \le T \le 200\ {}^\circ C \\ 2.7 & 200\ {}^\circ C < T \le 400\ {}^\circ C \\ 0.013T-2.5 & 400\ {}^\circ C < T \le 500\ {}^\circ C \\ 10.5-0.013T & 500\ {}^\circ C < T \le 600\ {}^\circ C \\ 2.7 & 600\ {}^\circ C < T \end{cases}$ Carbonate Aggregate Concrete $\rho c = \begin{cases} 2.566 & 20\ {}^\circ C \le T \le 400\ {}^\circ C \\ 0.1765T-68.034 & 400\ {}^\circ C < T \le 410\ {}^\circ C \\ 25.00671-0.05043T & 410\ {}^\circ C < T \le 445\ {}^\circ C \\ 2.566 & 445\ {}^\circ C < T \le 500\ {}^\circ C \\ 0.01603T-5.44881 & 500\ {}^\circ C < T \le 635\ {}^\circ C \\ 0.16635T-100.90225 & 635\ {}^\circ C < T \le 715\ {}^\circ C \\ 176.07343-0.22103T & 715\ {}^\circ C < T \le 785\ {}^\circ C \\ 2.566 & 785\ {}^\circ C < T \end{cases}$

Table B.1 (Continued): High temperature constitutive relationships for concrete

	ASCE Manual (1992)
Thermal Conductivity	Siliceous Aggregate Concrete. $$k_c = \begin{cases} -0.000625T + 1.5 & 20\ °C \le T \le 800\ °C \\ 1.0 & 800°C < T \end{cases}$$ Carbonate Aggregate Concrete. $$k_c = \begin{cases} 1.355 & 20\ °C \le T \le 293\ °C \\ -0.001241T + 1.7162 & 293\ °C < T \end{cases}$$
Thermal Strain	All types : $$\varepsilon_{th} = \left[0.004\left(T^2 - 400\right) + 6\left(T - 20\right)\right] \times 10^{-6}$$

Table B.1 (Continued): High temperature constitutive relationships for concrete

	Eurocode (2004)
Stress-strain relationships	$$\sigma_c = \frac{3\ \varepsilon\ f'_{c,T}}{\varepsilon_{c1,T}\left(2 + \left(\frac{\varepsilon}{\varepsilon_{c1,T}}\right)^3\right)} \quad , \varepsilon \leq \varepsilon_{cu1,T}$$ For $\varepsilon_{c1(T)} < \varepsilon \leq \varepsilon_{cu1(T)}$, the Eurocode permits the use of linear as well as nonlinear descending branch in the numerical analysis. For the parameters in this equation refer to Table A2
Thermal Capacity	Specific heat (J/kg C) $c = 900$, for $20°C \leq T \leq 100°C$ $c = 900 + (T - 100)$, for $100°C < T \leq 200°C$ $c = 1000 + (T - 200)/2$, for $200°C < T \leq 400°C$ $c = 1100$, for $400°C < T \leq 1200°C$ Density change (kg/m^3) $\rho = \rho(20°C)$ = Reference density for $20°C \leq T \leq 115°C$ $\rho = \rho(20°C)\ (1 – 0.02(T - 115)/85)$ for $115°C < T \leq 200°C$ $\rho = \rho(20°C)\ (0.98 – 0.03(T - 200)/200)$ for $200°C < T \leq 400°C$ $\rho = \rho(20°C)\ (0.95 – 0.07(T - 400)/800)$ for $400°C < T \leq 1200°C$ Thermal Capacity = $\rho \times c$

Table B.1 (Continued): High temperature constitutive relationships for concrete

	Eurocode (2004)
Thermal Conductivity	All types : Upper limit: $k_c = 2 - 0.2451\ (T / 100) + 0.0107\ (T / 100)2$ *for* $20°C \le T \le 1200°C$ Lower limit: $k_c = 1.36 - 0.136\ (T / 100) + 0.0057\ (T / 100)2$ *for* $20°C \le T \le 1200°C$
Thermal Strain	Siliceous aggregates: $\varepsilon_{th} = -1.8\times10^{-4}+9\times10^{-6}T+2.3 \times 10^{-11}T^4$ *for* $20°C \le T \le 700°C$ $\varepsilon_{th} = 14 \times 10^{-3}$ *for* $700°C < T \le 1200°C$ Calcareous aggregates: $\varepsilon_{th} = -1.2\times10^{-4}+6\times10^{-6}T+1.4\times10^{-11}T^3$ *for* $20°C \le T \le 805°C$ $\varepsilon_{th} = 12 \times 10^{-3}$ *for* $805°C < T \le 1200°C$

Table B.1 (Continued): High temperature constitutive relationships for concrete

	Lie and Kodur (1995b)
Stress-strain relationships	$$f_c = f'_c\left[1-\left(\frac{\varepsilon_{\max}-\varepsilon_c}{\varepsilon_{\max}}\right)^2\right] \quad , \varepsilon_c \le \quad \varepsilon_{\max}$$ $$f_c = f'_c\left[1-\left(\frac{\varepsilon_c-\varepsilon_{\max}}{3\varepsilon_{\max}}\right)^2\right] \quad , \varepsilon_c > \quad \varepsilon_{\max}$$ $$where \quad \varepsilon_{\max} = 0.003 + (7.0T + 0.05T^2)x10^6$$

c : Concrete specific heat. (J/kg °C)

k_c : Concrete thermal conductivity (W/m. °C)

f'_c : 28 days concrete compressive strength at room temperature (MPa)

$f'_{c,T}$: Concrete compressive strength at temperature T. (MPa)

T : Concrete temperature. ($^\circ C$)

$\varepsilon \quad or \quad \varepsilon_c$: Concrete mechanical strain.

ε_{th} : Concrete thermal strain.

$\varepsilon_{\mathrm{cu1,T}}$: Concrete ultimate strain at temperature T. (Eurocode model)

$\varepsilon_{\mathrm{c1,T}}$: Concrete strain at maximum stress at temperature T (Eurocode model)

$\varepsilon_{\mathrm{max,T}}$: Concrete strain at maximum stress at temperature T (ASCE 1992 and Kodur et al. 2004 models)

ρ(T): Density of concrete at temperature T. (kg/m^3)

ρ(20°C): Density of concrete at room temperature. (kg/m^3)

σ_{c} : Stress in concrete. (MPa)

Table B.2. Values for the main parameters of the stress-strain relationships for concrete at elevated temperatures (Eurocode 2004)

Temp. (°C)	Siliceous Agg.			Calcareous Agg.		
	$\frac{f'_{c,T}}{f'_c(20^\circ C)}$	$\varepsilon_{c1,T}$	$\varepsilon_{cu1,T}$	$\frac{f'_{c,T}}{f'_c(20^\circ C)}$	$\varepsilon_{c1,T}$	$\varepsilon_{cu1,T}$
20	1	0.0025	0.02	1	0.0025	0.02
100	1	0.004	0.0225	1	0.004	0.023
200	0.95	0.0055	0.025	0.97	0.0055	0.025
300	0.85	0.007	0.0275	0.91	0.007	0.028
400	0.75	0.01	0.03	0.85	0.01	0.03
500	0.6	0.015	0.0325	0.74	0.015	0.033
600	0.45	0.025	0.035	0.6	0.025	0.035
700	0.3	0.025	0.0375	0.43	0.025	0.038
800	0.15	0.025	0.04	0.27	0.025	0.04
900	0.08	0.025	0.0425	0.15	0.025	0.043
1000	0.04	0.025	0.045	0.06	0.025	0.045
1100	0.01	0.025	0.0475	0.02	0.025	0.048
1200	0	-	-	0	-	-

Table B.3. Strength reduction factors for SFRC as a function of temperature

Temp. (°C)	SFRC (SFPE 2002)	
	$\frac{f'_{c,T}}{f'_c(20^\circ C)}$	$\frac{f'_{t,T}}{f'_t(20^\circ C)}$
20	1	1.38
100	1.06	1.31
200	1.1	1.27
300	1.1	1.24
400	1.1	0.91
500	0.88	0.59
600	0.64	0.43
700	0.17	0.33
800	0	0.3
900	-	0.2

Table B.4: High temperature constitutive relationships of structural steel

	ASCE manual(1992)
Thermal Conductivity (W/m.°K)	For $T \le 900°C$ $k_S = -0.022T + 48$ For $T > 900°C$ $k_S = 28.2$
Specific Heat (J/kg.°K)	For $T \le 650°C$ $C_S = \dfrac{(0.004 \times T + 3.3) \times 10^6}{\rho_S}$ For $650°C < T \le 725°C$ $C_S = \dfrac{(0.068 \times T + 38.3) \times 10^6}{\rho_S}$ For $725°C < T \le 800°C$ $C_S = \dfrac{(-0.086 \times T + 73.35) \times 10^6}{\rho_S}$ For $T > 800°C$ $C_S = \dfrac{4.55 \times 10^6}{\rho_S}$ ρ_S is the density of steel.
Thermal strain(per °C.)	For $T < 1000°C$ $\dfrac{\Delta\ell}{\ell} = (0.004T + 12) \times 10^{-6}$ For $T \ge 1000°C$ $\dfrac{\Delta\ell}{\ell} = 16 \times 10^{-6}$

Table B.4 (Continued): High temperature constitutive relationships of structural steel

	ASCE manual(1992)
Temperature-stress-strain Relationship	$$\sigma_s = \begin{cases} \varepsilon \le \varepsilon_p & E_{s,T} \times \varepsilon \\ \varepsilon > \varepsilon_p & (c_1\varepsilon + c_2)F_{y,T} - \dfrac{c_3 \times F_{y,T}^2}{E_{s,T}} \end{cases}$$ Where $\varepsilon_p = \dfrac{c_2 F_{y,T} - c_3 F_{y,T}^2}{E_{s,T} - c_1 F_{y,T}}$
Elastic Modulus	$$\frac{E_{s,t}}{E_s} = \begin{cases} 1.0 + \dfrac{T}{C_9 \ln\left(\dfrac{T}{c_{10}}\right)}, & T \le 600°C \\ \dfrac{C_{11}\text{-}C_{12}T}{T - c_{13}}, & T>600°C \end{cases}$$
Yield Strength	$$\frac{F_{y,T}}{F_y} = \begin{cases} 1.0 + \dfrac{T}{c_4 \ln\left(\dfrac{T}{c_5}\right)}, & T \le 600°C \\ \dfrac{c_6 - c_7 T}{T - c_8}, & 600°C < T \end{cases}$$
Coefficients used in the equations	c_1 = 12.5; c_2 = 0.975; c_3 = 12.5; c_4 =900; c_5 = 1,750; c_6 = 340; c_7 = 0.34; c_8 = 240; c_9 = 2,000; c_{10} = 1,100; c_{11} = 690; c_{12} = 0.69; and c_{13} = 53.5.

Table B.4 (Continued): High temperature constitutive relationships of structural steel

	Eurocode 3 (2005)
Thermal Conductivity (W/m.°K)	For $T < 800°C$ $k_s = 54 - 3.33x10^{-2}T$ For $T \geq 800°C$ $k_s = 27.3$
Specific Heat (J/kg.°K)	For $T < 600°C$: $c_s = 425 + 7.73\times10^{-1}T - 1.69\times10^{-3}T^2 + 2.22\times10^{-6}T^3$ For $600°C \leq T < 735°C$ $c_s = 666 + \dfrac{13002}{738 - T}$ For $735°C \leq T < 900°C$ $c_s = 545 + \dfrac{17820}{T - 731}$ For $900°C \leq T \leq 1200°C$ $c_s = 650$
Thermal strain (per °C.)	For $T < 750°C$ $\dfrac{\Delta\ell}{\ell} = 1.2\times10^{-5}T + 0.4\times10^{-8}T^2 - 2.416\times10^{-4}$ For $750°C \leq T \leq 860°C$ $\dfrac{\Delta\ell}{\ell} = 1.1\times10^{-2}$ For $860°C < T \leq 1200°C$ $\dfrac{\Delta\ell}{\ell} = 2\times10^{-5}T - 6.2\times10^{-3}$

Table B.4 (Continued): High temperature constitutive relationships of structural steel

	Eurocode 3 (2005)
Temperature-stress-strain Relationship	$\sigma_s = \begin{cases} \varepsilon \le \dfrac{F_{p,T}}{E_{s,T}} \\ \quad E_{s,T} \times \varepsilon \\ \dfrac{F_{p,T}}{E_{s,T}} < \varepsilon < c_1 \\ \quad F_{p,T} - c + \dfrac{b}{a}\sqrt{a^2 - (c_1 - \varepsilon)^2} \\ c_1 < \varepsilon < c_3 \text{ and } T < 400°C \\ \quad \dfrac{(F_{u,T} - F_{y,T})\varepsilon + c_3 F_{y,T} - c_1}{(c_3 - c_1)} \\ c_3 < \varepsilon \le c_4 \text{ and } T < 400°C \\ \quad F_{u,T} \\ c_4 < \varepsilon < c_5 \text{ and } T < 400°C \\ \quad F_{u,T} \times \dfrac{(c_5 - \varepsilon)}{(c_5 - c_4)} \\ c_2 < \varepsilon \le c_4 \text{ and } T \ge 400°C \\ \quad F_{y,T} \\ c_4 < \varepsilon < c_5 \text{ and } T \ge 400°C \\ \quad F_{y,T} \times \left[1 - \dfrac{(\varepsilon - c_2)}{(c_3 - c_2)}\right] \\ \varepsilon \ge c_5 \\ \quad 0.0 \end{cases}$ Where $a^2 = (c_1 - F_{p,T}/E_{s,T})(c_1 - F_{p,T}/E_{s,T} + c/E_{s,T})$ $b^2 = c(c_1 - F_{p,T}/E_{s,T})E_{s,T} + c^2$ $c = \dfrac{(F_{y,T} - F_{p,T})^2}{(c_1 - F_{p,T}/E_{s,T})E_{s,T} - 2(F_{y,T} - F_{p,T})}$

Table B.4 (Continued): High temperature constitutive relationships of structural steel

	Eurocode 3 (2005)
Elastic Modulus	$$\frac{E_{s,T}}{E_s} = \begin{cases} 1.0, & T < 100°\text{C} \\ c_6 T + c_7, & 100°\text{C} \le T < 500°\text{C} \\ c_8 T + c_9, & 500°\text{C} \le T < 600°\text{C} \\ c_{10} T + c_{11}, & 600°\text{C} \le T < 700°\text{C} \\ c_{12} T + c_{13}, & 700°\text{C} \le T < 800°\text{C} \\ c_{14} T + c_{15}, & 800°\text{C} \le T < 1200°\text{C} \\ 0.0, & 1200°\text{C} \le T \end{cases}$$
Yield Strength	$$\frac{F_{p,T}}{F_y} = \begin{cases} 1.0, & T < 100^\circ C \\ c_{16} T + c_{17}, & 100^\circ C \le T < 400^\circ C \\ c_{18} T + c_{19}, & 400^\circ C \le T < 500^\circ C \\ c_{20} T + c_{21}, & 500^\circ C \le T < 600^\circ C \\ c_{22} T + c_{23}, & 600^\circ C \le T < 700^\circ C \\ c_{24} T + c_{25}, & 700^\circ C \le T < 800^\circ C \\ c_{26} T + c_{27}, & 800^\circ C \le T < 1200^\circ C \\ 0.0, & 1200^\circ C \le T \end{cases}$$ $$\frac{F_{y,T}}{F_y} = \begin{cases} 1.0, & T < 400°C \\ c_{28} T + c_{29}, & 400°\text{C} \le T < 500°\text{C} \\ c_{30} T + c_{31}, & 500°\text{C} \le T < 600°\text{C} \\ c_{32} T + c_{33}, & 600°\text{C} \le T < 700°\text{C} \\ c_{34} T + c_{35}, & 700°\text{C} \le T < 800°\text{C} \\ c_{36} T + c_{37}, & 800°\text{C} \le T < 900°\text{C} \\ c_{38} T + c_{39}, & 900°\text{C} \le T < 1200°\text{C} \\ 0.0, & 1200°\text{C} \le T \end{cases}$$ $$\frac{F_{u,T}}{F_y} = \begin{cases} c_{40}, & T < 300^\circ C \\ c_{41} T + c_{42}, & 300^\circ C \le T < 400^\circ C \\ 1.0, & 400^\circ C \le T \end{cases}$$

Table B.4 (Continued): High temperature constitutive relationships of structural steel

	Eurocode 3 (2005)
Coefficients used in the equations	$c_1 = 0.02$; $c_2 = 0.02$; $c_3 = 0.04$; $c_4 = 0.15$; $c_5 = 0.20$; $c_6 = -1\times10^{-3}$; $c_7 = 1.1$; $c_8 = -2.9\times10^{-3}$; $c_9 = 2.05$; $c_{10} = -1.8\times10^{-3}$; $c_{11} = 1.39$; $c_{12} = -4\times10^{-4}$; $c_{13} = 0.41$; $c_{14} = -2.25\times10^{-4}$; $c_{15} = 0.27$; $c_{16} = -1.933\times10^{-3}$; $c_{17} = 1.193$; $c_{18} = -0.6\times10^{-3}$; $c_{19} = 0.66$; $c_{20} = -1.8\times10^{-3}$; $c_{21} = 1.26$; $c_{22} = -1.05\times10^{-3}$; $c_{23} = 0.81$; $c_{24} = -2.5\times10^{-4}$; $c_{25} = 0.25$; $c_{26} = -1.25\times10^{-4}$; $c_{27} = 0.15$; $c_{28} = -2.2\times10^{-3}$; $c_{29} = 1.88$; $c_{30} = -3.1\times10^{-3}$; $c_{31} = 2.33$; $c_{32} = -2.4\times10^{-3}$; $c_{33} = 1.91$; $c_{34} = -1.2\times10^{-3}$; $c_{35} = 1.07$; $c_{36} = -5\times10^{-4}$; $c_{37} = 0.51$; $c_{38} = -2\times10^{-4}$; $c_{39} = 0.24$; $c_{40} = 1.25$; $c_{41} = -2.5\times10^{-3}$; and $c_{42} = 2$.

APPENDIX C

SAFIR Thermal Input File

% Anything above the space is considered notes

NPTTOT 1764 *%Number of points of integration*
NNODE 441 *%Number of Nodes*
NDIM 2 *%Number of global axis (2 thermal 2,3 structural)*
NDIMMATER 1 *%dimension of material law (1 thermal)*
NDDLMAX 1 *%nodal Dofs (1 thermal)*
EVERY_NODE 1 *%assignment of DOFs*
END_NDDL *%end current assignments*
TEMPERAT *%Start thermal analysis at t = 0*
TETA 0.9 *%time integration parameter (0 to 1)*
TINITIAL 20.0 *%initial temperature*
MAKE.TEM *%command to make .tem file*
LARGEUR11 40000 *%thermal stiffness matrix parameter (SAFIR will inform if too %small*
LARGEUR12 150 *%thermal stiffness matrix parameter (must be higher than restrained dofs)*
NORENUM *%do not allow equation renumbering*
ASTM150.tem *%Name of .tem file*
NMAT 3 *%number of materials used in the cross section*
ELEMENTS *%start the elements information*
SOLID 400 *%number of solid elements*
NG 2 *%number if integration points in each direction (2 %recommended)*
NVOID 0 *%number of internal voids*
END_ELEM *% End elements assignment*
NODES *%start node assignments two choices nodes - square %coordinates node number then coordinates (y,x), or nodes_cyd to use polar coordinates %node number then coordinates (r,theta)*
%nodes example:
NODE 1 0 0
%node_cyl example:
NODE 1 0.010015789 90
%these commands establish one node at a time, you can also repeat nodes using the following
REPEAT 12 0.01 0.00 5
%this will repeat the last 12 nodes (first number) incrementing nodes by 0.01 in the y %direction and (second number) and by 0.00 in the x direction (third number) and will do %it 5 times (fourth number)
....
NODELINE 0.203 0.0 *%location of neutral axis (y,x)*
YC_ZC 0.203 0.0 *%location of center of torsion (y,x)*
FIXATIONS *%start support sub group*
END_FIX *%end support sub group*
NODOFSOLID *%start element assignments*

ELEM 1 1 2 23 22 2 0 *%specify each element by the %coordinates it connects this line creates the element 1 connecting nodes 1,2,23,22 %numbering in ccw direction, followed by material assignment then residual stress.*
%can also use the repeat command:
REPEAT 12 13 5
%this will repeat the last 12 elements, increasing the node number by 13, and will do %this for 5 time
....
FRONTIER %starts specification of the exposed sides
F 20 NO ASTME119 NO NO %element to have the fire *%exposure specified using node number then either "no" of the fire name which can be inbuilt or "name.fct"*
GF 400 NO ASTME119 NO NO 20 *%this will increment the exposed %nodes from 20 to 400 in increments of 20 for the same fire exposure*
END_FRONT *%end frontier assignment*
SYMMETRY *%start symmetry*
REALSYM 421 441 *%define the first axis of symmetry*
REALSYM 1 421 *%define second axis of symmetry*
END_SYM *%end symmetry subgroup*
PRECISION 1.E-3 *%specify numerical precision (0.001 is good)*
MATERIALS *%start material subsection*
CALCONCEC2 *%material name (inbuilt)*
46 25 9 .56 *%material properties for concrete (water content, hot %surface convection coeff cold surface convection coeff, relative emissivity)*
STEELEC3 *%material name*
25 9 .5 *%material properties for steel (hot surface %convection coeff cold surface convection coeff, relative emissivity)*
TIME *%start time subgroup*
60 14400 *%time step and max time*
END_TIME *%end time subgroup*
IMPRESSION *%start output loop*
TIMEPRINT *%increments at which to print output*
60 14400 *%time step of printing and final time*
END_TIMEPR *%end time print group*

APPENDIX D

SAFIR Structural Input File

% Anything above the space is considered notes

NPTTOT 1764 *%Number of points of integration*
NNODE 441 *%Number of Nodes*
NDIM 2 *%Number of global axis (2 thermal 2,3 structural)*
NDIMMATER 1 *%dimension of material law (1 thermal)*
NDDLMAX 1 *%nodal Dofs (1 thermal)*
FROM 1 TO 41 STEP 1 NDDL 3 *%assignment of Dofs*
END_NDDL *%end current assignments*
STATIC PURE_NR *%specifies convergence criterion*
NLOAD 1 *%number of load vectors*
OBLIQUE 0 *%number of oblique supports*
COMEBACK 1 *%allow calculation back step*
LARGEUR11 40000 *%thermal stiffness matrix parameter (SAFIR will inform if too %small*
LARGEUR12 150 *%thermal stiffness matrix parameter (must be higher than restrained dofs)*
NORENUM *%do not allow equation renumbering*
NMAT 3 *%number of materials used in the cross section*
ELEMENTS *%start the elements information*
BEAM 20 2 *%type of element (truss, shell, beam), number of those %elements present and the number of thermal cross sections in the 20 elements*
NG 2 *%number if integration points in each direction (2 %recommended)*
NFIBER 1600 *%Number of longitudinal fibers (elements for the thermal %analysis)*
END_ELEM *%end the elements subsection*
NODES *%start node assignments, coordinates (x,y)*
NODE 1 0.00 0.20 *%Node example*
%these commands establish one node at a time, you can also repeat nodes using the following
GNODE 41 0.00000 6.00000 1 *%this will generate nodes from the previous %number to 41, the 41st node has coordinates 0,6 (x,y) and the step in node number will %be one*
....
FIXATIONS *%start support sub group*
BLOCK 1 F0 F0 F0 *%block restrict movement in the dofs when F0 %(f zero) is put in that spot, other supports can also be specified)*
END_FIX *%end support sub group*
NODOFBEAM %start importing thermal data
ASTM150.TEM *%name of thermal file to import (must be done for as many %sections as specified above)*
TRANSLATE 1 1 *%specify that thermal material correspond to structural in reference to the following order*
………………………
END_TRANS *%end translation of materials*

ELEM 1 1 2 3 2 *%element subgroup is started, defines element one %to connect nodes 1,2,3 with the cross section 2 just defied. Note beam elements have %three nodes, the center must have one dof while the ends at least 3*

…………………………………..

PRECISION 1.E-3 *%specify numerical precision (0.001 is good)*

LOADS

FUNCTION FLOAD *%specifies loading function FLOAD is a default*

NODELOAD 41 0 -4870000 0 *%Applies a node load at node 41 in %the directions stipulates (x,y,x)*

END_LOAD *%ends the load subgroup*

MATERIALS *%start material subsection*

CALCONCEC2 *%material name (inbuilt)*

0.25 48.1E6 0 0 *%material properties for concrete (Poisson's ratio, %compressive strength, tensile strength, place holder (0)*

STEELEC3 *%material name*

210.E9 0.3 350.0E6 *%material properties for steel (elastic modulus, Poisson's %ratio, material strength*

TIME *%start time subgroup*

60 14400 *%time step and max time*

END_TIME *%end time subgroup*

LARGEDISPL *%allow large displacements*

EPSTH *%Print stress information*

IMPRESSION *%start output loop*

TIMEPRINT *%increments at which to print output*

60 14400 *%time step of printing and final time*

END_TIMEPR *%end time print group*

PRINTMN *%print internal forces for beam elements*

PRINTREACT *%print reactions*

APPENDIX E

CFHSS Column Design Example

A CFHSS column located in a room 3 m high with a 6 m by 4 m floor that has a fuel load of 550 MJ/m^2 (of floor area) is to be designed. The room has one window opening 3 m wide by 2 m high. In this compartment, the architect has proposed a 273 mm diameter circular HSS column filled with plain concrete made with siliceous aggregate. The height of the column needs to be 3.81 m (to accommodate the drop ceiling and utilities) with fixed connections on both ends. The building code requires the column to have a 2-hour fire resistance rating. Now it is desired to know if this column will satisfy the code requirements by withstanding complete burnout of the fire that would occur within the compartment.

Room properties

Room dimensions: 6 m wide by 4 m deep by 3 m high

Ventilation: one window, 3 m wide by 2 m high

Fire load: 550 MJ/m^2

Lining material: concrete with the following properties

Thermal conductivity: k = 1.6 W/mK

Density: ρ = 2300 kg/m^3

Specific heat c_p = 980 J/kg K

Column properties:

Length: 3.81 m

Effective length factor: 0.65

Concrete compressive strength: 27.4 MPa

Diameter: 273.1 mm

Load: 750 kN

F = 0.07 (siliceous aggregate) 0.08 (carbonate aggregate)

Calculation of design fire as per Eurocode

Thermal inertia of concrete:

$$b = \sqrt{kpc_p} = \sqrt{1.6 * 2300 - 980} = 1900\ Ws^{0.5} / m^2 K$$

Floor area:

$$A_f = 6 * 4 = 24\, m^2$$

Area of internal surface:

$$A_t = 6*4*2 + 3*6*2 + 3*4*2 = 108\, m^2$$

Ventilation factor:

$$F_v = A_v \sqrt{H_v} / A_t = (3*2)\sqrt{2} / 108 = 0.079\, m^{0.5}$$

Fuel load energy density:

$$e_f = 550\,MJ/m^2$$

Total fuel load:

$$E = e_f A_f = 550 * 24 = 13,200\,MJ$$

Duration of fire:

$$t_d = 0.00013E/(A_v\sqrt{H_v}) = 0.00013*13200/(6*\sqrt{2}) = 0.202\,hours$$

Imaginary time used in Eurocode time-temperature relationship:

$$t* = t_d(F_v/0.04)^2/(b/1900)^2 = 0.202(0.079/0.04)^2/(1900/1900)^2 = 0.789\,hours$$

Time temperature relationship:

$$T = 1325(1-0324e^{-0.2t}*-0.204e^{-1.7t*}-0.472e^{-19t*})$$

Fire decay rate

Interpolate between a decay rate of 625 °C/hr for fire lasting ½ hour or less and 250 °C for fires lasting more than 2 hours = 553 °C/hr after 0.789 hours of combustion, see Fig. 6.4 for graphical representation of time temperature relationship for the design and standard fire

Calculation of ASTM fire resistance based on Eq. 1

1st Iteration:

The fire resistance (R) of a CFHSS column under standard fire exposure can be computed using Eq. [2.1]

$$R = f\frac{(f'_c+20)}{(KL-1000)}D^2\sqrt{\frac{D}{C}} = 0.07\frac{(27.4+20)}{(3810*.65-1000)}(273.1)^2\sqrt{\frac{273.1}{750}} = 101\,\text{min}$$

Area under ASTM E-119 time-temperature curve at 101 min: 1462 min°C
Area under the design fire time-temperature curve at 101 min: 1503 min°C

Since the area under the standard fire curve is less than that under the design fire the column will fail in the design fire. An alternative must be selected since this does not satisfy the 2 hour fire rating required for the column.

2nd Iteration:

By changing the aggregate type used in the concrete from siliceous to carbonate, the fire resistance of the column can be enhanced.

$$R = f\frac{(f'_c+20)}{(KL-1000)}D^2\sqrt{\frac{D}{C}} = 0.08\frac{(27.4+20)}{(3810*.65-1000)}(273.1)^2\sqrt{\frac{273.1}{750}} = 116\,\text{min}$$

Area under ASTM E-119 time-temperature curve at 116 min: 1701 min°C
Area under the design fire time-temperature curve at 116 min: 1626 min°C

Since the area under the standard fire curve is greater than that under the design fire the column will not fail in the design fire, thus the CFHSS column can be used in this application.

A detailed finite element analysis was carried out on this CFHSS column using the computer program SAFIR. Results from the analysis indicate that the column does not fail under the design fire but rather survives compartment burnout when carbonate aggregate are used. This is in agreement with the predictions from the proposed equivalent area approach that requires significantly less time and effort.

APPENDIX F

SFRC Floor Design Example

A room 3 m high with a 6 m by 4 m floor (with secondary beams spanning in the 6 m direction) and a fire load of 5.25 kN/m^2 is to be designed. The room has one window opening 3 m wide by 2 m high. The architect has indicated that the room below the considered compartment has the same dimensions and will have a fuel load of 550 MJ/m^2 (of floor area). Now, it is desired to know what thickness the floor needs to be to satisfy the code requirements by withstanding complete burnout of the probabilistic fire that would occur within the compartment.

Room properties

Room dimensions: 6 m wide by 4 m deep by 3 m high
Ventilation: one window, 3 m wide by 2 m high
Fire load: 550 MJ/m^2
Lining material: concrete with the following properties

Thermal conductivity: k = 1.6 W/mK
Density: ρ = 2300 kg/m^3
Specific heat c_p = 980 J/kg K

Calculation of design fire as per Eurocode

Thermal inertia of concrete:

$$b = \sqrt{kpc_p} = \sqrt{1.6*2300-980} = 1900\ Ws^{0.5}/m^2K$$

Floor area:

$$A_f = 6*4 = 24\,m^2$$

Area of internal surface:

$$A_t = 6*4*2 + 3*6*2 + 3*4*2 = 108\,m^2$$

Ventilation factor:

$$F_v = A_v\sqrt{H_v}\,/\,A_t = (3*2)\sqrt{2}\,/\,108 = 0.079\,m^{0.5}$$

Fuel load energy density:

$$e_f = 550\,MJ/m^2$$

Total fuel load:

$$E = e_f A_f = 550*24 = 13{,}200\,MJ$$

Duration of fire:

$$t_d = 0.00013E/(A_v\sqrt{H_v}) = 0.00013*13200/(6*\sqrt{2}) = 0.202\,hours$$

Imaginary time used in Eurocode time-temperature relationship:

$$t^* = t_d(F_v/0.04)^2/(b/1900)^2 = 0.202(0.079/0.04)^2/(1900/1900)^2 = 0.789\,hours$$

Time temperature relationship:

$$T = 1325(1-0324e^{-0.2t}*-0.204e^{-1.7t^*}-0.472e^{-19t^*})$$

Fire decay rate

Interpolate between a decay rate of 625 °C/hr for fire lasting ½ hour or less and 250 °C for fires lasting more than 2 hours = 553 °C/hr after 0.789 hours of combustion, see Fig. 6.12 for graphical representation of time temperature relationship for the design and standard fire

Determination of ASTM fire resistance

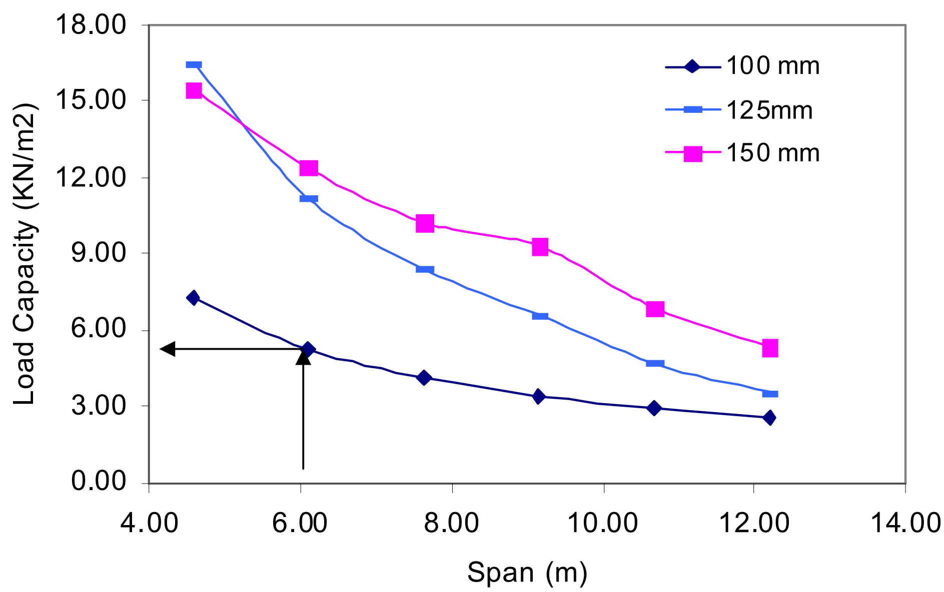

Fig. F.1: Load capacity of strip floor to achieve two hour fire resistance rating under ASTM E-119 fire exposure

1st Iteration:

Using Fig. E.1, the length of the span is found on the X-axis and a vertical line is drawn until the line for the desired slab thickness is intersected, in the case illustrated above when the slab thickness is 100 mm, the load capacity of the slab is found to be 5.5 kN/m^2

Based on a maximum design fire temperature of 1089 °C, the design fire burnout load is:

$$Design \quad Load \quad Capacity = \frac{ASTM \quad Load \quad Capacity}{\alpha \dfrac{t}{100}} = \frac{5.5KN/m^2}{\dfrac{1089°C}{1006°C}\dfrac{100mm}{100mm}} = 5.08KN/m^2$$

Given that the previous iteration yielded a load capacity less than the applied load capacity it is necessary to reiterate the process with a thicker floor slab assembly

2nd Iteration:
By entering Fig. E.2 (reproduced below to avoid confusion with multiple iterations) the load capacity of the 112.5 mm thick floor system is fond to be 8.5 kN/m^2

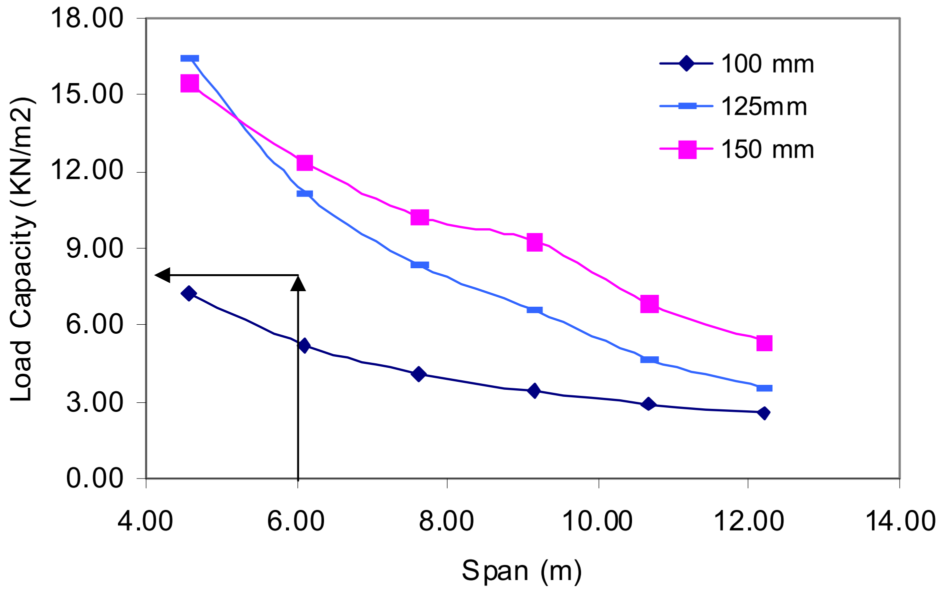

Fig. F.2: Load capacity of strip floor to achieve two hour fire resistance rating under ASTM E-119 fire exposure

Based on this load capacity, the burnout load capacity of the slab is found as follows

$$Design \quad Load \quad Capacity = \frac{ASTM \quad Load \quad Capacity}{\alpha \dfrac{t}{100}} = \frac{8.5KN/m^2}{\dfrac{1089°C}{1006°C}\dfrac{112.5mm}{100mm}} = 6.98KN/m^2$$

Since the burnout load capacity of the floor (6.98 kN/m^2) is greater than the applied load of 5.25 kN/m^2 the floor is sufficient to withstand compartment burnout and there is no need for applied external fire protection on the secondary beams,

REFERENCES

REFERENCES

1. Alfwakhiri, F., VKR Kodur, and G. Frater. *Temperature Field Modeling of the First Cardington Test*. Proc. of 3rd International Workshop - Structures in Fire, Ottawa. 2004. 1-11.

2. Anderberg, Y. "Modeling Steel Behavior." *Fire Safety Journal* 13 (1988): 17-26.

3. ASCE. "Minimum Design Loads for Buildings and Other Structures." *American Society of Civil Engineers* (2005).

4. ASCE/SFPE. *Standard Calculation Method for Structural Fire Protection*. Reston, VA: American Society of Civil Engineers, 1999. Ser. 29.

5. ASTM. *Standard Methods of Fire Test of Building Construction and Materials.* West Conshohocken, PA: American Society for Testing and Materials, 2001. Test Method E1 529-93

6. ASTM. *Standard Methods of Fire Test of Building Construction and Materials.* West Conshohocken, PA: American Society for Testing and Materials, 2007. Test Method E119-00

7. Bailey, C.G., and D.B. Moore. "The Structural Behavior of Steel Frames With Composite Floor Slabs Subject to Fire, Part 1: Theory." *The Structural Engineer* 78.11 (2000a): 19-27.

8. Bailey, C.G., and D.B. Moore. "The Structural Behavior of Steel Frames With Composite Floor Slabs Subject to Fire, Part 2: Design." *The Structural Engineer* 78.11 (2000b): 28-33.

9. Bailey, C.G., D.S. White, and B.D. Moore. "The Tensile Membrane Action Of Unrestrained Composite Slabs Simulated Under Fire Conditions." *Engineering Structures* 22 (2000): 1583-595.

10. Bentz, Dale P., and Kuldeep R. Prasad. *Thermal Performance of Fire Resistive Materials I. Characterization With Respect to Thermal Performance Models*. Rep. no. BFRL. Gaithersburg, MD, 2007. NTIS No. 7401.

11. Bond, G.V.L. *Fire and Steel Construction, Water Cooled Hollow Colums*. Constrado, Croydon, 1975.

12. British Steel. *The Behavior of a Multi-Storey Steel Framed Building Subject to Fire Attack*. Rotherdam, UK: British Steel Swinden Technology Center, 1998.

13. Buchanan, Andrew Hamilton. *Structural Design For Fire Safety*. New York: John Wiley and Sons Limited, 2005.

14. Cameron, N. *The Behaviour and Design of Composite Floor Systems in Fire*. Thesis. Edinburgh University. Edinburgh, Scotland, 2003.

15. Cashell, K.A., A. Y. Elghazouli, and B.A. Izzuddin. "Ultimate Behavior of Composite Floor Slabs at Ambient and Elevated Temperatures." Proc. of 5th International Conference on Structures in Fire, Singapore. 2008.

16. Chabot, M., and T.T. Lie. *Experimental Studies on the Fire Resistance of Hollow Steel Colums Filled With Bar-Reinforced Concrete*. Rep. no. 628. National Research Council of Canada, 1992.

17. Chen, J., B. Young, and B. Uy. "Behavior of High Strength Structural Steel at Elevated Temperatures." *ASCE Journal of Structural Engineering* (2006): 132-42.

18. Clark, C.L. *High Temperature Alloys*. Pitman, NY, 1953.

19. Cooke, G.M.E. "An Introduction to the Mechanical Properties of Structural Steel at Elevated Temperatures." *Fire Safety Journal* 13.1 (1988): 45-54.

20. Cooke, G.M.E., and D.J. Latham. "The Inherent Fire Resistance of a Loaded Steel Framework." *Steel Construction Today* 1 (1987): 49-58.

21. Dever, D.J. "Temperature Dependence of the Elastic Constrants in A-Iron Single Crystals: Relationships to Spin Order and Diffusion Anomalies." *Journal of Applied Physics* 43.8 (1972): 3293-301.

22. Duthinh, D. "2D Analysis of a Buidling Frame Under Gravity Load and Fire." Proc. of Computational and Experimental Engineering Sciences International Conference, Maderia, Portugal. 2004.

23. Elghazouli, A.Y., and B.A. Izzuddin. "Analytical Assessment of the Structural Performance of Composite Floor Subject to Compartment Fires." *Fire Safety Journal* 36 (2001): 769-93.

24. Elghazouli, A.Y., and B.A. Izzuddin. "Response of Idealized Composite Beam Slab Systems Under Fire Conditions." *Journal of Constructional Steel Research* 56 (2000): 199-224.

25. Eurocode 1. "General Actions – Actions on Structures Exposed to Fire." *European Committee for Standardization* ENV 1991 (2002): 1-2.

26. Eurocode 2. "Design of Concrete Structures - General Rules: Structural Fire Design." *European Committee for Standardization* ENV 1993 (2004): 1-2.

27. Eurocode 3. "Design of Steel Structures - General Rules: Structural Fire Design." *European Committee for Standardization* ENV 1993 (2005a): 1-2.

28. Eurocode 4. "Design of Composite Steel and Concrete Structure." *European Committee for Standardization* ENV 1994 (2005b): 1-2.

29. FEMA. "A Overview of Fire Protection in Buildings." (2003). Washington D.C.

30. FEMA. "High-Rise Office Building Fire One Meridian Plaza Philadelphia, Pennsylvania." (1994). Washington D.C.

31. FEMA. "Interstate Bank Building Fire Los Angeles California May 4th 1988." (1990). Washington D.C.

32. FEMA. "World Trade Center Building Performance Study: Data Collection, Preliminary Observations, and Recommendations." (2002). Washington D.C.

33. Fike, R.S., and VKR Kodur. "An Approach for Evaluating the Fire Resistance of CFHSS Columns Under Design Fire Scenarios." *Journal of Fire Protection Engineering* 19 (2009a): 229-60.

34. Fike, R.S., and V.K.R. Kodur. "Enhancing the Fire Resistance of Steel Framed Structures Through Beam-Slab Interactions." Proc. of 2009 Annual Stability Conference, Phoenix, AZ. 2009b.

35. Flint, G., A.S. Usmani, S. Lamont, B. Lane, and J. Torero. "Structural Response of Tall Buildings to Multiple Floor Fires." *ASCE Journal of Structural Engineering* 133.12 (2007): 1719-732.

36. Flint, G., A.S. Usmani, S. Lamont, J. Torero, and B. Lane. "Effect of Fire on Composite Long Span Truss Floor Systems." *Journal of Constructional Steel Research* 62 (2006): 303-15.

37. Franssen, J.M. "SAFIR: A Thermal/Structural Program for Modeling Structures Under Fire." *Engineering Journal* 42.3 (2005): 143-55.

38. Franssen, J.M., V.K.R. Kodur, and J. Mason. *User Manual for SAFIR 1998: A Computer Program for Analysis of Structures Submitted to Fire.* Belgium: University of Leige, 2000.

39. Genes, D.C. "Predicted Fire Endurance of Steel Structures." Proc. of American Society of Civil Engineering Conference, Las Vegas and New York. 1982. ASCE

40. Gillie, M., A.S. Usmani, and J.M. Rotter. "A Structural Analysis of The Cardington British Steel Corner Test." *Journal of Constructional Steel Research* 58 (2002): 427-42.

41. Gillie, M., A.S. Usmani, and J.M. Rotter. "A Structural Analysis Of The First Cardington Test." *Journal of Constructional Steel Research* 57 (2001a): 581-601.

42. Gillie, M., A.S. Usmani, J.M. Rotter, and M. O'Connor. "Modeling of Heated Composite Floor Slabs With Reference to The Cardington Experiments." *Fire Safety Journal* 36 (2001b): 745-67.

43. Gilvary, K., and R. Dexter. *Evaluation of Alternative Methods for Fire Rating Structural Elements*. Gaithsburg, MD: NST Building and Fire Research Laboratory, 1997.

44. Grandjean, G., J.P. Grimault, and L. Petit. *Determination De La Durée Au Feu Des Profils Creux Remplis De Béton*. Rep. no. Final. Luxembourg: Commission Des Communautés Européennes, 1981. Recherche Technique Acier

45. Harmathy, T., and W. Stanzak. *Elevated-Temperature Tensile and Creep Properties of Some Structural and Prestressing Steels*. Publication. Special ed. American Society for Testing and Material, 1970. Pgs. 186-208

46. Hayes, B. *A Study of the Design of Reinforced Concrete Slabs*. Thesis. University of Manchester. Manchester, England, 1968.

47. Huang, Z.H., and K.H. Tan. "Analytical Fire Resistance of Axially Restrained Steel Columns." *ASCE Journal of Structural Engineering* 129.11 (2003): 1531-537.

48. Huang, Z.H., I.W. Burgess, and R.J. Plank. "Modeling Membrane Action of Concrete Slabs in Composite Buildings in Fire, I: Theoretical Development." *ASCE Journal of Structural Engineering* 129.8 (2003a): 1093-102.

49. Huang, Z.H., I.W. Burgess, and R.J. Plank. "Modeling Membrane Action of Concrete Slabs in Composite Buildings in Fire, II: Validations." *ASCE Journal of Structural Engineering* 129.8 (2003b): 1103-112.

50. Huang, Z.H., I.W. Burgess, and R.J. Plank. "Non-Linear Structural Modeling of a Fire Test Subject to High Restraint." *Fire Safety Journal* 31 (2001): 795-814.

51. Huang, Z.H., I.W. Burgess, and R.J. Plank. "Three-Dimensional Analysis Of Composite Steel-Framed Buildings In Fire." *ASCE Journal of Structural Engineering* 126.3 (2000): 389-97.

52. Huang, Z.H., K.H. Tan, and S.K. Ting. "Heating Rate and Boundary Restraint Effects on Fire Resistance of Steel Columns with Creep." *Engineering Structures* 28 (2006): 805-17.

53. ISO 834. *Fire Resistance Tests – Elements of Building Construction*. Geneva, Switzerland: International Organization for Standardization, 1975.

54. Kirby, B.R., and R.R. Preston. "High Temperature Properties of Hot-Rolled, Structural Steels for Use in Fire Engineering Design Studies." *Fire Safety Journal* 13 (1988): 27-37.

55. Klingsch, W., and F.W. Wittbecker. *Fire Resistance of Hollow Section Composite Columns of Small Cross Sections*. Rep. Wuppertal, Germany: Bergische Universität, 1988. pp. 103

56. Kodur, V.K.R., and D.H. MacKinnon. "Fire Endurance of Concrete-Filled Hollow Structural Steel Columns." *AISC Steel Construction Journal* 37.1 (2000): 13-24.

57. Kodur, V.K.R., and R.S. Fike. "Performance-based Fire Design of Concrete-Filled Steel Columns." Proc. of 2009 Application of Structural Fire Engineering Conference, Prague, Czech Republic. 2009a.

58. Kodur, V.K.R., and R.S. Fike. "Performance-Based Fire Resistant Design for Concrete-Filled HSS Columns." Proc. of 2008 Annual Stability Conference, Nashville. 2008.

59. Kodur, V.K.R., and R.S. Fike. "Response of Concrete-Filled HSS Columns in Real Fires." *AISC Engineering Journal* 46.4 (2009b).

60. Kodur, V.K.R., and T.T. Lie. "Evaluation of Fire Resistance of Rectangular Steel Columns Filled With Fiber-Reinforce Concrete." *Canadian Journal of Civil Engineering* 24 (1997): 339-49.

61. Kodur, V.K.R., and T.T. Lie. *Experimental Studies on the Fire Resistance of Circular Hollow Steel Columns Filled With Steel Fiber Reinforced Concrete*. Rep. no. 691. National Research Council of Canada, 1995a.

62. Kodur, V.K.R., and T.T. Lie. "Fire Performance of Concrete-Filled Hollow Steel Columns." *Journal of Fire Protection Engineering* 7.3 (1995b): 89-98.

63. Kodur, V.K.R., and T.T. Lie. "Fire Resistance of Circular Steel Columns Filled With Fiber-Reinforced Concrete." *ASCE Journal of Structural Engineering* 122.7 (1996): 776-82.

64. Kodur, V.K.R., D.I. Nwosu, M.A. Sultan, and J.M. Franssen. "Application of the SAFIR Computer Program for Evaluating Fire Resistance." Proc. of Third International Conference on Fire Research Engineering, Chicago. 1999. 287-98.

65. Kodur, V.K.R., M.S. Dwaikat, and R.S. Fike. "High Temperature Properties of Steel for Fire Resistance Modeling of Structures." *ASCE Materials Journal* 22.5 (2010).

66. Kodur, V.K.R. "Performance-Based Fire Resistance Design of Concrete-filled Steel Columns." *Journal of Constructional Steel Research* 51 (1999): 21-36.

67. Lamont, S., and B. Lane. "Behavior of Structures in Fire and Real Design – A Case Study." *Journal of Fire Protection Engineering* 16 (2006): 5-31.

68. Latham, D.J., B.R. Kirby, and G. Thomson. "The Temperature Attained by Unprotected Structural Steelwork in Experimental Natural Fires." *Fire Safety Journal* 12 (1987): 139-72.

69. Lew, H.S., R.W. Bukowski, and N.J. Carino. *Federal Building and Fire Safety Investigation on the World Trade Center Disaster: Design, Construction, and Maintenance of Structural and Life Safety Systems*. Rep. no. NCSTAR. Gaithsburg, MD, 2005. NTIS No. 1-1.

70. Li, G.Q., S.C. Jiang, Y.Z. Yin, and M.F. Li. "Experimental Studies on the Properties of Constructional Steel at Elevated Temperatures." *ASCE Journal of Structural Engineering* 129.12 (2003): 1717-721.

71. Lie, T. T. *Structural Fire Protection. ASCE Manual*. New York, NY: American Society of Civil Engineers, 1992. Ser. 78.

72. Lie, T.T., and D.C. Stringer. "Calculation of Fire Resistance of Steel Hollow Structural Steel Columns Filled With Plain Concrete." *Canadian Journal of Civil Engineering* 21.3 (1994): 382-85.

73. Lie, T.T., and M. Chabot. *Experimental Studies on the Fire Resistance of Hollow Steel Columns Filled With Plain Concrete*. IRC Internal Report 611. National Research Council of Canada, 1992.

74. Lie, T.T., and S.E. Caron. *Fire Resistance of Circular Hollow Steel Columns Filled with Carbonate Aggregate Concrete: Test Results*. IRC Internal Report 573. National Research Council of Canada, 1988.

75. Lie, T.T., and V.K.R. Kodur. *Effect of Temperature on Thermal and Mechanical Properties of Steel-Fiber Reinforced Concrete*. IRC Internal Report 695. National Research Council of Canada, 1995a.

76. Lie, T.T., and V.K.R. Kodur. *Mechanical Properties of Fiber Reinforced Concrete at Elevated Temperatures*. IRC Internal Report 687. National Research Council of Canada, 1994.

77. Lie, T.T., and V.K.R. Kodur. *Thermal Properties of Fiber-Reinforced Concrete at Elevated Temperatures*. IRC Internal Report 683. National Research Council of Canada, 1995b.

78. Lie, T.T., R.J. Irwin, and M. Chabot. *Factors Affecting the Fire Resistance of Circular Hollow Steel Columns Filled With Plain Concrete*. IRC Internal Report 612. National Research Council of Canada, 1991.

79. Lim, L., A. Buchanan, P. Moss, and JM Franssen. "Numerical Modeling of Two-Way Reinforced Concrete Slabs in Fire." *Engineering Structures* 26 (2004): 1081-091.

80. Magnusson, S.E., and S. Thelandersson. "Temperature-Time Curves of Complete Process of Fire Development; Theoretical Study of Wood Fuel Fires in Enclosed Spaces." *Civil Engineering and Building* 65th ser. (1970). Acta, Polytechnica, Scandinavia

81. Mäkeläinen, P., J. Outinen, and J. Kesti. "Fire Design Model for Structural Steel S420M Based Upon Transient-State Tensile Test Results." *Journal of Constructional Steel Research* 48.1 (1998): 47-57.

82. Moss, P.J., and G.C. Clifton. "Modeling Of The Cardington LBTF Steel Frame Building Fire Tests." *Fire and Materials* 28 (2004): 177-98.

83. National Building Code of Canada. *National Research Council of Canada* (2005).

84. Newman, G.M., J.T. Robinson, and C.G. Bailey. *Fire Safe Design: A New Approach To Multi-Storey Steel-Framed Buildings*. 2nd ed. Silwood Park, Ascot, Berkshire: Steel Construction Institute, 2006.

85. NIST. *Fire Protection of Structural Steel in High Rise Buildings*. Gaithersburg, MD: National Institute of Standards and Technology, 2004.

86. Nwosu, D.I., and V.K.R. Kodur. "Behavior of Steel Frames Under Fire Conditions." *Canadian Journal of Civil Engineering* 26 (1999): 156-67.

87. Outinen, J., and P. Mäkeläinen. "Mechanical Properties of Structural Steel at Elevated Temperatures and After Cooling Down." *Fire and Materials* 28 (2004): 237-51.

88. Outinen, J., J. Kesti, and P. Mäkeläinen. "Fire Design Model for Structural Steel S355 Based Upon Transient State Tensile Test Results." *Journal of Constructional Steel Research* 42.3 (1997): 161-69.

89. Outinen, J. *Mechanical Properties of Structural Steels at High Temperatures and After Cooling Down*. Thesis. Helsinki University of Technology Laboratory of Steel Structures, 2007. Publication 32

90. Parkinson, D.L., and V.K.R. Kodur. "Performance-Based Design of Structural Steel for Fire Conditions – A Calculation Methodology." *International Journal of Steel Structures* 7.3 (2007): 219-26.

91. Petersson, O., and S.E. Magnusson. *Fire Engineering Design of Steel Structures*. Publication no. 50. Stockholm: Swedish Institute of Steel Construction, 1976.

92. Poh, K.W. "Stress-strain-temperature Relationship for Structural Steel." *Journal of Materials in Civil Engineering* 13.5 (2001): 371-79.

93. Ponto, M. "Citadel High School: A Performance-Based Solution for Unprotected Structural Steel." *Advantage Steel* 26 (2006). Canadian Institute for Steel Construction

94. Powel, R.W., and R.P. Tye. "High Alloy Steels for Use as a Thermal Conductivity Standard." *British Journal of Applied Physics* 11 (1960): 195-98.

95. Rempe, J.L., and D.L. Knudson. "High Temperature Thermal Properties for Metals Used in LWR Vessels." *Journal of Nuclear Materials* 372.2-3 (2008): 350-57.

96. Rubert, A., and P. Schaumann. "Structural Steel and Plane Frame Assemblies Under Fire Action." *Fire Safety Journal* 10 (1986): 173-84.

97. SFPE. *Handbook of Fire Protection Engineering*. Bethesda, MD: Society of Fire Protection Engineers, 2002.

98. SFPE. *Handbook of Fire Protection Engineering*. Bethesda, MD: Society of Fire Protection Engineers, 2005.

99. Sorathia, U., T. Gracik, and J. Ness. "Evaluation of Intumescent Coatings for Shipboard Fire Protection." *Journal of Fire Sciences* 21 (2003): 423-50.

100. *Steel Construction Manual.* 13th ed. [Chicago, Ill.]: American Institute of Steel Construction, 2005.

101. Stirland, C. *Steel Properties at Elevated Temperatures for Use in Fire Engineering Calculations*. Document ISO/TC92/WG15, No. 14. Teeside Laboratories, U.K: British Steel Corporation, 1980.

102. Talamona, D. "A Quadrilateral Shell Finite Element for Concrete and Steel Structures Subject to Fire." *Journal of Fire Protection Engineering* 15 (2005): 237-64.

103. Thomas, I.R., and Et Al. *The Effect of Fire in the Building at 140 William Street Office Building*. Rep. BHP Research-Melbourne Laboratories, 1992.

104. Touloukian, Y. "Thermal Radiative Properties for Non Metallic Solids." *Thermal Physical Properties* 8 (1972): 142.

105. Twilt, L. *Stress-strain Relationships of Structural Steel at Elevated Temperatures: Analysis of Various Options and European Proposal – Part F: Mechanical Properties*. TNO-rapport BI-91-015. Delft, 1991.

106. Usmani, A.S. "Stability of the World Trade Center Twin Towers Structural Frame in Multiple Floor Fires." *Journal of Engineering Mechanics* 131.6 (2005): 654-57.

107. Usmani, A.S., Y.C. Chung, and J.L. Torero. "How Did the WTC Towers Collapse: A New Theory." *Fire Safety Journal* 38.6 (2003): 501-33.

108. Wald, F., L. Silva, D. Moore, T. Lennon, M. Chladna, A. Santiago, M. Benes, and L. Borges. "Experimental Behavior of a Steel Structure Under Natural Fire." *Fire Safety Journal* 41.7 (2006): 509-22.

109. Wang, Y.C., and V.K.R. Kodur. "Research Toward the Use of Unprotected Steel Structures." *Journal of Structural Engineering* 126.12 (2000): 1442-450.

110. Wellman, E., A. Varma, R.S. Fike, P. Pakala, and V.K.R. Kodur. "Experimental Evaluation of Composite Floor Assemblies Under Fire Loading." *Submitted to Journal of Engineering Structures* (2010).

111. Wellman, E. *Experimental Evaluation of Composite Floor Assemblies Under Fire Loading*. Thesis. Purdue University. West Lafayette, Indiana, U.S. 2010.

112. Witteveen, J., L. Twilt, and F.S. Bijlaard. "The Stability of Braced and Un-braced Frames at Elevated Temperatures." International Symposium of Stability of Steel Structures. 1977. Lecture.

113. Yawata Iron and Steel Co. "WEL-TEN 80 Material Datasheet." (1969): 142-64. Japan

114. Zhang, N.S., and G.Q. Li. "A New Method to Analyze the Membrane Action in Composite Floor Slabs in Fire Conditions." Proc. of 5th International Conference on Structures in Fire, Singapore. 2008.